Spring 2004

Development of hydraulic relationships for estimating in-bank river discharge using remotely sensed data

David Michael Bjerklie
University of New Hampshire, Durham

DEVELOPMENT OF HYDRAULIC RELATIONSHIPS FOR ESTIMATING IN-BANK RIVER DISCHARGE USING REMOTELY SENSED DATA

BY

David Michael Bjerklie

BS, University of Maine, 1977

MS, University of New Hampshire, 1980

MSCE, University of Alaska, 1987

DISSERTATION

Submitted to the University of New Hampshire

in Partial Fulfillment of

the Requirements for the Degree of

Doctor of Philosophy

In

Earth Sciences

May, 2004

This dissertation has been examined and approved.

S. Lawrence Dingman

S. Lawrence Dingman, Professor of Hydrology and Water Resources

Charles J. Vörösmarty, Director Water Systems Analysis Group, Institute for the Study of Earth, Oceans and Space

Carl H. Bolster

Carl H. Bolster, Assistant Professor of Hydrology

Russell G. Congalton

Russell G. Congalton, Professor of Remote Sensing and GIS

G. Robert Brakenridge

G. Robert Brakenridge, Research Associate and Professor of Geography, Dartmouth College

22 January 2004

Date

ACKNOWLEDGEMENTS

First and foremost I would like to acknowledge my wife and family who have encouraged and patiently supported me through this process. My advisor, S. Lawrence Dingman, Department of Earth Science, provided both the foundation and the continued encouragment that I needed to compelete this research. I would also like to acknowledge the valuable input, guidance and review comments from my graduate committee: Charles J. Vorosmarty, Complex Systems Research Center, University of New Hampshire; Carl H. Bolster and Russell G. Congalton Department of Natural Resources, University of New Hampshire; and G. Robert Brakenridge, Department of Geography, Dartmouth College. I also received valuable comments from William Kirby of the United States Geological Survey. In addition, I am indebted to Balazs Fekete, Research Scientist at the Institute for the Study of Earth, Oceans and Space at the University of New Hampshire for providing insight, ideas and data which contributed to much of this work; Ellen Douglas and all of the staff and colleagues in the Water Systems Analysis Group at the Complex Systems Research Center, University of New Hampshire for providing input, comments and support; and Delwyn Moller at JPL-NASA and Laurence Smith at UCLA for valuable input and comments to this work. Elements of this research were funded by NASA grant numbers NAG5 – 7601 and NAG5 – 8683. My interaction with NASA researchers as a partcipant in the NASA grant program has been both rewarding and professionally encouraging.

TABLE OF CONTENTS

LIST OF TABLES

PAGE

LIST OF FIGURES

PAGE

ABSTRACT

DEVELOPMENT OF HYDRAULIC RELATIONSHIPS FOR ESTIMATING IN-BANK RIVER DISCHARGE USING REMOTELY SENSED DATA

by

David M. Bjerklie

University of New Hampshire, May, 2004

An evaluation river hydraulic data currently or potentially available from satellite and other remote platforms was completed, and a set of discharge estimation models proposed that can use the remotely sensed information to estimate discharge with reasonable accuracy. Reasonable accuracy is defined as within +/- 20% of the observed on average for a large number of estimates. The proposed estimation models are based on the Manning and Chezy flow resistance equations, and utilize combinations of potentially observable variables including water-surface width, maximum-channel (or bankfull) width, mean water depth, mean maximum-channel depth, mean water velocity, and channel slope. Both stastistically and rationally derived prediction models are presented, developed and calibrated on a data base of river discharge measurements and a quasi-theoretical data base of synthetic data. It was found that the channel slope can be used in lieu of a measured water surface slope with very little reduction in prediction accuracy when considering many estimates. Notably absent from this list is a resistance variable, which is included in both the Manning and Chezy equations, because this variable cannot be observed or directly measured. One of the key outcomes of the research is that an exponent of 0.33 on the slope explains much of the variablity in the resistance variable, and provides better predictive qualities than the traditional value of 0.5. A dimensionally homogeneous form of the Manning equation was developed which derives the slope exponent of 0.33 based on stable-bed

grain size considerations. The prediction models were tested on two data sets of remotely sensed hydraulic information that included width, maximum channel width, and channel slope. Predictions were also made from a single radar image that also included remotely sensed surface velocity, demonstrating the potential for greatly improved accuracy with this additional information. Additionally, the prediction models were tested with channel slope information derived from a digital elevation model, and used to define river channel geometry for a continental scale runoff model.

CHAPTER I

INTRODUCTION

Currently, less than 60% of the runoff from the continents is monitored at the point of inflow to the oceans (Fekete, 1999). The distribution of runoff within the continents is even less well monitored. Despite the importance of river discharge information, a comprehensive global river-monitoring network faces numerous technological, economic, and institutional obstacles. As a result, gaging stations and access to river-discharge information have been declining since the 1980s (Vörösmarty et al. 1999; IAHS, 2001). Hydrographic data obtained from satellites and other remote sources offer the possibility of broad and potentially frequent global coverage of river-discharge estimates (Barrett, 1998). Thus, a method that uses remotely sensed data to estimate river discharge would provide a means to maintain or even increase the global streamflow-monitoring network and may, in the long run, be a cost-effective method to obtain needed river-discharge data on a global scale.

Remotely sensed information can be appled to the science of estimating river discharge in two fundamental ways: 1) by providing data necessary to the watershed-runoff modeling process such as soil type, land cover, precipitation, topography, air temperature, solar radiation and wind speed such that runoff can be estimated and the discharge inferred from a routing scheme; or 2) by directly observing the hydraulic variables of flow in a river channel and estimating discharge from hydraulic functions that use this information. Although watershed modeling can provide estimates of river discharge, the discharge estimate is itself a by-product of a set of modeling assumptions and simplifications and cannot be said to be directly measured or estimated.

Additionally, it would not be independent of spatial and temporal complexities that are subject to various scaling and model-input limitations. Without ground-based discharge calibration data for a specific watershed, discharge estimates made from the first approach may or may not be accurate. The spatial and temporal complexities of the watershed runoff process and the modeling of that process suggest that a general approach to estimating discharge in this way would be inherently unreliable without watershed-specific calibration. In general, the number of variables required to track the variability and describe the mechanics of discharge in a river system is much less than those necessary to understand and track the variability of the watershed-runoff process. It is because of these issues that estimating discharge with the second approach is preferred and is the focus of this study.

The goal of this dissertation is to develop, demonstrate, and evaluate the accuracy and application of methods suitable for estimating the discharge in rivers from remotely sensed river channel information. The specific objectives of the research are to:

- Document the type and quality of river channel information that can be potentially observed from remote platforms;
- Evaluate the potential application and accuracy of the observed data to estimate discharge using hydraulic relationships developed from ground-based river-discharge data;
- Develop suitable hydraulic relationships from general hydraulic principles;
- Develop and test a method derived from the hydraulic analysis to estimate discharge from currently available information;

- Evaluate the hydraulic methods within the context of general discharge modeling application that maximizes the use of remotely obtained or modeled river discharge and channel variables.

The use of remotely sensed information, including water-surface elevation, water-surface velocity and water-surface area, to track changes in river discharge has been shown to be feasible and potentially useful where ground-based data are difficult to obtain (Kuprianov, 1973; Koblinsky et al., 1993: Birkett, 1998; Brakenridge et al., 1994;and Brakenridge et al., 1998, Horritt et al., 2001, Jasinski et al., 2001). These studies suggest that remotely sensed river hydraulic data could be used to directly estimate the discharge at a specific location, if ground-based discharge measurements are used to develop discharge ratings in conjunction with the remotely observed variable(s). This strategy, however, does not capitalize on the advantage of using remotely sensed data because ground measurements of discharge are still a fundamental aspect of the approach.

If remotely sensed river hydraulic data were used to directly estimate the discharge without the need for ground-based calibration data, then remote observation platforms could be used to estimate discharge over large areas in many rivers. A bankside system that remotely obtains the cross-sectional area of flow and surface velocity of rivers has been demonstrated by Costa et al. (2000), however, this system would still require ground-based installation and maintenance. Thus, if satellite or aerial platforms could be used to obtain sufficient amount of information to estimate discharge, the need for ground-based measurements could be eliminated and would enable the potential of remote observation systems to obtain information over large geographic areas, including those areas that are difficult to access, to be realized.

Estimating discharge in rivers from hydraulic information obtained solely from aerial and satellite platforms has been explored and summarized by Smith et al. (1996 and 1997). The water-surface width (estimated from water-surface area), channel slope and mean channel width (estimated from channel surface area) can all be obtained from existing remote sources. The surface velocity of rivers can also be observed remotely using various forms of Doppler radar or lidar (Vörösmarty et al., 1999; Emmitt, 2000 personal communication; Moller, 2003 personal communication).

This study further explores the potential for, and the accuracy of, estimating discharge from remote observations of the river channel. Hydraulic relationships and a reasonably accurate methodology are developed for this purpose. The relationships are applied to a set of aerial photos and SAR images and hydraulic modeling and mapping applications also explored.

CHAPTER II

THE POTENTIAL FOR ESTIMATING RIVER DISCHARGE AND MEASURING HYDRAULIC VARIABLES REMOTELY

The measurement of river discharge from space will fundamentally require a knowledge of the hydraulic relationship between river characteristics that can be observed from space-based platforms and river discharge. This chapter reviews the types of river hydraulic information that can potentially be observed from space-based platforms and develops several general relationships that can use this information to estimate discharge. Hydraulic data from more than 1,000 flow measurements in a wide range of rivers are used to develop and validate the relationships. An analysis of the impact of measurement error on prediction accuarcy is also undertaken. The approaches reviewed here are based on fundamental in-stream hydraulic relationships that are independent of watershed or basin predictor variables. Thus, the prediction methods are independent of regional and temporal climatic and physiographic variability and can be considered to be generally applicable to fluvial environments.

Estimating River Discharge from Hydraulic Variables

For most rivers, discharge (Q) cannot be measured directly, but rather must be calculated from measurements of the pertinent hydraulic elements of the flow. Discharge at a river cross-section, from continuity, is the volumetric flow rate through that cross-section and is given by

$$Q = VWY = VA \qquad (2\text{-}1)$$

where V is the average velocity, W is the water-surface width, Y the average water depth, and A the cross-sectional area perpendicular to the flow. Traditionally, Q is measured at selected cross-sections in a river by measurement of the velocity, depth, and width at incremental vertical stations across the channel, and the incremental flow estimates are summed to obtain the discharge through the cross-section. These periodic velocity-area measurements of discharge are then correlated with measured water-surface elevation (stage) to develop a stage-discharge "rating" for the cross-section. The stage-discharge rating equation takes the general form (Rantz et al., 1982; Herschy, 1998)

$$Q = a(Z-e)^m \tag{2-2}$$

where Z is the stage and the coefficients a and m are characteristic of the specific channel cross-section, and e is the elevation of zero flow.

For the periods between measurements of Q, the stage (Z) is recorded and Q is inferred from the rating curve. Since the value of e represents the elevation of zero flow, the term (Z-e) may be viewed as equivalent to the effective flow depth (Y) and thus the rating provides an estimate of discharge from the hydraulic flow depth. A rating equation such as equation (2-2) is developed for a particular river channel or cross-section, and would not be expected to be applicable to any other river location (Rantz et al., 1982). This is because change in stage (or depth) is used as an index to change in width and velocity, and is specific to the channel characteristics of the reach being measured. Thus, single variate discharge ratings cannot be generalized without a substantial loss in accuracy. Inclusion of additional hydraulic infromation into the rating model would improve the accuracy of the rating by accounting for more of the variability at any specific location.

Recently, Jasinski et al. (2001) used river stage obtained from satellite (TOPEX/Poseiden) altimetry data to develop discharge ratings for several locations in the Amazon basin by comparing the altimetry data with stage and discharge measured at existing gaging stations. The accuracy of the ratings varied depending on distance between the altimetry observation and the ground-measured discharge, and on the topography and the width of the river. This study demonstrated the feasibility of using satellite altimetry as a source of remote river-stage information. However, ground-based discharge data were required to develop the rating, and the derived ratings could not be extrapolated to other rivers or reaches of the Amazon. While such a system might have advantages in some situations, it does not solve the problems imposed by the costs of establishing and periodically measuring discharge on-the-ground, and would not offer the prospect of expanding the global coverage of discharge observations. Thus, a general rating that can estimate discharge from remotely obtained hydraulic data without ground-based measurements of discharge provides the best opportunity to capitaltize on satellite and other remote data sources.

A more general depth-discharge rating equation can be developed from the Manning equation which is widely viewed as generally applicable to natural rivers (Chow, 1959). Assuming a wide (W >10Y) rectangular channel, the depth-discharge rating defined from the Manning equation is

$$Q = aY^{1.67} \tag{2-3}$$

with

$$a = WS^{0.5}/n. \tag{2-4}$$

where S is the friction slope (slope of the total energy grade line but equivalent to the water surface or bed slope assuming uniform flow conditions) and n is the Manning resistance coefficient. In equation (2-3), the average depth is the dynamic predictive variable and the coefficient a can be directly calculated from channel properties and is comprised of a geometric component defined by W and a channel component defined by $S^{0.5}/n$ (which represents the balance between the gravitational energy supplied to the reach, S and the flow resistance, n). In a rectangular channel, W is constant and thus if S and n are constant, the coefficient a is constant. To the extent that S and n vary with depth, the exponent of equation (2-3) may also vary.

If a parabolic shape is assumed for the channel cross-section, a common assumption for natural channels (Chow, 1959), the width is related to the depth by $W^x=aY$ where x is the parabolic order. The derived depth-discharge rating from this assumption is

$$Q = aY^{(1/x + 1.67)} \tag{2-5}$$

with

$$a = (W_m/Y_m^{1/x})(S^{0.5}/n) \tag{2-6}$$

The variable W_m is the maximum or bank-full width and Y_m the maximum or bank-full average depth.

A similar equation can also be developed that uses width as the rating variable:

$$Q = aW^{(1.67x + 1)} \tag{2-7}$$

with

$$a = (Y_m^{1.67}/ W_m^{1.67x})(S^{0.5}/n) \tag{2-8}$$

Equations (2-5) and (2-7) can be regarded as generally applicable discharge ratings for within-bank flow to the extent that the Manning equation is generally applicable, under the assumption of a parabolic cross-section shape.

The channel resistance cannot be measured directly but is usually inferred from specific channel conditions including bed and bank material, channel irregularity (both in cross-section and planform shape) and other factors. In practice, the channel resistance is difficult to estimate with accuracy (Dingman and Sharma, 1997) and often varies considerably with discharge (Dingman, 1984). However, statistical studies by Riggs (1976), Jarrett (1984) and Dingman and Sharma (1997) have shown that reasonably accurate estimates of Q for within-bank flows can be obtained without resistance as an input variable, because the resistance varies with the channel geometry. Assuming that the hydraulic radius of the cross-section is equivalent to the mean depth (which would be expected for a wide channel), Dingman and Sharma (1997) show using multiple regression analysis that for a wide range of rivers discharge can be estimated as:

$$Q = 4.62W^{1.17}Y^{1.57}S^{0.34} \quad (2\text{-}9)$$

with all variables in SI units. Equation (2-9) was calibrated with over 500 flow measurements in 128 rivers and provides estimate accuracies, on average, in the range of 20% or better. This relationship can be considered a generally applicable multi-variate discharge rating because it includes the fundamental elements of uniform flow including the width, depth and slope. Additionally, since resistance is not an input variable, all of the necessary data can be measured either directly or remotely. However, equation (2-9) is fundamentally limited by the data used to develop it and therefore cannot be said to be generally applicable in all situations. In addition, because of this limitation, specific knowledge of the variation in the coefficient or exponents of the equation as they may relate to known channel conditions cannot be incorported into the model.

An equation similar to (2-9), which assumes that resistance is a function of the channel slope and geometry, can also be developed for situations where depth cannot be effectively measured, but velocity could be, such as in channels where there is substantial bed movement or bottom debris. The equation is developed by equating (2-1) with a general uniform flow equation such as equation (2-9), solving for the depth in terms of W, V and S, and then substituing this back into (2-1). Carrying through these operations yields an equation of the form:

$$Q = cW^{b}V^{f}S^{g} \quad (2\text{-}10)$$

In many situations it is difficult to establish the hydraulically meaningful channel slope that should be used in a theoretically or statistically based equation. Davidian (1984) suggests that a hydraulically meaningful slope should be measured over a reach length on the order of 75 times the water depth. However, the water-surface slope in a channel reach may vary spatially and temporally due to unsteady and non-uniform flow conditions (Davidian, 1984), and because of this, the reach length and timing associated with the slope measurement can alter the "true" uniform hydraulic slope associated with a particular discharge and channel geometry. Thus, consistent definitions of channel and water-surface slope will be important in attempting to apply equations involving those quantities. Given the potential difficulties of consistently measuring a water-surface slope that is hydraulically meaningful, a slope index may be used that considers the slope to be a constant rather than a variable. Such an index could be the topographic slope of the channel and thus might be related to channel morphology.

Alternatively, a relationship between discharge and an index velocity can be developed (Rantz, et al., 1982) which eliminates the slope variable. Since the average velocity in a channel is generally considered to be proportional to the square root of slope and 2/3 power of the depth via the Manning equation (or to the square root of slope and depth via the Chezy equation), the mean velocity could be substituted for the depth and slope to obtain a width-velocity relationship that avoids the need to measure depth and slope but that still provides estimates over a wide range of flow conditions. The form of this equation would be

$$Q = cW^hV^i \tag{2-11}$$

where c is a coefficient, and the exponents h and i reflect the relationships between depth and both width and velocity.

Measurement of Hydraulic Variables from Remote Platforms

Few studies have attempted to estimate river discharge entirely from satellite and/or other remotely obtained information, although the potential has been pointed out (Koblinsky, et al., 1993). Estimating the discharge in rivers via equations (1-1), (1-5), (1-7), (1-9), (1-10) and (1-11) requires a measure of the water-surface width, depth and water velocity, and/or river channel information including the water-surface slope, bank-full width and bank-full depth. The channel resistance is not a directly measurable quantity in the sense that it cannot be measured using an instrument, however it is related to the other geometric variables of the channel (Leopold et al., 1964; Bray, 1978; Dingman and Sharma, 1997) or can be evaluated by comparison with channel charcteristics where resistance values are known.

Satellite-based sensors and other remote data sources can be used to determine channel and water-surface width and water-surface area, water-surface elevation, channel slope and channel morphology (Table 2.1). In addition, there is a possibility that surface velocity can be measured at discrete locations across the river channel (Vörösmarty et al., 1999; Emmitt, personal communication, 2001). The key hydrographic variables that cannot be directly measured from satellite information or other remote data sources are average depth and average cross-sectional velocity. Thus, average depth and average cross-sectional velocity will need to be related, at least implicitly, to stage and surface velocity, respectively, if these variables are used for estimating discharge. Recently, Costa et al. (2000) have demonstrated that surface velocity measurements can effectively be used to estimate the mean velocity in a channel section.

Numerous studies have employed satellite-based imagery to estimate flood inundation area (Smith, 1997). However, few have used satellite derived data to track variability in river and flood stage elevations, and even fewer have attempted to quantitatively estimate river discharge. Landsat 7 multi-Spectral Scanner (MSS), Thematic Mapper (TM), and other visible/infrared spectrum sensors, and synthetic-aperture radar (SAR) imagery from satellites have proven to be useful in tracking changes in water-surface area (and widths) in floodplains and large rivers (Smith,1997). Sippel et al. (1994) determined the inundation area of the Amazon River floodplain using a scanning multi-channel microwave radiometer (SMMR) mounted on the Nimbus 7 satellite. The SMMR sensor measures the microwave emission of the earth's surface,

Table 2.1 **Satellite and Remote Data Sources**

Data Source	Hydrographic Data Type	Resolution	Relative Cost	Limitations/Advantages	Coverage
Aerial Photography	Surface features including width and channel shape. Stereoscopic Pairs can also provide surface roughness and slope.	High Resolution Depending on Scale	Low	Limited by inability to see through cloud cover Can provide high resolution and detail and provides direct interpretation and yields from a range of spectral bands	Spatial - Depends on Scale Temporal - Infrequent coverage
Visible Spectrum Digital Imagery	Surface features including width, channel shape and coupled with a DEM surface roughness and slope.	Depends on sensor, platform and orbital characteristics Aerial Imagery such as Emerge(1) Photography can be 1m or less Satellite Based Imagery such as Landsat 7 typically 10m or less	Moderate to high depending on coverage (large areas are expensive)	Limited by inability to see through cloud cover Provides direct interpretation and yields information from a range of spectral bands	Spatial - Can be large depending on desired resolution Temporal - Depends on orbital period and weather
Radar Imagery	Surface features including width, channel and roughness and used with interferometric methods can provide slope and possibly surface velocity using SAR with interferometry.	Space based 10m to 30m SAR surface velocity (not verified). Higher resolution with aerial	High.	Interpretation may be difficult Can see through cloud cover and yields information from a range of spectral bands	Spatial - can be 150 km X 150 km or less depending on desired resolution. Temporal - depends on orbital period.
Radar Altimetry	Elevation at discrete points which can be used to determine water surface heights (stage) and and possibly slope.	Space based elevations typically 0.5 m but possible to 10 cm Higher resolution with aerial	High	Limited range of information Can see through cloud cover	Provides discrete point data with coverage that depends on the orbital period (frequency of repeat orbits).
Lidar	Surface velocity, water surface slope and stage.	Possible to 10cm/s for velocity (not verified) 5 cm elevation	Not evaluated	Limited by cloud cover and range of information is limited Interpretation of return may be simpler than radar	Provides discrete point data with coverage that depends on the orbital period (frequency of repeat orbits).
Topographic Maps and GIS	Static channel shape and slope and other static surface features.	Depends on Scale	Low	Temporally limited because it is a static data base Interpretation is direct	Spatial - depends on scale Temporal - static.
EPA Reach data base and other comparable data bases	Potentially reach lengths, channel types and other channel feaatures	Depends on data	Low	Temporally limited because it is a static data base Interpretation is direct	Dependent on available data

which can be correlated to ground saturation and open water at the surface; however the resolution is low, on the order of 25 km, and the signal is attentuated by atmospheric moisture. Vörösmarty et al. (1996) correlated SMMR signals with discharge in the Amazon River, thus developing a discharge rating based on general moisture conditions within the basin. Brakenridge et al. (1994) used SAR images from ERS-1 to delineate flood inundation area coupled with topographic information to determine water-surface elevations during the 1993 Mississippi floods. Horritt (2000), Bates and DeRoo (2000) and Horritt et al. (2001) have used SAR imagery to delineate flood boundaries and calibrate river hydraulic models.

A method to estimate river discharge from aircraft has been developed that couples ground-based channel geometry information with surface velocity measurements made by photographing floats or other tracking substance introduced into the river by aerial drop (Kuprianov, 1978). The mean velocity is estimated from the surface velocity using an assumed vertical velocity distribution, and the channel geometry is measured on the ground and assumed to be constant thereafter. This method has a reported accuracy of 10% or better where winds are moderate (2 to 3 m/s) and water-surface velocity is in the range of 1 to 2 m/s. Although this method relies on instruments introduced into the streamflow (the floats) to measure velocity, the measurement is made entirely from a remote platform (the aircraft) once the appropriate ground measurements are made.

Smith et al. (1996) estimated the discharge in three braided glacial rivers using reach-averaged water-surface area obtained from RADARSAT SAR imagery. That study correlated the water-surface area in braided reaches (lengths on the order of 10 km) with discharge obtained from existing ground-based gaging stations to derive power-function discharge ratings that use effective width (water-surface area divided by the reach length) as the predictor variable. The accuracy of the ratings varied in each river, ranging from 1.5% (for 11 estimated values) to 54%

(19 estimated values). A single best-fit power function was also developed as a general rating for all of the rivers. Error associated with this function was much larger, providing accuracy only within a factor of 2 (100% error).

Smith et al. (1996) also pointed out that the total sinuosity was an important discriminator between the rivers studied. To test the predictive power of sinuosity, we used the data from Smith et al. (1996) to develop a general multi-parameter power function with reach-averaged width as the dynamic variable and the average sinuosity as a channel constant to predict discharge in all the three braided rivers (data not shown). This relation reduced the standard error of the estimate by 30% and improved the slope of the regression compared to the width-only relationship reported by Smith et al. (1996). These results suggest that morphologic features of a river channel that can be observed remotely and that are related to the energy-dissipation process may be useful for remote- discharge estimation. These features may include, in addition to channel sinuosity, meander wavelength, meander radius of curvature, bankfull width, width/depth ratio, and others (Leliavsky, 1966; Dury, 1976; Osterkamp et al., 1983; Rosgen, 1994).

In principle, it would seem that a width-discharge rating might be developed for a wide range of rivers, because width generally increases with increasing discharge. However, in nearly rectangular channels, or channels with highly irregular cross-sectional shape, width may change very little or in a highly non-linear way with discharge. This is illustrated in Figure 2.1, which shows changes in width with discharge over a range of flows for the Mississippi River at Thebes, Illinois, and the Connecticut River at Thompsonville, Connecticut (USGS, 2001). The graphs demonstrate that in the Mississippi at Thebes width does indeed change linearly with discharge and could be used as an index to flow variation, whereas in the Connecticut at Thompsonville it changes non-linearly with very little change at higher discharges. Similarly, width changes very little with discharge in the Amazon River narrows at Obidos (Oltman, 1968). This condition may be common at many locations in larger rivers, and suggests that multi-variate discharge ratings that

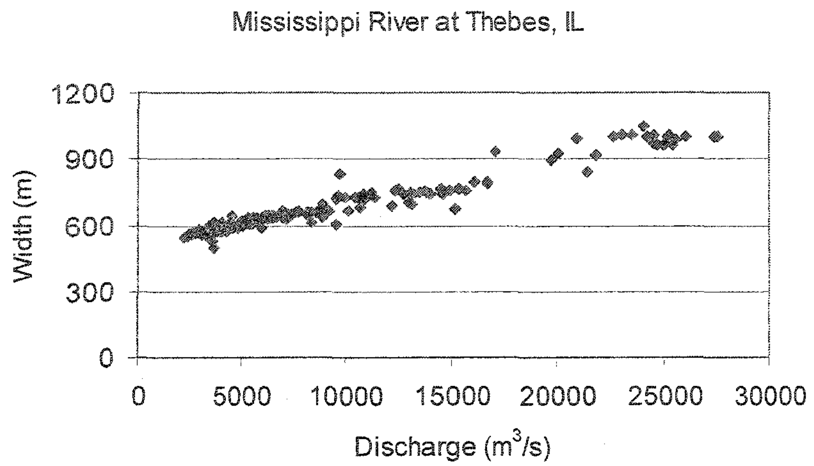

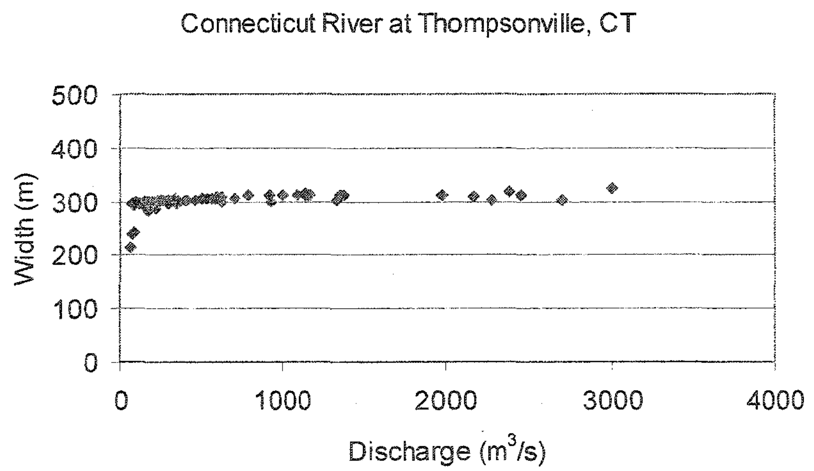

Figure 2.1 – Width versus discharge over a range of flows for the Mississippi River at Thebes, Illinois and the Connecticut River at Thompsonville, Connecticut (Source of discharge measurements: U.S. Geological Survey).

reflect general hydraulic relationships would be more universally applicable than relations based only on width. This also suggests that the best locations for evaluating river discharge from space, where width is the most readily observed hydraulic variable, are those channel reaches where width variation with dischage is most pronounced (Smith et al., 1997).

Measurement of Width

Both channel width and water-surface width (and also the water-surface area) can be measured from a variety of sensors and imagers mounted on satellites and aircraft (Table 2.2), including panchromatic and infrared imagers, digital photography, and synthetic aperture radar (SAR) (Barrett, 1998; University of Wisconsin Environmental Remote Sensing Center, 2001). The resolution of satellite-mounted digital panchromatic sensors is within the same range as aircraft- mounted sensors, indicating that satellite observation of width, because of the larger coverage, may be the preferred method to obtain this type of data. SAR is the only sensor that can measure the width in any atmospheric condition (Smith, 1997).

Panchromatic imagers have spatial resolution as fine as 1 or 2 m and SAR imagers as fine as 10 m (University of Wisconsin Environmental Remote Sensing Center, 2001). However, the accuacy of a sensor to observe surface-area or width change is not limited solely by the resolution. Improved measurement accuracy can be obtained by averaging resolution errors over the observed reach, such that relatively coarse resolution imagery may provide measurement accuracy significantly better than the resolution may imply. In addition, the ability to use different sensor bands to observe the surface area, each with its own observation qualities, can be used to complement each other and achieve potentially greater measurement accuracy.

The key objective of measuring surface area and width, as for any dynamic variable, is to detect change from one scene to another. Change detection is not necessarily restricted to resolution because identification of a pixel as either water or not-water depends on sub-pixel size qualities that are also detected. It is difficult to evaluate the true "error" that might be associated with the measurement of width and surface area from remote platforms, especially considering

Table 2.2 Examples of River Hydraulic Variables Observable from Existing Space Based Sensors

Observed Variable	Satellite/Sensor	Data Type	Data Resolution	Repeat Observation Frequency	Observational Issues
Water Surface Width and Channel Morphology	TERRA/ASTER	Visible Infrared Thermal Infrared Shortwave Infrared	15m	1-2 days	Cannot detect through clouds Banks may be obscured by vegetation and shadows
	EROS A & B	Visible to Infrared	1.5m	daily (with a constellation of satellites)	Cannot detect through clouds Banks may be obscured by vegetation and shadows
	ERS2	SAR	12-26m	6 days	Banks may be obscured by vegetation and wet soils
	SPOT 4	Panchromatic visible	10m	26 days	Cannot detect through clouds Banks may be obscured by vegetation and shadows
	LANDSAT 7	Panchromatic visible	15-60m	16 days	Cannot detect through clouds Banks may be obscured by vegetation and shadows
	IKONOS	Panchromatic visible	1-4 m		Cannot detect through clouds Banks may be obscured by vegetation and shadows
	RADARSAT	SAR	8-30m	1-6 days	Banks may be obscured by vegetation and wet soils
Water Surface Stage and slope	ERS-2 TOPEX/Posiedon	Radar Altimeter	10cm	10 days	Repeat observations limited to large rivers Using Interferometry coupled with Altimetry (unproven)
	RADARSAT	SAR	1cm	1-6 days	
Water Surface Velocity		Lidar Radar SAR	NA NA NA		Signal obscured by surface wind and waves Sensors have not been tested in rivers

that the error would be a function of many factors including the observed reach length, the resolution, the spectral bands used for pixel identification and processing technique. Based on these considerations, we could easily assume that a "typical" measurement error for a reach-averaged width measurement could be on the order of 10 m or less.

Width estimates using any imager would be subject to errors associated with vegetation obscuring the water's edge and the bank and, in the case of SAR, wet ground, vegetation, wind roughening and rocks can also obscure the edge of water. With a combination of SAR imagery (to observe through cloud cover) and digital panchromatic imagery, it is conceivable that width could be observed with near global coverage on a repeat cycle of nearly one week.

Measurement of Stage and Depth

Radar altimetry has been successfully used to track water-level elevations (stage) in large rivers, lakes and floodplains. Koblinsky et al. (1993) were able to use Geosat altimeter data to track elevation changes at several locations in the Amazon River basin with an accuracy on the order of 0.7 m. The altimeter footprint ranges from 0.2 to 2 km so target must be at least this wide to obtain a return unique to the water body. More recently, Birkett (1998) and Birkett et al. (2002) measured water-surface elevation changes in several rivers (including rivers in the Amazon Basin, the Okavango River, the Indus River and the Congo River) using water-surface elevation data obtained from the TOPEX/Posiedon (T/P) altimeter and reported an accuracy ranging from 11 to 60 cm.

With the currently deployed T/P altimeter, the theoretical minimum river width that can be observed ranges from 0.58 to 1.16 km (Birkett et al. 2002) with accuracies ranging from 10 cm to 1 m. However, it is possible that the altimeter can obtain accurate water-surface elevation measurements on rivers with widths as low as 50 meters by altering the signal-filtering algorithms (Ernesto Rodriquez, personal communication, 2001). The accuracy of the T/P altimeter (and altimeters in general) is strongly dependent on the surface conditions being observed (Birkett et al., 2002). Laser altimeters (lidar) such as GLAS (NASA, 1997), which will be deployed on ICESAT, can track elevation changes to within 15 cm, and thus may provide significantly higher accuracies in river environments than possible with currently deployed radar altimeters.

Depth cannot be measured directly from remote data (Table 2.1 and 2.2). Thus, this variable will need to be estimated, at least in part, from measurements of stage coupled with other observable characteristics of the channel. Depth could be derived from repeated observations of stage over a wide range of flow conditions provided accurate topographic data or altimetric measurements of sufficient accuracy were available to determine the exposed bank elevation at each observed water level. However, in large rivers low flow depths may never be observed, necessitating the estimation of the bank-full depth or other depth reference so that stage measurements can be converted to average water depths.

An estimate of the depth can be developed from a time series of stage measurements provide it is long enough to identify the bottom (zero flow) elevation, or the elevation of the top of bank. If the zero flow elevation (Z_0) is known, then computation of depth from observations of stage can be made directly. If the top of bank elevation is known, then Z_0 could be estimated if width observations are also available, by statistically relating the width and stage observations through linear regression, with the intercept being equal to Z_0. Another approach would be to assume a specific cross-section shape (e.g. a parabola) and then solve for Z_0 given stage and width observations that include the top of bank elevation and bankfull width.

Measurement of Water-Surface Slope

Water-surface slopes on the Amazon River and some of its larger tributaries have been estimated by Mertes et al. (1996) and Dunne et al. (1998) using SEASAT and Birkett et al. (2002) using T/P. All of these estimates have been made from sea-level (the mouth of the Amazon) to an inland point hundreds or thousands of kilometers upstream. The long reaches that were evaluated minimized the impact of altimeter accuracy on the estimates. Birkett et al. (2001) were also able to observe temporal changes in water-surface slope in the mainstem of the Amazon over long reaches.

In the Amazon River at Obidos, the water depth is on the order of 40 to 50 m and hydraulically meaningful water-surface gradients are on the order of 1 cm/km (Oltman, 1968). Thus, given an optimistic altimeter error of 10 to 20 cm, a reach of 5 to 10 km could conceivably result in slope estimates ranging from negative values to 8 times the actual value. This suggests that slope information obtained from the current generation of altimeters would not provide sufficient spatial resolution to be hydraulically meaningful. Averaging the slope obtained from a large sampling of slope measurements may be the most meaningful slope information that can be considered reliable.

One approach to obtaining more accurate water-surface slope measurements could be through the use of interferometric SAR. With this technique, water-surface elevation changes on the order of 1 cm can be detected in large rivers and flooded areas (Alsdorf et al. 2000, Alsdorf et al. 2001) and, when coupled with high resolution topographic information, could be used to estimate water-surface slopes across a flooded area as well as within a river. Laser altimeters may also provide a means to accurately measure hydraulically meaningful water-surface slopes because the altimeter could simultaneously measure the elevation at two points in a channel reach.

Measurement of Water-Surface Velocity

Surface velocity in rivers is potentially measurable from satellites with doppler lidar or radar. However, surface winds and waves on the water body could significantly interfere with the measurement (Vörösmarty et al. 1999), although observing limitations have not been fully evaluated. Theoretical (e.g. the Prandtl-von Karman velocity profile) or empirical relations would be required to translate surface velocity to average velocity; however, surface velocity could potentially provide an index of average flow velocity and hence be directly useful in predicting discharge.

Based on information supplied by Emmitt (personal communication, 2001), a satellite mounted doppler lidar sensor that could observe surface velocity would have a footprint of approximately 10 m with 75 m between observations along a track, and have a measurement accuracy on the order of 0.1 m/s. Given these specifications, the lidar could observe two to three surface-velocity "points" across a 200 meter wide river reach. There is no guarantee that the satellite track would cross the river reach perpendicular to the flow, thus the point measurements may be skewed across the channel. This should not be a problem provided the distance to each bank can be evaluated from another source (e.g. a concurrent image of the channel and knowledge of the satellite track) and the correction made. Despite the potential limitations, if surface velocity were measured and can be used to infer average velocity, there is the potential for measuring all elements of equation (2-1) simultaneously and thus enabling direct calculation of discharge.

Observation of Channel Morphology

Valley and channel features such as the channel sinuosity, channel slope, meander length, and meander radius of curvature can be observed from a variety of data sources, including visible- and infrared-spectrum images, SAR images, DEMs, and topographic map information. Because these features are considered relatively stable over short time frames, the frequency and timing of observations is not a limiting factor, and therefore high-resolution panchromatic images could be used to measure them when weather conditions permit.

Estimating River Discharge

Based on the above discussion, there is a possibility that the hydraulic elements of equation (2-1) can all be measured simultaneously from satellites. If so, discharge could be calculated directly, with an accuracy dependent on the accuracy and precision of the individual measurements of water-surface width, surface velocity, and stage and of the estimations of mean velocity and mean depth from observations of surface velocity and stage. Because there is a potential that stage or surface velocity will not be observed with confidence (e.g. under strong winds or where topography obscures the signal) there will be many situations when all three of the key variables cannot be observed at the same time. In these situations statistically based relationships such as described by equations (2-9), (2-10) and (2-11) may be useful.

Statistically Based Estimation Methods

To explore the predictive characteristics of different combinations of potentially observable (or estimated) river-hydraulic variables, a set of generally applicable river-discharge estimation equations (models) were developed based on equations (2-5), (2-7), (2-9), (2-10) and

Table 2.3 **Range of Hydraulic Parameters in Calibration and Validation Data Sets**

Parameter	Symbol	Units	Mean	Stdev	Coeff. Var.	Maximum	Minimum
Calibration Data N = 506							
Discharge	Q	m^3/s	1585	12260	7.74	216000	0.01
Top Width	W	m	146	206	1.41	2290	2.90
Average Depth (Hyd. Radius)	Y	m	2.48	3.56	1.44	48.03	0.18
Average Velocity	V	m/s	1.12	0.66	0.59	5.10	0.02
Water Surface Slope (average)	S	m/m	0.00278	0.00572	2.06	0.04	0.0000007
Valdiation Data N = 506							
Discharge	Q	m^3/s	1666	13184	7.91	283170	0.05
Top Width	W	m	158	211	1.34	2300	5.40
Average Depth (Hyd. Radius)	Y	m	2.73	3.53	1.29	50.33	0.14
Average Velocity	V	m/s	1.13	0.61	0.54	3.61	0.07
Water Surface Slope (average)	S	m/m	0.00243	0.00474	1.95	0.04	0.0000007

(2-11). The models were derived using multiple-regression analysis of hydraulic data from 1,012 discharge measurements in 102 rivers in the United States and New Zealand, including 4 measurements from the Amazon River at Obidos. The data include a wide range of river conditions (Table 2.3) and was randomly divided into a calibration data set and a validation data set each containing 506 measurements. The 4 Amazon River measurements were equally divided between the calibration and validation data sets.

The data base includes 569 discharge measurements with reach averaged (generally three or more cross-sections representing a reach length 5 or more times the width) values of water-surface width, average water-surface depth, average velocity, and water-surface slope measured concurrently with the discharge. These data were obtained from Barnes (1967), Hicks and Mason (1992) and Coon (1998). Because these data are reach-averaged, the hydraulic-geometry and velocity values are representative of the energy and resistance relationships within the channel, and less a reflection of conditions at a single cross-section. In addition, the reported width approximates the water-surface area divided by the reach length, consistent with Smith et al. (1996). To this extent, the data are consistent with what might be obtained from remote imagery capable of providing reach averaged width, channel slope, and surface velocity.

The reach-averaged data include only two discharge measurements greater than 10,000 m^3/s. In order to include more large flows in the data base, 443 additional measurements representative of the larger rivers of North America were obtained from the USGS (2001) and data from four measurements for the Amazon River at Obidos, Brazil were also included (Oltman, 1968; Dury, 1976). These large discharge measurements are not reach averaged, and therefore have a certain incompatibility with the rest of the data in the data base. However, it is anticipated that hydraulic variability between the measurement section and the reach as a whole is not large, and that the number of observations will average out the variability. In addition, inspection of the channel characteristics at the measurement sections for these rivers do not indicate any channel constraints from bridges or other structures (however, some of the river hydraulics may be affected by bedrock outcrops and canyons).

The discharge data are all in-bank and do not represent overbank-flow conditions. In general, the data were obtained from relatively straight single-thread channel sections, and therefore do not necessarily reflect the hydraulic conditions in more complex or less constrained channel patterns. Because of this, the derived regression coefficients may be biased towards these types of channels, reflecting typical relationships between width and depth, depth and resistance, and velocity and depth that would be found in straight channels. However, because the models are based on, and include, the fundamental hydraulic variables of uniform flow, the resultant regression equations are considered to remain generally representative of uniform-flow relationships for any defined channel.

Similar to Dingman and Sharma (1997), the predictive models were assumed to be multiplicative. The form of the prediction equations (models) that were developed are based on Equations (2-5), (2-7), (2-9), (2-10) and (2-11) as follows:

Model 1 (Equation 2-9): $Q = c_1 W^a Y^b S^d$ (2-12)

Model 2 (Equation 2-11): $Q = c_2 W^e V^f S^g$ (2-13)

Model 3 (Equation 2-10): $Q = c_3 W^e V^f$ (2-14)

Model 4 (Equation 2-5): $Q = c_4 W_m{}^g Y_m{}^h S^i Y^j$ (2-15)

Model 5 (Equation 2-7): $Q = c_5 W_m{}^k Y_m{}^l S^m W^n$ (2-16)

Models 1, 2, 4 and 5 use the water-surface slope as a prediction variable. However, the USGS discharge measurement data base does not include slope as a measured parameter. Therefore, a channel slope for these river stations was measured manually from 1:24,000 scale USGS topographic maps over one contour interval. This results in a constant slope value for all of the flow measurements at a particular river station, implying slope as a geomorphic characteristic of the river.

The implication of using a constant slope is explored by comparing two realizations of Model 1 developed from the reach averaged data base, that includes a unique measured slope for all discharge measurements (minimum of five) at each river station (excluding the Barnes (1967) data, which includes only one flow measurement at each station). The first model uses slope as a dynamic variable and the second uses a slope obtained by averaging all of the measured slopes over the entire discharge range at each river station. The comparison shows nearly identical regression models (Table 2.4). Based on this comparison, we conclude that using an average slope, or a channel slope obtained from topographic information that is a constant for a river reach, can be used in lieu of a measured slope, thus obviating the need to track water surface slope as a dynamic prediction variable.

These results also indicate that the USGS flow measurement data, which includes width, average depth, average velocity, and discharge (but not slope) can be combined with the reach averaged data base (which includes a measured slope) using a slope measured from 1:24,000 scale USGS topographic maps for each station. In the remainder of this paper, all of the regression models and all discussion of slope as a prediction variable assume a constant slope for each river station, developed either as an average of many measured values, or obtained from topography.

Using the entire calibration data set (N= 506), the following regression models are developed (in SI units):

Model 1: $$Q = 7.22W^{1.02}Y^{1.74}S^{0.35} \quad (2\text{-}17)$$

Model 2: $$Q = 0.09W^{1.21}V^{1.53}S^{-0.30} \quad (2\text{-}18)$$

TABLE 2.4 **COMPARISON OF REGRESSION MODELS USING CONSTANT AND VARIABLE SLOPE**

Model	Regression Statistics N	R^2	Std. Error Regression		Relative Residual (Q* - Q)/Q	Log Residual (logQ* - logQ)	Actual Residual (Q* - Q) (m^3/s)	Coefficients	Value	Std. Error	Upper 95%	Lower 95%	p
Variable Slope $Q = 4.57W^{1.18}Y^{1.74}S^{0.35}$	545	0.95	0.19	Mean	0.12	0.001	14.6	Intercept	4.57	1.14	5.97	3.50	<0.0001
				Stdev	0.69	0.189	113.8	W	1.18	0.03	1.24	1.12	<0.0001
								Y	1.74	0.04	1.82	1.67	<0.0001
								S	0.35	0.02	0.38	0.32	<0.0001
Constant Slope $Q = 4.60W^{1.17}Y^{1.76}S^{0.35}$	545	0.95	0.20	Mean	0.14	-0.001	11.4	Intercept	4.60	1.16	6.21	3.42	<0.0001
				Stdev	0.87	0.202	113.0	W	1.17	0.03	1.23	1.10	<0.0001
								Y	1.78	0.04	1.86	1.69	<0.0001
								S	0.35	0.02	0.39	0.31	<0.0001

Model 3: $Q = 0.23W^{1.46}V^{1.39}$ (2-19)

Model 4: $Q = 3.55W_m^{1.19}Y_m^{-0.84}S^{0.30}Y^{2.17}$ (2-20)

Model 5: $Q = 1.07W_m^{-1.61}Y_m^{1.11}S^{0.08}W^{2.65}$ (2-21)

The values for Y_m and W_m used in the regresssion analysis are obtained as the maximum value for all of the flow measurements at each river station, and thus are constant for each station. The possiblity that the Amazon River measurements skewed the regression results was evaluated by removing them from the calibration data set and re-running the regression analysis. It was found that the Amazon data did not significantly impact the regression results.

The four regression models varied in their ability to describe the observed data. Comparative statistics between the models are shown on Table 2.5 and indicate that Models 1, 2 and 3 perform comparably well, and that Model 4 does not perform as well as Models 1, 2 and 3 but is better than Model 5. The intercept and coefficient of the slope for Model 5 are not significantly different than zero at the 95% confidence level. Since the form of the model is based on the Manning equation, slope would be expected to be a significant predictor variable as it is in Model 1. The reason for this outcome may be due to the fact that width by itself is not an especially good predictor variable at many specific river stations (as indicated by Figure 2.1), and thus a constant slope at each river station does not contribute to explaining at-a-station variation. The standard error of the estimate (standard deviation of the log residuals) for Model 5 is nearly twice as large as the standard errors for Model 1, 2 and 3, and indicates that 67% of the predictions using this model fall within a wide margin (factor of 2.75). Because of the relatively poor performance of Model 5 it is not evaluated further.

For comparative purposes, Table 2.5 also lists regression results for three single-variate models that use each element of equation (2-1) (W, Y and V) to predict Q. These models indicate that depth, by itself, predicts discharge better than width and has a lower standard error than

TABLE 2.5 **REGRESSION MODEL COMPARISON**

Model	Regression Statistics R^2	Std. Error Regression	Coefficients	Value	Std. Error	upper 95%	lower 95%	t stat	p
Model 1									
$\log Q = 0.86 + 1.02\log W + 1.74\log Y + 0.35\log S$	0.95	0.23	Intercept	0.86	0.06	0.98	0.73	13.40	<0.0001
$(Q = 7.22W^{1.02}Y^{1.74}S^{0.35})$			W	1.02	0.03	1.07	0.96	35.16	<0.0001
			Y	1.74	0.04	1.82	1.66	42.07	<0.0001
			S	0.35	0.02	0.40	0.31	15.27	<0.0001
Model 2									
$\log Q = -1.06 + 1.21\log W + 1.53\log V - 0.30\log S$	0.97	0.19	Intercept	-1.06	0.04	-0.98	-1.14	-26.22	<0.0001
$(Q = 0.09W^{1.21}V^{1.53}S^{-0.30})$			W	1.21	0.02	1.25	1.16	53.65	<0.0001
			V	1.53	0.03	1.59	1.47	51.85	<0.0001
			S	-0.30	0.02	-0.26	-0.33	-15.29	<0.0001
Model 3									
$\log Q = -0.63 + 1.46\log W + 1.39\log V$	0.95	0.23	Intercept	-0.63	0.04	-0.56	-0.70	-17.93	<0.0001
$(Q = 0.23W^{1.46}V^{1.39})$			W	1.46	0.03	1.45	1.32	40.98	<0.0001
			V	1.39	0.02	1.50	1.43	80.57	<0.0001
Model 4									
$\log Q = 0.55 + 1.19\log Wm - 0.84\log Ym + 0.3\log S + 2.17\log Y$	0.93	0.28	Intercept	0.55	0.11	0.76	0.34	5.19	<0.0001
$(Q = 3.55W_m^{1.19}Y_m^{-0.84}*S^{0.30}Y^{2.17})$			W_m	1.19	0.06	1.29	1.08	21.42	<0.0001
			Y_m	-0.84	0.11	-0.63	-1.06	-7.64	<0.0001
			S	0.30	0.03	0.37	0.24	9.48	<0.0001
			Y	2.17	0.05	2.27	2.06	42.11	<0.0001
Model 5									
$\log Q = 0.03 - 1.61\log Wm + 1.11\log Ym + 0.08\log S + 2.65\log Y$	0.83	0.44	Intercept	0.03	0.17	0.36	-0.30	0.17	0.86
$(Q = 1.07W_m^{-1.61}Y_m^{1.11}S^{0.08}W^{2.65})$			W_m	-1.61	0.16	-1.30	-1.92	-10.24	<0.0001
			Y_m	1.11	0.16	1.42	0.79	6.86	<0.0001
			S	0.08	0.05	0.18	-0.02	1.53	0.13
			W	2.65	0.13	2.90	2.39	20.00	<0.0001
Comparative Single-Variate Models									
Q-W									
$\log Q = -0.98 + 1.62\log W$	0.79	0.49	Intercept	-0.97	0.07	-0.84	-1.11	-13.74	<0.0001
$(Q = 0.11W^{1.62})$			W	1.62	0.04	1.69	1.55	43.85	<0.0001
Q-Y									
$\log Q = 1.49 + 2.46\log Y$	0.84	0.43	Intercept	1.49	0.02	1.54	1.45	70.33	<0.0001
$(Q = 30.90Y^{2.46})$			Y	2.46	0.05	2.55	2.37	51.64	<0.0001
Q-V									
$\log Q = 2.07 + 1.96\log V$	0.33	0.87	Intercept	2.07	0.04	2.15	2.00	52.92	<0.0001
$(Q = 117.49V^{1.96})$			V	1.95	0.12	2.20	1.72	15.90	<0.0001

Model 5. The standard error is the standard deviation of the log residual, and its antilog is representative of the standard deviation of the fractional errors between the predicted and observed values on a log scale, and can be used as an approximation of the percent expected error provided there are not too many extreme values in the residual distribution. Using this approach (for comparative purposes), the depth by itself would be expected to predict discharge to within a factor of 2.7 67% of the time, width by itself would be expected to predict discharge within a factor of 3 67 % of the time, and velocity by itself would predict discharge within a factor of 7.4 67% of the time. Relative to depth and width, velocity by itself is a poor indicator of discharge.

The validation statistics for Models 1, 2, 3 and 4 and the Dingman and Sharma Model (Equation 2-9) are compared in Table 2.6. Comparative statistics include the mean and standard deviation of the following quantities:

$$\text{Relative Residual} = (Q' - Q)/Q \qquad (2\text{-}16)$$

$$\text{Log Residual} = \log(Q') - \log(Q) \qquad (2\text{-}17)$$

$$\text{Actual Residual} = Q' - Q \qquad (2\text{-}18)$$

In addition, the number of predictions within a specified percent-error interval (percent different than the observed) are also tabulated for 20%, 50% and 100% error. Figure 2.2 shows the predicted discharge (Q') plotted against the observed discharge (Q) for each model, along with an upper- and lower-envelope curve defined by the +/- 50% error in the observed value.

The log and actual residuals indicate that Model 1 and the Dingman and Sharma model tend to over-predict discharge and Models 2, 3 and 4 tend to under-predict discharge (Table 2.6 and Figure 2.2). Model 1 shows the least overall prediction bias, and the Dingman and Sharma model has the highest. The mean relative error indicates the average percent error of the predictions. Model 2 performs the best in this regard, with an average relative error of 10%. Average relative error for Model 1, 3 and 4 are less than 20%. The antilog of the mean of the log

TABLE 2.6 REGRESSION MODEL VALIDATION STATISTICS

Model	Validation Statistics	Relative Residual $(Q^* - Q)/Q$	Log Residual $(\log Q^* - \log Q)$	Actual Residual $(Q^* - Q)$ (m^3/s)	Percent of predictions within 20, 50 and 100% of the observed: 20%	50%	100%
Model 1 $Q = 7.22W^{1.02} * Y^{1.74} * S^{0.35}$	Mean	0.16	0.004	243	39%	82%	90%
	Stdev	0.81	0.207	5059			
Model 2 $Q = 0.09W^{1.21}V^{1.53}S^{-0.3}$	Mean	0.07	-0.017	-615	37%	79%	94%
	Stdev	0.58	0.195	7129			
Model 3 $Q = 0.23W^{1.46}V^{1.39}$	Mean	0.10	-0.024	-790	32%	71%	93%
	Stdev	0.71	0.231	9946			
Model 4 $Q = 3.55W_m^{1.19}Y_m^{-0.84}S^{0.30}Y^{2.17}$	Mean	0.17	-0.016	-119	28%	73%	89%
	Stdev	0.99	0.243	5333			
Dingman and Sharma Model $Q = 4.62W^{1.17}Y^{1.57}S^{0.34}$	Mean	0.43	0.092	763	41%	74%	86%
	Stdev	1.01	0.215	7644			

residuals indicates the fractional error between the predicted and observed discharge (the log residual can also be expressed as log(Q'/Q) such that the antilog is the ratio Q'/Q), which can be regarded as a correction factor. This measure of error shows that Model 1 has the highest mean accuracy (with a ratio of less than 1%), and that Models 2, 3 and 4 all show mean accuracy within 5%. Model 2 shows the least overall prediction error variability, as indicated by the standard deviation of the relative error and the log residual. The error percentiles indicate that Models 1, 2 and the Dingman and Sharma model are comparable.

Inspection of Figure 2.2 indicates that the predictive characteristics of the models vary for different ranges of discharge. These differences are evaluated by comparing the distribution of the relative residual with observed discharge. To facilitate comparison, the mean and standard deviation of the relative residuals have been averaged within four categories of discharge range (0-10, 10-100, 100-1,000 and >1,000 m^3/s). Models 1, 4 and the Dingman Sharma model tend to over-predict primarily in the low discharge range (0-10 m^3/s). This suggests that these models will have the best results in medium to large rivers where discharge typically ranges above 10 m^3/s.

The reason for this may be that the relationship between resistance and the channel geometry cannot be fully represented by a single regression intercept (model coefficient). Models 2 and 3 also tends to over-predict discharge in the low range (0-10 and 10-100 m^3/s) but also under-predicts in the high discharge range (>1,000 m^3/s). This result indicates that Models 2 and 3 would do better if the coefficients varied with discharge, i.e. different model coefficients were calculated for different flow ranges. The Dingman and Sharma Model shows a consistent over-prediction for all flow ranges, which may result because it was developed from a data set with fewer large rivers (also suggesting that statistical models such as these would be improved if they were developed for specific flow ranges).

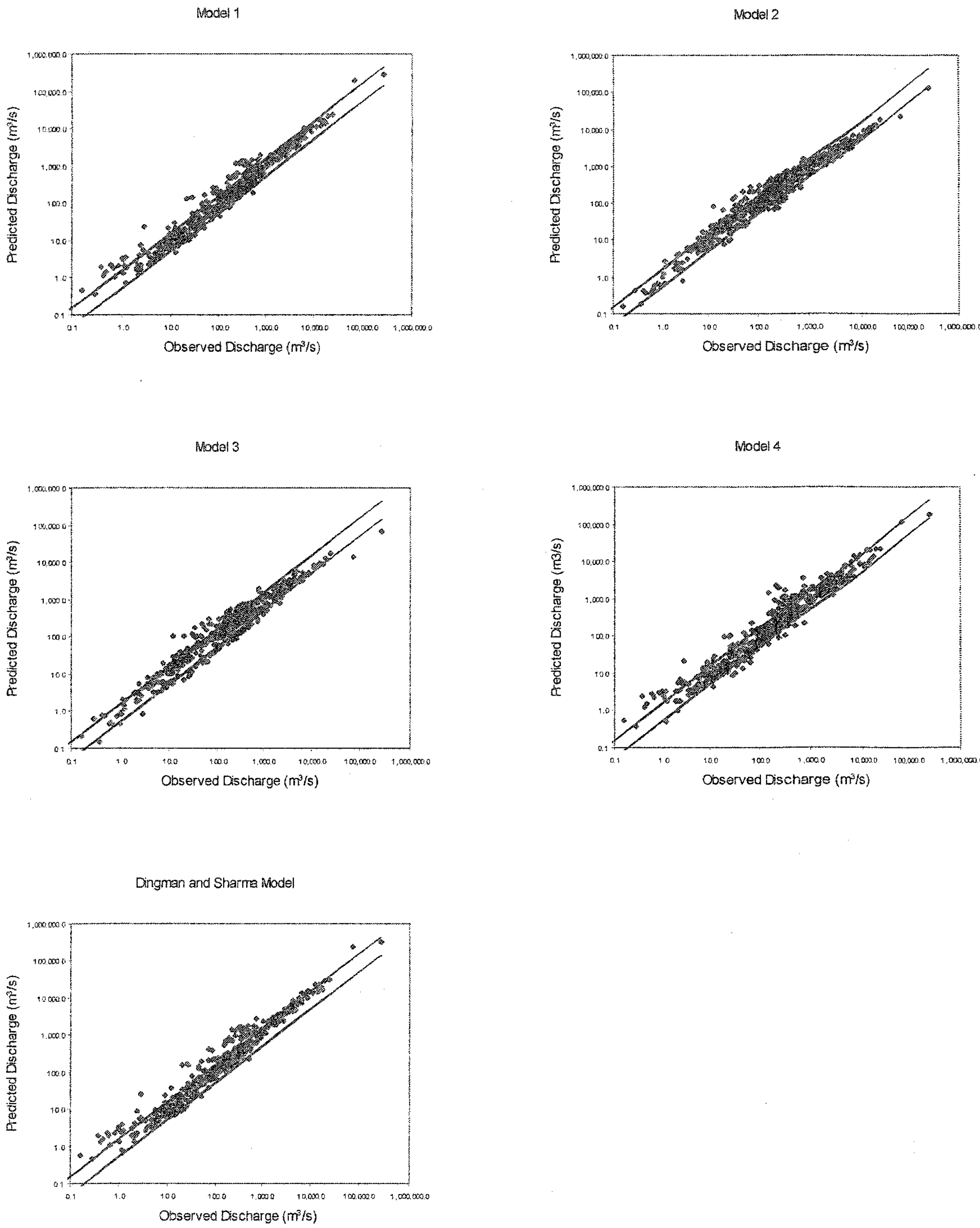

Figure 2.2 – Predicted Discharge plotted against observed discharge for the validation data set using Models 1, 2, 3, 4, and the Dingman and Sharma Model. The envelope curves represent +/- 50% of the observed discharge.

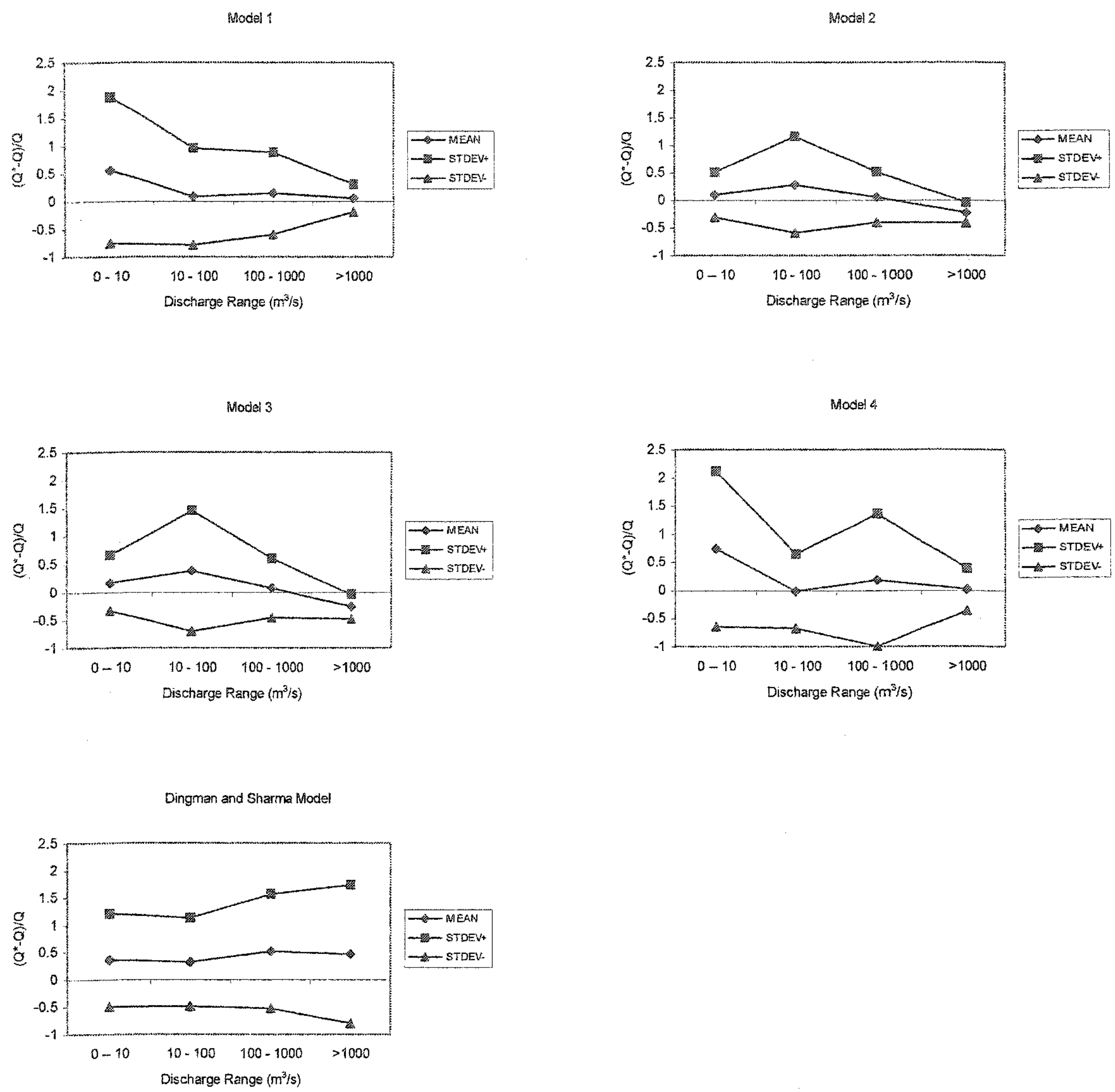

Figure 2.3 – Variation of the mean and standard deviation of the relative residuals averaged within ranges of observed discharge. The upper and lower lines are +/- one standard deviation from the mean. Multiplying the relative residual by 100 gives the percent error. The number of observastions in each range are 71, 132, 209, and 94 from lowest to highest.

Prediction variability, as indicated by the upper and lower standard deviation of the relative residuals, is reduced in the highest discharge range for Models 1, 2, 3 and 4 (Figure 2.3). This indicates that model precision is improved for the larger rivers. The Dingman and Sharma model does not follow this trend, which again may be due to the presence of fewer large rivers in the data base used to develop it. The validation statistics indicate that prediction models based on Models 1, 2, 3 and 4 could all be used as general discharge estimating models, with mean accuracy of less than 20% in all cases. The variability of the estimates would be expected to be within +/- 50% of the acutal value on the order of 2/3 of the time. The prediction accuracy would be improved for medium and large rivers.

As a comparison, under good measurement conditions, the accuracy of a discharge measurement made on the ground with standard techniques is assumed to be in the range of 2 to 4% of the actual value at least 2/3 of the time (Rantz et al., 1982, Herschy, 1998). The accuracy of measurements made using the slope-area method (usually for large discharges that could not be meausred using standard techniques), which is based on after-the-fact measurements of the flow width, depth, energy slope and flow resistance using the Manning or comparable uniform flow equation, are not explicitly known because it depends on field judgement and the quality of the measured data (Kirby, 1987). However it is often reported that good measurements have an accuracy between 10 and 20% (Herschy, 1998).

The development of the rating curve averages out some of the error associated with the discharge measurements, however interpolation from the rating curve may also introduce error, especially if the rating curve is subject to change over time. The accuracy of estimates made from the rating curve diminishes with extrapolation beyond the highest and lowest measured discharges because the nature of the "true" rating beyond the measured values is not known. Additionally, hysteresis effects may not be adequately reflected in the rating. Dickerson (1967) suggests that accuracy in estimating future (uncalibrated) discharge values from a rating curve may range from +13% and -11% at the 80% confidence level, and from + 21% to -17% at the 95% confidence level.

Measurement Uncertainty Analysis

Models 1, 2, 3 and 4, and equation (2-1) enable exploration of the impact that potential uncertainty (error) in measurement of the dynamic variables W, Y and V would have on the accuracy of discharge predictions. To do this, (the measured variables were assumed to be error free which is not really the case), typical measurement accuracies were assigned to each variable, and then varied randomly assuming a normal distribution such that the mean measurement uncertainty for the entire data base is zero and 95% of the uncertainties are within the assigned accuracy. The modified data were then used to re-estimate the discharge in the validation data base and then these values were compared via the relative residual to the estimates that assumed no uncertainity. A maximum and minimum measurement accuracy is assumed for each dynamic variable.

For W, the minimum assumed measurement uncertainty is 1 m and the maximum is 10 m, which would be consistent with the resolution of many of the current SAR and visible spectrum sensors (Table 2.2). Although, accuracy in width (surface area) measurement greater than 10 m may be routinely possible over longer reach lengths and by using complimentary observation bands, the range selected for the error analysis is not considered to be unreasonable for the purpose of this analysis. The minimum assumed measurement uncertainity in water-surface elevation (as a proxy for Y) is 0.1 m and the maximum is 0.5 m, consistent with the range associated with current satellite altimeters (Birkett, 1998, Birkett et al., 2002). The minimum measurement uncertainty in V is assumed to be 0.1 m/s, which is the low end of the anticipated accuracy of a surface velocity measurement (Emmitt, personal communication, 2001), and the maximum was arbitrarily chosen to be 0.5 m/s (since the measurement of surface velocity from satellites has not been tested).

This analysis does not consider the potential uncertainity in estimating channel slope or the other characteristic channel values W_m and Y_m. These variables could be determined by a number of methods, including: 1) estimation from topographic mapping and geomorphologic considerations; 2) measurement from repeated satellite observations; and 3) measurement via field surveys. The magnitude of uncertainty associated with determining the channel characteristics will depend in large part on the accuracy of available topographic information and availability of channel survey data. The analysis also does not consider the uncertainity associated with estimating the average velocity from the surface velocity measurements or the uncertainty associated with converting stage to average depth. However, Costa et al. (2000) has shown that the surface velocity can be used to estimate the mean velocity in a single cross-section with good overall results by using a simple correction factor of 0.85 (Rantz et al., 1982).

The assumed measurement uncertainties are distributed with a mean of zero such that the mean value of the prediction residuals would not change. Because of this, the measure used to evaluate the effect of the measurement uncertainty on the predictions is the standard deviation of the relative residuals. The standard deviation of the relative residuals as a function of discharge category for the maximum assumed uncertainty (error), the minimum assumed uncertainty, and the case with no uncertainity are shown on Figure 2.4. The least variability is associated with using equation (2-1) because there is no associated statistical error. All of the plots in Figure 2.4 show that the impact of maximum measurement uncertainty on prediction variability, relative to the no uncertainity case, becomes pronounced below a discharge of 10 m^3/s. The impact of maximum uncertainty for discharge above 10 m^3/s is greatest for equation (2-1) and Models 2 and 3. This result shows the effect of compounding errors in the case of equation (2-1), which includes uncertainty in all three dynamic variables, and indicates that uncertainty in V has a larger impact on prediction variability than does uncertainty in Y (comparing Model 1 and 2).

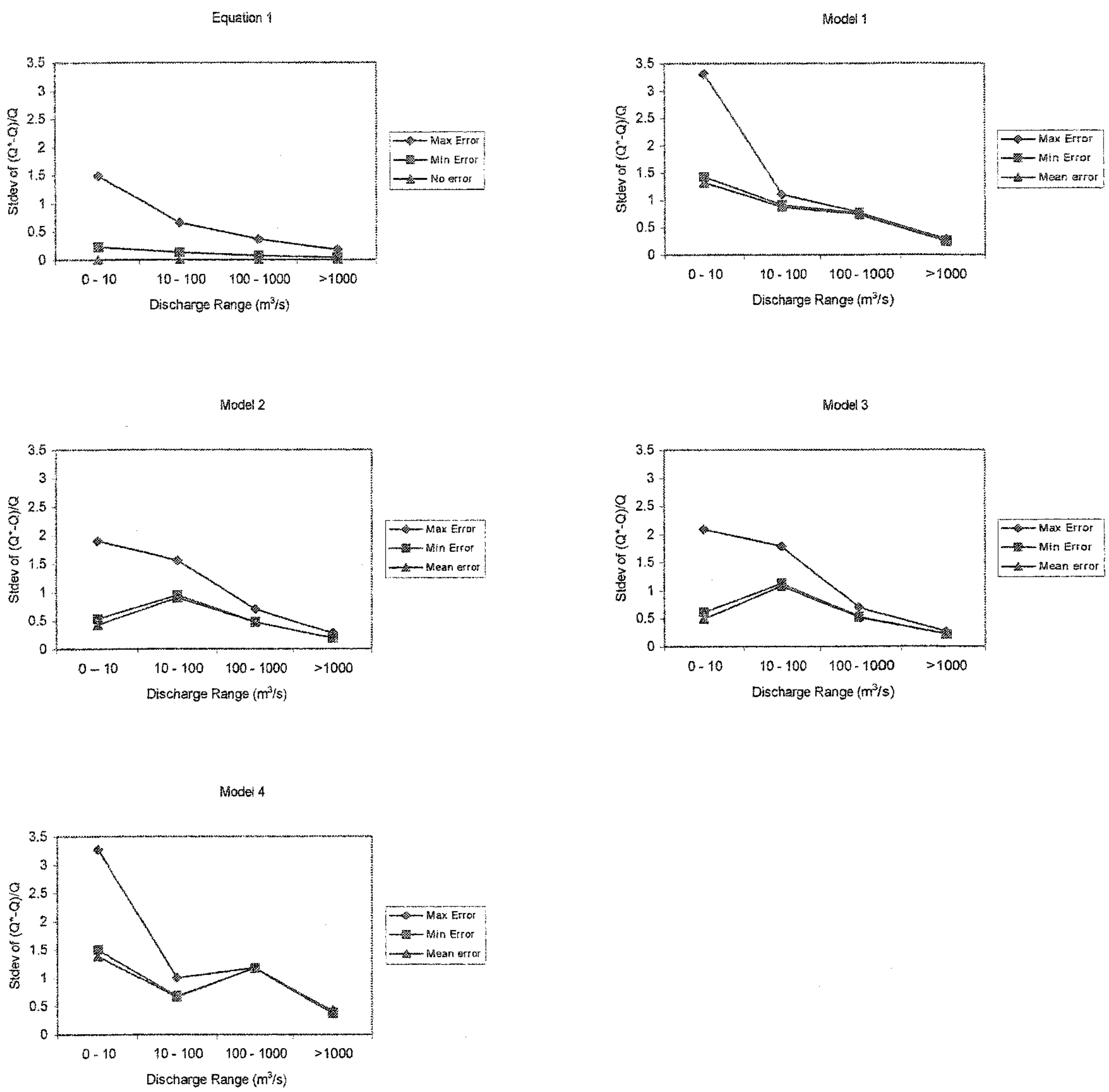

Figure 2.4 – Variation of the standard deviation of the relative residuals assuming a high (maximum) and low (minimum) measurement error in the dynamic variables as compared to no (mean) assumed measurement error. The dynamic variables are W, Y, and V. Ninety five percent of the assumed maximum errors are within +/- 10 m for W, +/- 0.5 m for Y, and +/- 0.5 m/s for V. Ninety five percent of the minimum errors are within +/- 1 m for W, +/- 0.1 m for Y, and +/- 0.1 m/s for V.

The impact of minimum uncertainty is not large within any discharge category, although as in the maximum uncertainty case it is most pronounced for discharge below 10 m^3/s. However, if the minimum measurement uncertainty is achieved for all dynamic variables, predicting discharge with equation (2-1) would result in a standard deviation in the relative residual (percent error) of less than 25% for discharges less than 10 m^3/s, less than 15% for discharge in the range 10 - 100 m^3/s and less than 10% for discharge greater than 100 m^3/s. The impact of minimum measurement uncertainty using Models 1, 2, 3 or 4 is less than 15% for discharge less than 10 m^3/s, and less than 10% for all other discharge categories. The plots in Figure 2.4 show that if the minimum measurement uncertainty can be achieved, uncertainty in the estimated discharge using the statistically based models is well below the uncertainty associated with the model itself (no error case).

As suggested by comparing the plots for Model 1 and Models 2 and 3 in Figure 2.4, there appears to be a different error response between Y and V. The differences in measurement uncertainty impact associated with the three dynamic variables were evaluated by introducing error into one variable at a time, and then comparing the standard devaition of the relative residuals. The results of this analysis are shown in Figure 2.5 for equation (2-1), and Models 1 and 3. The plot for equation (2-1) shows that error in V has greater impact on the discharge estimate than does error in Y, and that error in W has the least impact. Comparing Models 1and 3 shows that error in Y has the largest impact relative to W and V at low discharge (less than 10 m^3/s), and that error in V has a greater impact than error in Y for discharge greater than 10 m^3/s.

Discussion

The advantage of a satellite-based river-discharge-monitoring system is that it has the potential to fill in gaps where there is little or no information and obtain data over large areas simultaneously. Another advantage that satellite (or aerial) based measurement of hydraulic variables (particularly width) could provide is the ability to observe variation over a reach, thus enabling a reach-averaged value to be derived and minimizing the local variability that is specific to single cross sections. Development of a general method to estimate river discharge using river-channel hydraulic information observed from existing space or aerial platforms can be accomplished with statistical relationships developed from river data bases. If the water surface velocity of a river can be observed with Doppler lidar and used to estimate the average cross-sectional velocity and if the water-surface elevation can be used to estimate the average depth, all elements of equation (2-1) can be obtained remotely and the discharge in the river can be directly calculated.

The use of equation (2-1) is the preferred method to estimate discharge because it does not rely on a statistical derivation, shows the least overall prediction variance, and is applicable to any river under any flow conditions. However, it is likely that not all elements of equation (2-1) can be observed at the same time with confidence, thus in these situation statistically based models such as described by Models 1, 2, 3 and 4 can be used with reasonable accuracy, averaging +/- 20% or less, with accuracy within approximately +/- 50% 2/3 of the time. This level of accuracy compares favorably with estimates derived from extrapolation of ground-based ratings and slope-area measurements of discharge. Measurement error analysis indicates that with anticipated maximum uncertainty in the values of the observed variables, the variability of discharge estimates is increased substantially for discharges less than 100 m^3/s, however assuming, a reasonable minimum measurement uncertainty (0.1 m accuracy in depth, 1 m accuracy in width and 0.1 m/s) prediction error variability is only slightly increased over the no-error case.

Models that use width and surface-velocity only to estimate discharge (Model 3) can be used in situations where slope cannot be measured, or where anthropogenic control of slope

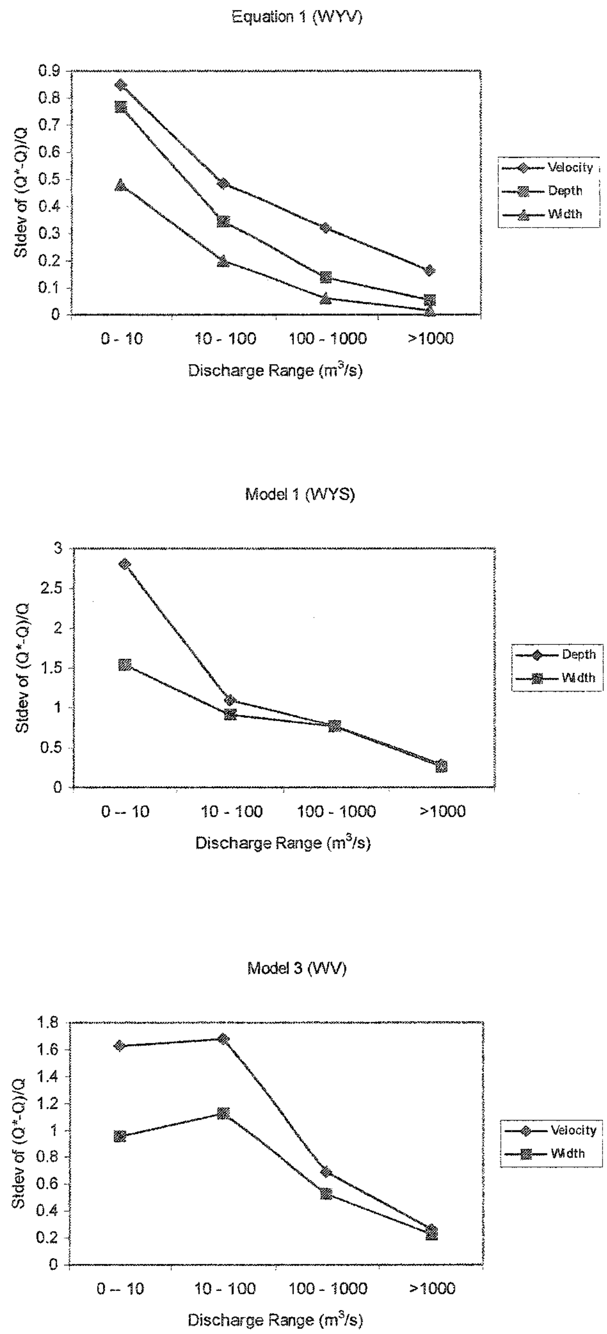

Figure 2.5 – Variation in the standard deviation of the realtive residuals for prediction methods with more than one dynamic variable assuming error in only one variable at a time, showing the relative impact that error in the different dynamic variables has on prediction variability.

violates the hydraulic assumptions inherent in Models 1 and 2, assuming surface velocity can be effectively measured. However, width-velocity models appear to have a bias trend across a wide range of discharge.

The predictive models described above are applicable to within-bank discharge only, because these models did not include over-bank flow in the data base used to develop and evaluate them. However, estimating over-bank discharge would require the same information, i.e. the width of flow, the average depth of flow and the average velocity of flow. Alsdorf et.al. (2000) has shown the feasibility of using interferometric SAR to map the surface relief of an inundated region of the Amazon, thus demonstrating that mapping flow paths within a flooded area is possible. With this information, the discharge within the flooded area could be estimated and resolved in the downstream direction using floodplain topography and water-surface elevation to estimate the flow depths across the inundated area. As shown by Brakenridge et al. (1998), Bates and DeRoo (2000), and Horritt (2000), this information could also be used in conjunction with a hydraulic model to estimate the discharge within a flooded region. Brakenridge and Knox (1998) used satellite images obtained from ERS-1 coupled with topographic information to develop a three dimensional picture of the flooded area (inlcuding depth and areal extent) which were then used to track the flood wave and estimate flood discharge using the HEC-2 river hydraulic model.

The successful use of equation (2-1) and Models 2 and 3 will depend on the ability to measure surface velocity from space. To this end, development and verification of this technology will greatly enhance the potential ability to measure river discharge from space. Additionally, use of equation (2-1) and Models 1, 2, 3 and 4 all depend on the ability to translate surface measurements of stage and/or velocity into average values for the channel section under observation. Thus, techniques to estimate the average water depth in a channel section based on observation of water-surface elevation and techniques to estimate the average velocity in channel section based on measurements of surface velocity need to be developed and verified. Another issue of concern is that currently deployed altimeters cannot accurrately obtain water-surface elevations on rivers less than several hundred meters wide. However, there is an indication that these same altimeters can observe much smaller rivers with similar accuracy by effecting a change in the on-board signal processing (personal communication, Ernesto Rodriguez). Also, laser altimeters may provide much greater accuracy with reduced observation size limitations relative to radar altimeters. The potential improvements in river-stage measurement indicated by these developments need to be evaluated.

CHAPTER III

DEVELOPMENT OF GENERALLY APPLICABLE EQUATIONS FOR ESTIMATING RIVER DISCHARGE

Because width is the most readily and reliably measured hydraulic element of the channel from remote sources, relationships that use width with either of the other two elements of the continuity equation (depth and velocity) along with characteristic channel variables such as maximum width and channel slope, would provide the most flexibility in measuring discharge from remote platforms or sources. Estimating discharge from relationships that use width as the only variable do not provide sufficient information to characterize the range of river discharge variability with reasonable accuracy (e.g. a mean prediction accuracy within 20% or less of the expected value with, 67% of the predictions within 50% of the expected value), and consequently do not yield generally applicable models.

Additionally, models based on width only cannot be derived from hydraulic principles without over-simplification of in-channel hydraulic relationships, and are therefore limited to uniquely derived statistical relationships for a given reach. Thus, there is advantage to developing discharge-estimating equations that rely on measured width and geomorphic characteristics that can be readily observed and one of the other two dynamic variables of continuity, depth or velocity. Developing generally applicable models with the fewest possible independently measured variables that can provide reasonable estimation accuracy will minimize compounding error; and provide a way of estimating discharge when all of the elements of flow continuity cannot be observed or accurately estimated.

Generally applicable statistical relationships developed from multiple-regression analysis, that use width, channel slope, and either mean depth or mean velocity to estimate river discharge, as described in Chapter 2, have shown that discharge can be estimated with reasonable accuracy. However, regression models do not allow for improvements in the estimates if there is better knowledge of the behavior of one river as opposed to another. The coefficients and exponents of the models are fixed by the errors and variability within the data set used to develop them, and even if the data set represented the entire population of flows, variability that is not explained by the regression cannot be reduced by inclusion of more specific knowledge that may be available for a specific river. For this reason, rationally based equations that are developed from physical principles would provide more general and adaptable models for estimating discharge in rivers. In addition, rationally based models can be calibrated to specific rivers where additional or better knowledge is available.

This chapter develops and evaluates the use of generally applicable river-discharge estimating equations that are based on width, channel slope and either mean depth or mean velocity. Both statistically and rationally derived equations are developed from a flow-measurement data base similar to that used in Chapter 2 and a synthetic discharge data base that is based on principles of river hydraulics. Comparison and applications of these relationships are discussed including their use with other types of hydrologic information.

Hydraulic Data

A large discharge-measurement data base was developed in order to derive, calibrate and compare statistically based discharge-prediction models with similar models developed from physical principles. The data base includes 1,037 flow measurements from 103 rivers in the United States and New Zealand. At each river station, from five to twenty in-bank discharge measurements obtained for as wide a range of flow as possible, were incorporated into the data base. The data base includes a measured width and/or cross-sectional area, mean depth and/or hydraulic radius, a mean velocity for the measurement section or reach, and an average or topographic channel slope for the reach (see Chapter 2). In addition, the maximum depth and width for the set of measurements at each station were included as a separate channel-shape variable. Approximately half of the measurements consisted of values averaged for a given reach, and the remainder of the data were obtained from single measurement cross-sections.

The data were obtained from Barnes (1967), Hicks and Mason (1991), Coon (1998) and from the U.S. Geological Survey's on-line NWIS data base (USGS, 2001), and all represent single-thread channels. The data include rivers that do not exhibit any control on the slope (no back-water effects), and no large expansion or contraction of the flow within the reach where the data were collected (thus, rivers that were contracted by a bridge or natural feature such as a canyon or narrows were not included in this data). These data are referred to as the channel-control data base (Appendix 1). The channel-selection criteria were implemented so that the hydraulic variables could all be considered adjusted to the channel slope. The channel characteristics of each river in the data base were evaluated based on information available from the data sources, or from inspection of topographic maps of the channel at each station. For comparative purposes, the channel-control data base was randomly divided into a calibration data set ($N = 680$) and a validation data set ($N = 357$). The range of data in each sub-set is shown on Table 3.1.

Approximately 90% of the data in the channel control data base is the same as that used for the multiple regression analysis presented in Chapter 2. Eight large rivers, including the

Amazon, were excluded from this data base because the data were judged to be affected by channel constrictions (both natural and anthropogenic) or other controls on the water-surface slope. Nine additional rivers with no slope control were substituted for those that were excluded in order to maintain a similar size data set.

As discussed above, there are advantages to developing hydraulic models from physical principles rather than basing the relationships solely on the statistics of particular data sets. For this reason, a theoretically derived river-channel and discharge data set was generated from which various hydraulic relationships were statistically extracted and analyzed. The synthesized data set was developed from the Prandtl-von Karman universal velocity distribution law assuming a uniform channel with a parabolic channel cross-section shape. The following describes the steps taken in developing the data base.

The Prandtl von-Karman universal velocity distribution law states that the velocity (v) in a vertical profile varies with distance from the bottom (y) as a log-function of the vertical distance above an assumed roughness height. This relationship is given by:

$$v = 2.5V^* \ln(y/k) \qquad (3\text{-}1)$$

where V^* is the shear velocity ($V^*=(gYS)^{1/2}$, g is the acceleration due to gravity, Y and S are mean depth and bed slope respectively) and k is a constant that is proportional to the surface roughness of the streambed, and is equal to 0.033 times the roughness height (k_s) (Chow, 1959). The roughness height is considered to be the effective height of surface irregularities that intrude

Table 3.1 **Range of Hydraulic Parameters in Data Sets**

Parameter	Symbol	Units	Mean	Stdev	Coeff. Var.	Maximum	Minimum
Calibration Data N = 680							
Discharge	Q	m^3/s	860	2434	2.83	27576	0.01
Top Width	W	m	128	159	1.24	1009	2.9
Average Depth (Hyd. Radius)	Y	m	2.38	2.24	0.94	12.39	0.1
Average Velocity	V	m/s	1.15	0.62	0.54	5.1	0.02
Water Surface Slope (average)	S	1	0.0029	0.0056	1.93	0.04	0.000043
Validation Data N = 357							
Discharge	Q	m^3/s	717	1960	2.73	17837	0.02
Top Width	W	m	126	146	1.16	765	3.1
Average Depth (Hyd. Radius)	Y	m	2.33	2	0.86	12.7	0.18
Average Velocity	V	m/s	1.11	0.59	0.53	3.53	0.02
Water Surface Slope (average)	S	1	0.0021	0.0042	2.00	0.04	0.000043
Synthetic Data Set N = 380							
Discharge	Q	m^3/s	4985	12559	2.52	98233	0.14
Top Width	W	m	337	405	1.20	2000	30
Average Depth (Hyd. Radius)	Y	m	3.43	3.59	1.05	21.78	0.1
Average Velocity	V	m/s	1.4	0.63	0.45	3	0.15
Water Surface Slope (average)	S	1	0.0012	0.0021	1.75	0.01	0.00002

beyond the laminar sub-layer for hydraulically rough flow conditions (which is the case in most natural rivers)(Chow, 1959). The relation between k (used in the following theoretical development) and the roughness height (k_s) was developed from hydraulic experiments performed by J. Nikuradse in 1933 (Chow, 1959).

A general discharge equation can be derived in terms of velocity as:

$$Q = \iint v \, dy \, dx \tag{3-2}$$

where y is the mean distance above the bottom (depth) and x is the top width at y. Integrating v in equation (3-1) with respect to y

$$q = 2.5V^* \int \ln(y/k) \, dy \tag{3-3}$$

gives the unit discharge in the vertical (the flow per unit distance along the cross section):

$$q = 2.5V^* \, y(\ln(y/k) - 1) \tag{3-4}$$

The unit discharge can now be integrated with respect to dx to obtain the total discharge in the cross-section assuming a regular geometric cross-sectional shape. To conduct the integration, a parabolic cross-section shape is assumed (Fekete, 2002; Chow, 1959). A parabolic shape is often used to represent self-formed river channel cross-sections (Chow, 1959), and in many cases are comparable to those obtained from assuming other regular geometric shapes commonly used such as a semi-ellipse, trapezoid, or higher order paraboloid. Additionally, hydraulically efficient stable channel cross-sections developed from theoretical considerations can be represented by cosine functions that are nearly equivalent to parabolic sections (Henderson, 1966; Ferguson, 1986). This indicates that the assumption of a parabolic shape as representing the "typical" self-formed channel is reasonable.

The integration of Equation (3-4) involves inverting the parabola to obtain the proper integration under the curve such that $y = y_m - c\,x^2$ where y_m is the maximum depth within the section bounded by x. The inversion is illustrated on Figure 3.1. The coefficient c is a geometric constant for the parabola defined at maximum width and depth, equal to $1/(W_m^2/Y_m)$. Substituting this into Equation (3-4) and setting $w_m/2 - \varepsilon = X$, where ε is an arbitrarily small number gives:

$$Q = 2.5V^* \int_0^X (y_m - c\,x^2)[\ln((y_m - c\,x^2)/k) - 1]\,dx \qquad (3\text{-}5)$$

Integrating equation 3-5 gives (webMathematica, 2002):

$$Q/2 = 2.5V^*[-7y_m x/3 + 5cx^3/9 + (4y_m^{1.5}/3c^{0.5})(\mathrm{ArcTanh}[c^{0.5}x/y_m^{0.5}]) + (y_m x - cx^3)\ln[(y_m - cx^2)/k] \qquad (3\text{-}6)$$

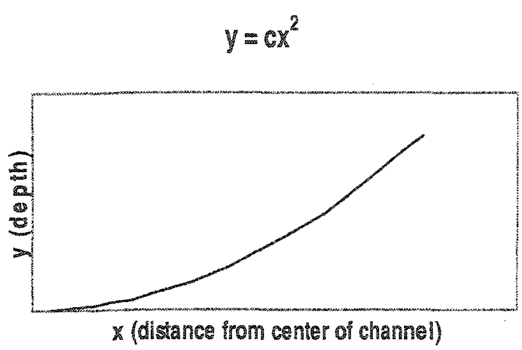

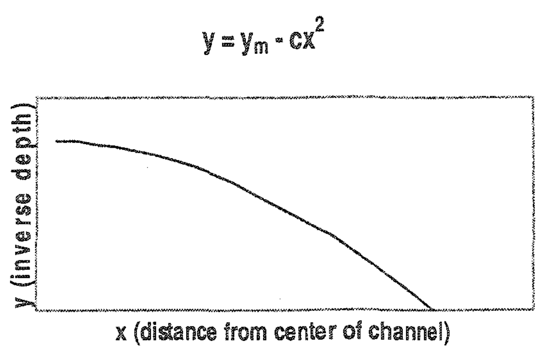

Figure 3.1 - Definition sketch: integration of the parabolic section

Numerous studies have shown that rivers exhibit general hydraulic relationships between depth, slope, width, velocity and resistance (Leopold et al, 1964; Henderson, 1966; Rosgen, 1996). In order to avoid inclusion of unrealistic channels in the synthesized data base, general rules for estimating the maximum depths and roughness heights were used. The rule for estimating the maximum depth was developed based on multiple-regression analysis of a bank-full hydraulic geometry data set compiled from various sources for 521 river reaches (Schumm, 1960; Barnes, 1967; Osterkamp et al., 1982; Church and Rood, 1983; and Dingman and Palaia, 1999) (Appendix 3). Based on the analysis of this data, it was found that maximum depth (Y_m) could be predicted from the maximum width (W_m) and the slope (S) according to the following relation:

$$Y_m = 0.08W_m^{0.39}/S^{0.24} \tag{3-7}$$

In equation (3-7) all units are in meters. The width and slope in equation (3-7) explains approximately 73 % of the variation in maximum depth ($r^2 = 0.73$).

The roughness height was estimated directly from theoretical considerations based on an initial assumption that the Manning resistance coefficient (n) is a function of the slope (Bray, 1979) as follows:

$$n = 0.1S^{0.18} \tag{3-8}$$

Chow (1959) presents a dimensional relationship between the Chezy C and Manning n based on the hydraulic radius (in feet), and a theoretical relationship between the Chezy C and roughness height (in feet) as follows

$$C = 1.49R^{0.17}/n \tag{3-9}$$

$$C = 32.6\log(12.2R/k_s) \tag{3-10}$$

Equations (3-8), (3-9) and (3-10) were used to compute the roughness height (k_s) for a given slope assuming that $R = Y_m$. The value of k in equation (3-6) is then computed as 0.033 times the roughness height. Thus, the channel dimensions and hydraulic characteristics of the synthesized data base are derived from maximum width and channel slope, and the assumption of a parabolic channel shape.

The range of slopes and widths used to develop the synthetic data base were within the same range of values included in the flow-measurement data base (Table 3.1). It is recognized that small streams may take on a large range of slopes, but typically larger rivers will only exhibit relatively flat slopes. However, no such behavioral rule between width and slope was invoked to generate the synthetic data. Instead, the slope and width were treated as independent variables, and the range of values were selected to be comparable to actual rivers.

The derived synthetic data base consists of 380 flows with associated values for width, mean depth, mean velocity and slope (a constant value for each synthetic river channel) in units of meters and seconds (Appendix 4). Comparison of the synthetic and measurement data bases was accomplished by analyzing the behavior of the dimensionless Froude number. In both the synthetic and flow measurement data bases, the Froude number was found to be predictable from a dimensionless velocity head index given by $V^2/(2gW)$. The velocity head index (VHI) is used here because it does not include a depth term, and therefore would be more useful in a predictive capacity (because depth is not readily available from remote data). The Froude-number-VHI relationship derived from the synthetic data is:

$$F = 2.20[V^2/(2gW)]^{0.27} \qquad (3\text{-}11)$$

The same relationship derived from the measurement data is:

$$F = 2.32[V^2/(2gW)]^{0.31} \qquad (3\text{-}12)$$

Although not equivalent at the 95% confidence level, the similarity of these equations indicates the general comparability of the two data sets.

The Froude relationship for both the measurement data and the synthetic data are shown on Figures 3.2a and 3.2b. Further analysis of the relationship between the Froude number and

VHI for the synthetic data revealed that the variability in the general relation given by equation (3-11) can be reduced by using the maximum width and the slope to predict the coefficient and exponent of the equation. Multiple regression analysis of (W_m) and (S) on the coefficient (c) and exponent (m) of equation (3-11) gives the following:

$$c = 23.7 W_m^{0.125} S^{0.449} \tag{3-13}$$

and

$$m = 0.881 W_m^{-0.046} S^{0.148} \tag{3-14}$$

Figures 3.2c and 3.2d shows the predictive characteristics of the general relation between Froude number and VHI derived from the synthetic data base applied to both the synthetic and measurement data. Figures 3.2e and 3.2f show the improvement in predictability by using the relationships given by equation (3-13) and (3-14). The improvement in prediction for the synthetic data can be readily observed. The improvement in prediction for the measurement data was measured by computing the mean and standard deviation of the relative residual (predicted minus observed divided by the observed) and the log-residual (log of the predicted minus log of the observed) of the estimate. The mean relative residual and log-residual associated with Figure 3.2d is 36% and 29% respectively, and the mean relative residual and log-residual associated with Figure 3.2f is 23% and 17% respectively, indicating that knowledge of W_m and S can substantially reduce Froude-number estimating errors. The standard deviation of the errors were also reduced. Thus, the hydraulic characteristics of the synthetic data can be used to derive relationships that help explain variability within the measurement data, indicating that the theoretically derived data is a useful representation of real-world rivers.

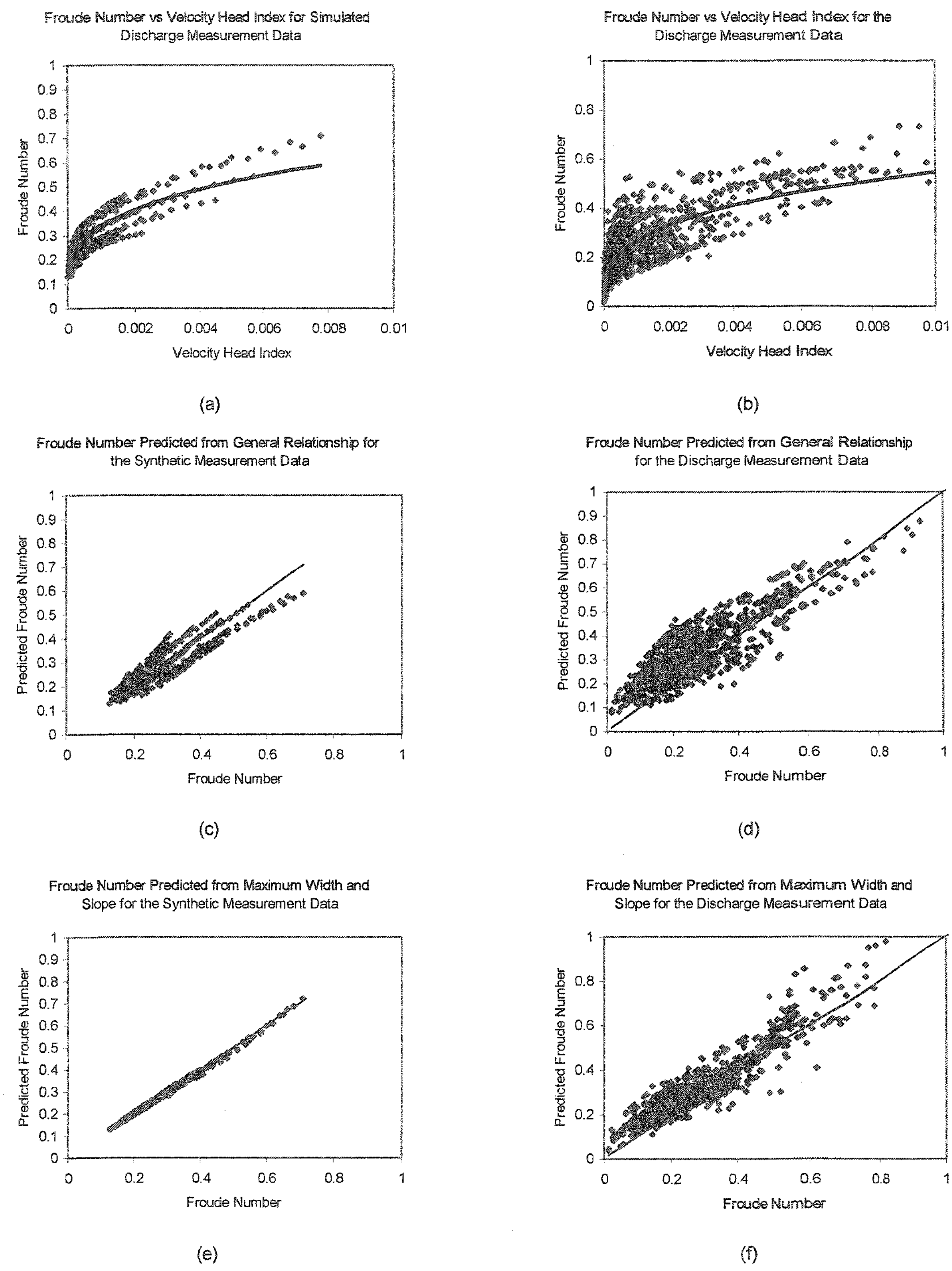

Figure 3.2 – Froude number plotted against the VHI for the synthetic (a) and measurement (b) data; actual Froude number plotted against the Froude number predicted from the general relation for the synthetic (c) and measurement (d) data; improvement in prediction using the width-slope correction for the synthetic (e) and measurement (f) data.

Statistically Based Discharge Estimating Models

For comparison, a set of regression models parallel to those proposed in Chapter 2 were developed from regression analysis of the channel-control calibration data. These models are:

		r^2	std. error	
Model 1:	$Q = 4.24W^{1.10}Y^{1.63}S^{0.33}$	0.97	0.19	(3-15)
Model 2:	$Q = 0.08W^{1.16}V^{1.65}S^{-0.33}$	0.97	0.19	(3-16)
Model 3:	$Q = 0.23W^{1.48}V^{1.45}$	0.95	0.24	(3-17)
Model 4:	$Q = 4.74W_m^{1.04}Y_m^{-0.58}S^{0.29}Y^{2.11}$	0.94	0.27	(3-18)

The regression results differ from those presented in Chapter 2 because a somewhat different data base was used to develop them, although approximately 90% of the data in the channel-control data set are the same. Thus, even with a large amount of data in common, the statistically based models would, in general, provide different predictive results, indicating one a key limitation of statistically derived models. Comparing these models with those derived in Chapter 2 (Table 2.6), it is found that the magnitude of the slope exponent for Models 1 and 2 were the same at the 95% confidence level, whereas the values for the width, depth and velocity exponents were not always the same between these models. This suggests that slope is an effective discriminating variable even where the interaction of width and velocity may vary. Model 3 is similar for both data bases at the 95% confidence level.

The exponents of Model 4, with the exception of slope and depth, are also different, however an interesting aspect of this model is that the exponents on the maximum width and maximum depth are near the expected values (1.0 for W_m and -0.5 for Y_m) if the "typical" channel shape were a parabola (2nd order paraboloid). This suggests that self-formed single thread channels tend towards parabolic shapes, further verifying the assumption underlying the development of the synthetic data base.

The exponents associated with Model 1 suggest a similarity to the Manning equation which is given as:

$$Q = (u/n)AR^{2/3}S^{1/2} \tag{3-19}$$

where u is a proportionality constant and n is a resistance coefficient. The exponent on the depth term is near the expected value of 1.67 and the exponent on the width is near the expected value of 1. However, the exponent on slope is closer to 0.33 rather than 0.5, as formulated by Manning (1895).

Comparable regression models were also developed for the Prandtl-von Karman synthetic data base. Model 4 was not developed from these data because the maximum depth was derived from the maximum width and the slope (and thus is perfectly correlated with maximum width and slope). The resultant regression models are:

		r^2	std. error	
Model 1:	$Q = 8.42W^{0.98}Y^{1.74}S^{0.31}$	1.00	0.04	(3-20)
Model 2:	$Q = 0.06W^{1.07}V^{2.25}S^{-0.38}$	1.00	0.06	(3-21)
Model 3:	$Q = 0.12W^{1.53}V^{1.85}$	0.99	0.13	(3-22)

Model 1 derived from the synthetic data shows nearly the same exponents as those derived from the measured data bases (although different at the 95% confidence level with the exception of the slope exponent), and are similar to the Manning equation except for the exponent on the slope, which is also nearer to the cubed root rather than the square root. The exponents on Model 2 and 3 are different than those for the regression models derived from the measurement data.

The regression models from each of the data bases suggests that a general form of Model 1 could be represented by the Manning equation with an exponent of 0.33 (cubed root) on slope rather than the square root. However, the regression models do not immediately suggest any general form for Model 2 or 3. The consistent behavior of the regression statistics with regard to Model 1 suggests a robustness with regard to a general form, and its similarity to the Manning equation is encouraging. Additionally, the result that the slope exponent is always nearer 0.33 as opposed to 0.5 suggests that there is an underlying principle of natural rivers that relates the resistance to $S^{0.17}$, thus resulting in a slope exponent of 0.33 (as indicated by equation 3-8).

General Discharge Estimating Equations

Open-channel flows are often modeled as one-dimensional gradually varied steady or unsteady flows. Such flows satisfy three fundamental relations including: 1) continuity, requiring the conservation of mass; 2) the energy equation, characterizing the apportionment of mechanical energy and its spatial and temporal rates of change; and 3) a constitutive relation, characterizing the relation between energy gradient and flow rate. The constitutive relation is generally described as,

$$V = Kg^{1/2}R^{p}S^{q} \tag{3-23}$$

where K is a channel conductance and S in the general sense can be taken as the friction slope (slope of the energy grade line). Specification of the constitutive relation is not straightforward because there is uncertainty about the values of p and q (Manning, 1889; Golubstov, 1969) and the way in which the velocity conductivity coefficient, K, varies with flow and boundary characteristics.

The most widely used constitutive relation is the Manning equation. However, studies that have established a sound theoretical basis for this relation or have unequivocally demonstrated that it governs all uniform flows are not evident in the literature. A number of studies before and after publication of the papers on which wide acceptance of the Manning equation are based (Manning 1889, 1895) have discussed the appropriate values of p and q and the question of whether and how the conductance coefficient varies with flow and channel characteristics. As is well known, Manning himself felt that the constitutive equation should be dimensionally correct and was uncomfortable with the form of the equation that came to bear his name (Manning, 1895).

One major problem with the Manning equation – and of many other proposed forms of the constitutive relation - is that there is no universally accepted way of determining the appropriate value of the conductance/resistance parameter from measurable channel characteristics for *a priori* or *a posteriori* applications. In addition, the Manning equation violates at least two of the principles that should be satisfied by a constitutive relation (Bear 1972): (1) consistency with principles of momentum balance and (2) dimensional homogeneity. The Manning equation is an empirical modification of the Chezy equation,

$$V = C \cdot g^{1/2} \cdot R^{1/2} \cdot S_e^{\ 1/2} \tag{3-24}$$

which can be derived from force-balance relations and is dimensionally homogeneous. However, the Chezy equation is based on the dimensionally-motivated assumption that resistance is proportional to V^2. As Leopold et al. (1960) pointed out, that assumption may only be true if resistance associated with the flow boundary does not change with V, in other words resistance is constant for all velocities. This condition is generally true for pipe flow but not for open channels where the boundary changes substantially with discharge.

Manning (1889) himself cited empirical studies that showed various values for p and q, and subsequent empirical and even theoretical (Leopold et al. 1960) and quasi-theoretical (Henderson 1966) studies have found wide variation in both p and q. Several studies, including Golubtsov (1969), Riggs (1976), Jarrett (1984), and Dingman and Sharma (1997), have not only used statistical analysis to reveal different apparent values of p and q, but also to suggest that a very wide range of flows can be successfully modeled using a universal value for the velocity (conductance) coefficient (K). This latter point is especially important, because confirmation of this finding would free the modeler from the inherently subjective and highly uncertain (HEC, 1986) process of estimating the resistance. Lane's stable-channel analysis (Henderson, 1966) also suggests that it may be possible to model open-channel flows using a constant conductance coefficient for all channels, at least to the accuracy obtainable by the usual subjective methods for estimating reach-specific resistance/conductance. Thus, it is of interest to compare the variability of K over all flows in the data bases using different assumptions for the values of p and q.

Four discharge-estimating models with exponents selected *a priori* based on the Chezy, Manning and regression equations were used to evaluate the variability of K as a function of p and q. These are:

$$Q = k_1 W Y^{1.67} S^{0.5} \tag{3-25}$$

$$Q = k_2 W Y^{1.67} S^{0.33} \tag{3-26}$$

$$Q = k_3 W Y^{1.5} S^{0.5} \tag{3-27}$$

$$Q = k_4 W Y^{1.5} S^{0.33} \tag{3-28}$$

The discharge coefficients (k_1 through k_4) were determined for each flow measurement in the channel-control data base and their distributions plotted as histograms in Figure 3.3. The coefficient of variation for the distributions is also indicated on Figure 3.3. Comparison of the historgrams indicates that the discharge coefficient is bi-modally distributed when a slope exponent of 0.5 is used (k_1 and k_3), and there is significantly less overall variability in the conductance coefficient when an exponent of 0.33 is used (k_2 and k_4). This indicates that there would be less estimation error and greater accuracy when using constituitve equations that assume a slope exponent of 0.33 for natural rivers.

The improved predictive qualities of the models when using a slope exponent of 0.33 can be explained, in part, by assuming that the principal source of resistance is the boundary roughness, and that the boundary roughness is directly related to a characteristic stable grain size. The stable grain diameter is proportional to the maximum channel hydraulic radius (or depth) times the slope (Henderson, 1966), such that $D = \phi Y_m S$ with D equal to the stable grain diameter and ϕ is a coefficient that accounts for the Shields entrainment function and the specific gravity of the sediment (solid:fluid density ratio). Given that bed shear stress is related to the size of the bed material, the stable-bed resistance coefficient would also be related to grain size (Chow, 1959; Henderson, 1966). Resistance is also known to be a function of the depth of flow (Chow, 1959), consistent with the concept of relative roughness (Engelund, 1966;Limerinos, 1970; Hey, 1979; Arcement et al., 1989). Thus, an expression for the stable-bed resistance should include the maximum depth and slope ($Y_m S$) to account for the resistance associated with the size of the stable-bed material, and the flow depth (Y) to account for the relative roughness. With these assumptions a dimensionally homogeneous constitutive equation based on the Chezy equation would take the form:

$$Q = C^* g^{0.5} W Y^{1.5} S^{0.5} / (Y_m S/Y)^f \qquad (3\text{-}29)$$

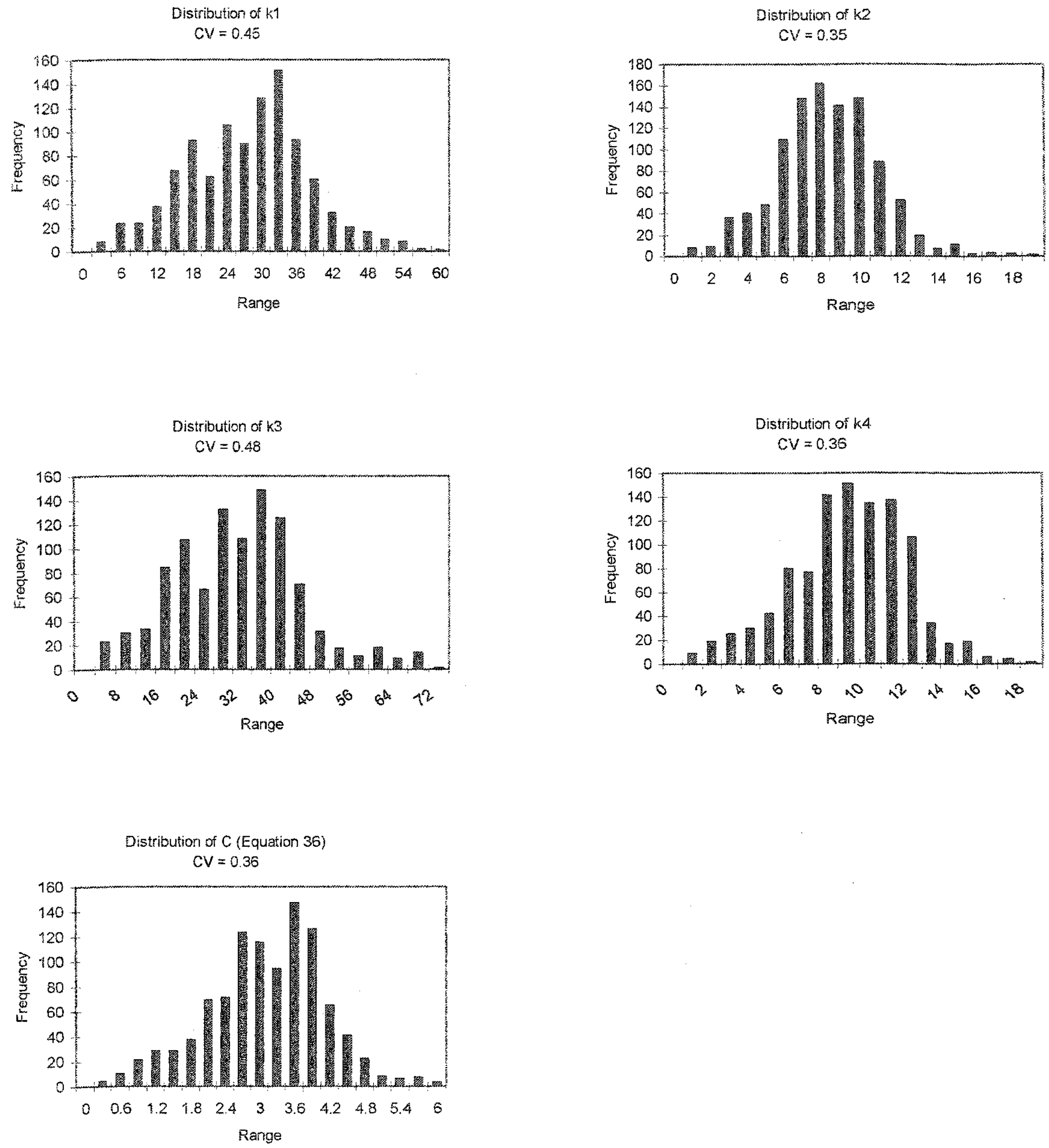

Figure 3.3 – Distribution of the discharge coefficient for the channel-control data for the various forms of Model 1 showing the coefficient of variation for each distribution.

where f is an exponent relating the stable grain size to resistance, and C^* is a constant of proportionality that may vary with flow conditions. The value of C^*, determined by minimizing the log-residual of error using the channel-control data, is estimated to be 2.74. This equation maintains dimensionality by including the ratio Y_m/Y, which also accounts for the effect of relative roughness. Studies by Lacey (Bray 1979) have indicated that bankfull (or regime) resistance, as expressed in the Manning equation, in natural gravel bed channels is a function of slope to the 1/6th power (i.e. resistance is proportional to $S^{0.17}$). This general relationship was further substantiated by Bray (1979). Accepting this relation (f = 0.17) would result in a slope exponent of 0.33 and a depth exponent of 1.67 for Model 1, which confirms the results from the regression analyses. The distribution of C^* for this model has a smaller range than the k values for the comparable models as shown on Figure 3.3.

Because the variables used in equation (3-29) are rationally developed and provide a more complete representation of the geometric contributions to resistance, this equation is considered to be a more physically complete formulation of Model 1 compared to equations (3-25) through (3-28). Deriving the form of equation (3-29) from regression analysis of the channel control data (N=1037) yields the following equation:

$$Q = 0.84g^{0.5}W^{1.25}Y^{1.70}S^{0.27}Y_m^{-0.43} \qquad r^2 = 0.97 \quad \text{std error} = 0.18 \qquad (3\text{-}30)$$

An interesting aspect of this equation is that it is very nearly dimensionally homogeneous. This suggests that the correct variables are included in the model, and thus also are included in equation (3-29). However, the magnitude of the exponents are significantly different than those proposed for equation (3-29), indicating that equation (3-29) is not a completely satisfactory physical representation of Model 1. Equation (3-30) suggests that width and other factors related to slope and maximum depth are important in defining the resistance.

Equation (3-29), if applied to the bankfull flow condition, would reduce to a form similar to the Chezy equation, except that the exponent on the slope is 0.33 rather than 0.5, because $Y = Y_m$. Leopold et al. (1960) suggested that rivers in regime tend towards a constant bankfull

Froude number. Figure 3.4 shows the Froude number plotted against discharge for 22 rivers in the United States over a wide range of flows (several orders of magnitude) obtained from the USGS NWIS data base. The plots show two distinctive patterns. One is a logarithmic increase in Froude number which converges to a constant value at high discharge, and the other is a random scatter at low discharge which also converges to a constant at high discharge. In either case, there appears to be a tendency for the Froude number to reach a constant value as discharge increases toward the bankfull or regime flow.

The rivers shown on Figure 3.4 represent channels that are unrestricted (as determined by inspection of topographic maps of the river stations) and therefore the Froude number would not reflect backwater or accelerating flow conditions. It is not known (because it was not recorded in the data base) whether any of the discharges shown on the plots are greater than bankfull. However, it can be surmised that if the Froude number reaches a constant value at high discharge, the asymptote would occur at or near the bankfull discharge, and may persist in overbank flow conditions assuming that the majority of flow even in floods remains in the channel (which may be the case for smaller overbank flood events).

The asymptotic Froude number for each river shown on Figure 3.4 was estimated by inspection and tabulated in Table 3.2 along with the channel slope measured from topographic maps. These data are plotted on Figure 3.5 and show that the asymptotic Froude number is a function of the channel slope and can be fit to the following equation, which is plotted as the trend line given by:

$$F = 3.5S^{0.33} \tag{3-31}$$

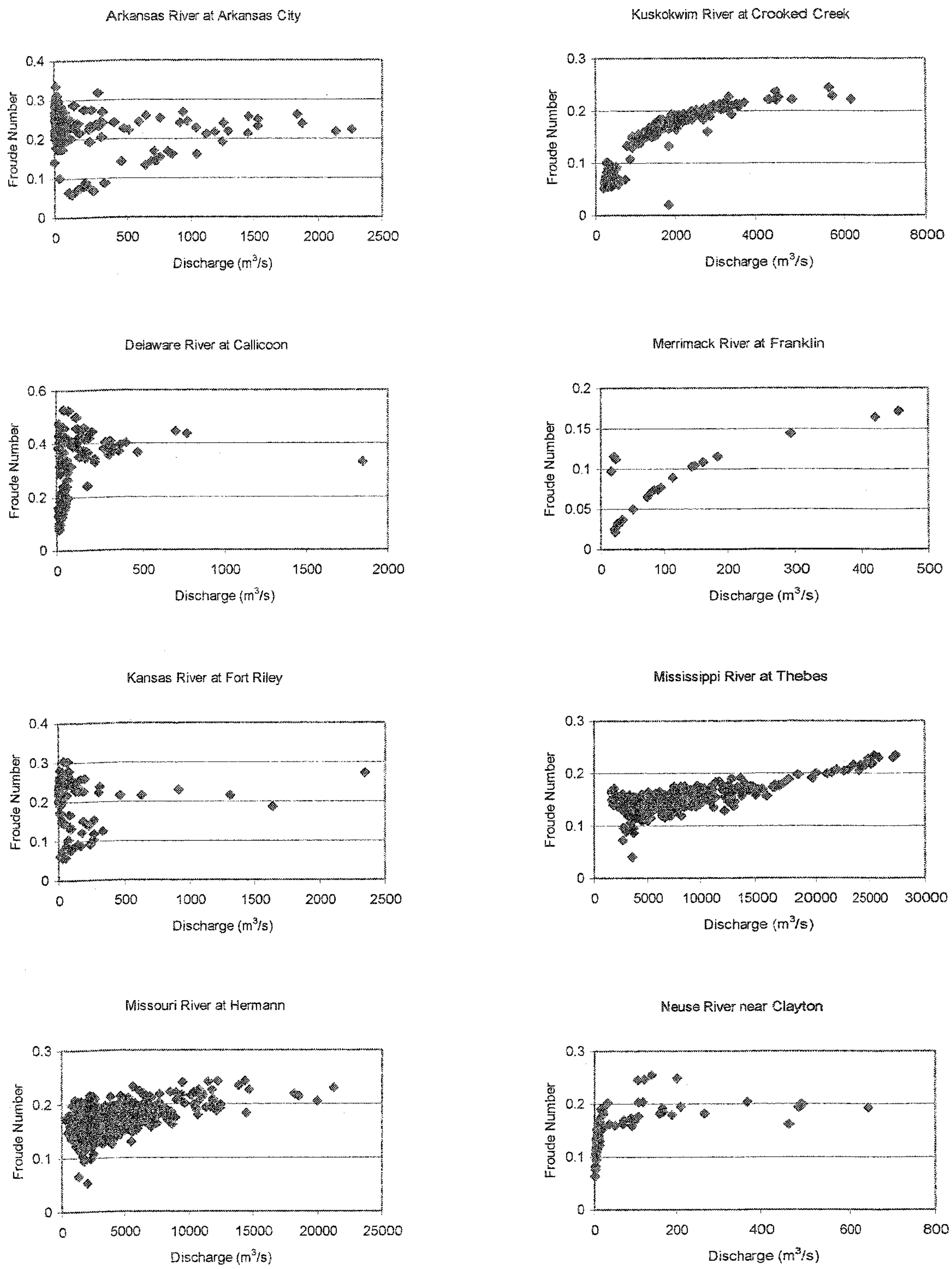

Figure 3.4 – Froude number as a function of discharge at 22 gaging stations.

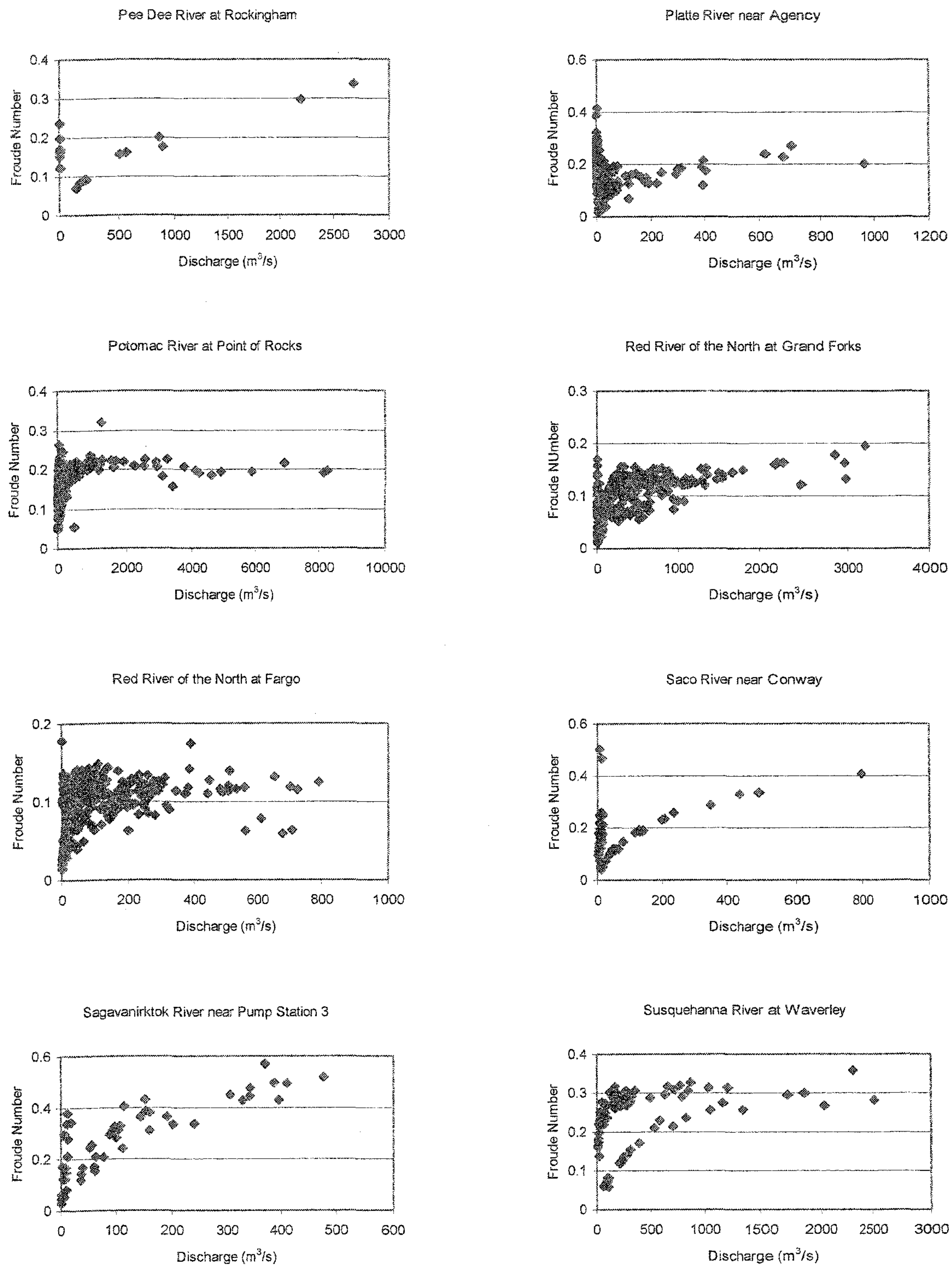

Figure 3.4 – (continued)

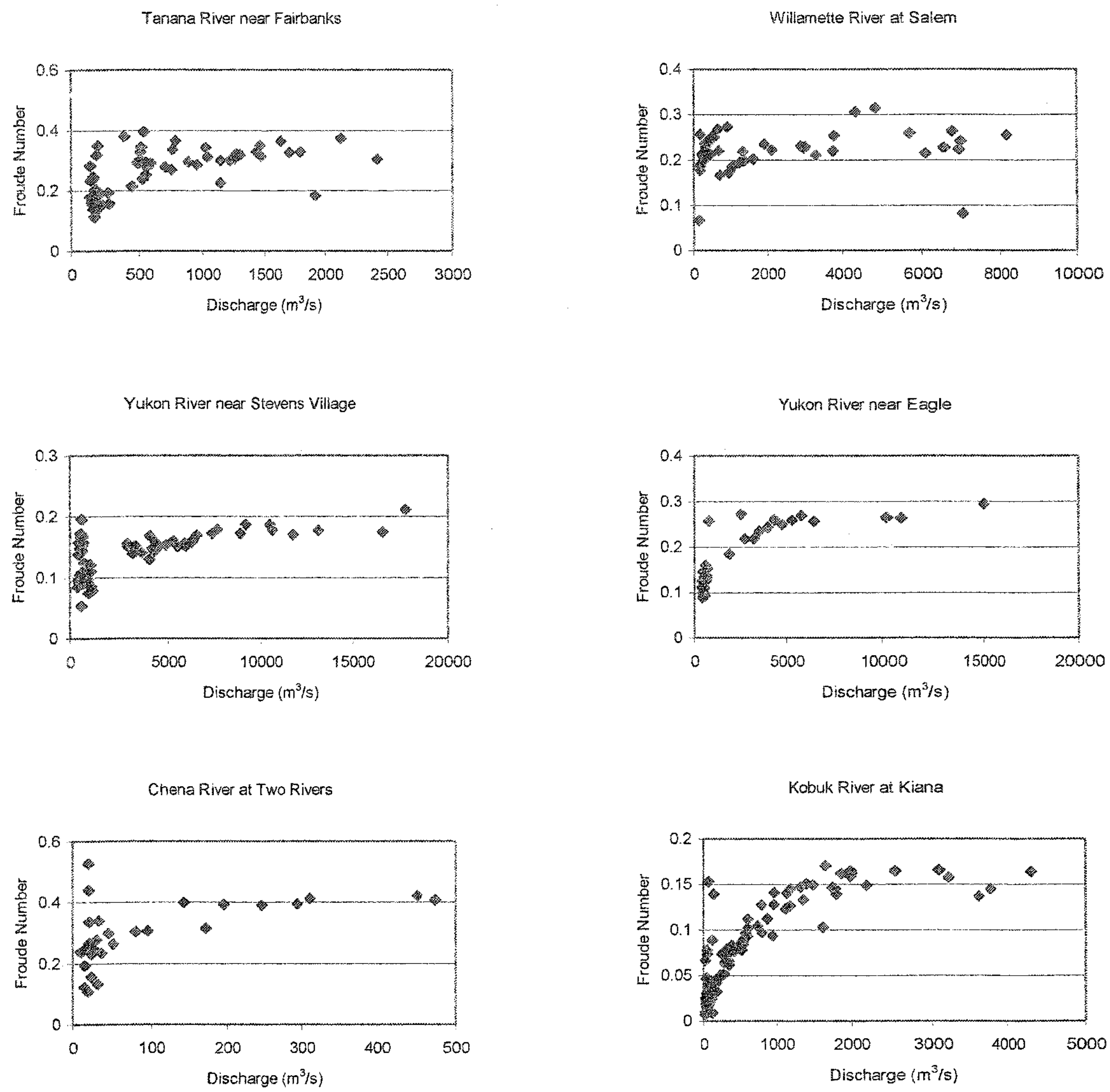

Figure 3.4 – (continued).

TABLE 3.2 - High Flow Froude Numbers and Channel Slopes

River Gaging Station	Channel Slope [1]	Froude Number [2]
Arkansas River at Arkansas City, Kansas	0.000685	0.25
Delaware River at Callicoon, New York	0.00107	0.4
Kansas River at Fort Riley, Kansas	0.00049	0.25
Kuskokwim River at Crooked Creek, Alaska	0.000198	0.25
Mississippi River at Thebes, Illinois	0.000137	0.25
Missouri River at Hermann, Missouri	0.00013	0.23
Platte River near Agency Missouri	0.00046	0.22
Red River of the North at Fargo, North Dakota	0.00009	0.12
Willamette River at Salem, Oregon	0.00032	0.25
Yukon River at Stevens Village, Alaska	0.000068	0.18
Yukon River at Eagle, Alaska	0.00036	0.3
Saco River at Conway, New Hampshire	0.0018	0.4
Chena River at Two Rivers, Alaska	0.00136	0.4
Kobuk River at Kiana, Alaska	0.00008	0.15
Sagavanirktok River near Pump Station 3, Alaska	0.00274	0.5
Merrimack River at Franklin, New Hampshire	0.0002	0.18
Neuse River at Clayton, North Carolina	0.00028	0.2
Pee Dee River at Rockingham, North Carolina	0.00068	0.35
Potomac River at Point of Rocks, Maryland	0.00027	0.2
Susquehanna River at Waverley, New York	0.00048	0.3
Tanana River near Fairbanks, Alaska	0.00043	0.35
Red River of the North at Grand Forks, North Dakota	0.000043	0.18

Notes:
1 - Channel slope measured from topographic maps
2 - Froude number based on inspection of Figure 3.4

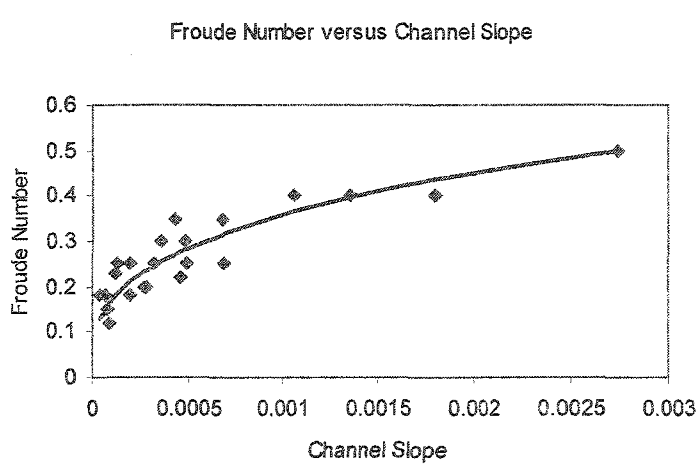

Figure 3.5 – Asymptotic Froude number (F) as a function of the channel slope for the rivers shown on Figure 3.5 and Table 3.2.

Substituting the definition for the Froude number, $F = V/(gY)^{0.5}$, into equation (3-31), re-arranging and multiplying by the cross-sectional area yields the following equation for bankfull discharge:

$$Q = 3.5g^{0.5}W_mY_m^{1.5}S^{0.33} \qquad (3\text{-}32)$$

which verifies the form of equation (3-29) if Y_m is substituted for Y. The different discharge coefficient in equation (3-29) compared to equation (3-31) (i.e. 3.5 versus 2.74 respectively) is probably due in part to the small data set used to develop equation (3-31), but may also indicate that the discharge coefficient varies with flow conditions.

Thus, equation (3-29) is considered to be a rational form of Model 1. However, a model that requires an estimate of both the depth and maximum depth, as would be needed for equation (3-29), increases the potential for compounding errors because depth cannot be directly measured remotely and would need to be estimated. Therefore, a more practical general formulation for Model 1 would be that given by equation (3-26). This equation appears to have comparable (possibly somewhat better) predictive characteristics compared to equation (3-29) after calibration of the discharge coefficient (Figure 3.2; also see Table 3.3 following this section).

Model 1, as described by equation (3-26) can be used to develop a general form of Model 2, (which does not require an estimate of the depth) by re-arranging and solving for depth, and then equating it to continuity, Q = WYV. The resulting form of Model 2 is:

$$Q = kWV^{2.5}S^{-0.5} \qquad (3\text{-}33)$$

This form of Model 2 is more similar to the equivalent model developed from regression analysis of the synthetic data base, compared to the equivalent model developed from regression analysis of the measurement data. However, because it can be easily developed from Model 1, it is viewed as an appropriate general form for Model 2.

Model 3 can be developed assuming that the concept of predictable river hydraulic geometry (Leopold et al., 1964) can be considered a physical principle. Within this conceptual framework, theoretical and observed values for the down-the-channel and at-a-station relationship between discharge and depth both tend towards approximately the same relationship, $Y = kQ^{0.4}$ (Leopold et al. 1964). Thus, Model 3 can be developed by substituting $kQ^{0.4}$ for Y in the continuity equation yielding:

$$Q = kW^{1.67}V^{1.67} \qquad (3\text{-}34)$$

Model 4 is a special case of Model 1 (as represented by equations (3-26) and (3-29)), developed by assuming width is a function of depth. Based on the previous discussion, an appropriate assumed geometric shape for a channel cross-section is a parabola. With this assumption, the form of Model 4 would be

$$Q = kW_mY_m^{-0.5}Y^{2.17}S^{0.33} \qquad (3\text{-}35)$$

or in a more complete rational form

$$Q = Cg^{0.5}W_mY_m^{-0.5}Y^{2.0}\ S^{0.33}/(Y_mS/Y)^{0.17} \qquad (3\text{-}36)$$

derived by substituting the equation of a parabola in terms of depth in to Model 1 for the width, i.e. $W^2 = aY$ where $a = W_m/Y_m^{0.5}$.

Calibration of General Equations and Comparison with Comparable Regression Models

To facilitate a comparison between the derived general prediction models and corresponding statistically based models (derived from the measurement and synthetic data), the channel-control data base was randomly divided into a calibration (N = 680) and validation (N = 387) data set. Table 3.1 compares the range of data in both the calibration and validation data sets. The conductance (or discharge) coefficients for the general prediction models were optimized by finding the constant value that minimized the log-residual of the predicted minus observed discharge for the calibration data. The log-residual was chosen for the minimization process because the discharge estimates are bounded by zero at the low end, with no constraint at the upper end.

The regression and general models were used to predict the discharge for the validation data set and the prediction errors of the various models were compared. The comparative error statistics included the log-residual, relative residual, actual residual (predicted minus observed) and the root mean square error (RMSE) of the predictions. Both the relative residual and the anti-log of the log-residual are measures of the percent error of the estimates. The comparative validation statistics of the models are shown on Table 3.3. The log-residuals for all of the general models are unbounded and in general are normally distributed as illustrated on Figure 3.6. The actual residuals and the relative residuals are not normally distributed because they are bounded by zero on the low end, with no upper boundary, thus they tend to have a skewed probability distribution.

The error statsitics indicate that the models derived from the synthetic data performed the worst. However, similar statistical results can be obtained using the synthetic data models if the coefficient is optimized from the calibration data in a similar manner as the general model (Table 3.3). This suggests that the general form of the synthetic models are applicable provided they are calibrated, similar to the general models. An interesting apsect of the synthetic models is that Model 1 (width-depth-slope) tends to overpredict discharge, whereas Models 2 and 3 (width-velocity-slope and width-slope) tend to underpredict discharge. These results suggest that the theoretical data used to develop the synthetic models under-represents the magnitude of resistance in the channel – with a subsequent smaller depth and higher velocity. This feature of the synthetic data would not be expected to affect the previous conclusions regarding the prediction of Froude number from the velocity head index, because these variables are dimensionless.

The various forms of Model 1, with the exception of the one based on the non-optimized synthetic data, all performed similarly, suggesting that any of the general forms of Model 1 can be used with the same confidence as a model developed from multiple- regression analysis. The expected accuracy of this model, using ground-measured depth and width, and slope measured from a topographic map, would be better than 5% on average, and approximately +/- 50% two thirds of the time. Model 2 and 3 performed reasonably well, with mean accuracies of less than+/- 6% for all forms of the models except those derived from the non-optimized synthetic data. However, the estimates exhibit more variabilty than those using Model 1, with 67% of the estimates falling within a factor of 2. In general, Model 2 performed better than Model 3 and the regression models developed from the measurement data performed the best. The form of Model 4 developed from the measurement data performed the least well of all of the regression models; however the general form of this model performed as well if not slightly better than Models 2 and 3. Additionally, the rational form of Model 4 performed as well if not slightly better than the same model developed from regression.

TABLE 3.3 MODEL COMPARISON

Model Type Regression Models	Validation Statistics	Relative Residual (Q' - Q)/Q	Actual Residual (Q' - Q) (m^3/s)	Log Residual log(Q'/Q)	Root Mean Square Error RMSE (m^3/s)
Measurement Data					
Model 1					
$Q = 4.84W^{1.10}Y^{1.63}S^{0.33}$	Mean	0.14	71.8	0.001	30
	Stdev	0.92	562.1	0.192	
Model 2					
$Q = 0.08W^{1.16}V^{1.65}S^{-0.34}$	Mean	0.19	-99.3	0.018	36.7
	Stdev	0.75	687.7	0.199	
Model 3					
$Q = 0.23W^{1.48}V^{1.45}$	Mean	0.16	-103.2	0.001	32.8
	Stdev	0.57	613	0.249	
Model 4					
$Q = 4.74W_m^{1.04}Y_m^{-0.58}Y^{2.11}S^{0.29}$	Mean	0.32	5.1	-0.002	37.4
	Stdev	1.52	707.4	0.284	
Synthetic Data					
Model 1					
$Q = 8.42W^{0.98}Y^{1.74}S^{0.31}$	Mean	0.49	257.2	0.110	51.4
	Stdev	1.27	938.6	0.200	
Model 2					
$Q = 0.06W^{1.07}V^{2.25}S^{-0.38}$	Mean	-0.21	-218.9	-0.161	42.6
	Stdev	0.36	776.1	0.257	
Model 3					
$Q = 0.12W^{1.53}V^{1.85}$	Mean	-0.24	-199.8	-0.201	42.3
	Stdev	0.45	774	0.290	
Synthetic with Optimized Coefficient					
Model 1					
$Q = 6.54W^{0.98}Y^{1.74}S^{0.31}$	Mean	0.15	39.7	0.001	25.8
	Stdev	0.99	486.2	0.199	
Model 2					
$Q = 0.09W^{1.07}V^{2.25}S^{-0.38}$	Mean	0.19	30.2	0.015	29.2
	Stdev	0.54	552.2	0.257	
Model 3					
$Q = 0.18W^{1.53}V^{1.85}$	Mean	0.15	59	-0.025	30.5
	Stdev	0.68	574.7	0.29	

TABLE 3.3 (Continued)

Model Type **Regression Models**	**Validation Statistics**	Relative Residual (Q' - Q)/Q	Actual Residual (Q' - Q) (m^3/s)	Log Residual log(Q'/Q)	Root Mean Square Error RMSE (m^3/s)
Calibrated General Models					
Model 1					
$Q = 7.14WY^{1.67}S^{0.33}$	Mean	0.15	-24.6	-0.003	23.2
	Stdev	1.04	437.7	0.195	
Model 1 (Rational)					
$Q = 2.74g^{0.5}WY^{1.67}S^{0.33}Y_m^{-0.17}$	Mean	0.15	-132.0	-0.007	31.7
	Stdev	1.21	585.9	0.201	
Model 2					
$Q = 0.05WV^{2.5}S^{-0.5}$	Mean	0.18	134.9	0.001	47.6
	Stdev	0.57	889.6	0.296	
Model 3					
$Q = 0.1W^{1.67}V^{1.67}$	Mean	0.18	183.9	-0.020	38.1
	Stdev	0.8	697.7	0.297	
Model 4					
$Q = 6.87W_mY_m^{-0.5}Y^{2.17}S^{0.33}$	Mean	0.34	49.0	0.007	40.0
	Stdev	1.49	755.6	0.283	
Model 4 (Rational)					
$Q = 2.64g^{0.5}W_mY_m^{-0.67}Y^{2.17}S^{0.33}$	Mean	0.34	-68.2	0.004	36.2
	Stdev	1.61	681.4	0.287	

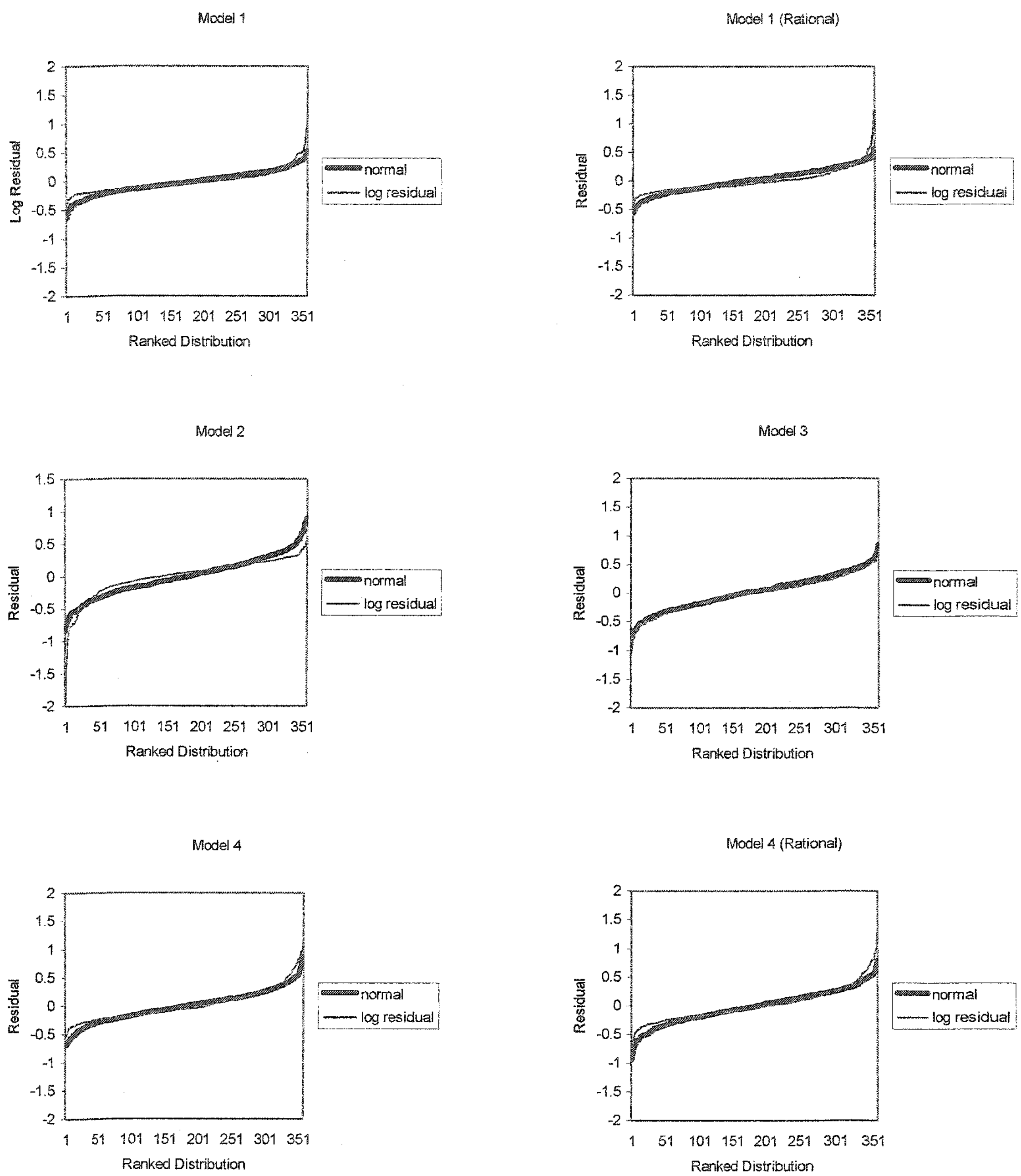

Figure 3.6 – Log-residual distribution from the validation data for Models 1 through 4 plotted with the equivalent normal distribution assuming the same standard deviation and mean of zero.

Slope-Controlled Reaches

The relationships that have been developed provide a set of equations that can be used to estimate in-bank river discharge depending on the type of information that is available. However, all of the relationships are based on an underlying assumption that the channel is adjusted to a characteristic slope. There are many river reaches where the channel is not adjusted to the slope, such as behind run-of-the-river dams, and where rivers are constricted by both natural and manmade features. In order to evaluate the use of the equations developed here for these types of rivers, a data set of discharge measurements were obtained from the USGS NWIS data base for rivers judged to exhibit control on the slope.

Selected flow measurements that did not meet the criteria for the channel-control data described in the hydraulic data section, were compiled into a slope-control data base that includes 293 measurements from 17 rivers, including the Amazon River at Obidos narrows (Oltman, 1968). The slope-control data includes rivers where there is an identifiable feature that creates a backwater or in other ways controls the hydraulic slope of the channel. These features include bridges or canyons that constrict the channel, and measurement stations that are located within run-of-the-river reservoirs behind dams or are suspected of being affected by backwater from dam and lock systems.

A data set of river stations where slope could not be effectively measured from topographic maps, and where large wetland and swamp systems are associated with the river channel were also compiled. These latter stations are presumed to exhibit significant lateral water exchange with the associated wetlands and swamps, and therefore the traditional concept of channel slope being the only significant mechanism driving the downstream motion may not be appropriate.

Figure 3.7 shows the predicted versus observed discharge for these data using the general models as compared to the same models applied to the channel control validaton data set. Figure 3.7 also shows that the estimates for the non-conforming reaches are generally subject to greater error. The mean prediction errors are significantly greater when applied to these data for all of the models. However, the standard deviation of the errors are comparble to those obtained for the channel control data. This suggests that in rivers where slope is controlled by hydraulic features, correction factors could be applied to the various models. Using the anti-log of the log residual as the best measure of prediction accuracy, the mean error for Model 1 is approximately 35% and the mean error for Model 2 is -58%. The mean error using Model 3, which does not use slope as a predictor variable is less than 5%, indicating that this model is the preferred model for situations where channel slope is not the primary hydraulic control. Interestingly, Model 4 showed the lowest mean error (less than 1%) suggesting that the additional information provided by the maximum width compensates to some degree for the effects of hydraulic control.

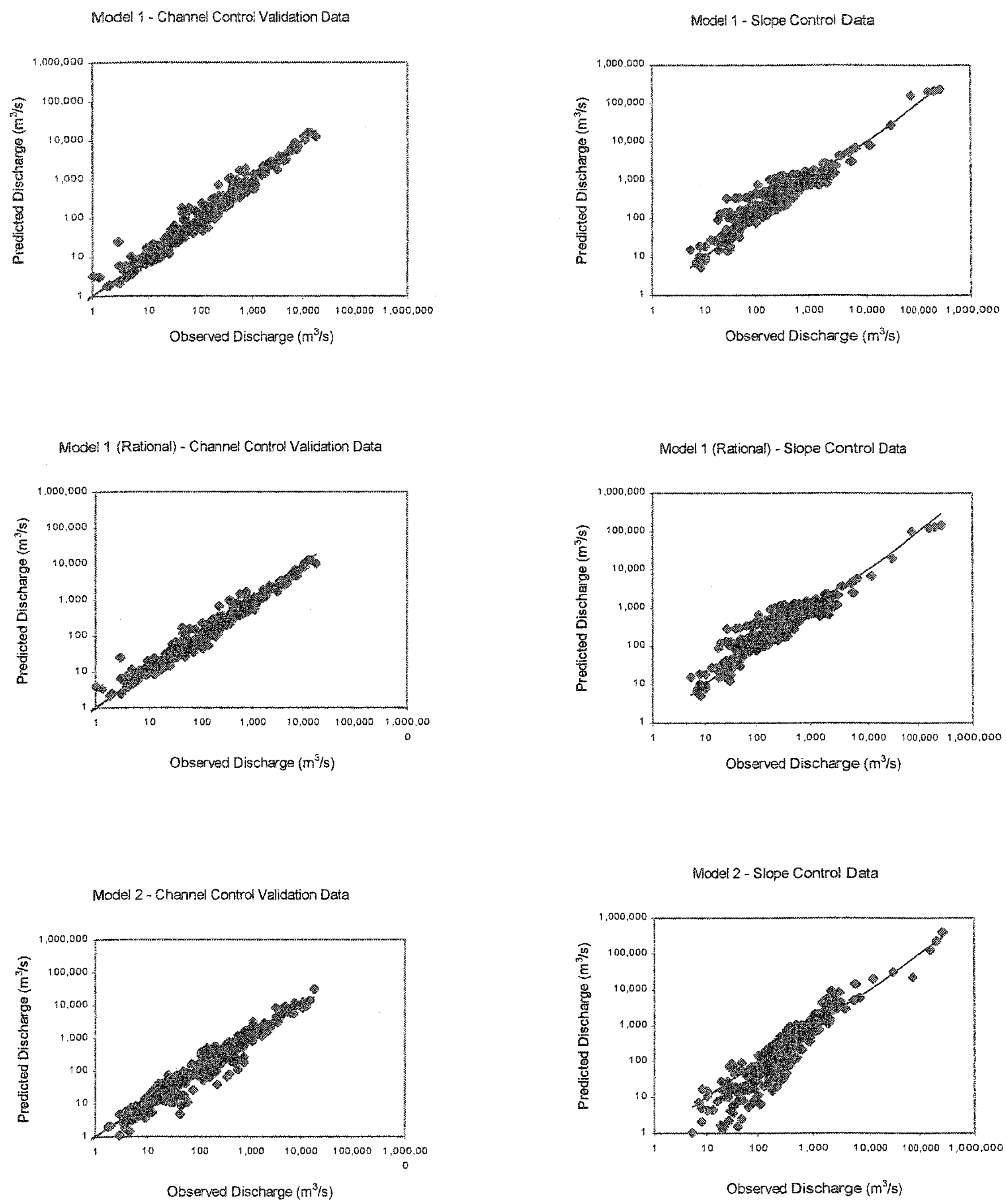

Figure 3.7 – Observed versus predicted discharge for the validation data and the slope-control data. The validation data are plotted on the left and the non-conforming data on the right.

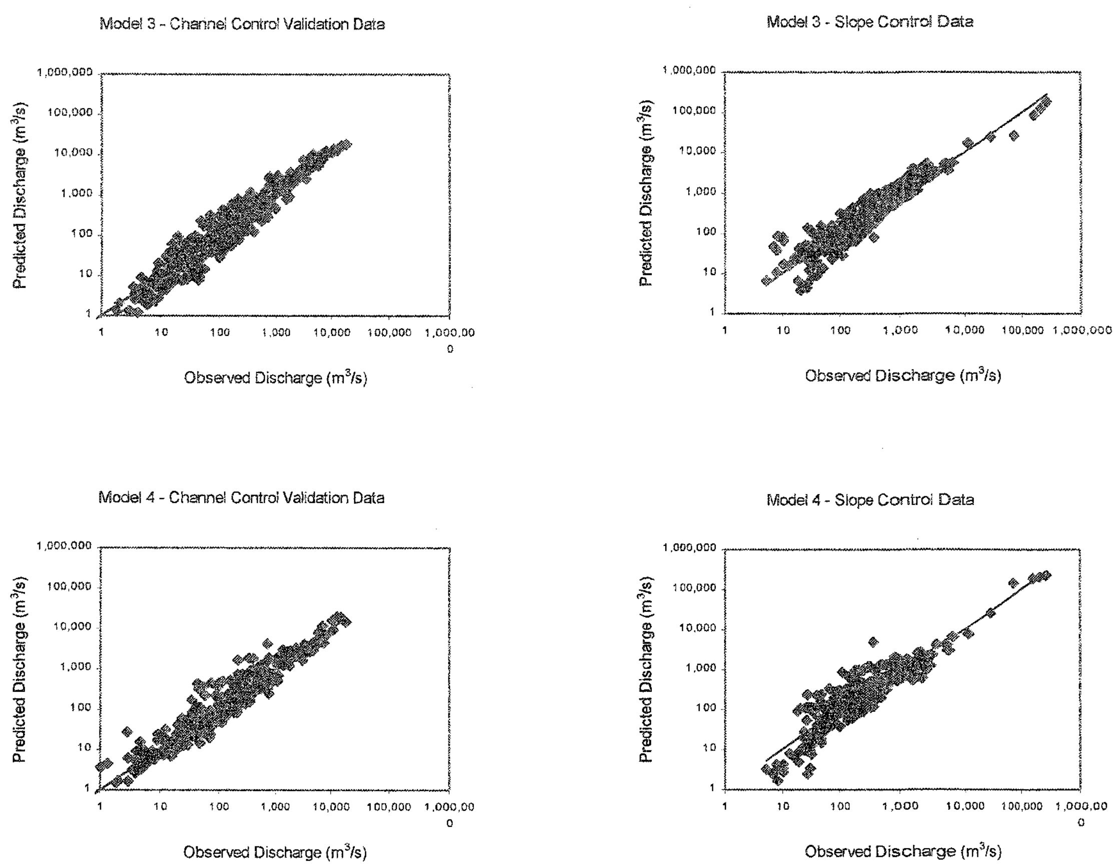

Figure 3.7 – (continued).

Discussion

Based on these comparisons, the calibrated general models and the models developed from the synthetic data base can be considered as useful and applicable as the regression models based on observed data. This suggests that river discharge is predictable from fundamentalhydraulic principles and can be estimated with reasonable accuracy for a wide range of flow conditions using constant values for coefficients calibrated on observations. An important finding is that uniform flow equations that use a slope exponent of 0.33 rather than 0.5 tend to have better predictive qualities in natural rivers, including less variation of the discharge coefficient and greater predictive accuracy. An advantage to using the general equations developed here rather than multiple-regression-based models is that they can be adapted to any flow conditon because they are based on well founded hydraulic principles and considerations rather than specific data sets. Thus, the assigned discharge coefficients can be adjusted based on knowledge of specific river reaches, for example where some ground-based data is available, without changing the predictive qualities of the model.

The general relationships provide a means to estimate in-bank river discharge from limited hydraulic information potentially obtained completely from remote sources. Model 2 or 3 combined with equations (3-11), (3-13) and (3-14), at a minimum, provides a method to estimate in-bank river discharge given knowledge of the bank-full width, wetted dynamic width and the channel slope. These variables can all be directly measured from remote platforms and available topographic information. The accuracy of the relationships vary, however the ability to use theoretically based synthetic data to generate models that predict as well as models developed from measured data suggests the general applicability of the formulations. Rationally derived relationships enable the predictive models to be calibrated and updated as specific knowledge is gained regionally or for individual rivers. In addition to the potential use of these relationships to estimate discharge in rivers from remotely obtained data, they can also be used in combination as tools to synthesize and map hydraulic geometry of rivers, and to interpolate hydraulic conditions in rivers based on limited field data or output from land-surface hydrology models.

CHAPTER IV

ESTIMATING DISCHARGE IN RIVERS USING REMOTELY SENSED HYDRAULIC INFORMATION

As discussed in Chapter 2, a mean water-surface width for a river can be readily measured (by measuring the wetted surface area and then dividing by the reach length) from a variety of existing remote imagery sources over large portions of the earth,. However, existing remote data sources do not provide coverages of river water-level elevations in areas where discahrge measurements are also readily available, and data sets of remote surface velocity mesurements are unavailable. Thus, at the present time, measurements of the water-surface width of rivers, combined with channel features such as the maximum channel width and the channel slope could be used to develop estimates of river discharge in remote areas or between river stations.

This chapter tests a methodology, based on the hydraulic relationships described in Chapter 3, to estimate in-bank river discharge using remotely sensed width information and channel-slope information obtained from topographic maps. Additionally, the use of water-surface velocity information observed from a single SAR image (Moller, 2002 personal communication) is used to evaluate the application and improvement in discharge estimates that can be achieved with this additional source of information. The results of these tests contribute to an assessment of the data requirements and potential accuracy of space-based discharge estimating methods.

Images and Remote Data

A data base of hydraulic information measured from various remote sources was compiled for this study. River reaches selected for analysis were located at or near established river gaging stations so that measured discharge values were available for comparison with estimates made from the remotely-sensed data. Mean daily discharge observations were obtained from the USGS NWIS on-line data base or from the Water Survey of Canada (Smith et al., 1996). Although the discharge estimates made from the remote data strictly only apply to the moment when the remote observation was made, the mean daily discharge, in all cases, did not vary widely through the day when the remote data were obtained. Thus, the average daily discharge is considered to be nearly equivalent to the instantaneous discharge at the time of the remote measurement.

Fourteen air photos, taken as part of the National Aerial Photography Program (NAPP), were obtained from the USGS EROS Data Center for analysis. The photos depicted the channel reach of 7 different rivers in New England near the corresponding USGS gaging station on each river during different flow conditions. These photos are geo-referenced and routinely taken as part of the USGS topographic mapping program . The photos were printed at a scale of 1:10,000. The mean water-surface width and mean maximum channel width were measured by averaging many equally spaced sections perpendicular to the channel banks.

Eleven digital orthophoto quadrangles (DOQs) available from the National Digital Orthophoto Program (NDOP), showing the selected river reach in 9 large rivers, were also obtained from the EROS data center for analysis. The resolution of the DOQs is 1 m. The water-surface width and maximum channel widths were measured from the DOQs by delineating the total water surface and channel surface areas within the reach by defining the area of interest within a series of polygons. The polygons were fit as closely as possible to the observed boundaries, and then the total area of the polygons summed and divided by the total reach length to obtain the mean-width estimate.

The maximum channel width measured from the aerial photos and the DOQs was assumed to be the active channel (Figure 4.1), identified by the presence of sand and gravel bars, marked changes in vegetation on the channel banks (typically sparse) that suggest a riparian zone with frequent inundation, and areas where recent scour or deposition could be observed. Islands with prominent point bars and sparse riparian vegetation were included in the maximum width. Islands with stable vegetation and areas that appeared to be old meander scars or scars from scour were not included. The extent of the maximum channel width often varied considerably along the channel reach (Figure 4.1). In some cases, the maximum channel width was not an obvious feature and a certain amount of operator judgment was required to define its extent. Thus, determination of the maximum channel width is a source of operator error. Comparing the channel surface area delineated for the Missouri River and the Sacramento River in Figure 4.1, this source of operator error is most likely greater in highly active and irregular channels.

The localized variability is minimized by using aerial mean averages of width (and other variables) that more closely approximate the mean conditions in a channel, thus defining the appropriate reach length is a key element of the data collection. Leopold et al. (1964) and Leopold (1994) suggest that mean values for determining channel geometry should be averaged over at least one meander length (typically 11 channel widths) because this length reflects the energy dissipation regime of the reach. Rosgen (1994) suggests that data be averaged over a minimum of two meander lengths in order to provide the most meaningful values. For this study,

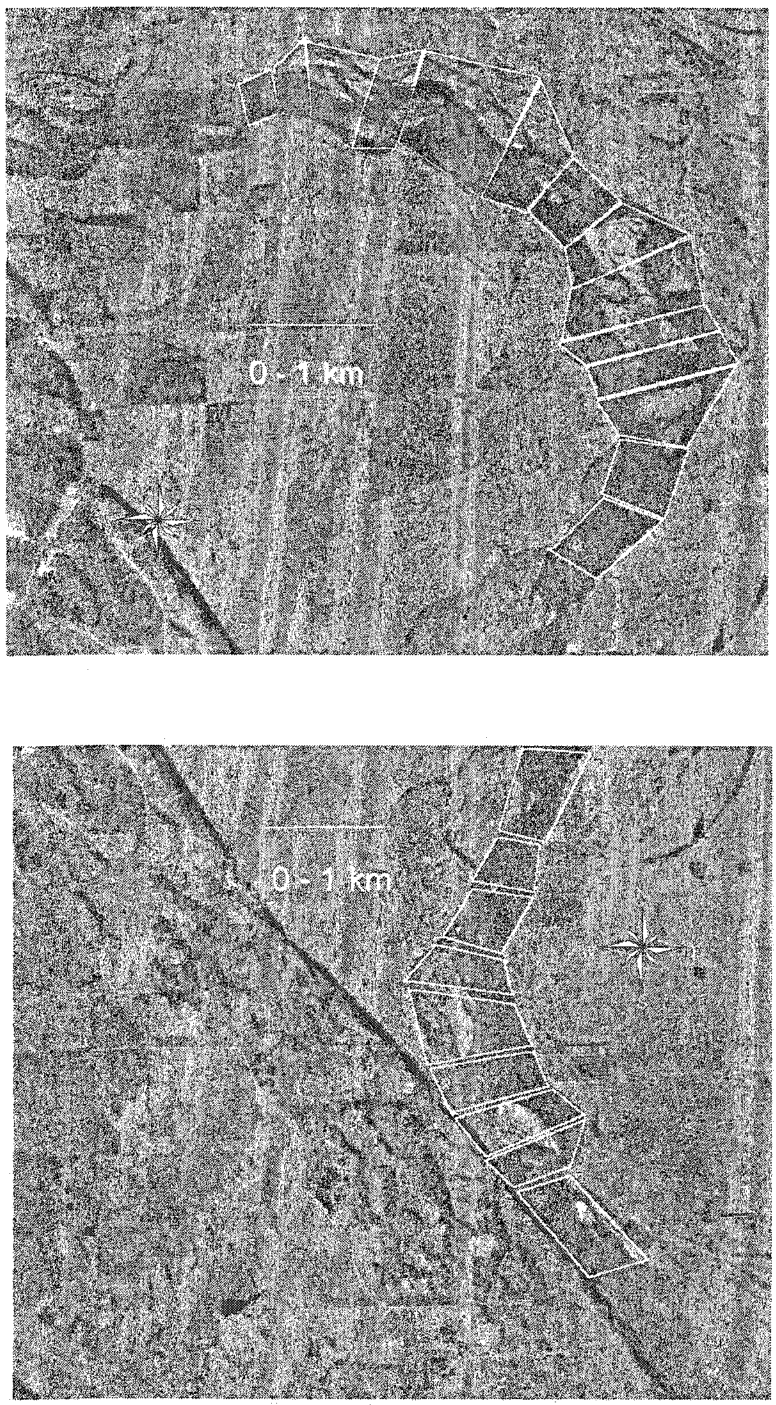

Figure 4.1 – Missouri River near Elk Point South Dakota, showing digitized plygons delineating the maximum channel surface area (Source: 3.75 minute DOQs for Elk Point (top) and Ponca (bottom) South Dakota, National Digital Orthophoto Program (NDOP)).

Figure 4.1 (continued) – Sacramento River near Red Bluff California, showing digitized polygons delineating the maximum channel surface area (Source: 3.75 min. DOQ for Bend, Califronia, National Digital Orthophoto Program (NDOP)).

the widths were averaged over a reach length that included at least one meander wavelength and was limited to a length that did not inlcude any tributary inflow or change in morphology.

The channel slope for all of the river reaches was measured from the corresponding USGS 1:24,000 scale topographic map by measuring the channel length between consecutive contour lines (approximately 3 meter contour interval). All of the images were obtained for river reaches at or near USGS stream gaging stations, and thus the mean daily discharge for the day of each image was available for comparison with the discharge estimates made from the images.

A time series set of SAR images obtained from ERS-1, were analyzed by Smith et al. (1996) to measure the water-surface area at different discharges in three large braided rivers (the

Tanana and Taku Rivers in Alaska, and the Iskut River in British Columbia). The resolution of the images was 25m with a processed pixel resolution of 12.5 m, and were collected at C-band. A total of 41 water- surface areas were obtained for the three rivers, 19 for the Iskut, 11 for the Taku, and 11 for the Tanana. The water-surface area estimates were made by summing all pixels classified as water based on a procedure developed by Smith et al. (1996). The total water-surface area within the braided channel system observed was divided by the valley length to obtain a mean or "effective" water-surface width for the reach. A measurement uncertainty was not reported (for more detail on these data and on the processing techniques used to extract the effective widths from the SAR images, refer to Smith et al. (1996)).

The reach lengths observed ranged from 9 to 16 km (approximately 20 to 30 times the effective width). The channel slope was assumed to be represented by the valley slope for the braided rivers, and was measured from topographic maps. A maximum channel width was not specifically measured by Smith et al. (1996). The maximum water-surface width from the time series was assumed to represent the maximum channel width for the purposes of this analysis. In each river, the maximum observed width occurred during high flow conditions, and likely reflects a high flow event that is near the mean annual flood. This assumes that the maximum channel width would generally correspond to a discharge near the mean annual flood (Leopold, 1964).

An airborne along-track interferometric (ATI) SAR imager (AirSAR), flown by NASA-JPL, obtained an image of the Missouri River near Elk Point South Dakota on March 25, 2002 (Figure 4.2). The resolution of the image was 5 m and was collected at C-Band. The water-surface width and the surface velocity were obtained from the image. The surface velocity was obtained using a Doppler technique developed by JPL (Goldstein et. al. 1994). Figure 4.2 shows the AirSAR radial velocity estimate projected onto the water surface. Note that in this figure positive velocities are flowing away from the radar to the south.

The velocities have also been corrected for the Bragg-resonant effect (Bragg 1913) whereby short wind-driven waves on the river surface have the effect of biasing the velocity estimate by their phase speed (Kinsman 1965). In this case the Bragg velocity is approximately 0.23 m/s although the correction increases with range due to the increasing incidence angle. At the time of the image, a mild wind blowing in the direction of the river flow (approximately 10 knots) was inferred from the nearby weather station in Sioux City, Iowa. Given the flat topography it is reasonable to assume that the wind direction in the imaged area will be consistent with the weather station's observation. Without the Bragg correction, the south-bound wind would have the effect of biasing the velocities high.

Because the ATI-SAR measures velocity in the radial direction only, the portion of the river which is oriented nearly parallel to the flight direction detects very low velocities (Figure 4.2). As such, for this case study, the analysis includes the region where the river is directed toward the radar. Techniques to alleviate this limitation are suggested in the discussion. The slope of the river channel was obtained from USGS topographic mapping, and the approximate maximum channel width was measured from a recent DOQ of the same reach (photo taken on April 4, 1993). The reach of river where the image was taken is characterized by large sand and gravel bars, and is much wider than both upstream and downstream sections of the river. This reach of river is considered atypical of the Missouri River for the region.

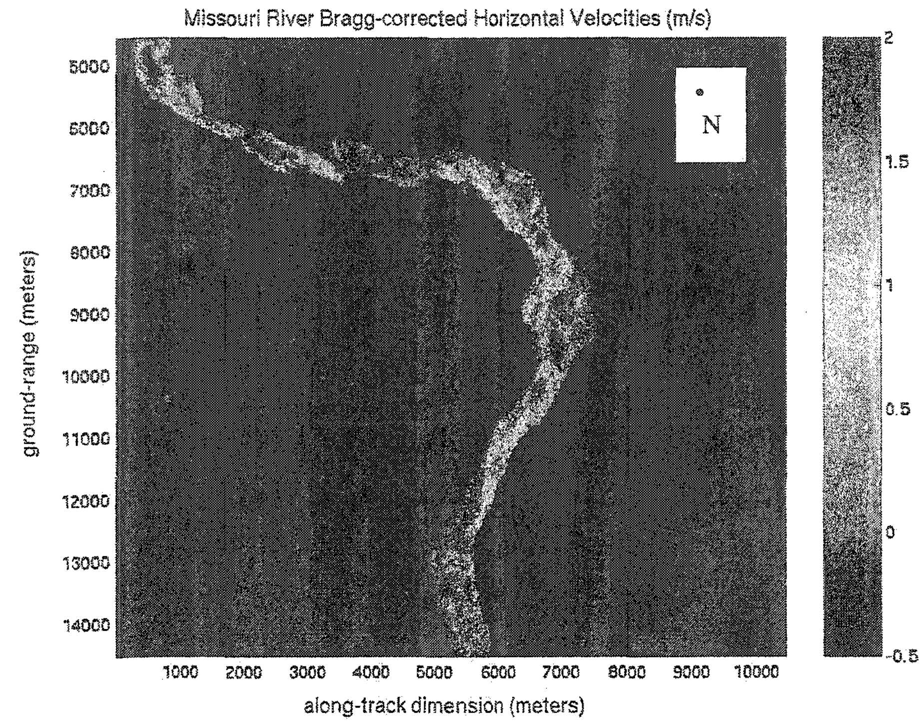

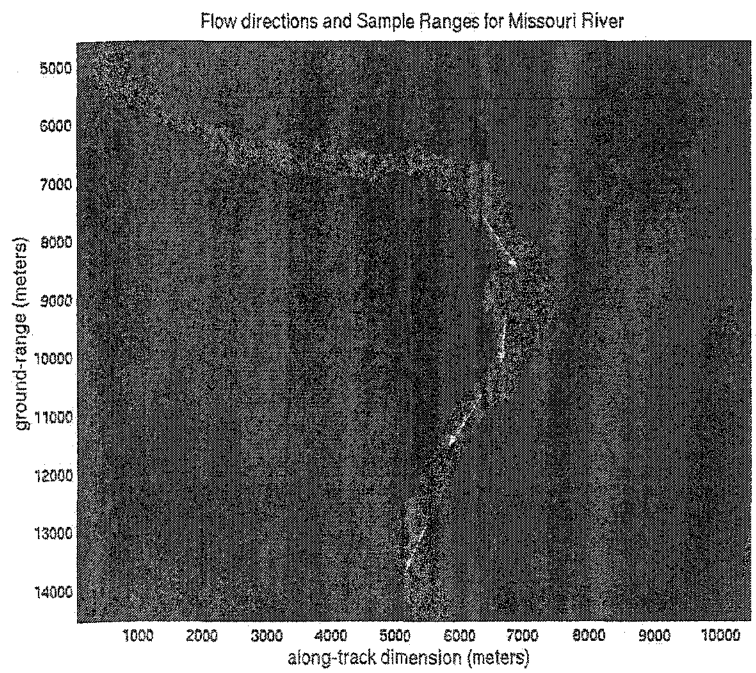

Figure 4.2 – C-band SAR image of the Missouri River near Elk Point, Souoth Dakota showing radial surface velocity projected onto the horizontal plan (upper) and inferred flow direction (lower) indicated by arrows (Source:NASA-JPL Air SAR).

Because of the large sand and gravel bars, estimating the effective water-surface width was problematic. It was decided not to include shallow or sluggish water that did not contribute significantly to the flow. For this reason, the effective water-surface width was assumed to include only those regions where the surface velocity was greater than a threshold value. Taking this approach avoids potential complications associated with non-parallel flow lines, which would more likely be present over the shallow bars, and reduces the potential for assigning too much weight to generally non-contributing flow regions. The threshold velocity value used to estimate the mean water-surface width and velocity field was 0.15 m/s, thus velocities lower than this number were excluded when estimating mean velocities and river widths. This velocity threshold was chosen because below this value, the velocity estimate becomes too uncertain. This approach, while simplistic, was effective in excluding the sand-bar regions which would otherwise bias the velocity and width estimates.

A mean cross-channel width and velocity were determined for four portions of the observed river reach that were oriented towards the radar, and which were able to provide reliable estimates of both width and velocity. Vector velocity estimates were inferred from the radial velocities by assuming that the direction of flow was parallel to the river direction. Figure 4.2 shows the inferred direction of flow and regions of the river that were used to obtain four discharge estimates.

The river lengths varied in absolute range depending on the estimated direction of flow. Note that the flow direction estimates in Figure 4.2 are biased toward the high-flow regions and exclude the obvious sandbars (compare with upper frame of Figure 4.2). The absolute ranges were [1107, 765, 976, 730] m respectively (from north to south) while the estimated water-surface width (adjusted for the direction of flow and excluding sand-bar regions) was 330 m on average (previously mentioned velocities <0.15 m/s were excluded from the estimation process). Although the range-to-width ratio is quite low, this was necessitated by the meandering nature of the river.

The accuracy of the water-surface and maximum-channel width estimates measured from the images are, in part, a function of the resolution of the images and the accuracy of the measuring tool. Thus, the resolution of the DOQs (1m) and the SAR images (10 m ERS-1 SAR, and 5m NASA-JPL AirSAR) indicate the accuracy of an estimated width measurement if it were a single measured value. However, the widths were estimated by measuring the total water-surface area of the reach divided by the reach length. This procedure would likely improve the accuracy of the estimate due to averaging. However, the methods used to measure the surface area may introduce additional unknown error. In the case of the NAPP aerial photos, the image resolution is a function of the ability to sharply see the boundary of the defined object (since these are not digital). It is estimated that the resolution of these photos at 1:10000 scale is approximately 4 m. The width estimates made from the photo is assumed to be somewhat better than the resolution implies, however, due to averaging along the reach (i.e. the balance of positive and negative estimte errors would tend to improve the overall estimate for the reach). Overall, the accuracy of the width estimates made from the various images is not precisely known.

Discharge Estimating Methodology

The observed water-surface width (W), bank-full (or maximum) channel width (W_m), and the channel or valley slope (S) can be used to estimate the river discharge at the time of the observation for the SAR images obtained by Smith, and for the 26 NAPP photos. This is accomplished by estimating the mean velocity (V) using a general relationship for estimating the

Froude number (F) and a relationship to estimate the discharge using width, velocity and slope as developed in Chapter 3. The Froude number estimate is obtained from the following general form of equation (3-13):

$$F = c(V^2/2gW)^m \tag{4-1}$$

where $c = \alpha W_m^{0.12} S^{0.449}$ (4-2)

$$m = 0.881 W_m^{-0.046} S^{0.148} \tag{3-14}$$

The equations for determining c and m were developed from the synthetic flow-measurement data base, as described in Chapter 3. The coefficient α is assumed, for convenience, to be a calibration coefficient that reflects specific channel conditions. Calibration procedures for α are described later.

As can be seen from equation (4-1) and the variables used to predict c and m, all of the variables needed to compute F are obtained from the image except V. Combined with a dimensionally formulated discharge-estimating equation that uses width, velocity and Froude number given as:

$$Q = g^{-1} W V^3 F^{-2} \tag{4-3}$$

where g is the accleration due to gravity, and equation (3-33) given below

$$Q = 0.05 W V^{2.5} S^{-0.5},$$

an estimate of the velocity can be made by substituting F from equation (4-1) (with the values of c and m determined from W_m and S) into equation (4-3), then equating this to (3-33) and re-arranging. Once V is estimated, the discharge is then computed directly from equation (4-3). Thus, a discharge estimate can be made from a minimum of three variables all obtained from remote sources including: 1) observed water-surface width (W) measured from an image, 2) the maximum (or bankfull) channel width (W_m) measured from an image, and 3) the channel slope (S) measured from a topographic map.

In order to evaluate the magnitude of the calibration coefficient α, the observed discharge measurements in the channel-control data base (Chapter 3) were used to calibrate equation (4-2). The best fit value of α found by minimizing the mean of the log residual of the estimates is 20. Figure 4.3a shows that the distribution of F, estimated using a constant value for α (= 20) is non-linear at low values (F less than about 0.2). The distribution was linearized by adjusting the value of α for observed inflection points in the distribution. Accordingly, for Froude numbers in the range 0 to 0.1, α was adjusted to 11.3, for Froude numbers in the range 0.1 to 0.2, α was adjusted to 17.7, and for Froude numbers in the range 0.2 to 0.4 and larger, α was adjusted to 22.3 (Figure 4.3b). The linearized values of α provide a means to self-calibrate equation (4-2) as follows: the Froude number determined from an intial value for α is used to determine a new value of α according to the Froude number ranges described above. The value of α is then adjusted accordingly. When the predicted Froude number and the value of α used to determine the Froude number are in the appropriate range class, the self calibration is complete (usually after one adjustment).

Discharge Estimation Results

Initial estimates of the discharge for the single-channel data were made using a value of 20.0 for α. Table 4.1 lists the observed data and the estimated discharges for the single-channel rivers derived from the air photos. The mean and standard deviation of the relative and log residuals of the estimates are also provided. Using the average value for the calibration coefficient resulted in very poor discharge estimate accuracy. Improvements in the estimates for

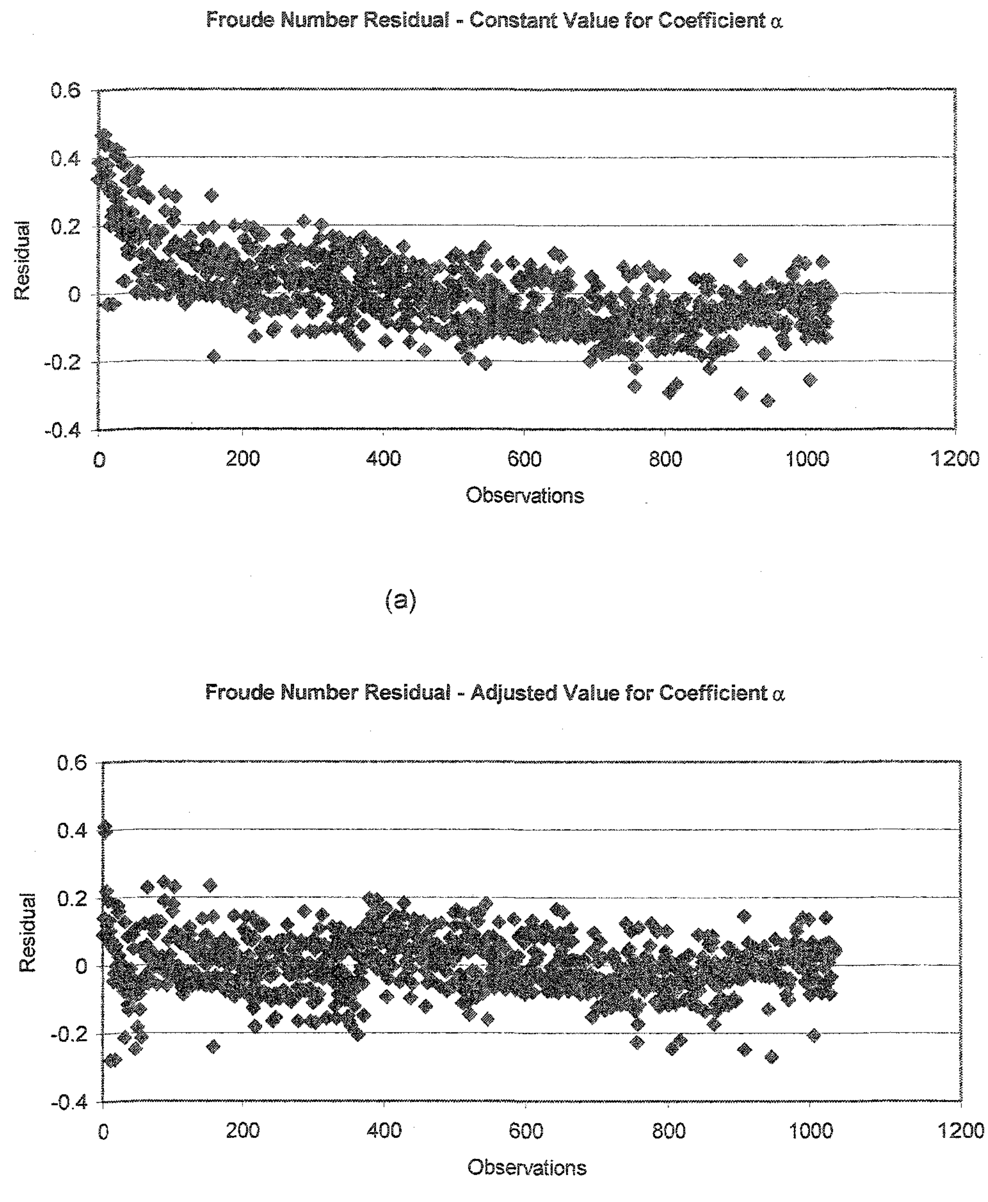

Figure 4.3 – Residuals of the predicted and observed Froude numbers when α constant value of a is used (Plot a), and when α is adjusted for Froude number ranges between 0 – 0.1, 0.1 – 0.2 and greter than 0.2, showing that the distribution becomes more linear.

the single channel rivers were made by adjusting the calibration coefficient as a function of the Froude number, as described above.

The initially estimated Froude numbers for the single-channel estimates greater than 0.2 were recomputed using $\alpha = 22.3$, and the initial Froude number estimates between 0.1 and 0.2 were recomputed using $\alpha = 17.7$. If the adjustment in α forced the Froude number out of range for the value of α used, then the previous α and the adjusted α were averaged. If the revised Froude number remained in range for the adjusted α, no additional adjustments were made. This approach does not require any new information or assumptions to be introduced into the calibration, and thus is considered to be a self calibration process. The revised discharge estimate accuracy is much improved (Table 4.1) using this calibration procedure.

An alternative calibration procedure was also explored by observing that the optimal value for α, determined by adjusting it until the predicted discharge equaled the observed discharge, was correlated with the maximum width of the river channels that were analyzed. Best-fit linear predictive relationships (Figure 4.4) between W_m and the optimized α were determined for rivers where $W_m < 200$m and $W_m > 200$m given by:

$$\alpha = -0.075W_m + 23.7 \text{ and} \qquad r^2 = 0.38 \qquad \text{for } W_m < 200\text{m} \qquad (4\text{-}4)$$

$$\alpha = -0.005W_m + 20.3 \qquad r^2 = 0.79 \qquad \text{for } W_m > 200\text{m} \qquad (4\text{-}5)$$

Table 4.1 - Hydraulic Data and Discharge Estimate Statistics for Single Channel Rivers

River	Maximum Channel Width (m)	Channel Slope	Water Surface Width (m)	Observed Discharge (m^3/s)	α = 20.0				Adjusted α from Froude number				Adjusted α from maximum width function			
					Estimated Froude Number	Estimated Discharge (m^3/s)	Percent Error	Log Residual	Estimated Froude Number	Estimated Discharge (m3/s)	Percent Error	Log Residual	Estimated Froude Number	Estimated Discharge (m3/s)	Percent Error	Log Residual
Pemigewassett River at Plymouth, NH	82	0.0017	69.2	43.0	0.30	99.4	131.2	0.364	0.27	39.2	-8.8	-0.040	0.28	59.2	37.7	0.139
Pemigewassett River at Plymouth, NH	82	0.0017	78.6	78.0	0.30	151.7	94.5	0.289	0.28	59.8	-23.3	-0.115	0.29	90.4	15.9	0.064
Pemigewassett River at Plymouth, NH	82	0.0017	73.2	59.0	0.30	119.8	103.1	0.308	0.27	47.3	-19.9	-0.098	0.28	71.4	21.0	0.083
Pemigewassett River at Woodstock, NH	67.1	0.0026	54.6	26.0	0.33	73.0	180.9	0.449	0.31	32.3	24.4	0.095	0.31	40.7	56.7	0.195
Pemigewassett River at Woodstock, NH	67.1	0.0026	51.4	20.0	0.33	60.3	201.3	0.479	0.30	26.7	33.4	0.125	0.31	33.6	68.0	0.225
White River at West Hartford, Vermont	83.5	0.0012	78.6	93.0	0.27	135.3	45.5	0.163	0.24	48.3	-48.0	-0.284	0.26	77.6	-16.6	-0.079
Ammonoosuc River at Bethlehem, NH	27.9	0.0075	26.8	9.9	0.45	34.1	244.5	0.537	0.43	19.0	92.0	0.283	0.43	17.7	78.5	0.252
Ammonoosuc River at Bethlehem, NH	27.9	0.0075	15.7	6.4	0.41	7.2	11.7	0.048	0.39	4.0	-37.7	-0.206	0.38	3.7	-42.1	-0.237
Baker River near Rumney, NH	23.5	0.0013	19.9	5.4	0.26	16.1	198.1	0.474	0.24	6.6	22.0	0.087	0.23	5.7	5.0	0.021
Baker River near Rumney, NH	23.5	0.0013	16.9	3.5	0.25	9.4	169.3	0.430	0.23	3.9	10.3	0.042	0.22	3.3	-5.1	-0.023
Smith River at Bristol, NH	18.6	0.0037	17.7	11.0	0.36	16.5	50.4	0.177	0.33	8.5	-23.0	-0.113	0.33	7.3	-33.4	-0.177
Smith River at Bristol, NH	18.6	0.0037	13.6	6.1	0.34	7.5	22.4	0.088	0.32	3.8	-37.3	-0.203	0.31	3.3	-45.8	-0.266
Pomperaug River at Southbury, CT	18.4	0.0021	16.3	3.8	0.30	13.0	241.2	0.533	0.27	6.0	58.0	0.199	0.27	5.1	33.4	0.125
Pomperaug River at Southbury, CT	18.4	0.0021	13.1	3.3	0.28	6.5	98.0	0.297	0.26	3.0	-8.3	-0.038	0.26	2.6	-22.6	-0.111
Mississippi River at Thebes, IL	801	0.000137	710.0	14326.0	0.10	34.5	-99.8	-2.619	0.14	1444.5	-89.9	-0.996	0.18	18107.2	26.4	0.102
Mississippi River at Thebes, IL	801	0.000137	657.0	4700.0	0.09	21.5	-99.5	-2.339	0.14	901.8	-80.8	-0.717	0.18	11305.2	140.5	0.381
Potomac River at Point of Rocks, MD	381	0.00027	280.0	144.0	0.14	75.8	-47.4	-0.279	0.18	776.9	439.5	0.732	0.17	373.0	159.0	0.413
Missouri River near Elk Point, SD	651	0.00023	466.0	680.0	0.12	50.3	-92.6	-1.131	0.16	762.4	12.1	0.050	0.18	1764.8	159.5	0.414
Missouri River near Elk Point, SD	651	0.00023	336.0	450.0	0.11	9.7	-97.8	-1.667	0.14	147.0	-67.3	-0.486	0.16	340.3	-24.4	-0.121
South Platte River near Kersey, CO	125	0.00093	78.0	38.0	0.23	48.2	26.9	0.103	0.20	15.2	-60.1	-0.399	0.22	43.9	15.6	0.063
Missouri River near Culbertson, MT	343	0.000156	258.0	484.0	0.11	34.7	-92.8	-1.145	0.15	673.8	39.2	0.144	0.14	206.1	-57.4	-0.371
Kansas River at Fort Riley, KS	115	0.00049	77.0	17.5	0.18	40.7	132.5	0.366	0.18	40.7	132.5	0.366	0.18	31.0	76.9	0.248
Sacramento R. below Bend near Red Bluff, CA	163	0.000575	92.0	459.0	0.19	32.4	-92.9	-1.151	0.19	32.4	-92.9	-1.151	0.19	53.8	-88.3	-0.931
Willamette River at Salem, OR	219	0.00032	164.0	221.0	0.16	79.0	-64.2	-0.447	0.20	589.2	166.6	0.426	0.17	154.0	-30.3	-0.157
Delaware River at Port Jervis, DE	221	0.00098	162.0	172.0	0.24	167.9	-2.4	-0.011	0.21	50.2	-70.8	-0.535	0.25	264.8	54.0	0.187
Wenatchee River at Monitor, WA	126	0.0032	69.0	37.0	0.34	54.8	48.0	0.170	0.31	24.2	-34.5	-0.184	0.33	51.8	40.0	0.146
Mean							50.4	-0.212			12.6	-0.116			23.9	0.023
Standard Deviation							114.4	0.899			108.5	0.421			64.1	0.285

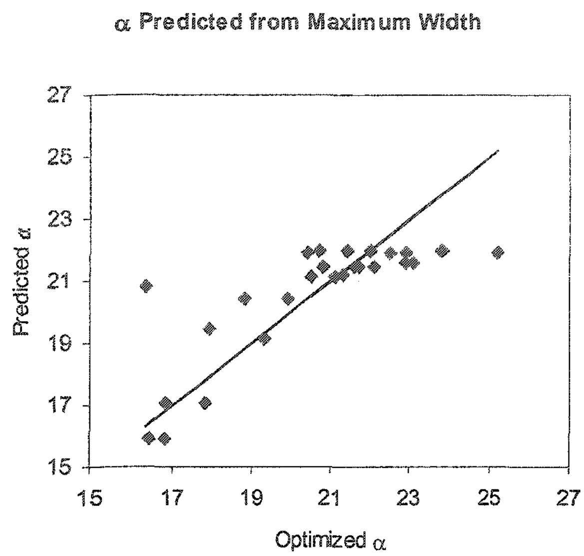

Figure 4.4 – Optimized α plotted against α predicted from maximum width relationships.

These calibration relationships improve the discharge predictions particularly for the Mississippi River, however they are based on limited data and are somewhat spurious because they are derived from the observed data (which for application purposes would be unknown). Both of the calibration procedures used to improve the discharge estimates indicate that specific channel characteristics (W_m) and the energy regime of the river reach (Froude number) are important to consider when applying the methods developed in this paper. Figure 4.5 a, b and c show the predicted discharge plotted against the observed discharge for the single-channel rivers using each of the calibration options described above.

Table 4.2 lists the discharge estimates developed for the braided channels derived from the SAR images by Smith et al. (1996). All of the Froude-number estimates for the braided channels were above 0.2, indicating that a value of 22.3 for α should be used to recompute the discharge. However, if this is done, the estimation accuracy becomes poor, with all of the estimates biased low. This suggests that the calibration for braided river channels is different than for single- channel rivers. This would not be surprising, as mean values of depth and velocity, averaged across the braided channel system (i.e. the water-surface area) reflect somewhat different dynamics compared to the single channels. Many researchers have found that there is a distinct regime threshold between braided and single channel rivers (Henderson, 1966; Ferguson, 1986). Figure 4.5d shows the predicted discharges plotted against the observed discharges for the braided rivers.

The accuracy of the discharge estimates developed from channel width, water-surface width, and channel slope varied depending on the calibration procedure used. The error was evaluated from the relative residual ([Q' – Q]/Q) and the log residual (logQ' – logQ) where Q' is the predicted discharge and Q the observed discharge. For the single channel rivers, assuming a constant value for α, the estimates were rather poor (Table 4.1), exhibiting a mean error on the order of +/- 50%. The standard deviation of the error was large using either error index and a distinct break in the predictive quality for larger rivers was evident (Figure 4.5). The Froude number calibration markedly improved the predictions, with a mean over-prediction of 12% based on the relative residual and an under-prediction of 23% based on the anti-log of the log residual. The standard deviation of the errors was also markedly reduced and the distinct break in predictive quality for the larger rivers nearly eliminated. Even further improvement in the accuracy of the estimates was made using the width-based calibration method.

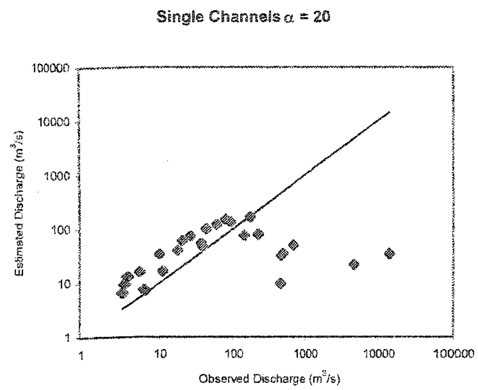

a)

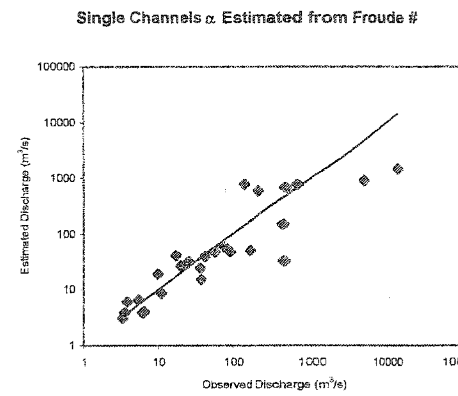

b)

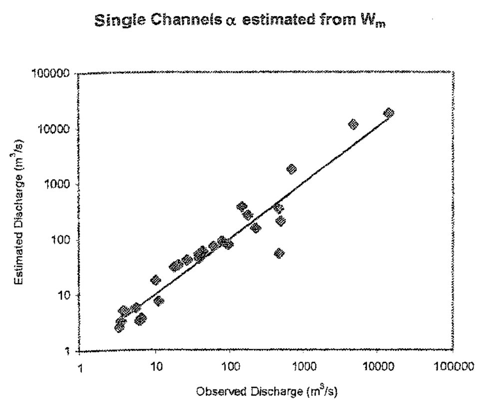

c)

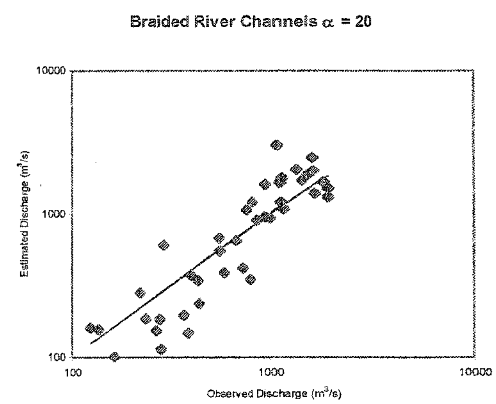

d)

Figure 4.5 – Plots a, b, and c show the predicted discharge for the single channel rivers plotted against the observed discharge using differetn estimates of α. Plot d shows the predicted discharge plotted against the observed discharge for the braided rivers using a constant value for α.

The prediction error for the braided rivers was generally less than the error for the single-channel rivers even though there was no calibration (Table 4.2, Figure 4.5d). This suggests that the braided rivers constitute a more homogeneous data set. These results suggest that grouping rivers by channel type, size and energy regime may provide a means to improve overall estimation accuracy, and that improved and more robust self-calibration methods could be developed based on experience.

The SAR image obtained by NASA-JPL for the Missouri River provided both the surface velocity and water-surface width, enabling the use of equation (3-33) directly. The mean velocity for the cross-section was estimated by applying a correction factor of 0.86 to obtain the mean velocity in the vertical (Rantz et al., 1982). Recent experiments by Costa et al. (2000) in several rivers in which surface velocity was measured using bank-side and helicopter-borne radar showed that this correction factor appears to provide reasonable estimates of mean velocity in the cross-section.

Table 4.3 provides the measured values of water-surface width and mean velocity in four relatively short sections of river within the observed reach. The nearest USGS gaging station on the Missouri River is located at Sioux City, Iowa, approximately 20 miles downstream of the observed reach. For the date of the SAR image, the discharge at this station was approximately 450 m^3/s. There are no major tributaries entering the River between the observed reach and the gaging station at Sioux city, so the discharge at Sioux City is assumed to be approximately the same as for the observed reach.

The discharge estimate using equation (3-33) is approximately 70% higher than the observed discharge. This is within the expected accuracy of the statistical model (Model 2), which indicates that approximately 67% of the estimates would be within a factor of 2 (Chapter 3). Given that the reach is non-conforming, i.e. it is atypical for the river, the relatively large error is not surprising. As a comparison, the width and mean velocity for two discharge measurements made at the Sioux City gage on March 6 and March 13, 2002 with approximately the same discharge (442 and 476 m^3/s respectively) were 173 m and 165 m for width, and 1.00 m/s and 0.96 m/s for mean velocity. The channel slope at the gage is approximately the same as for the observed reach. Using equation (3-33) with these data provides estimates of discharge of 597 and 514 m^3/s respectively (errors of +8 and +35%).

Table 4.2 - Hydraulic Data and Discharge Estimate Statistics for Braided Channel Rivers

River	Maximum Channel Width (m)	Slope	Water Surface Width (m)	Observed Discharge (m^3/s)	α = 20.0 Estimated Froude Number	Estimated Discharge (m^3/s)	Percent Error	Log Residual
Iskut River, British Columbia	700	0.0022	437.0	292	0.32	604.1	106.9	0.316
	700	0.0022	579.0	951	0.34	1603.0	68.6	0.227
	700	0.0022	656.0	1570	0.35	2471.7	57.4	0.197
	700	0.0022	584.0	1110	0.34	1651.5	48.8	0.173
	700	0.0022	490.0	862	0.33	898.6	4.2	0.018
	700	0.0022	393.0	735	0.31	418.1	-43.1	-0.245
	700	0.0022	291.0	388	0.29	147.5	-62.0	-0.420
	700	0.0022	261.0	164	0.28	101.1	-38.3	-0.210
	700	0.0022	316.0	370	0.29	196.3	-47.0	-0.275
	700	0.0022	621.0	1320	0.35	2043.7	54.8	0.190
	700	0.0022	596.0	1140	0.34	1772.2	55.5	0.192
	700	0.0022	498.0	948	0.33	950.5	0.3	0.001
	700	0.0022	694.0	1080	0.36	3004.7	178.2	0.444
	700	0.0022	533.0	1121	0.33	1203.0	7.3	0.031
	700	0.0022	534.0	818	0.33	1210.8	48.0	0.170
	700	0.0022	446.0	681	0.32	648.4	-4.8	-0.021
	700	0.0022	311.0	235	0.29	185.7	-21.0	-0.102
	700	0.0022	294.0	266	0.29	152.8	-42.6	-0.241
	700	0.0022	381.0	403	0.31	375.5	-6.8	-0.031
Taku River ,Alaska	580	0.0015	301.0	277	0.26	183.5	-33.8	-0.179
	580	0.0015	358.0	436	0.27	342.1	-21.5	-0.105
	580	0.0015	541.0	1840	0.30	1508.0	-18.0	-0.086
	580	0.0015	520.0	1840	0.30	1308.0	-28.9	-0.148
	580	0.0015	360.0	801	0.27	349.1	-56.4	-0.361
	580	0.0015	229.0	309	0.24	68.7	-77.8	-0.653
	580	0.0015	339.0	221	0.27	281.3	27.3	0.105
	580	0.0015	288.0	136	0.26	156.6	15.1	0.061
	580	0.0015	290.0	124	0.26	160.5	29.5	0.112
	580	0.0015	574.0	1480	0.31	1865.4	26.0	0.101
	580	0.0015	491.0	765	0.30	1064.4	39.1	0.143
Tanana River , Alaska	865	0.0010	820.2	1764	0.26	1670.2	-5.3	-0.024
	865	0.0010	782.1	1617	0.26	1390.7	-14.0	-0.065
	865	0.0010	733.3	1158	0.25	1085.2	-6.3	-0.028
	865	0.0010	562.2	595	0.23	390.2	-34.4	-0.183
	865	0.0010	494.4	445	0.23	237.9	-46.5	-0.272
	865	0.0010	407.9	283	0.21	113.5	-59.9	-0.397
	865	0.0010	614.6	566	0.24	549.9	-2.8	-0.013
	865	0.0010	704.8	1000	0.25	931.6	-6.8	-0.031
	865	0.0010	825.9	1413	0.26	1715.4	21.4	0.084
	865	0.0010	857.7	1586	0.26	1983.9	25.1	0.097
	865	0.0010	649.1	561	0.24	678.5	21.0	0.083
Mean							3.8	-0.033
Standard Deviation							49.5	0.217

Table 4.3 SAR Image Missouri River near Elk Point South Dakota
Discharge Estimates Using Equation (3)

Cross-section	Width (m)	Surface Velocity (m/s)	Estimated Mean Velocity (m/s)	Channel Slope	Estimated Discharge (m^3/s)	Discharge at Sioux City (m^3/s)	Percent Error
1	315	1.13	0.97	0.00023	966.8	450	114.9
2	313	1.07	0.92	0.00023	838.2	450	86.3
3	370	0.80	0.69	0.00023	478.9	450	6.4
4	321	1.05	0.90	0.00023	820.0	450	82.2
Average	330	1.01	0.87		776.0		72.4

Discharge Estimate Using Maximum Width
$\alpha = 22.3$

Cross-section	Width (m)	Mean Velocity (m/s)	Estimated Maximum Width (m)	Channel Slope	Estimated Froude Number	Estimated Discharge (m^3/s)	Discharge at Sioux City (m^3/s)	Percent Error
Mean	336	0.88	651	0.00023	0.2	435	450	-3.3

The discharge estimate can be improved if the maximum channel width is also used in the analysis. The maximum channel width for the reach coincident with the SAR image was measured from recent DOQs (Figure 4.1, taken April 4, 1993), and estimated to average 651 m. Assuming that this value has not changed between 1993 and 2002, the method described previously to estimate discharge from the single-thread and braided river reaches was used to develop the discharge estimate with the inclusion of the measured surface velocity rather than the estimated velocity. The resulting discharge estimate was 434 m^3/s, which is within 5% of the observed discharge at Sioux City. Thus, discharge estimates developed from two channel variables (maximum channel width and channel slope) and two dynamic variables (water-surface width and velocity) appear to provide an optimum set of hydraulic information for prediction (based on one observation).

Discussion

This analysis indicates that relatively accurate estimates of in-bank river discharge can be made from remote observations of water-surface width in rivers provided two channel-characteristic variables are also known or measured remotely, the maximum channel width and the channel slope. However, it may be difficult to automate or readily obtain the maximum (bank-full) channel data, especially considering that a certain amount of judgment is required to define the maximum areal extent of the active channel. Assuming that the channel dimensions and the channel slope are relatively constant (at least over a period of years), inventories of this information can be developed from air photo and map analysis and from field surveys. These data can then serve as baseline information that is coupled with dynamic tracking of water-surface width to obtain time series estimates of river discharge over large areas or selected sets of rivers.

Another approach to defining the maximum channel width of rivers would be based on accumulated water-surface width measurements developed over time. Similar to the Smith et al. (1996) braided river-width data, a sufficiently long time series of widths would enable the maximum channel width to be identified and catalogued. This approach would be preferable to methods that rely on the identification of the active channel from morphologic features, because the water is relatively easy to identify. Additionally, identification of water surface areas and widths can be automated depending on the type of imagery (for example color infrared, SAR, and panchromatic) because water can be readily distinguished from surrounding land.

The accuracy of the discharge estimates reported on Table 4.1 and 4.2 indicate that robust calibration procedures will be necessary to successfully develop discharge estimates from imagery and other remotely sensed information. Experience may provide the data necessary to develop these methods, as there is strong indication from this analysis that characteristic channel features, including maximum width and channel type, can be used as calibration tools. Additionally, there is an indication from this analysis that self-calibration methods based on the Froude number can be developed. As data sets of remotely sensed water-surface widths, velocities, maximum channel widths, and channel slopes are collected and associated with channel-type information, robust methods for assigning calibration coefficients can be developed.

The successful use of SAR imagery to simultaneously observe water-surface width and velocity holds great promise as a tool for substantially improving the accuracy of river-discharge estimates, especially when coupled with maximum-channel width and channel-slope information. Surface- velocity measurements require information about surface wind speed and direction in order to correct for these effects. For rivers in deep gorges one can generally assume that the wind will blow in the direction of the river banks and ameliorate this restriction. An additional limitation, whereby river flow orthogonal to the radar line-of-sight results in extreme radial velocities, may be addressed by flight lines that cross the river from alternate directions and deriving the vector velocities by assuming, as was done here, that the flow is parallel to the banks or by combining directionally diverse paths. A further preferable alternative is a system that can measure velocity in a single pass by means of directionally diverse multi-beam interferometric measurement capability (Moller et.al. 2002, Frasier and Camps 2001).

The equations developed in Chapter 3 indicate that discharge-estimating models that include width, depth, and slope have generally greater accuracy, especially for larger rivers, compared to models that use width and slope only; or width, slope, and velocity. Inclusion of remotely observed stage (water-surface elevation) from altimetry (Birkett, 1998) may provide an additional dynamic variable that can be used to estimate the depth and thus improve the accuracy of estimates even further. Depth estimates could be developed from stage if knowledge of the river-bottom elevation is available, or from time series of stage observations over a range of water levels.

Observation of water-surface area (and width) and river-channel characteristics can be made with currently operating satellites, frequently and over much of the globe on a routine basis from a variety of sensors (Chapter 2). However, surface velocity and stage data may be available only on an occasional basis depending on the orbits of satellites, sensor capabilities and availability. In these circumstances, more accurate discharge estimates could be made when these data (surface velocity and stage) are available and used to calibrate routinely made estimates based on measured widths and map slopes. This approach would maximize the use of the more readily available data (water-surface area and channel slope) and enable less frequently available data (surface velocity and stage) to be successfully incorporated into a river-discharge observing strategy.

This analysis has shown that water-surface width, maximum channel width and channel slope can be used to estimate in-bank river discharge with an accuracy of 20% or better on average, however the standard deviation of the error could be 50 to 100% depending on the type of river and calibration technique. Additional data, including surface velocity (and stage) are likely to markedly improve the discharge estimates. Development of time-series data sets of water-surface area (and thus width), stage, and surface velocity of rivers will be key to fully developing robust estimating methods, calibration tools, and channel morphology inventories that will provide the basis for remotely tracking and estimating river discharge on large scales from space.

CHAPTER V

APPLICATION OF RIVER CHANNEL SLOPES DERIVED FROM A SIX MINUTE DEM FOR HYDRAULIC MODELING OF RIVERS

The water-surface slope is one of the key indicators of the hydraulic conditions within the river, and is an important predictor of the velocity, channel resistance, and stable channel geometry (Henderson, 1966). Most hydraulic models of river flow, sediment transport, bank stability, flooding, flood routing, and habitat conditions rely on an independently derived energy or water-surface slope as an input variable. Many hydraulic modeling applications (such as floodplain modeling) assume uniform flow between measurement points in a channel network, and thus inherently assume that the channel slope derived from channel-bottom elevations is equivalent to the water-surface and energy slope (Chow, 1959). With this assumption, the channel slope can be considered to be representative of the average energy slope in a river reach. Thus channel slopes obtained from topographic maps can be used in lieu of field-measured slopes in hydraulic models (as shown in Chapter 2), and provide a way of remotely obtaining estimates of channel slope.

However, measuring channel slopes from topographic maps is usually done manually, and is therefore labor intensive. Additionally, the scale of the map used to derive the slope is critical to its accuracy. Altimeters mounted on aircraft or satellites have the potential for measuring channel and water-surface slopes over large areas; however there are problems of accuracy inherent in these measurements due to the low slopes that rivers exhibit relative to surrounding topography and the accuracy of the altimeters themselves (Birkett, 1998).

Digital elevation models (DEMs) can be used to obtain river channel slopes with automated routines, thus eliminating the labor intensive task of meausring slope from topographic maps. However, the use of DEM derived slopes for instream hydraulic studies is limited due to the difficulty of obtaining hydraulically meaningful values. This problem arises because routines used to develop the DEM cannot effectively determine the exact channel location and water-surface elevations within any specific grid cell. Often, a channel slope derived from a DEM will have large variability within a channel network, exhibiting sharp rises and troughs between adjacent grid cells. Fekete (2002, personal communication) has developed a method to estimate the channel slope by a technique that smooths large slope fluctuations between grid cells and maintains a continuous downstream slope direction.

This Chapter evaluates the application of a river-channel slope field generated from a six minute DEM by Fekete (2002, personal communication) for modeling of rivers. The river-channel slopes obtained from the DEM are used in conjunction with river hydraulic variables potentially obtained or estimated from remote data sources to estimate discharge in rivers using a set of general hydraulic relationships based on the Manning equation. The potential accuracy of discharge estimating equations, which rely on slope as an input variable, is evaluated and some potential applications of using the DEM-derived slope and the hydraulic relationships are explored and discussed.

Data and Methods

River discharge measurements obtained from the USGS National Water Information System (NWIS) flow measurement data base were downloaded (http://www.water.usgs.gov/nwis/measurements/) for more than 5,000 gaging stations in the

United States. This data base consists of nearly one million records each providing measured discharge, flow width, flow cross-sectional area, mean velocity and other information about the gaging station and measurement conditions for stations across the United States. A DEM-derived slope was also available for each station (Fekete, 2002 personal communication).

The mean annual flow (Q_a) was used as a characteristic discharge for each station because it is considered to be correlated with the general morphological characteristics of the channel (Leopold et al., 1964; Osterkamp and Hedman, 1982) such that the water-surface slope associated with Q_a is assumed to be approximately the same as the general topographic channel slope. Additionally, the mean annual flow is assumed to be subject to fewer potential backwater effects from upstream or downstream controls, such as bridges, and is more reliably identified

For this analysis, the mean annual flow was determined from a composite flow field developed by Fekete (2002), which combines USGS long-term flow records with estimates made from a continental water-balance model (Vörösmarty et al., 1999). These data were used because the inclusion of the modeled flow data in the mean-annual discharge field provides a means to compensate for the varying record lengths inherent in the USGS flow data. The USGS flow measurement (Q_c) nearest to the estimated mean annual flow was extracted from NWIS flow measurement data base for analysis.

The USGS gaging station data were linked to a 6-minute gridded river network (STN-06, Fekete, 2002) for spatial analysis. The USGS-reported basin area was compared with the STN-06 calculated basin area, and all stations where the difference between the two basin areas was greater than 15% were discarded. This eliminated those stations with basin area less than the size of the 6 minute grid cell (approximately 100 km^2). Stations with missing mean-annual flow data or missing channel-geometry data were also eliminated from the data base. The resultant data base included mean-annual-flow measurement data for 2,256 stations.

The characteristic flow measurement (Q_c) data were used with Model 1 (equation 3-26) to estimate an associated hydraulic slope. Model 1 is given by:

$$Q_c = KWY^{1.67}S_c^{0.33} \qquad (5\text{-}1)$$

and is rearranged to calculate the slope:

$$S_c = [Q_c/(KWY^{1.67})]^3 \qquad (5\text{-}2)$$

where S_c = the characteristic hydraulic slope

Q_c = the characteristic discharge (m^3/s)

W_c = the characteristic water-surface width (m)

Y_c = the characteristic mean flow depth (m)

K = a discharge coefficient

The hydraulic slope calculated from equation (5-2) represents a general or "typical" slope associated with the particular flow and channel geometry obtained from the characteristic-flow data. A constant value of K was determined through a calibration process that minimized the log-residual between the predicted and observed discharge from an independent data set consisting of over 1,000 flow measurements in 81 rivers (Chapter 3). The optimized estimate of K is 7.2, +/- 3.9 within one standard deviation. Because of the range of variability in the estimate of K, the calculated hydraulic slope has an associated uncertainty that reflects this variability.

Because the characteristic slope is derived directly from a calibrated hydraulic model, comparing this slope and the DEM-derived slope provides a means to evaluate the efficacy of the DEM slope for use in general hydraulic models. Additionally, evaluating the differences, or error, between the two slope estimates can provide insight into range of applicability of the DEM slope in hydraulic models.

The DEM derived slope (S_{dem}) was used in conjunction with the USGS measured hydraulic variables for each station as input to Model 1, Model 2 (equation 3-33) and Model 3 (equation 3-34) to estimate the discharge. Model 1 is given by equation (5-1), and Models 2 and 3 are respectively given as (Table 3.3):

$$Q = 0.05 W_c V_c^{2.5} / S_{dem}^{0.5} \tag{5-3}$$

$$Q = 0.1 W_c^{1.67} V_c^{1.67} \tag{5-4}$$

where V_c = the characteristic mean velocity (m/s).

The discharge coefficients for Model 2 and 3 were optimized on the same data set as Model 1. Models 1 and 2 use S_{dem} and the measured characteristic values for width (W_c) and either depth (Y_c) or velocity (V_c) as input. Model 3 uses the measured characteristic width (W_c) and velocity (V_c), and thus is independent of slope. Discharge was estimated using the three models and compared against the measured characteristic discharge from the USGS NWIS data for each station. Because Model 3 is independent of slope, the effect of potential error in the slope can be evaluated by comparing the variability of this Model against the other two models.

Analysis and Results

The spatial distribution of the DEM-derived slope and the calculated hydraulic slope for the 2,256 river stations are shown on Figure 5.1. Figure 5.1 also shows the spatial distribution of the log residuals (error) between the hydraulic and DEM slopes. The log residual was chosen as the best measure of error because the error is bounded by zero on the low end and is not bounded on the high end. The log residual is calculated as:

$$\text{Error} = \log(S_{dem}) - \log(S_c) \qquad (5\text{-}5)$$

The log residual can also be expressed as the log of the ratio of the two slopes:

$$\text{Error} = \log(S_{dem}/S_c) \qquad (5\text{-}6)$$

Equation (5-6) shows that the antilog of the residual is the ratio of the DEM slope and the hydraulic slope, and thus can be thought of as a correction factor between the two slopes. This characteristic of the residual provides a direct measure of the percent difference between the slope estimates.

Inspection of Figure 5.1 shows that the distribution of the DEM slope appears to be consistent with the general topographic trends of the continental United States. The distribution of the hydraulic slope shows greater variability, possibly indicating the effects of smaller scale topographic relief on channel slope. Many of the slope residuals are quite large, in the range of several orders of magnitude. The mean residual between the two slopes is ($10^{-0.1}$) and the standard deviation of the residuals indicates that the difference between the two slopes is nearly one order of magnitude (Table 5.1).

Figure 5.2 and Table 5.1 show the discharge prediction results for the three models, with Model 1 and Model 2 using the DEM slope as input. It can be seen that the DEM slope provides reasonably accurate results using the models, and that results for Model 1 and 2, which use the DEM slope, are comparable to Model 3 which does not. Model 3 is comparable to Model 1 and 2 when a map-derived slope is used (Chapter 2 and 3). This suggests that the DEM slope provides results, on average, with the same accuracy as a map derived slope even considering some of the rather large deviations between the DEM slope and the hydraulic slope.

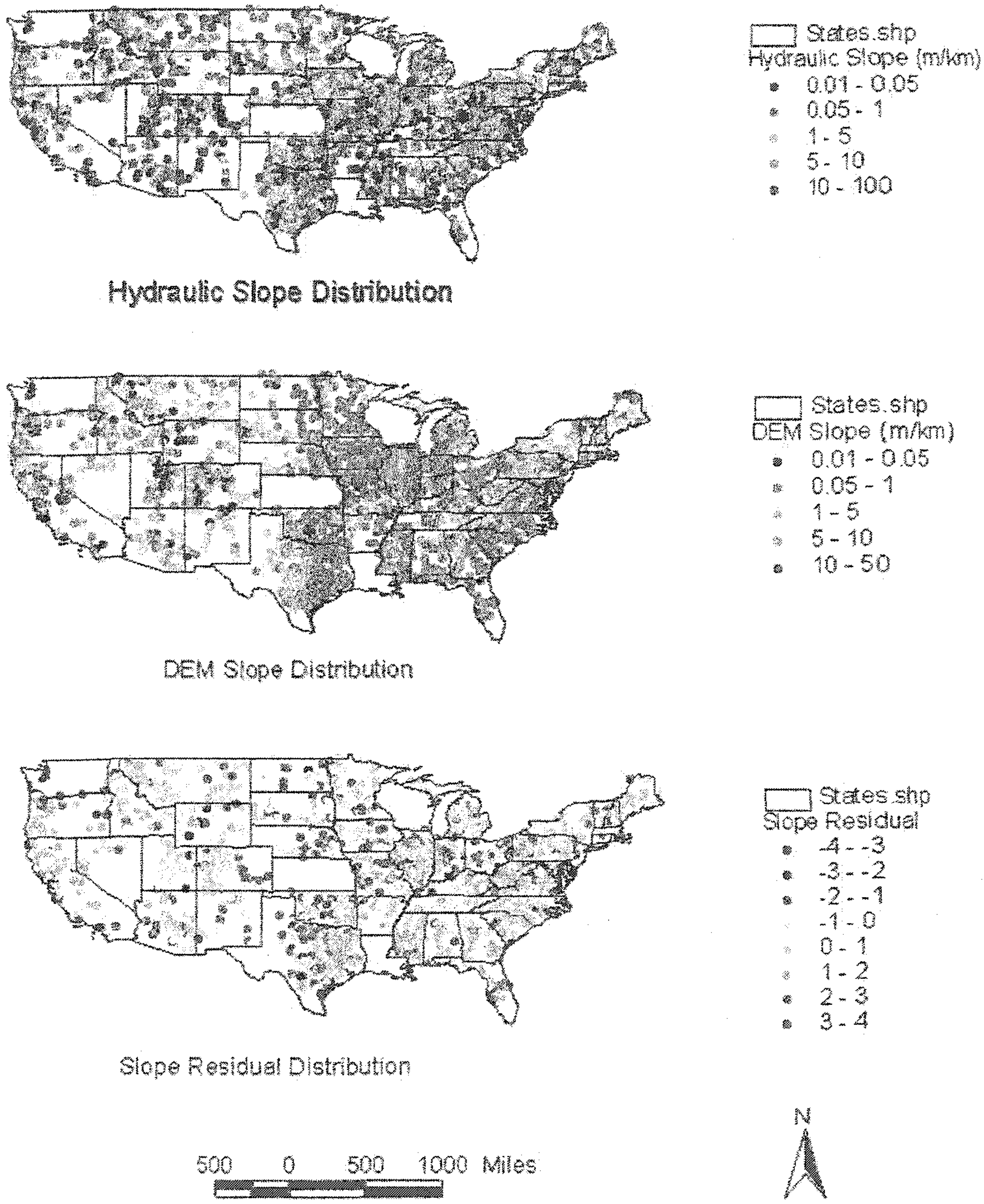

Figure 5.1 – Distribution of the hydraulic slope, DEM slope and the slope residual determined at 2,223 gaging stations in the continental United States.

Table 5.1 - Mean and Standard Deviation of the Log Residuals

Percent of Data	Condition		Residuals Slope $\log(S_{dem}/Sc)$	Model 1 $\log(Q'/Q)$	Model 2 $\log(Q'/Q)$	Model 3 $\log(Q'/Q)$
100%	All Slope Data	Mean	-0.10	0.06	-0.09	-0.04
		Stdev	0.86	0.29	0.43	0.32
90%	Upper and Lower 5% Maximum Deviation of Difference Between DEM and Characteristic Slope	Mean	-0.11	0.05	-0.08	-0.03
		Stdev	0.65	0.22	0.32	0.29
80%	Upper and Lower 10% Maximum Deviation of Difference Between DEM and Characteristic Slope	Mean	-0.12	0.05	-0.07	-0.02
		Stdev	0.53	0.18	0.26	0.27
70%	Upper and Lower 15% Maximum Deviation of Difference Between DEM and Characteristic Slope	Mean	-0.13	0.04	-0.07	-0.01
		Stdev	0.44	0.15	0.22	0.25

note:

S_{dem} = the DEM derived slope
Sc = the characteristic hydraulic slope
Q' = the predicted discharge
Q = the measured characteristic discharge

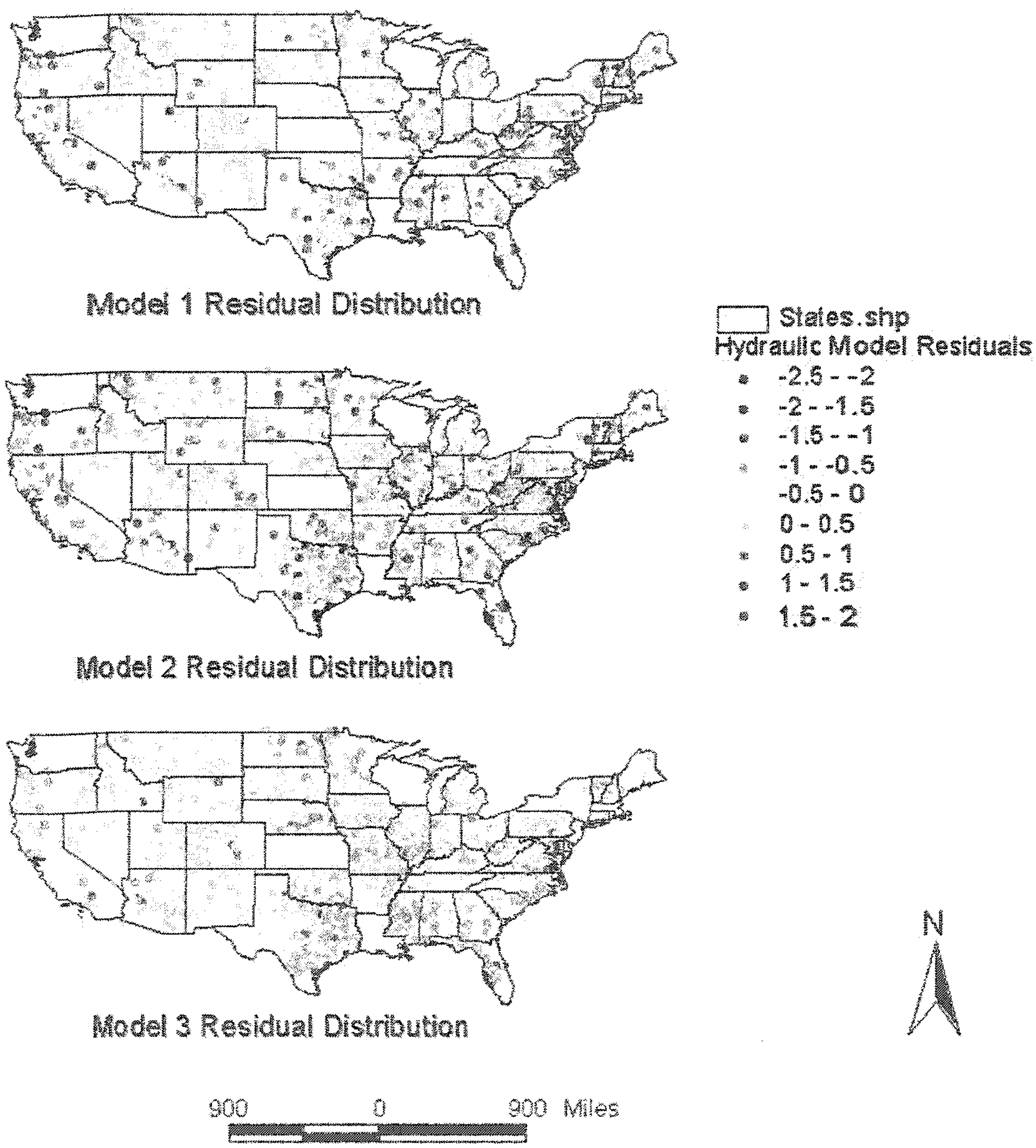

Figure 5.2 – Distribution of the discharge estimate residuals for discharge estimating Models 1, 2 and 3 determined at 2,223 gaging stations in the continental United States.

This conclusion, considering the large deviations between the DEM and hydraulic slopes, indicates that the discharge estimates using Models 1 and 2 are not highly sensitive to the slope, and that the DEM derived slope can be used in hydraulic river modeling with an acceptable level of confidence. However, given the rather large variation in DEM slopes compared to the calculated hydraulic slopes, understanding the variables that control the error could provide insight into the applicability and constraints of using the DEM slope for hydraulic modeling.

The slope residual and the residuals for each of the three models are normally distributed as seen on Figure 5.3. This indicates that inferential statistics regarding probable accuracy can be made when using the DEM derived slope and the hydraulic models. The ranked distributions also indicate that the DEM slope is unbiased relative to the hydraulic slope. This is indicated by the coincident residual distribution relative to a normal distribution with a mean of zero and the same standard deviation. However, the residuals from Models 1, 2 and 3 appear to be biased, as shown by the fact that the residuals plot either above (in the case of Model 1) or below (in the case of Model 2 and Model 3) the normal distribution. This suggests that these models could be linearly corrected by adjusting the magnitude of the coefficient of each model. However, because the models are used to predict only the mean annual flow, adjusting the model coefficients could result in greater errors for higher and lower flows if the models were used to predict a wider range of discharge at each station.

As an example, if the largest 5, 10, and 15% of the positive and negative deviations between the DEM slope and the hydraulic slope are eliminated from the data base, the discharge estimates improve significantly, as seen on Figure 5.4 and Table 5.1. This can also be seen on Figure 5.3, which shows that the largest residuals occur at the extreme ends of the ranked residual distributions for each model. Thus if the occurrence of the largest slope deviations can be

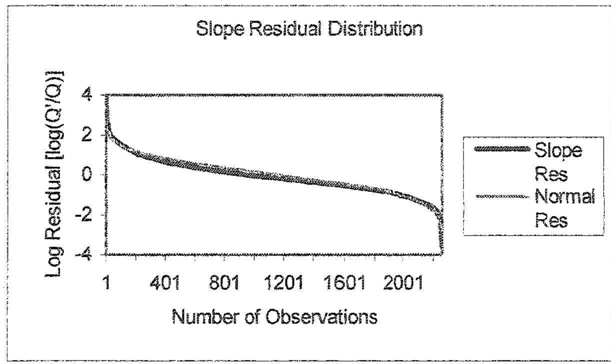

a)

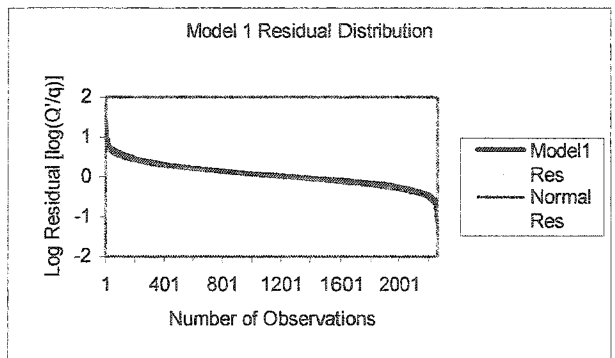

b)

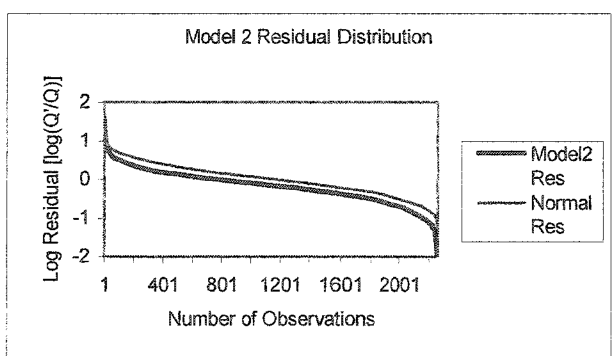

c)

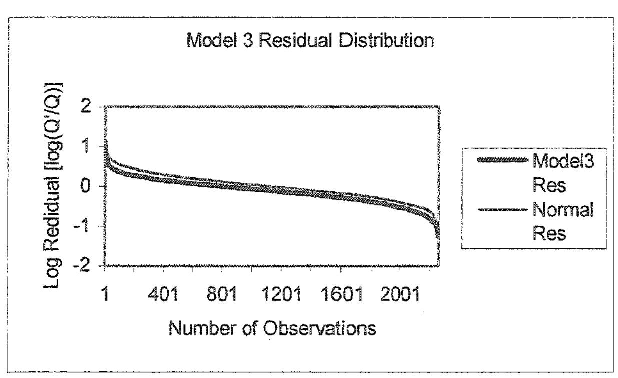

d)

Figure 5.3 – Ranked log-residual distribution for the a) DEM and hydraulic slope; b) Model 1; c) Model 2; d) Model 3, plotted with a normally distributed residual with a mean of zero and the same standard deviation for comparison.

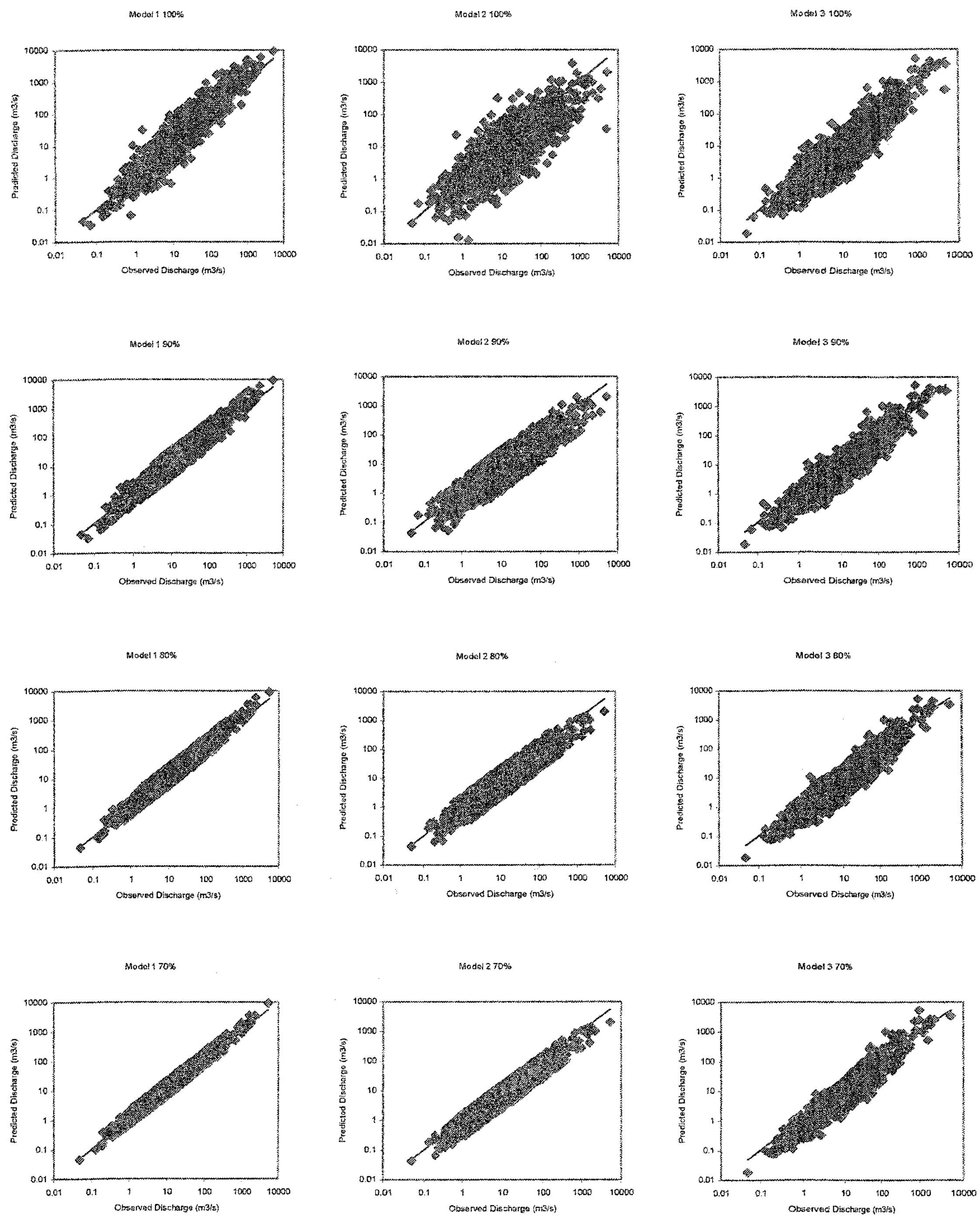

Figure 5.4 – Improvement in discharge prediction after eliminating the indicataed percentage of extreme positive and negative slope residuals.

predicted, application of the DEM slope for these streams can be understood to be subject to large error, and other slope measures obtained from maps or field surveys could be used for these reaches.

It can be reasoned that the slope deviations may be related to the variability in micro-topography that is not captured adequately by the DEM, and error associated with using the general discharge coeffcient. Based on this, an initial assumption was that the smaller streams may be subject to more small scale topographic variation. However, measures of stream size including discharge, width, and basin area did not explain very much of the variation in the deviation either individually or combined, as evidenced by low correlation coefficients and high standard errors obtained from regression analysis. A combined variable, the width times the DEM slope, provided marginal improvement in predictability. This combined term indexes both stream size and potential energy gradient. Based on this, it was reasoned that these terms would provide a good index for predicting the deviation.

The Froude number, obtained from the USGS measurements, was chosen as an indicator of the balance between inertial and gravitational (retarding) forces in the channel. As it turned out, the Froude number was much more strongly correlated to the deviations than any of the stream size indices. This is evidence that the general dishcarge coefficient, which is related to the FRoude number, can explain much of the resdual error. Since the width-slope term provided some predictability, multiple regression of the Froude number and the width-slope term were used as predictor variables, and found to provide a good predictive model of the slope residual. Inclusion of the basin area as a predictor further improved the estimating relationship, as shown on Table 5.2 and Figure 5.5.

Table 5.2 - Prediction of Log Slope Residual

Regression Equation $\log(S_{dem}/S_c) = -2.794 + 0.794(\log[WS_{dem}]) - 3.000(\log[F]) - 0.180(\log[A])$

Regression Statistics		*Coefficients*		*Standard Err*	*t Stat*	*P-value*	*Lower 95%*	*Upper 95%*
Multiple R	0.96091	Intercept	-2.794	0.028	-99.651	0.000	-2.849	-2.739
R Square	0.923348	log[WS]	0.794	0.009	93.000	0.000	0.777	0.811
Standard E	0.238142	log[F]	-2.999	0.020	-149.019	0.000	-3.039	-2.960
Observatio	2257	log[A]	-0.180	0.007	-24.285	0.000	-0.195	-0.166

notes: S_{dem} = DEM slope
S_c = characteristic hydraulic slope
W = water surface width (m)
F = Froude Number
A = Contributing basin area (km^2)

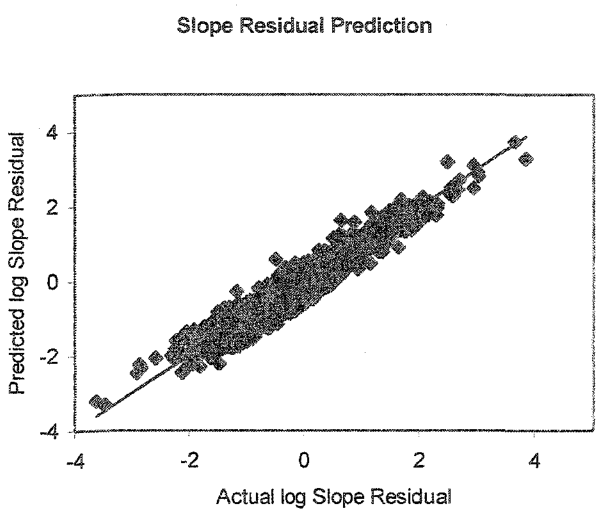

Figure 5.5 – Predicted slope residual plotted against actual slope residual.

With knowledge of the DEM derived slope, channel width and basin area, all which can be obtained remotely, coupled with a modeled or a-priori estimate of the Froude number, rivers which may provide relatively poor candidates for hydraulic modeling using the DEM slope can be identified. The question arises, however, as to the range of Froude numbers which are likely to result in relatively poor discharge estimates. This was evaluated by using the slope-deviation prediction equation with the width, basin area and DEM slope from the data base.

Keeping all of the values of width, slope, and basin area constant, and varying only the Froude number, the mean and standard deviation of the log-residual discharge-prediction errors were determined assuming various ranges of the Froude number. It was found that within a Froude number range of 0.09 to 0.45, the prediction accuracy of the models was comparable to the case where the upper and lower 10% of the ranked slope residual errors were removed from the data (Table 5.1). The mean and standard deviation, respectively, of the errors within the above Froude number range was 0.03 and 0.22 for Model 1, -0.143 and 0.34 for Model 2, and –0.1 and 0.26 for Model 3. Thus, it is concluded that the slope-residual predictive relation can provide selective knowledge about which streams can be modeled most accurately, and that relatively good predictability can be obtained for rivers that exhibit a range of Froude numbers between 0.09 and 0.45. This Froude number range is typical for many natural rivers, as evidenced by data compiled in Chapter 3 (Appendix) and as discussed by Leopold et al., (1964). Thus, if Froude numbers determined from modeling are outside of this range, the discharge estimate should be considered to be relatively inaccurate.

For comparison, a box plot of the log-residual range for the slope (slp) and the discharge prediction (Mod1, Mod2 and Mod3) have been summarized by physiographic province in the continental United States on Figure 5.6. The physiographic province boundaries were obtained from the USGS (http://www.water.usgs.gov/pub/dsdl/physio.e00.gz) and represent regions of similar topography, rock types, and geologic/geomorphologic history. The residuals for a fourth discharge estimating model (Modws) that requires only slope and width as predictor variables is also shown on Figure 5.6 to illustrate the effect of using only one dynamic variable (width) to predict the discharge. This prediction model is developed by equating Models 2 and 3 (equations 5-3 and 5-4) and then solving for the velocity. With velocity estimated, equation 5-3 is then used to estimate the discharge.

Figure 5.6 shows that Modws has the largest potential prediction bias and range of error, as anticipated. In general, the largest mean prediction bias for the other models occurs in the Atlantic plains region. The lowest prediction bias for these models occurs in western and interior regions. For Mod1, Mod2 and Mod3, the range of prediction error is greatest for Mod2, and is comparable for Mod1 and Mod3 across all regions. Mod2 also shows the largest potential (negative) bias, and Mod1 shows the largest potential for positive bias.

The slope residual shows a general low bias in the interior regions, and a high bias in the Atlantic Plains region, similar to Figure 5.1. The error in Mod1, Mod2 and Modws, which use slope as a predictor, does not always follow the slope error. This is due to the opposite predictive effective that the Froude number and the combined WS parameter have on estimating the magnitude of the slope residual. The trend and variability of the discharge-estimate residuals illustrated in Figure 5.6 indicate that the models will provide the most accurate estimates in the Interior Plains and Rocky Mountain System regions because of less variability in the slope residual. This may indicate that channel slope generally conforms to the topographic slope in these regions with less small-scale variation. Additonally, the error distribution suggests that regional adjustments to the discharge coefficients could be made to account for the observed variance. For example, in the Atlantic Plain region, a lower coefficient value using Model 1 and a higher coefficient value using Model 2 would correct much of the error using these models in this physiogrtaphic region.

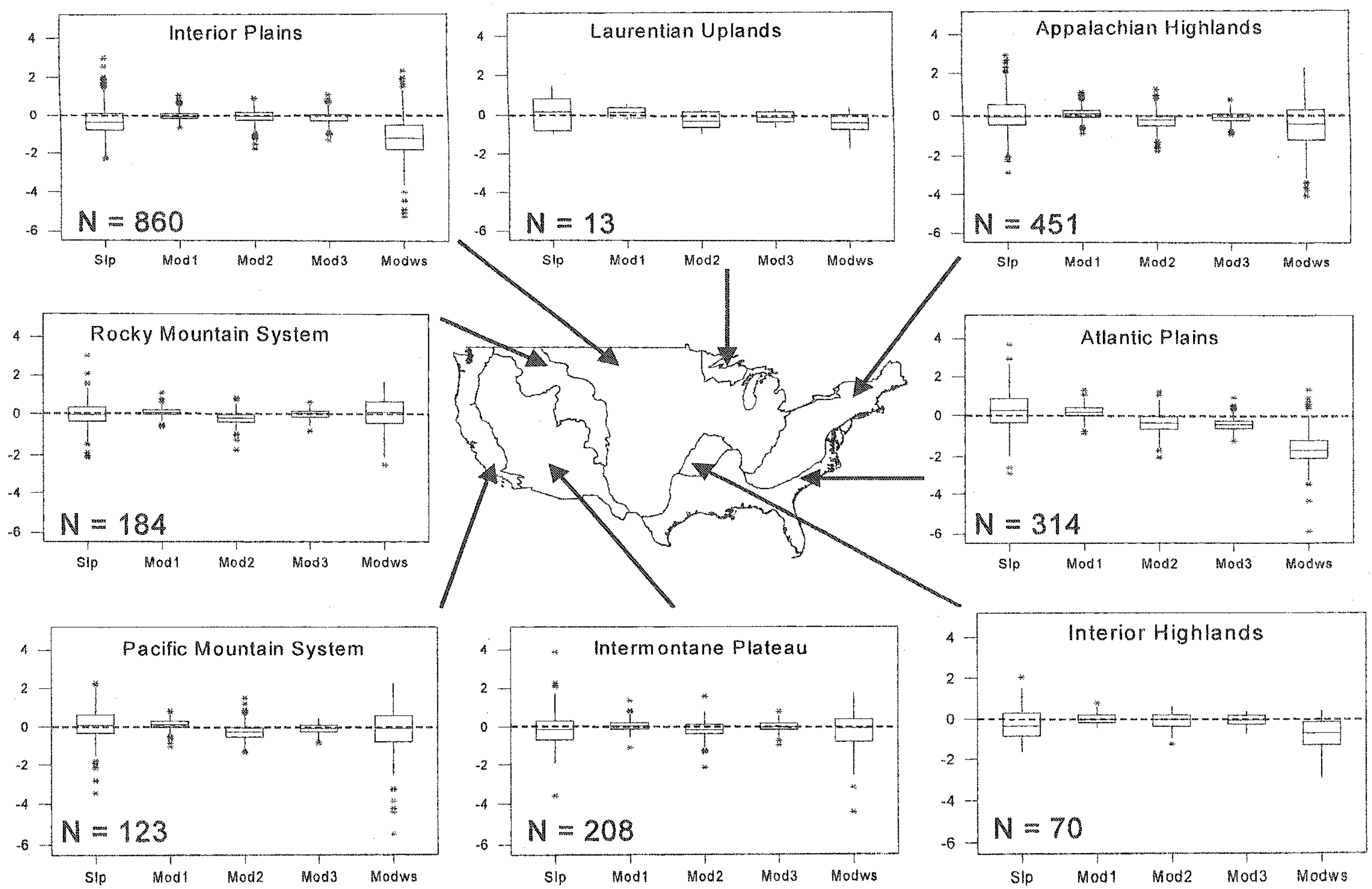

Figure 5.6 – Boxplots of the log-residual of the slope (slp), Model 1 (Mod1), Model 2 (Mod2), Model 3 (Mod3), and the width-slope model (Modws) summarizing the regional distribution.

Applying the DEM Slope to Large Scale River Modeling

The general hydraulic relationships developed in Chapter 3, used in combination, enable the discharge to be estimated from a minimum of necessary data including the maximum or bankfull channel width, the dynamic width (i.e. the water surface width at the time of the observation) and the channel slope. Conversely, these relationships can also be used to develop channel geometries if the discharge, width and slope are known. This latter capability is of special application to large-scale land-surface water-balance and runoff modeling because it provides the framework for development of realistic river-routing schemes. Assigning realistic channel geometry to the river network can also provide an estimate of the channel capacity, and hence the occurrence of over bank flooding can be modeled.

An example of the application of these relationships in this capacity can be demonstrated using a high-resolution runoff field developed by combining a water-balance runoff model (WBM) with observed discharge from ground-based discharge monitoring networks (Fekete and Vörösmarty, 2002). The mean annual discharge values are derived for a gridded river network at a 30 minute spatial resolution to obtain a mean annual discharge field for North America. An approximation of the bankfull-channel width is then estimated for every 30-minute grid cell along the river-channel network using a general regime relationship (Leopold et al, 1964) that relates the bankfull channel width with the mean annual discharge. Osterkamp and Hedman (1982) have statistically developed the coefficients of this relationship from a large data base of rivers in the Missouri River Basin

$$W_b = 8.1 Q_a^{0.58} \tag{5-7}$$

where Q_a = the mean annual discharge (m^3/s)

W_b = the bankfull or regime channel width (m).

A similar relationship correlating the bankfull width to the mean annual flood, taken to be equivalent to the bankfull discharge (Leopold et al, 1964) has also been determined from a data base of bank-full channel geometry compiled from various sources (Schumm, 1960; Barnes, 1967; Osterkamp and Hedman, 1982; Church and Rood, 1983; Dingman and Palaia, 1999) (see Chapter 3, and Appendix3). The channel geometry data were measured in the field and the bank-full discharge estimated according to various methods for 521 rivers in North America. The resulting relationship is

$$Q_b = 0.24W_b^{1.64} \qquad (5\text{-}8)$$

where Q_b = the mean annual flood (m^3/s).

The estimated bankfull width and discharge, obtained from the mean annual discharge via equations (5-7) and (5-8), are coupled with a general physically based discharge relationship (equation 3-29) to estimate the bank-full depth and velocity, thus defining the bankfull channel geometry and flow regime. For the condition where the dynamic wetted width (W) equals the bankfull width and the dynamic mean depth (Y) equals the bank-full depth, the bankfull depth can be calculated given the bankfull discharge from (equation 3-29):

$$Q = 2.74g^{0.5}WY^{1.67}S^{0.33}/Y_b^{0.17} \qquad (5\text{-}9)$$

The slope can be taken as S_{dem}, and the bankfull velocity can then be estimated from the equation of continuity, $V_b = Q_b/(W_bY_b)$. Figures 5.7 and 5.8 show the estimated mean bankfull depth and estimated mean bankfull velocity plotted as a function of the estimated bankfull discharge for grid cells coinciding with 2,256 USGS gaging stations. These are compared to similar plots obtained from the bankfull channel geometry data base.

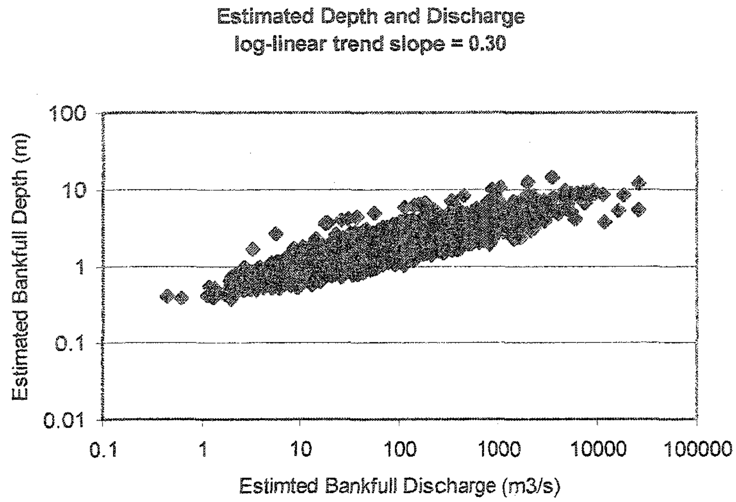

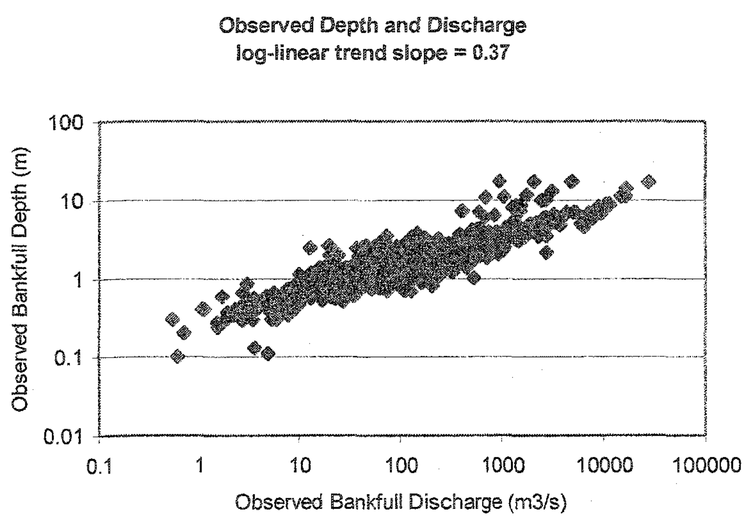

Figure 5.7 – Mean bankfull depth plotted against bankfull discharge for the estimated and observed data showing the general distribution patterns.

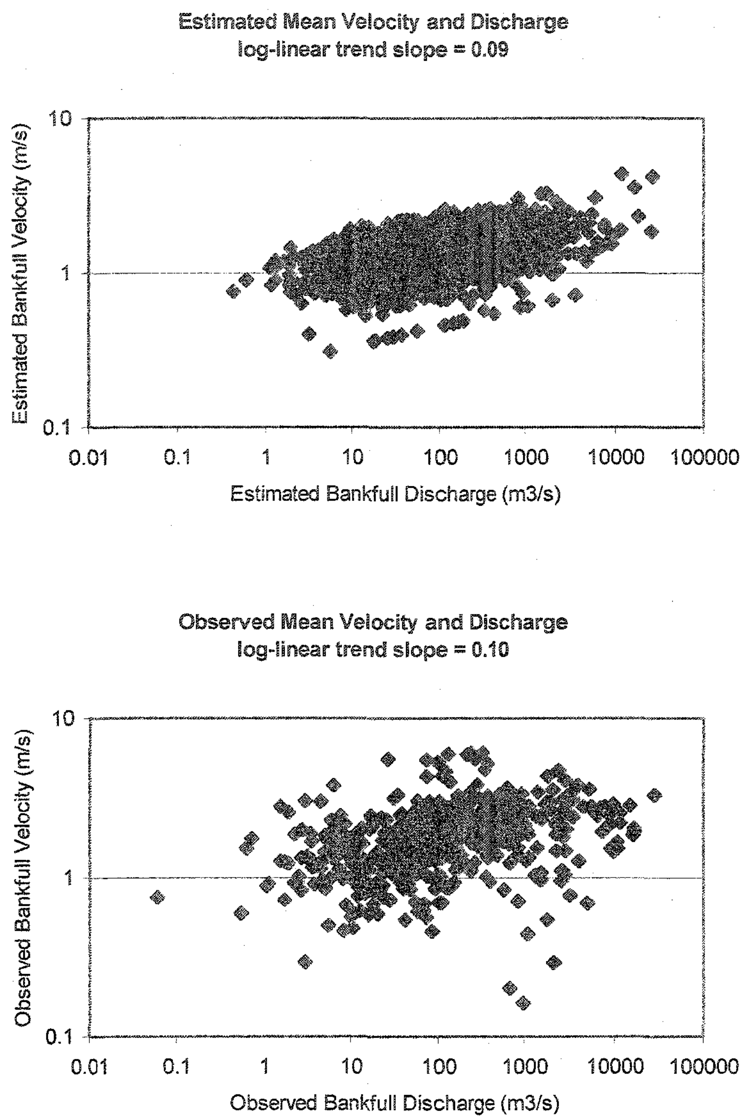

Figure 5.8 – Mean bankfull velocity plotted against bankfull discharge for
The estimated and observed data showing the general distribution patterns.

Figure 5.7 shows that the estimated depths have a similar pattern of variability compared to the observed depths, however the trend slope for the estimated values is less steep. The estimated velocities (Figure 5.8) show a similar trend compared to the observed data, but with less overall variability. In, general, the estimated depth and velocity compare well with the observed relationships.

A similar approach would combine the estimated bankfull width and discharge to calculate the bankfull velocity using a width-velocity relationship (that does not require slope) as described by equation 5-4, or other forms of Model 3 developed in Chapter 3 (Table 3.3) shown as equations (5-10) and (5-11) below:

$$Q = 0.23 W^{1.48} V^{1.45} \qquad (5\text{-}10)$$

$$Q = 0.18 W^{1.53} V^{1.85} \qquad (5\text{-}11)$$

Once velocity is estimated, the bankfull depth is calculated from continuity. The estimated bankfull depth, therefore is dependent on which equation is used to compute the mean bankfull velocity.

Histograms of the approximated values for the bankfull discharge and width developed from the mean annual discharge field for North America using equation (5-7) and (5-8) are shown on Figure 5.9. The mean width for 10043 30 minute grid cells (approximate land surface of North America) is 113 m, and for velocity and depth it is 1.59 m/s and 2.64 m using equation (5-4), 1.62 m/s and 2.32 m using equation (5-10), and 1.46 and 2.68 using equation (5-11). Figure 5.9 also shows histrograms of the approximated values for bankfull velocity and depth derived from equations (5-4), (5-10) and (5-11). Figure 5.9 indicates that bankfull velocity is much less variable than either bankfull width or depth, suggesting that it is relatively constant for a wide range of river channels. This is in agreement with general predictions of regime theory, which indicates a small velocity exponent when correlated with the bankfull discharge (Savenije, 2003; Lacey, 1935; and Leopold, 1964). However, observed values (Bray, 1979; Williams, 1978; and Church and Rood, 1983) of bankfull velocity tend to have a much wider range than predicted here or suggested by regime theory, thus the velocity derived from equation (5-1), which is based on statistical analysis of actual discharge measurements, appears to be the most realistic.

If equation (5-10) is used to estimate velocity, then the estimated depth is lower (Figure 5.7) than if equations (5-4) or (5011) are used. Thus, equation (5-10) may bet he most appropriate if the goal is to model velocity, and equations (5-4) or (5-11) would be most appropriate if the goal is to model depth. Equation (5-11) yields a greater range of velocity than equation (5-4), with a similar range of depth, thus equation (5-11) appears to provide the best overall values for both depth and velocity. The inclusion of slope in the development of the channel geometry would introduce more site specific information and would therefore result in a larger range of velocity and depth which would be more realistic, as demonstrated by Figures 5.7 and 5.8. Figure 5.10 shows the spatial distribution of the estimated bankfull width, depth and velocity assigned to the river network for North America using equations (5-7), (5-8) and (5-11).

Once the bank-full channel geometry is defined, a depth-discharge rating can also be defined. This is accomplished using equation (5-9) assuming a suitable channel cross-section shape. If a parabola is assumed, the following general discharge equation for in-bank channel depths is obtained from equation (5-9):

$$Q = 2.74g^{0.5}(W_b/Y_b^{0.67})Y^{2.17}S^{0.33} \qquad (5\text{-}12)$$

Because W_b, Y_b and S are constant values, equation (5-12) defines a unique depth-discharge rating for depths ranging from 0 to Y_b.

A depth can be calculated from equation (5-12) for any in-bank discharge estimate generated from the WBM. Given the assumed channel cross-section shape, a width and velocity can also be calculated, thus defining the necessary routing parameters for the channel network. Thus, an explicit river runoff routing scheme for the WBM model can be developed. Because the bank-full depth is prescribed, when the model-estimated discharge results in a depth exceeding this value, over bank flooding is assumed to be occurring. When over-bank flow occurs, routing can be adjusted to account for over- bank storage. Additionally, this capability can be used to evaluate

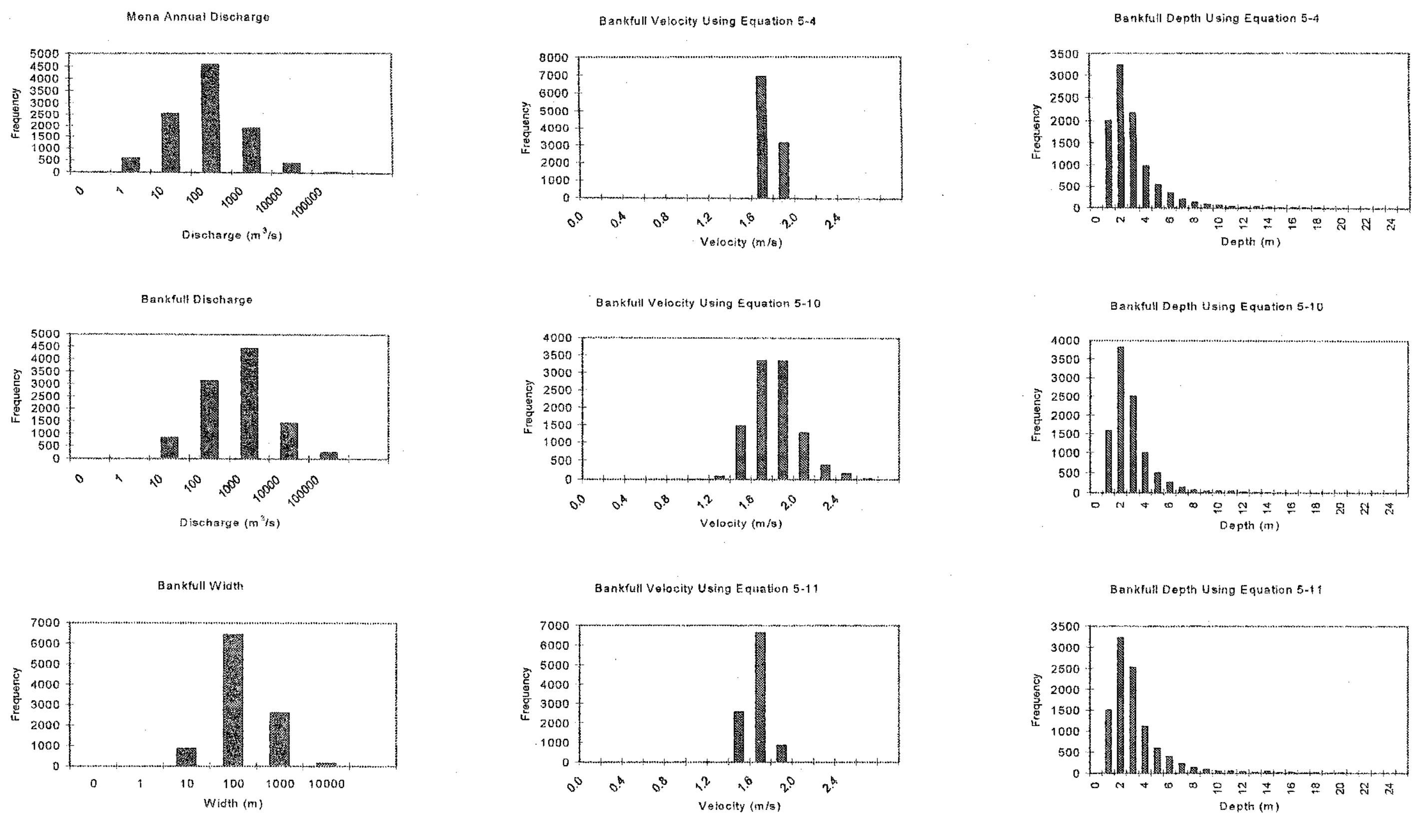

Figure 5.9 – Histograms showing the 30 minute distribution of approximated bankfull hydraulic variables for North America including discharge, width, velocity and depth. Velocity and depth distributions estimated from equations (5-4), (5-10), (5-11) are shown.

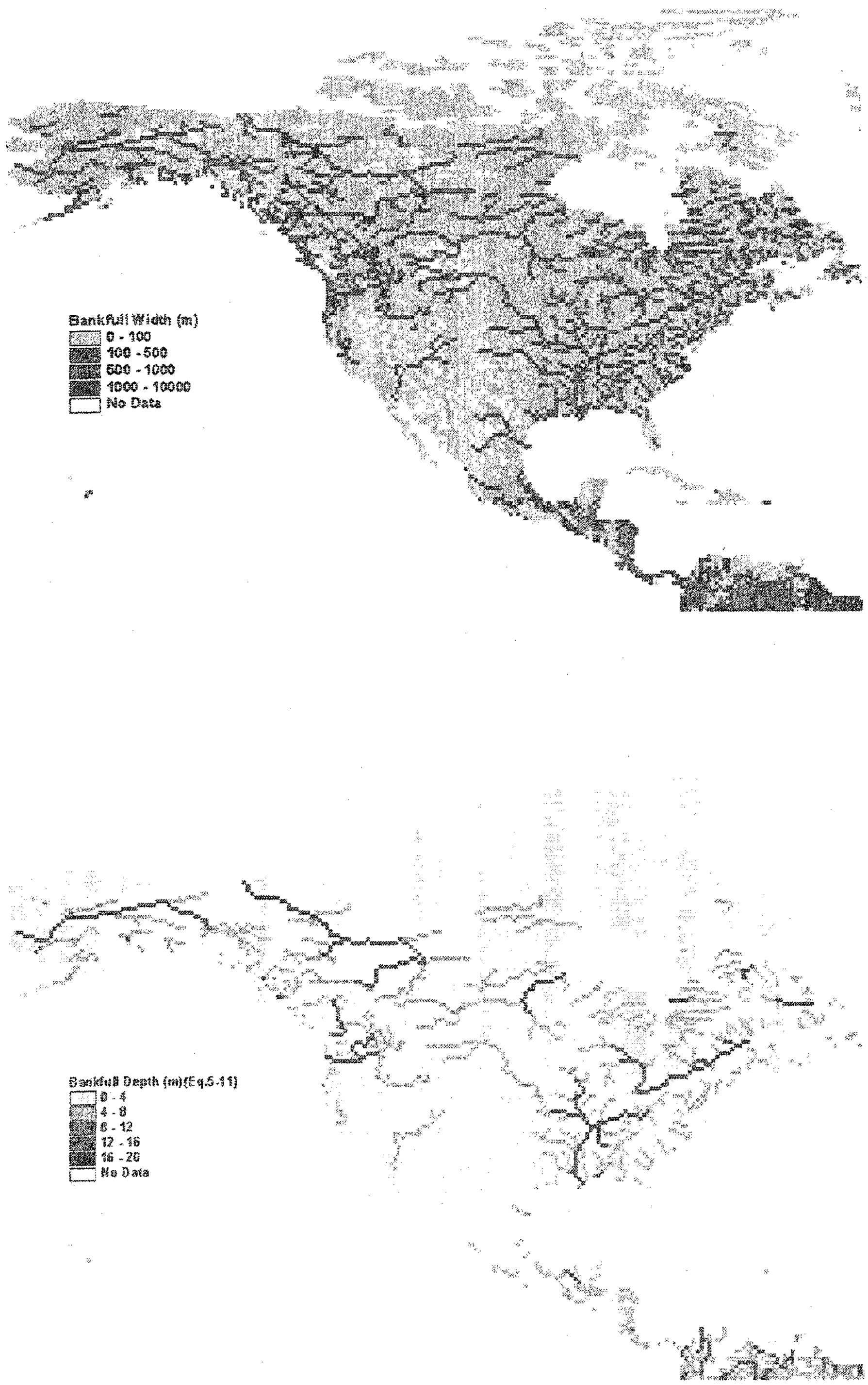

Figure 5.10 – Distribution of estimated bankfull width (top) and bankfull depth (bottom) for North America based on general width-discharge function and equation (5-11).

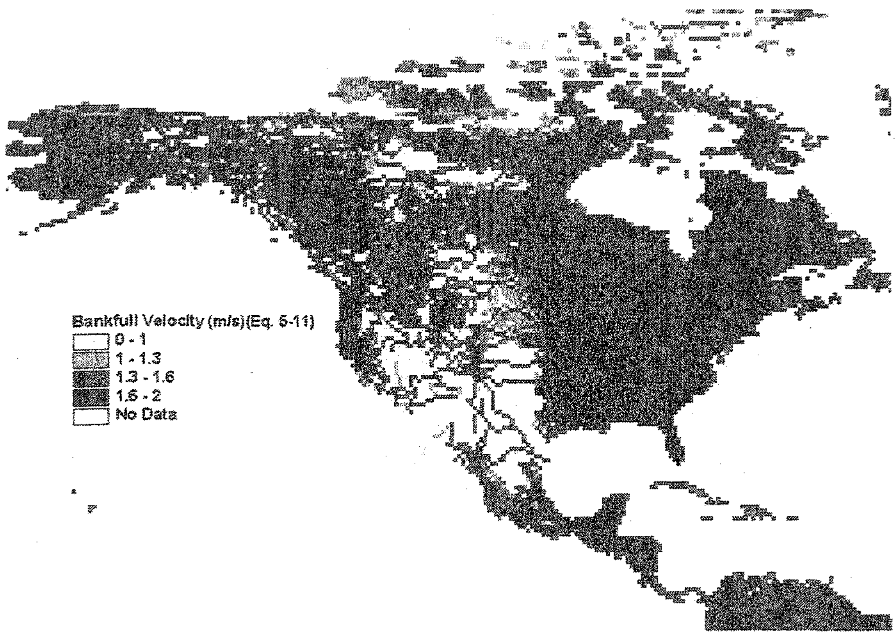

Figure 5.10 (continued)– Distribution of estimated bankfull velocity for North America based on general width-discharege function and equation (5-11).

the frequency of over bank flooding generated by the model, and coupled with the DEM, could define the areal extent of flooding.

The strategy outlined above cannot provide reach-specific rating curves because equations (5-7) and (5-8) represent relationships fitted to data from diverse geographic and hydrologic regions, with relatively large potential estimation errors. In order to evaluate the specific prediction errors associated with the procedure developed above, equation (5-9) was used to calculate the expected depth associated with the mean annual discharge, which was then compared to the observed depth associated with the mean annual discharge obtained for the 2,256 USGS gaging stations.

Figure 5.11 compares the estimated and observed mean flow depth, and shows relatively poor agreement, tending to under-estimate at high depth, and over-estimate at low depth. This suggests that the initial estimates of the bank-full width and the bank-full discharge, obtained from equations (5-7) and (5-8), do not adequately reflect the channel-specific conditions at the gaging stations. In order to provide greater site specificity, observed elements of the actual channel geometry within each reach would be needed. Bank-full widths obtained from imagery would provide sufficient additional site-specific information such that equation (5-7) would not be necessary. Additionally, if dynamic widths were also available, a unique channel cross-section shape need not be assumed, because equation (5-9), which does not assume a specific cross-section shape, could be used to develop the rating. Thus, it is anticipated that a more accurate river routing scheme can be developed by coupling the general hydraulic relationships with observed channel width (bankfull), the dynamic water-surface width and the channel slope.

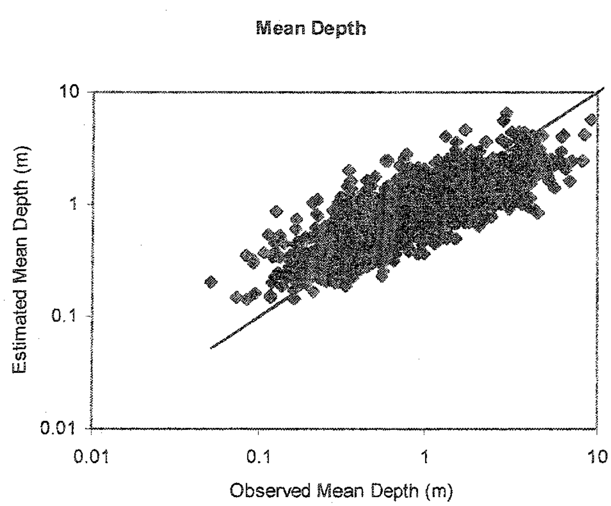

Figure 5.11 – Estimated mean depth plotted against the observed mean depth for the mean annual flow data.

Discussion

River-channel slopes developed from a 6-minute DEM using the Fekete method can be effectively used in general uniform-flow hydraulic models of river flow. This enables the large-scale application of river-flow models that require an independently derived channel slope as an input variable. General flow-routing models applied on a global or continental scale can therefore be effectively developed and linked to large-scale water-balance and runoff models. Additionally, large-scale evaluation of in-stream hydraulic conditions in rivers can be made where high accuracy in any given reach is not critical. The DEM slope could also be coupled with remotely sensed estimates of river channel and dynamic width to estimate discharge in rivers over large areas.

Errors associated with using the DEM-derived slope are normally distributed over a wide range of rivers in the United States. The magnitude of the error between the DEM slope and the functional hydraulic slope associated with each discharge measurement is a function of the DEM slope, the river width, the contributing drainage area, and the Froude number of the flow. Because the error associated with using the DEM slope in lieu of a hydraulic slope is normally distributed and predictable, straight-forward statistical evaluation of modeling results can be undertaken, and those rivers that exhibit conditions conducive to greater modeling errors can be identified.

With improvements in the accuracy of DEM models, it can be assumed that estimates of the channel slope would improve, enabling even better hydraulic-modeling results in the future. The DEM slope could also be used in conjunction with available field data and in-stream hydraulic information to develop an improved composite field of the hydraulic slope in rivers.

CHAPTER VI

SUMMARY AND CONCLUSIONS

The development of methods to estimate the discharge of rivers using remotely sensed data will provide the means to increase the streamflow measurement network globally. This component of the land-surface water-budget is currently measured at ground-based gaging stations for many of the larger rivers in populated regions, however large rivers in remote areas and small to intermediate sized rivers over much of the globe are not currently monitored. Additionally, the global river-gaging network and access to these data have been decreasing in recent years. Because of these trends, the current ground-based streamflow gaging network does not provide adequate spatial coverage for many scientific applications, including verification of the land-surface runoff contribution to the oceans and the spatial distribution of intra-continental runoff.

Calibration of continental scale runoff and climate models depend on adequate spatial density and length of streamflow records. Remote sensing of river discharge has the potential to provide this needed data by filling in gaps within the existing streamflow gaging network, and by adding new information from inaccessible regions that have not been gaged in the past. Generally applicable open-channel hydraulic equations, including the Manning and Chezy equations, have been in use for decades, and can be adapted to remote sensing applications because the dynamic constitutive elements of the equations can all be measured or potentially measured remotely, provided a general estimate of the resistance can be made.

This research has shown that much of the variance associated with resistance can be predicted and measured through its effect on other elements of flow, including depth, velocity and channel slope. In particular, the usual formulation of the Manning and Chezy equation states that velocity varies as the square root of slope, whereas this research has shown that greater variance in velocity can be explained if the cubed root of slope were used. A physical explanation of this phenomena has been developed, and modified forms of the Manning and Chezy equations described that minimize the uncertainty associated with the resistance term.

Additionally, this reseach has shown that estimating the in-bank discharge of rivers from remotely sensed hydraulic information can be accomplished with reasonable accuracy (on average within 20% of the ground measured value) given observations of reach averaged water-surface width and maximum-channel (bankfull) width coupled with channel slope. Additional information such as surface velocity, measured using Doppler lidar or SAR techniques, appear to enable much higher accuracies. Mean accuracy for large numbers of estimates can be expected to be within +/- 20% of the actual discharge, with a relatively wide range of variability. For example, the accuracy for 67% of a large number of estimates (one standard deviation) made over a wide range of rivers would be expected to be within +/- 50 to 100% depending on the model used and the data available.

Satellite and other remotely obtained images of the land surface have the capability of providing accurate measurments of the water-surface width of rivers around the globe on a nearly real-time basis. Additionally, satellite imagery and other remote sources of land-surface information can provide measurements of channel geomorphic characteristics including the bankfull (or active) channel width and the channel slope. There are potential difficulties in measuring water-surface slope; however measurement of slope from topographic information, and thus a channel constant for a particular river reach, can be used in lieu of a measured water-surface slope in discharge- estimating equations while maintaining reasonable accuracy.

There is an indication that general features of a river, such as its channel morphology and size (indicated by its maximum width), can be used to self-calibrate the estimation procedure, thereby improving the accuracy of remotely based estimates. Additionally, self-calibration methods based on the predicted Froude number also show promise with regard to improving estimate accuracy. As more river hydraulic data become available from satellites and aerial surveys, improved methods and calibration procedures can be developed. These improvements will be based on experience with large data sets of remotely sensed hydraulic and river-channel information.

Considering that traditional ground-based, non-contact discharge measurements (e.g. the slope-area method) may provide an expected accuracy in the range of +/- 20%, the mean estimate accuracy potentially provided from remotely sensed information is certainly comparable. Although discharge estimates made from aerial or satellite sensed information will likely never provide the level of accuracy that can be achieved from direct in-stream measurment of depth, velocity and width (using the velocity-area method), there are numerous applications for remote discharge estimates. Where data gaps in flow records exist, and in rivers that have poor accessibility and costs for obtaining ground-based discharge are high, satellite and aerial paltforms can be used to supplement the ground-based network. In addition, because of the potential for global coverage by satellites, relatively frequent and accurate estimates of discharge over large areas can provide much needed understanding of the spatial distribution of discharge across the continents on a near-real-time basis.

The equations and methods developed here to estimate river discharge are easily adapted to other hydrologic modeling applications. This is because they are based on general principles of open-channel flow, and therefore can be generalized to any river environment. Used in combination, the hydraulic relationships can be used to estimate river discharge from a minimum set of observed channel and hdyraulic data; conversely, they can also be used to estimate river-channel geometry and discharge ratings from estimates of discharge. Thus, the equations and relationships developed to estimate discharge from measurable hydraulic variables can be used in watershed-modeling applications to generate realistic river-routing parameters based on channel geometry, including a criteria for identifying the occurrence of overbank flow (i.e. flooding).

Although the various estimating equations and relationships developed here pertain to in-bank discharge and river flow conditions, the basic hydraulic relationships may also be adaptable to estimating discharge in overbank conditions, with adequate understanding of the variability of the discharge coefficient in these situations. Similar to the calibration of the equations for in-bank discharge, the calibration of the equations for overbank discharge will require a large and diverse data set of overbank flow measurements along with information about the nature of the flooded areas. Another key issue with regard to estimating the discharge of overbank areas would be the identification of those flooded areas where the flow direction cannot be assumed to be in the downstream direction, and identification of stagnant or flooded areas that do not contribute to downstream flow. Even though the surface area of a flooded reach can be measured remotely, and an average width determined, all of this area may not be contributing to downstream flow. This problem can be addressed through observations of surface velocity, as non-contributing reaches can be readily identified as those areas with a minimum downstream surface velocity vector.

The current generation of spaced-based and aerial imagers and sensors are adequate to measure river hydraulic variables and thus to provide estimates of river discharge. However, much of the data that is potentially available for this prupose has not been developed to provide large spatial and temporal data sets for analysis. These data sets are critical to formulating improved calibrations and more complete understanding of the error characteristics of the discharge estimates. Development of a comprehensive data set that includes remote observations of water-surface area, stage, surface velocity, channel slope and observed discharge for a large number of river reaches is particularly important.

LIST OF REFERENCES

1) Alsdorf, D.E., J.M. Melack, T. Dunne, L.A.K. Mertes, L.L. Hess and L.C. Smith, 2000. Interferometric radar measurements of water level changes on the Amazon River flood plain. Nature 404: 174 - 177.

2) Alsdorf, D.E, L.C. Smith and J.M. Melack, 2001. Amazon floodplain water level changes measured with interferometric SIR-C radar. IEEE Transactions on Geoscience and Remote Sensing 39 (2): 423-431.

3) Arcement, George J., and V.R. Schneider, 1989. Guide for selecting Mannings roughness coefficients for natural channels and flood plains, U.S. Geological Ssurvey Water-supply Paper 2339.

4) Barnes, H.H., 1967. Roughness characteristics of natural channels, USGS Water-Supply Paper 1849, 213p.

5) Barrett, E., 1998. Satellite Remote Sensing in Hydrometry. In: R.W. Herschey (Editor), Hydrometry: Principles and Practices. 2nd edition, John Wiley and Sons, Chichester, pp. 199-224.

6) Bates, P.D. and A.P.J. DeRoo, 2000. A simple raster-based model for flood inundation simulation. Journal of Hydrology 236: 54 - 77.

7) Bear, J. (1972) Dynamics of Fluids in Porous Media Flow. New York: American Elsevier.

8) Birkett, C.M., 1998. Contribution of the TOPEX NASA radar altimeter to the global monitoring of large rivers and wetlands. Water Resources Research 34 (5): 1223-1239.

9) Birkett, C.M, L.A.K. Mertes, T. Dunne, M.H. Costa and M.J. Jasinski, 2002. Surface water dynamics in the Amazon Basin: application of satellite radar altimetry. Presentation 2nd International LBA Scientific Conference, Manaus, Amazonas, Brazil july 7-10.

10) Bragg, W.L., 1913, The diffraction of short electromagnetic waves by a crystal, Proc. Cambridge Phil. Soc., 17: 43.

11) Brakenridge, G.R., J.C. Knox, E.D. Paylor and F.J. Magilligan, 1994. Radar remote sensing aids study of the Great Flood of 1993, American Geophysical Union Eos Trans., AGU 75 (45): 521-527.

12) Brakenridge, G.R., B.T. Tracy and J.C. Knox, 1998. Orbital SAR remote sensing of a river flood wave. J. Remote Sensing, 19 (7): 1439-1445.

13) Bray, D.I., 1979. Estimating average velocity in gravel-bed rivers. Journal of the Hydraulic Division ASCE HY9: 1103-1123.

14) Chow, Ven Te, 1959. Open-Channel Hydraulics. McGraw-Hill Book Company, New York. p. 680.

15) Church, M. and K. Rood, 1983. Catalogue of alluvial river channel regime data, Department of Geography, University of British Columbia, Vancouver, Canada edition 1.

16) Coon, W.F., 1998. Estimation of roughness coefficients for natural stream channels with vegetated banks. U.S. Geological Survey Water Supply Paper 2441. p. 133.

17) Costa, J.E., K.R. Spicer, R.T. Cheng, F.P. Haeni, N.B. Melcher and E.M. Thurman, 2000. Measuring stream discharge by non-contact methods: A proof-of-concept experiment. Geophysical Research Letters, 27 (4): 553-556.

18) Davidian, Jacob, 1984. Computation of water surface profiles in open channels, Book 3 Chapter A15 U.S. Geological Survey Techniques of Water-Resources Investigations p. 47.

19) Dickerson, W.T., 1967. Accuracy of discharge determinations. Hydrology Papers, Colorado State University, Fort Collins Colorado, No. 20.

20) Dingman, S.L. and K.P. Sharma, 1997. Statistical development and validation of discharge equations for natural channels. Journal of Hydrology 199:13-35.

21) Dingman, S.L., 1984 . Fluvial Hydrology. W.H. Freeman and Company, New York. p. 383.

22) Dingman, S.L. and K. Palaia, 1999. Comparison of models for estimating flood quantiles in New Hampshire and Vermont, Journal of the American Water Resources Association, 35: 1233-1243.

23) Dunne, T., L.A.K. Mertes, R.H. Meade, J.E. Richey and B.R. Forsberg, 1998. Exchanges of sediment between the floodplain and channel of the Amazon River in Brazil, GSA Bulletin 110(4):450-467.

24) Dury, G.H., 1976. Discharge prediction, present and former, from channel dimensions. Journal of Hydrology 30 (3):219-245.

25) Emmitt, G.D, 2001. Personal communication, Simpson Weather Associates, Charlottesville, VA.

26) Engelund, F., 1966. Hydraulic resistance of alluvial streams, Journal of the Hydraulic Division, American Society of Civil Engineers, HY2: 315-326.

27) Fekete, B.M., C.J. Vorosmarty and W. Grabs, 1999. Global, composite runoff fields based on observed river discharge and simulated water balance. WMO-Global Runoff Data Center Report 22. p 114.

28) Fekete, B.M., 2001. Spatial Distribution of Global Runoff and It's Storage In River Channels, unpublished PhD dissertation, University of New Hampshire.

29) Fekete, B.M., 2002. personal communication, Institure for Earth, Ocean Studies, Complex Systems Research University of New Hampshire, Durham, NH.

30) Ferguson, R.I., 1986.Hydraulics and hydraulic geometry, progress in physical geography, 10(1) pg. 1-31.

31) Frasier S.J. and A.J.Camps, 2001, Dual-beam interferometry for ocean surface current vector mapping, IEEE Transactions on Geophysical and Remote-sensing, 39(2), pg 401:414.

32) Goldstein R.M., T.P. Barnett, and H.A. Zebker, 1984, Remote Sensing of Ocean currents, Science 246 pg. 1282-1285

33) Golubstov, V.V., 1969. Soviet Hydrology: Selected Papers, Issue No. 5.

34) Hydrologic Engineering Center (1986) Accuracy of Computed Water Surface Profiles. U.S. Army Corps of Engineers Hydrologic Engineering Center Research Document 26.

35) Henderson, F.M., 1966. Open Channel Flow, MacMillan Publishing Company, New York.

36) Herschy, R.W., 1998. Flow measurement. In: R.W. Herschey (Editor), Hydrometry: Principles and Practices. 2nd edition, John Wiley and Sons, Chichester, pp. 9-83.

37) Hey, R.D., 1979. Flow resistance in gravel-bed rivers, Journal of the Hydraulics Division American Society of Civil Engineers, HY4:365-379.

38) Hicks, D.M. and P.D. Mason, 1991. Roughness Characteristics of New Zealand Rivers. New Zealand DSIR Marine and Freshwater Resources Survey, Wellington, NZ. p. 329.

39) Horritt, M.S., 2000. Calibration of a two-dimensional finite element flood flow model using satellite radar imagery, Water Resources Research 36(11):3279-3291.

40) Horritt, M.S.,D.C. Mason, and A.J. Luckman, 2001. Flood boundary delineations from synthetic aperture radar imagery using a statsitical active contour model, J. Remote Sensing, 22 (13): 2489 -2507.

41) IAHS Ad Hoc Committee, 2001. Global water data: a newly endangered species, EOS Transactions, American Geophysical Union 82 (5): 54, 56, 58.

42) Jarrett, R.D. (1984). Hydraulic of high gradient streams. ASCE Journal of Hydraulic Engineering 110:1519 - 1539.

43) Kirby, W.H., 1987.Linear error analysis of slope-area discharge determinations. Journal of Hydrology 100:315 – 339.

44) Koblinsky, C.J., R.T. Clarke, A.C.Brenner and H.Frey, 1993. Measurement of river level with satellite altimetry. Water Resources Research 29(6):1839-1848.

45) Kuprianov, V. V., 1978. Aerial methods of measuring river flow. In: Herschey (Editor), Hydrometry: Principles and Practices. 1st edition, John Wiley and Sons, Chichester, pp. 473-478.

46) Jasinski, M.J., C.M. Birkett, S. Chinn, and M.H. Costa, 2001. Abstract, NASA/NOAA GAPP and Hydrology Principal Investigators Meeting, April 30-May, Potomac MD.

47) Leliavsky, Serge 1966. An Introduction to Fluvial Hydraulics. Dover Publications New York. p. 257.

48) Leopold, L. B., R. A. Bagnold, M. G. Wolman, and L. M. Brush, Jr. (1960) Flow resistance in sinuous or irregular channels. U.S. Geological Survey Professional Paper 282-D.

49) Leopold, L.B., M.G. Wolman, and J.P. Miller, 1964. Fluvial Processes in Geomorphology. W.H. Freeman, New York. p. 522.

50) Leopold, L.B., 1994. A View of the River, Harvard University Press, London, England.

51) Knisman B., 1965, Wind waves, Prentice Hall Inc.

52) Limerinos, J.T., 1970. Determination of the Manning coefficient for measured bed roughness in natural channels, U.S. Geological Survey Water Supply Paper 1898-B.

53) Manning, R. (1889) On the flow of water in open channels and pipes. Transactions of the Institution of Civil Engineers of Ireland 20:161-207.

54) Manning, R. (1895) Supplement to 'On the flow of water in open channels and pipes'. Transactions of the Institution of Civil Engineers of Ireland 24:179-207.

55) Mertes, L.A.K., T. Dunne, and L.A. Martinelli, 1996. Channel-floodplain geomorphology along the Solimes-Amazon River, Brazil. GSA Bulletin 108 (9): 1089-1107.

56) Moller D.K., B. Pollard and E.Rodriguez 2002, Feasibiliy study for a spaceborne along-track interferometer/scatterometer, 2002 AirSAR Workshop Proceedings

57) Moller, Delwyn, 2002. NASA Jet Propulsion Laboratory, Pasadena Califronia, personal communication.

58) NASA Earth Observing System GLAS Science Team, 1997. Geoscience laser altimeter system (GLAS) science requirements. ICES-UTA-SPEC-001, GLAS-UTA-REQ-001.

59) Oltman, R.E., 1968. Reconnaissance investigations of the discharge and water quality of the Amazon River. U.S. Geological Survey Circular 552. p. 16.

60) Osterkamp, W.R. and E.R. Hedman, 1982. Perennial-streamflow characteristics related to channel geometry and sediment in Missouri River Basin, USGS Professinal Paper 1242, p. 37.

61) Osterkamp, W.R.,L.J. Lane and G.R. Foster, 1983. An analytical treatment of channel-morphology relations. U.S. Geological Survey Professional Paper 1288. p. 50.

62) Rantz, S.E. and others, 1982. Measurement and computation of streamflow: Volume 1 measurement of stage and discharge. U.S. Geological Survey Water Supply Paper 2175. p. 284.

63) Riggs, H. C., 1976. A simplified slope-area method for estimating flood discharges in natural channels. U.S. Geological Survey Journal of Research 4:285-291.

64) Rodriquez, Ernesto, 2001. personal communication, NASA/Jet Propulsion Laboratory.

65) Rosgen, D.L. 1994. A Classification of natural rivers, Catena Vol. 22: 169-199 Elsevier Science, B.V. Amsterdam.

66) Savenije, H.H.G, 2003. The width of a bankfull channel: Lacey's formula explained, Journal of Hydrology, article in press.

67) Schumm, S.A., 1960. The shape of alluvial channels in relation to sediment type, USGS Professional Paper 352-B.

68) Sippel, S.J., S.K. Hamilton, J.M. Melack and B.J. Choudhury, 1994. Determination of inundation area in the Amazon River floodplain using SMMR 37 GHz polarization difference. Remote Sensing Environment 48:70-76.

69) Smith, L.C., B.L. Isacks, A.L. Bloom and A.B. Murray, 1996. Estimation of discharge from three braided rivers using synthetic aperture radar satellite imagery. Water Resources Research 32 (7):2021-2034.

70) Smith, L. C., 1997. Satellite remote sensing of river inundation area, stage, and discharge: a review. Hydrological Processes 11: 1427 -1439.

71) University of Wisconsin Environmental Remote Sensing Center, 2001.

72) U.S. Geological Survey, 2001. NWIS Streamflow Measurement Data Base, www.water.usgs.gov/nwis/measurements .

73) Vörösmarty , C.J., C. Birkett, L. Dingman, D.P. Lettenmaier, Yunjin Kim, Ernesto Rodriguez, George D. Emmitt, William Plant and Eric Wood, 1999. NASA post-2002 land surface hydrology mission component for surface water monitoring, HYDRA_SAT. A report from the NASA Post 2002 LSHP Planning Workshop, Irvine CA April 12-14. p. 53.

74) Vörösmarty, C.J., C.J. Willlmott, B.J. Choudhury, A.L. Schloss, T.K. Stearns, S.M. Robeson, and T.J. Dorman, 1996. Analyzing the discharge regime of a large tropical river through remote sensing, ground-based climatic data and modeling. Water Resources Research 32: 3137-50.

75) webMathematica, 2002. http://www.integrals.wolfram.com, Wolfram Web Resources, Wolfram Research.

76) Williams, G.P., 1978. Bank-full discharge in rivers, Water Resources Research v. 14 no. 6:1141-1154.

APPENDIX
RIVER DISCHARGE AND CHANNEL HYDRAULIC DATA

Appendix 1 - Channel Control Flow Measurement Data

Table A1 - Channel Control Flow Measurement Data

River Name	Source	Discharge (m^3/s) Q	Width (m) W	Mean Depth (m) Y	Mean Velocity (m) V	Maximum Width (m) Wm	Maximum Depth (m) Ym	Slope (m/m) Sa	Froude Number F
Mississippi at Thebes	USGS-NWIS	27576.4	1002.7	11.21	2.45	1003	11.2	0.000137	0.233749
	USGS-NWIS	24547	1009.4	10.95	2.22	1003	11.2	0.000137	0.214305
	USGS-NWIS	19762.2	894.8	11.11	1.99	1003	11.2	0.000137	0.190714
	USGS-NWIS	14496	765	10.79	1.76	1003	11.2	0.000137	0.171155
	USGS-NWIS	12542.5	764.4	10.9	1.51	1003	11.2	0.000137	0.1461
	USGS-NWIS	10504	722.6	9.89	1.47	1003	11.2	0.000137	0.149316
	USGS-NWIS	9003.4	663.2	9.39	1.44	1003	11.2	0.000137	0.150112
	USGS-NWIS	8210.6	657.1	9.06	1.38	1003	11.2	0.000137	0.146454
	USGS-NWIS	7163.1	625.7	8.55	1.34	1003	11.2	0.000137	0.146389
	USGS-NWIS	6398.6	644.9	8.96	1.11	1003	11.2	0.000137	0.118456
	USGS-NWIS	5832.4	612	7.62	1.25	1003	11.2	0.000137	0.14465
	USGS-NWIS	5322.8	631.2	8.21	1.03	1003	11.2	0.000137	0.114829
	USGS-NWIS	4728.2	599.8	6.94	1.14	1003	11.2	0.000137	0.138233
	USGS-NWIS	4416.8	593.7	6.96	1.07	1003	11.2	0.000137	0.129559
	USGS-NWIS	4246.9	573	6.31	1.18	1003	11.2	0.000137	0.150056
	USGS-NWIS	3822.2	570.9	6.02	1.12	1003	11.2	0.000137	0.145817
	USGS-NWIS	3652.3	572.1	5.81	1.1	1003	11.2	0.000137	0.145778
	USGS-NWIS	3171	566	5.79	0.97	1003	11.2	0.000137	0.128771
	USGS-NWIS	2641.6	563.2	5.1	0.92	1003	11.2	0.000137	0.130134
	USGS-NWIS	2216.9	545	4.13	0.98	1003	11.2	0.000137	0.154042
Potomac at point of rocks	USGS-NWIS	8154	476.7	9.39	1.82	477	9.4	0.00027	0.189725
	USGS-NWIS	1687.4	333.1	3.76	1.34	477	9.4	0.00027	0.220749
	USGS-NWIS	860.7	307.2	2.55	1.1	477	9.4	0.00027	0.220044
	USGS-NWIS	543.6	300.2	2.01	0.9	477	9.4	0.00027	0.202783
	USGS-NWIS	393.5	285.9	1.63	0.84	477	9.4	0.00027	0.210171
	USGS-NWIS	328.4	258.5	1.59	0.8	477	9.4	0.00027	0.202665
	USGS-NWIS	264.4	281.3	1.43	0.66	477	9.4	0.00027	0.176304
	USGS-NWIS	213.5	276.1	1.09	0.71	477	9.4	0.00027	0.217236
	USGS-NWIS	166.8	276.7	1.09	0.55	477	9.4	0.00027	0.168282
	USGS-NWIS	140.7	246.9	1.06	0.54	477	9.4	0.00027	0.167544
	USGS-NWIS	105.9	259.1	0.9	0.45	477	9.4	0.00027	0.151523
	USGS-NWIS	91.7	288.6	0.82	0.39	477	9.4	0.00027	0.137577
	USGS-NWIS	70.8	253.3	0.6	0.46	477	9.4	0.00027	0.189701
	USGS-NWIS	69.6	235.3	0.56	0.52	477	9.4	0.00027	0.221971
	USGS-NWIS	67.1	248.4	0.66	0.4	477	9.4	0.00027	0.157281
	USGS-NWIS	59.7	240.5	0.78	0.32	477	9.4	0.00027	0.115742
	USGS-NWIS	54.9	234.4	0.53	0.44	477	9.4	0.00027	0.193064
	USGS-NWIS	48.7	221	0.48	0.46	477	9.4	0.00027	0.212092
	USGS-NWIS	34.8	235.9	0.41	0.36	477	9.4	0.00027	0.179596
	USGS-NWIS	15.6	192	0.34	0.24	477	9.4	0.00027	0.13148
Missouri at Hermann	USGS-NWIS	14439.4	602.3	10.21	1.83	602	10.2	0.00013	0.182947
	USGS-NWIS	13816.5	599.8	9.96	2.31	602	10.2	0.00013	0.233813
	USGS-NWIS	11268.4	737.6	8.61	1.77	602	10.2	0.00013	0.19269
	USGS-NWIS	8635.3	585.8	9.42	1.56	602	10.2	0.00013	0.162363
	USGS-NWIS	8323.9	437.4	10.58	1.8	602	10.2	0.00013	0.176773
	USGS-NWIS	7304.6	435.8	9.76	1.72	602	10.2	0.00013	0.175869
	USGS-NWIS	6993.2	432.8	9.27	1.74	602	10.2	0.00013	0.182556
	USGS-NWIS	6002.3	434.6	8.93	1.55	602	10.2	0.00013	0.165689
	USGS-NWIS	4954.7	424.9	8.35	1.4	602	10.2	0.00013	0.154765
	USGS-NWIS	4360.1	425.5	7.86	1.3	602	10.2	0.00013	0.148122
	USGS-NWIS	3822.2	404.1	7.03	1.33	602	10.2	0.00013	0.160236
	USGS-NWIS	3454.1	428.5	6.72	1.2	602	10.2	0.00013	0.147871
	USGS-NWIS	3001.1	424	6.53	1.09	602	10.2	0.00013	0.136256
	USGS-NWIS	2681.2	424	5.74	1.1	602	10.2	0.00013	0.146664
	USGS-NWIS	2406.6	384.6	5.94	1.05	602	10.2	0.00013	0.13762
	USGS-NWIS	2143.3	420.6	5.19	0.98	602	10.2	0.00013	0.137413
	USGS-NWIS	1865.8	303	5.55	1.11	602	10.2	0.00013	0.150509
	USGS-NWIS	1582.7	332.2	4.84	0.98	602	10.2	0.00013	0.142295
	USGS-NWIS	1274.1	324.6	3.89	1.01	602	10.2	0.00013	0.163581
	USGS-NWIS	784.3	237.1	3.66	0.96	602	10.2	0.00013	0.160294
Yukon at Stevens Village	USGS-NWIS	17836.9	597.4	12.7	2.35	698	12.4	0.000068	0.210646
	USGS-NWIS	16647.8	698	12.39	1.93	698	12.4	0.000068	0.175149
	USGS-NWIS	13165.3	644.6	11.1	1.84	698	12.4	0.000068	0.176418
	USGS-NWIS	10617.2	548.6	10.67	1.81	698	12.4	0.000068	0.177004
	USGS-NWIS	8890.1	527.3	9.94	1.7	698	12.4	0.000068	0.172243
	USGS-NWIS	7644.4	676.6	7.41	1.52	698	12.4	0.000068	0.17837
	USGS-NWIS	6540.2	655.3	7.1	1.41	698	12.4	0.000068	0.169035
	USGS-NWIS	5945.6	544	8.11	1.35	698	12.4	0.000068	0.151429

River Name	Source	Discharge (m³/s) Q	Width (m) W	Mean Depth (m) Y	Mean Velocity (m) V	Maximum Width (m) Wm	Maximum Depth (m) Ym	Slope (m/m) Sa	Froude Number F
	USGS-NWIS	4898.1	505.9	7.44	1.3	698	12.4	0.000068	0.152245
	USGS-NWIS	4530	509	7.08	1.26	698	12.4	0.000068	0.151266
	USGS-NWIS	4161.9	505.9	6.85	1.2	698	12.4	0.000068	0.146461
	USGS-NWIS	3624	527.3	6.25	1.1	698	12.4	0.000068	0.140553
	USGS-NWIS	3284.3	582.1	5.27	1.09	698	12.4	0.000068	0.151673
	USGS-NWIS	2916.2	594.3	4.67	1.05	698	12.4	0.000068	0.155209
	USGS-NWIS	1056.1	609.6	3.47	0.5	698	12.4	0.000068	0.085742
	USGS-NWIS	753.1	673.6	2.23	0.5	698	12.4	0.000068	0.106956
	USGS-NWIS	523.8	512	2.14	0.48	698	12.4	0.000068	0.104814
	USGS-NWIS	472.8	609.6	1.35	0.57	698	12.4	0.000068	0.156709
	USGS-NWIS	416.2	505.9	1.98	0.41	698	12.4	0.000068	0.093076
Willamette at Salem	USGS-NWIS	8188	516.6	7.27	2.15	517	7.3	0.00032	0.254717
	USGS-NWIS	6936.6	512.6	6.84	1.98	517	7.3	0.00032	0.241838
	USGS-NWIS	4869.8	463.3	4.85	2.17	517	7.3	0.00032	0.314757
	USGS-NWIS	4331.8	435.8	4.75	2.09	517	7.3	0.00032	0.306328
	USGS-NWIS	3793.9	289.5	6.48	2.02	517	7.3	0.00032	0.253484
	USGS-NWIS	3312.6	241.4	7.58	1.81	517	7.3	0.00032	0.210006
	USGS-NWIS	3029.4	248.4	6.62	1.84	517	7.3	0.00032	0.228442
	USGS-NWIS	2117.8	212.1	5.91	1.69	517	7.3	0.00032	0.222065
	USGS-NWIS	1922.4	206	5.46	1.71	517	7.3	0.00032	0.233769
	USGS-NWIS	1613.8	213.3	5.22	1.45	517	7.3	0.00032	0.202731
	USGS-NWIS	1373.2	207.3	4.89	1.37	517	7.3	0.00032	0.197903
	USGS-NWIS	1087.2	204.2	4.35	1.23	517	7.3	0.00032	0.188385
	USGS-NWIS	713.5	203.3	3.57	0.98	517	7.3	0.00032	0.165683
	USGS-NWIS	552.1	182.6	2.45	1.23	517	7.3	0.00032	0.25102
	USGS-NWIS	512.5	182	2.34	1.2	517	7.3	0.00032	0.250588
	USGS-NWIS	402	181	2.08	1.07	517	7.3	0.00032	0.236995
	USGS-NWIS	353.9	182.3	1.93	1.01	517	7.3	0.00032	0.232236
	USGS-NWIS	267.6	173.7	1.77	0.87	517	7.3	0.00032	0.208891
	USGS-NWIS	199.9	170.1	1.57	0.75	517	7.3	0.00032	0.191205
	USGS-NWIS	163.1	120.4	3.5	0.39	517	7.3	0.00032	0.066591
Red River of the North at Granc	USGS-NWIS	2972.8	304.8	7.92	1.17	351	7.9	0.000043	0.132804
	USGS-NWIS	2457.5	350.5	7.02	1	351	7.9	0.000043	0.120564
	USGS-NWIS	1797.8	182.9	7.62	1.29	351	7.9	0.000043	0.149279
	USGS-NWIS	1545.9	184.4	7.15	1.17	351	7.9	0.000043	0.139772
	USGS-NWIS	1285.4	182.9	6.04	1.16	351	7.9	0.000043	0.150774
	USGS-NWIS	982.4	157.3	6.26	1	351	7.9	0.000043	0.127673
	USGS-NWIS	724.8	130.4	5.58	1	351	7.9	0.000043	0.135229
	USGS-NWIS	560.6	110.3	5.27	0.93	351	7.9	0.000043	0.129409
	USGS-NWIS	526.6	91.4	5.88	0.98	351	7.9	0.000043	0.129099
	USGS-NWIS	501.1	90.5	5.52	1	351	7.9	0.000043	0.135962
	USGS-NWIS	472.8	103.6	5.32	0.86	351	7.9	0.000043	0.119105
	USGS-NWIS	421.9	88.4	5.17	0.92	351	7.9	0.000043	0.12925
	USGS-NWIS	359.6	85.3	4.69	0.9	351	7.9	0.000043	0.132753
	USGS-NWIS	302.9	84.1	4.15	0.87	351	7.9	0.000043	0.136421
	USGS-NWIS	273.5	78	4.14	0.85	351	7.9	0.000043	0.133446
	USGS-NWIS	222.5	77.4	3.53	0.81	351	7.9	0.000043	0.137716
	USGS-NWIS	193.9	76.5	3.45	0.73	351	7.9	0.000043	0.125545
	USGS-NWIS	128.3	76.2	3.18	0.53	351	7.9	0.000043	0.09494
	USGS-NWIS	98.8	74.4	3.07	0.43	351	7.9	0.000043	0.078395
	USGS-NWIS	44.5	71.3	3.33	0.19	351	7.9	0.000043	0.03326
Arkansas River at Arkansas Cit	USGS-NWIS	2265	278.6	5.14	1.58	285	5.1	0.000685	0.222619
	USGS-NWIS	2140.4	285.6	4.94	1.51	285	5.1	0.000685	0.21702
	USGS-NWIS	1874.3	285.3	4.27	1.54	285	5.1	0.000685	0.238064
	USGS-NWIS	1537.4	273.1	3.74	1.51	285	5.1	0.000685	0.249418
	USGS-NWIS	1291.1	271.3	3.63	1.3	285	5.1	0.000685	0.21796
	USGS-NWIS	971.1	266.1	2.84	1.29	285	5.1	0.000685	0.244522
	USGS-NWIS	719.1	105.2	6.15	1.11	285	5.1	0.000685	0.142979
	USGS-NWIS	475.7	179.8	2.41	1.1	285	5.1	0.000685	0.226345
	USGS-NWIS	404.9	162.5	2.22	1.12	285	5.1	0.000685	0.24012
	USGS-NWIS	342.6	139.3	4.3	0.57	285	5.1	0.000685	0.087807
	USGS-NWIS	305.8	153	1.96	1.02	285	5.1	0.000685	0.232734
	USGS-NWIS	263.9	123.7	4.7	0.45	285	5.1	0.000685	0.066306
	USGS-NWIS	246	146	1.77	0.95	285	5.1	0.000685	0.228099
	USGS-NWIS	219.4	106.7	4.06	0.51	285	5.1	0.000685	0.080853
	USGS-NWIS	174.4	149.3	1.44	0.81	285	5.1	0.000685	0.215621
	USGS-NWIS	139	151.5	1.02	0.9	285	5.1	0.000685	0.284662
	USGS-NWIS	111.8	150.6	1.12	0.66	285	5.1	0.000685	0.199215
	USGS-NWIS	74.7	135.6	0.75	0.73	285	5.1	0.000685	0.269265
	USGS-NWIS	54.9	150.3	0.63	0.58	285	5.1	0.000685	0.233424

River Name	Source	Discharge (m^3/s) Q	Width (m) W	Mean Depth (m) Y	Mean Velocity (m) V	Maximum Width (m) Wm	Maximum Depth (m) Ym	Slope (m/m) Sa	Froude Number F
	USGS-NWIS	39.4	127.1	0.64	0.48	285	5.1	0.000685	0.191663
Kuskokwim at Crooked Creek	USGS-NWIS	6189.1	408.4	7.8	1.94	442	7.8	0.000198	0.221892
	USGS-NWIS	4473.4	405.4	6.05	1.82	442	7.8	0.000198	0.236364
	USGS-NWIS	3595.7	426.7	5.44	1.55	442	7.8	0.000198	0.212285
	USGS-NWIS	3001.1	441.9	4.77	1.42	442	7.8	0.000198	0.20769
	USGS-NWIS	2641.6	389.5	5.01	1.35	442	7.8	0.000198	0.192665
	USGS-NWIS	2347.1	368.8	4.91	1.3	442	7.8	0.000198	0.187409
	USGS-NWIS	2081	381	4.39	1.24	442	7.8	0.000198	0.18905
	USGS-NWIS	1823.3	371.8	4.37	1.12	442	7.8	0.000198	0.171145
	USGS-NWIS	1528.9	349	4.31	1.01	442	7.8	0.000198	0.155407
	USGS-NWIS	1449.6	350.5	3.92	1.05	442	7.8	0.000198	0.169408
	USGS-NWIS	1435.4	362.7	4.1	0.97	442	7.8	0.000198	0.153027
	USGS-NWIS	1404.3	350.5	4.19	0.96	442	7.8	0.000198	0.149814
	USGS-NWIS	1217.4	347.5	3.88	0.9	442	7.8	0.000198	0.145953
	USGS-NWIS	1078.7	327.6	3.88	0.85	442	7.8	0.000198	0.137845
	USGS-NWIS	730.5	381	4.34	0.44	442	7.8	0.000198	0.067468
	USGS-NWIS	560.6	411.5	3.84	0.35	442	7.8	0.000198	0.057054
	USGS-NWIS	515.3	362.7	2.87	0.49	442	7.8	0.000198	0.092394
	USGS-NWIS	498.3	364.8	2.88	0.47	442	7.8	0.000198	0.088468
	USGS-NWIS	376.6	350.5	3.23	0.33	442	7.8	0.000198	0.058654
Platte near Agency	USGS-NWIS	965.5	156	4.59	1.35	156	4.6	0.00046	0.201286
	USGS-NWIS	707.8	137.2	3.35	1.54	156	4.6	0.00046	0.268773
	USGS-NWIS	622.9	134.1	3.38	1.37	156	4.6	0.00046	0.23804
	USGS-NWIS	404.9	53	5.8	1.32	156	4.6	0.00046	0.175084
	USGS-NWIS	396.4	106.7	3.14	1.18	156	4.6	0.00046	0.212718
	USGS-NWIS	393.5	64	6.49	0.95	156	4.6	0.00046	0.119121
	USGS-NWIS	390.7	103.6	3.43	1.1	156	4.6	0.00046	0.189729
	USGS-NWIS	314.3	57	4.48	1.23	156	4.6	0.00046	0.185632
	USGS-NWIS	222.8	48.8	5.09	0.9	156	4.6	0.00046	0.12743
	USGS-NWIS	119.2	53.6	3.19	0.7	156	4.6	0.00046	0.125196
	USGS-NWIS	82.7	48.2	2.76	0.62	156	4.6	0.00046	0.119213
	USGS-NWIS	54.4	44.5	2.78	0.44	156	4.6	0.00046	0.084298
	USGS-NWIS	45.6	41.8	2.38	0.46	156	4.6	0.00046	0.095248
	USGS-NWIS	39.1	39.6	1.5	0.66	156	4.6	0.00046	0.172141
	USGS-NWIS	30.9	43.3	1.21	0.59	156	4.6	0.00046	0.171335
	USGS-NWIS	23.4	41.5	1.1	0.52	156	4.6	0.00046	0.158378
	USGS-NWIS	19.5	43.3	3.22	0.14	156	4.6	0.00046	0.024922
	USGS-NWIS	12.9	34.7	2.91	0.13	156	4.6	0.00046	0.024344
	USGS-NWIS	5.6	26.8	0.58	0.36	156	4.6	0.00046	0.150999
	USGS-NWIS	3.6	24.4	0.38	0.39	156	4.6	0.00046	0.202097
Sagavanirktok near Pump Stati	USGS-NWIS	478.5	233.2	1.17	1.76	233	1.6	0.00274	0.519765
	USGS-NWIS	410.5	131.1	1.6	1.96	233	1.6	0.00274	0.494975
	USGS-NWIS	387.9	132.9	1.52	1.91	233	1.6	0.00274	0.494878
	USGS-NWIS	342.6	129.5	1.53	1.72	233	1.6	0.00274	0.444191
	USGS-NWIS	328.4	131.1	1.52	1.65	233	1.6	0.00274	0.427513
	USGS-NWIS	305.8	129.5	1.41	1.67	233	1.6	0.00274	0.449256
	USGS-NWIS	239.5	132	1.44	1.26	233	1.6	0.00274	0.33541
	USGS-NWIS	201.6	128.3	1.31	1.2	233	1.6	0.00274	0.334913
	USGS-NWIS	191.1	126.2	1.21	1.26	233	1.6	0.00274	0.365902
	USGS-NWIS	160.5	125.9	1.05	1.22	233	1.6	0.00274	0.380323
	USGS-NWIS	113.8	102.1	0.92	1.21	233	1.6	0.00274	0.402975
	USGS-NWIS	88.9	83.8	1.1	0.97	233	1.6	0.00274	0.295435
	USGS-NWIS	60.3	96.9	1.11	0.56	233	1.6	0.00274	0.169791
	USGS-NWIS	52.9	96	0.8	0.69	233	1.6	0.00274	0.246429
	USGS-NWIS	39.4	86.9	0.91	0.5	233	1.6	0.00274	0.167431
	USGS-NWIS	18	131.1	0.25	0.54	233	1.6	0.00274	0.344993
	USGS-NWIS	12.5	91.7	0.35	0.39	233	1.6	0.00274	0.21058
	USGS-NWIS	9.2	81.7	0.39	0.29	233	1.6	0.00274	0.148336
	USGS-NWIS	6.9	67.1	0.23	0.44	233	1.6	0.00274	0.293073
	USGS-NWIS	4.6	67.1	0.32	0.22	233	1.6	0.00274	0.124232
Kansas at Fort Riley	USGS-NWIS	2349.9	337.7	4.06	1.71	338	4.3	0.00049	0.271094
	USGS-NWIS	1641.8	320	4.27	1.2	338	4.3	0.00049	0.185504
	USGS-NWIS	1308	332.2	3.24	1.21	338	4.3	0.00049	0.214734
	USGS-NWIS	908.8	315.5	2.53	1.14	338	4.3	0.00049	0.228945
	USGS-NWIS	622.9	213.3	2.66	1.1	338	4.3	0.00049	0.215446
	USGS-NWIS	458.7	206.6	2.21	1	338	4.3	0.00049	0.214877
	USGS-NWIS	331.3	147.8	3.2	0.7	338	4.3	0.00049	0.125
	USGS-NWIS	305.8	195.4	1.64	0.95	338	4.3	0.00049	0.236967
	USGS-NWIS	262.2	131.1	2.59	0.77	338	4.3	0.00049	0.152837
	USGS-NWIS	234.1	96	4.18	0.58	338	4.3	0.00049	0.090621

River Name	Source	Discharge (m^3/s) Q	Width (m) W	Mean Depth (m) Y	Mean Velocity (m) V	Maximum Width (m) Wm	Maximum Depth (m) Ym	Slope (m/m) Sa	Froude Number F
	USGS-NWIS	219.7	116.9	2.63	0.7	338	4.3	0.00049	0.137882
	USGS-NWIS	190.3	178.3	1.2	0.89	338	4.3	0.00049	0.259529
	USGS-NWIS	132.5	174.6	1.01	0.76	338	4.3	0.00049	0.241568
	USGS-NWIS	103.1	171.3	0.86	0.7	338	4.3	0.00049	0.241121
	USGS-NWIS	75.6	78.3	2.09	0.46	338	4.3	0.00049	0.101642
	USGS-NWIS	47	104.5	0.75	0.6	338	4.3	0.00049	0.221313
	USGS-NWIS	35.7	92.7	0.63	0.61	338	4.3	0.00049	0.245497
	USGS-NWIS	19.3	64.3	0.55	0.55	338	4.3	0.00049	0.236902
	USGS-NWIS	12.9	59.4	0.44	0.49	338	4.3	0.00049	0.23597
Kobuk at Kiana	USGS-NWIS	4331.8	528.8	6.34	1.29	533	6.3	0.00008	0.163656
	USGS-NWIS	3765.6	533.4	6.25	1.13	533	6.3	0.00008	0.144386
	USGS-NWIS	3199.3	509	5.53	1.16	533	6.3	0.00008	0.157573
	USGS-NWIS	3086.1	475.5	5.39	1.2	533	6.3	0.00008	0.16511
	USGS-NWIS	2556.6	475.5	4.77	1.13	533	6.3	0.00008	0.165275
	USGS-NWIS	2197.1	472.4	4.64	1	533	6.3	0.00008	0.148295
	USGS-NWIS	1865.8	437.4	4.14	1.03	533	6.3	0.00008	0.161705
	USGS-NWIS	1628	463.3	4.93	0.71	533	6.3	0.00008	0.102146
	USGS-NWIS	1327.9	408.4	3.68	0.88	533	6.3	0.00008	0.146536
	USGS-NWIS	968.3	344.4	3.67	0.77	533	6.3	0.00008	0.128394
	USGS-NWIS	739	304.8	3.81	0.64	533	6.3	0.00008	0.104738
	USGS-NWIS	608.7	283.5	3.57	0.6	533	6.3	0.00008	0.101439
	USGS-NWIS	526.6	274.3	3.66	0.52	533	6.3	0.00008	0.086826
	USGS-NWIS	489.8	274.3	3.66	0.49	533	6.3	0.00008	0.081817
	USGS-NWIS	410.5	265.2	3.48	0.44	533	6.3	0.00008	0.075344
	USGS-NWIS	342.6	259.1	3.18	0.42	533	6.3	0.00008	0.075235
	USGS-NWIS	252.3	246.9	2.69	0.38	533	6.3	0.00008	0.074011
	USGS-NWIS	144.7	231.6	2.76	0.23	533	6.3	0.00008	0.044224
	USGS-NWIS	59.2	222.5	1.75	0.15	533	6.3	0.00008	0.036221
Missouri nr Culbertson	USGS-NWIS	1155.2	205.7	3.71	1.51	206	3.7	0.000156	0.250425
	USGS-NWIS	1092.9	202.7	3.14	1.72	206	3.7	0.000156	0.310063
	USGS-NWIS	761.6	204.2	3.62	1.03	206	3.7	0.000156	0.17293
	USGS-NWIS	566.3	205.7	3	0.92	206	3.7	0.000156	0.169674
	USGS-NWIS	461.5	207.3	2.58	0.86	206	3.7	0.000156	0.171031
	USGS-NWIS	396.4	198.1	2.22	0.9	206	3.7	0.000156	0.192954
	USGS-NWIS	393.5	193.5	2.52	0.81	206	3.7	0.000156	0.162994
	USGS-NWIS	365.2	192.9	2.63	0.72	206	3.7	0.000156	0.141821
	USGS-NWIS	328.4	175.9	2.4	0.78	206	3.7	0.000156	0.160833
	USGS-NWIS	297.3	192	2.23	0.69	206	3.7	0.000156	0.147599
	USGS-NWIS	275.5	160	2.43	0.71	206	3.7	0.000156	0.145493
	USGS-NWIS	239	150.9	2.28	0.69	206	3.7	0.000156	0.145972
	USGS-NWIS	213.2	164.6	2.03	0.64	206	3.7	0.000156	0.143489
	USGS-NWIS	175.3	157	1.88	0.59	206	3.7	0.000156	0.137455
	USGS-NWIS	145.8	181.3	1.28	0.63	206	3.7	0.000156	0.177878
	USGS-NWIS	144.1	181.3	1.56	0.51	206	3.7	0.000156	0.130435
	USGS-NWIS	138.4	179.8	1.36	0.57	206	3.7	0.000156	0.156132
	USGS-NWIS	116.4	117.3	1.54	0.64	206	3.7	0.000156	0.164743
	USGS-NWIS	109.3	149.3	1.75	0.42	206	3.7	0.000156	0.101419
	USGS-NWIS	98.2	172.2	1.07	0.53	206	3.7	0.000156	0.163671
S. Platte near Kersey	USGS-NWIS	436	195.1	1.91	1.17	203	1.9	0.00093	0.270431
	USGS-NWIS	402	202.7	1.72	1.16	203	1.9	0.00093	0.282541
	USGS-NWIS	207.8	139.6	1.52	0.98	203	1.9	0.00093	0.253917
	USGS-NWIS	139.6	129.8	1.32	0.82	203	1.9	0.00093	0.227969
	USGS-NWIS	72.8	105.2	0.95	0.73	203	1.9	0.00093	0.239248
	USGS-NWIS	36.5	73.1	0.61	0.82	203	1.9	0.00093	0.335379
	USGS-NWIS	33.1	72.5	0.6	0.77	203	1.9	0.00093	0.317543
	USGS-NWIS	32.3	68.9	0.64	0.73	203	1.9	0.00093	0.291487
	USGS-NWIS	28.3	65.5	0.61	0.71	203	1.9	0.00093	0.290389
	USGS-NWIS	27.6	69.5	0.56	0.71	203	1.9	0.00093	0.303076
	USGS-NWIS	24.4	71.3	0.49	0.7	203	1.9	0.00093	0.319438
	USGS-NWIS	22	66.1	0.5	0.66	203	1.9	0.00093	0.298158
	USGS-NWIS	19.6	67.7	0.45	0.64	203	1.9	0.00093	0.304762
	USGS-NWIS	15.7	57.6	0.42	0.65	203	1.9	0.00093	0.320388
	USGS-NWIS	14.4	48.5	0.47	0.64	203	1.9	0.00093	0.298207
	USGS-NWIS	13.9	57	0.4	0.61	203	1.9	0.00093	0.308097
	USGS-NWIS	13.5	47.9	0.44	0.64	203	1.9	0.00093	0.308206
	USGS-NWIS	12.2	49.7	0.41	0.6	203	1.9	0.00093	0.299327
	USGS-NWIS	10	45.1	0.36	0.61	203	1.9	0.00093	0.324762
Chena near Two Rivers	USGS-NWIS	458.3	73.1	2.9	2.16	74	2.9	0.00136	0.405174
	USGS-NWIS	311.4	73.8	2.2	1.92	74	2.9	0.00136	0.413501
	USGS-NWIS	294.5	72.8	2.21	1.83	74	2.9	0.00136	0.393226

River Name	Source	Discharge (m^3/s) Q	Width (m) W	Mean Depth (m) Y	Mean Velocity (m) V	Maximum Width (m) Wm	Maximum Depth (m) Ym	Slope (m/m) Sa	Froude Number F
	USGS-NWIS	246	71.9	1.99	1.72	74	2.9	0.00136	0.389483
	USGS-NWIS	195.1	70.1	1.72	1.62	74	2.9	0.00136	0.394582
	USGS-NWIS	171.3	65.5	1.91	1.37	74	2.9	0.00136	0.316658
	USGS-NWIS	143	68.9	1.4	1.48	74	2.9	0.00136	0.399562
	USGS-NWIS	95.1	65.8	1.32	1.1	74	2.9	0.00136	0.305839
	USGS-NWIS	80.1	66.1	1.18	1.03	74	2.9	0.00136	0.302889
	USGS-NWIS	51.5	66.1	0.96	0.81	74	2.9	0.00136	0.264081
	USGS-NWIS	45.3	69.2	0.79	0.83	74	2.9	0.00136	0.298299
	USGS-NWIS	36.5	66.1	0.83	0.66	74	2.9	0.00136	0.231415
	USGS-NWIS	32.8	67.7	0.59	0.82	74	2.9	0.00136	0.341016
	USGS-NWIS	31.7	52.1	1.29	0.47	74	2.9	0.00136	0.132187
	USGS-NWIS	30	68	0.64	0.69	74	2.9	0.00136	0.275516
	USGS-NWIS	25.3	64.9	0.63	0.62	74	2.9	0.00136	0.249522
	USGS-NWIS	23.5	65.5	0.82	0.44	74	2.9	0.00136	0.155215
	USGS-NWIS	19.1	59.1	0.34	0.96	74	2.9	0.00136	0.525919
	USGS-NWIS	15.7	56.4	0.6	0.47	74	2.9	0.00136	0.193825
Delaware at Callicoon	USGS-NWIS	1851.6	290.5	3.4	1.86	290	3.4	0.00107	0.322226
	USGS-NWIS	767.3	239.3	1.77	1.82	290	3.4	0.00107	0.43699
	USGS-NWIS	696.5	243.8	1.56	1.74	290	3.4	0.00107	0.445014
	USGS-NWIS	464.3	160.9	1.77	1.52	290	3.4	0.00107	0.364959
	USGS-NWIS	390.7	160.9	1.55	1.57	290	3.4	0.00107	0.402829
	USGS-NWIS	359.6	164.9	1.43	1.48	290	3.4	0.00107	0.395349
	USGS-NWIS	314.3	157.9	1.34	1.4	290	3.4	0.00107	0.386334
	USGS-NWIS	305.8	163.7	1.32	1.33	290	3.4	0.00107	0.369787
	USGS-NWIS	268.4	162.8	1.24	1.33	290	3.4	0.00107	0.381529
	USGS-NWIS	217.2	156	1.18	1.12	290	3.4	0.00107	0.329355
	USGS-NWIS	188.6	146.9	0.93	1.32	290	3.4	0.00107	0.43724
	USGS-NWIS	166.5	157.9	0.94	1.13	290	3.4	0.00107	0.372307
	USGS-NWIS	135.3	147.8	0.73	1.15	290	3.4	0.00107	0.429955
	USGS-NWIS	109.6	147.2	0.66	1.05	290	3.4	0.00107	0.412861
	USGS-NWIS	79.6	145.4	0.65	0.79	290	3.4	0.00107	0.313009
	USGS-NWIS	52.4	184.7	0.64	0.44	290	3.4	0.00107	0.175691
	USGS-NWIS	32.3	182.9	0.55	0.32	290	3.4	0.00107	0.137834
	USGS-NWIS	26.8	213.3	0.35	0.36	290	3.4	0.00107	0.194382
	USGS-NWIS	19.8	183.2	0.33	0.33	290	3.4	0.00107	0.183503
	USGS-NWIS	12.4	113.1	0.2	0.54	290	3.4	0.00107	0.385714
Kansas at DeSoto	USGS-NWIS	4784.8	205.7	9.71	2.4	206	9.7	0.00035	0.24603
	USGS-NWIS	4473.4	217	7.79	2.65	206	9.7	0.00035	0.303294
	USGS-NWIS	3624	187.4	8.42	2.3	206	9.7	0.00035	0.253197
	USGS-NWIS	3114.4	182.9	7.92	2.15	206	9.7	0.00035	0.244041
	USGS-NWIS	2944.5	182.9	8.03	2	206	9.7	0.00035	0.225455
	USGS-NWIS	1990.4	175.3	7.1	1.6	206	9.7	0.00035	0.191813
	USGS-NWIS	1823.3	178.3	6.1	1.68	206	9.7	0.00035	0.217286
	USGS-NWIS	1625.1	178	5.38	1.7	206	9.7	0.00035	0.234123
	USGS-NWIS	1415.6	175.3	5.27	1.53	206	9.7	0.00035	0.212899
	USGS-NWIS	1192	175.9	4.91	1.38	206	9.7	0.00035	0.198941
	USGS-NWIS	971.1	170.7	4.33	1.31	206	9.7	0.00035	0.201101
	USGS-NWIS	671	172.2	3.71	1.05	206	9.7	0.00035	0.174136
	USGS-NWIS	535.1	170.7	3.1	1.01	206	9.7	0.00035	0.183243
	USGS-NWIS	492.6	171.9	2.8	1.02	206	9.7	0.00035	0.194719
	USGS-NWIS	419	169.8	2.23	1.11	206	9.7	0.00035	0.237442
	USGS-NWIS	353.9	163.4	2.14	1.01	206	9.7	0.00035	0.220547
	USGS-NWIS	294.5	167	1.94	0.91	206	9.7	0.00035	0.208702
	USGS-NWIS	213.8	164	1.68	0.77	206	9.7	0.00035	0.189768
	USGS-NWIS	106.2	151.5	1.21	0.58	206	9.7	0.00035	0.168431
	USGS-NWIS	50.4	142.6	0.78	0.45	206	9.7	0.00035	0.162762
Neuse near Clayton	USGS-NWIS	648.4	96	5.02	1.35	96	5	0.00028	0.192473
	USGS-NWIS	489.8	95.7	4.07	1.26	96	5	0.00028	0.199508
	USGS-NWIS	461.5	78.6	5.13	1.14	96	5	0.00028	0.16078
	USGS-NWIS	370.9	92.3	3.41	1.18	96	5	0.00028	0.204123
	USGS-NWIS	269.5	74.1	3.44	1.06	96	5	0.00028	0.182563
	USGS-NWIS	211.8	72.5	2.84	1.03	96	5	0.00028	0.195238
	USGS-NWIS	190	71.6	2.81	0.94	96	5	0.00028	0.179127
	USGS-NWIS	160.5	53	3.05	0.99	96	5	0.00028	0.181081
	USGS-NWIS	140.4	51.8	2.26	1.2	96	5	0.00028	0.254985
	USGS-NWIS	107.6	45.7	2.4	0.98	96	5	0.00028	0.202073
	USGS-NWIS	71.6	46.6	2.03	0.76	96	5	0.00028	0.170393
	USGS-NWIS	49.8	48.5	1.62	0.63	96	5	0.00028	0.158114
	USGS-NWIS	36.5	45.7	1.36	0.59	96	5	0.00028	0.16161
	USGS-NWIS	32.8	41.1	1.17	0.68	96	5	0.00028	0.200818

River Name	Source	Discharge (m^3/s) Q	Width (m) W	Mean Depth (m) Y	Mean Velocity (m) V	Maximum Width (m) Wm	Maximum Depth (m) Ym	Slope (m/m) Sa	Froude Number F
	USGS-NWIS	22.2	41.1	0.97	0.56	96	5	0.00028	0.181631
	USGS-NWIS	17.3	43	0.77	0.52	96	5	0.00028	0.189298
	USGS-NWIS	15.9	42.4	0.84	0.45	96	5	0.00028	0.156841
	USGS-NWIS	13.1	40.8	0.73	0.44	96	5	0.00028	0.164505
	USGS-NWIS	10.4	38.1	0.67	0.41	96	5	0.00028	0.160005
	USGS-NWIS	7.6	41.1	0.62	0.3	96	5	0.00028	0.121706
Red R. of the North at Fargo	USGS-NWIS	792.8	204.2	4.64	0.84	204	4.8	0.00009	0.124568
	USGS-NWIS	724.8	193.5	4.78	0.78	204	4.8	0.00009	0.113964
	USGS-NWIS	702.2	189	4.65	0.8	204	4.8	0.00009	0.118509
	USGS-NWIS	654	180.4	4.26	0.85	204	4.8	0.00009	0.131553
	USGS-NWIS	557.8	167	4.34	0.77	204	4.8	0.00009	0.118068
	USGS-NWIS	532.3	178.3	4.08	0.73	204	4.8	0.00009	0.115446
	USGS-NWIS	506.8	176.8	3.87	0.74	204	4.8	0.00009	0.120161
	USGS-NWIS	447.3	164.6	3.6	0.76	204	4.8	0.00009	0.127953
	USGS-NWIS	342.6	152.7	3.41	0.66	204	4.8	0.00009	0.11417
	USGS-NWIS	308.6	142.6	3.1	0.72	204	4.8	0.00009	0.130629
	USGS-NWIS	278	109.7	3.67	0.69	204	4.8	0.00009	0.115054
	USGS-NWIS	250	108.2	3.35	0.69	204	4.8	0.00009	0.120424
	USGS-NWIS	200.7	91.4	3.23	0.68	204	4.8	0.00009	0.120863
	USGS-NWIS	185.7	85.3	3.25	0.67	204	4.8	0.00009	0.118719
	USGS-NWIS	163.1	76.2	3.75	0.57	204	4.8	0.00009	0.094026
	USGS-NWIS	132.5	73.1	3.53	0.51	204	4.8	0.00009	0.08671
	USGS-NWIS	101.9	44.2	3.47	0.66	204	4.8	0.00009	0.113179
	USGS-NWIS	74.7	39.6	3.21	0.59	204	4.8	0.00009	0.105193
	USGS-NWIS	45.6	43.9	3.01	0.34	204	4.8	0.00009	0.062601
	USGS-NWIS	35.4	37.8	2.24	0.42	204	4.8	0.00009	0.089642
Saco at Cornish	USGS-NWIS	744.6	79.2	5.56	1.69	81	5.6	0.0006	0.228948
	USGS-NWIS	676.7	80.8	5.35	1.57	81	5.6	0.0006	0.216825
	USGS-NWIS	543.6	80.8	4.69	1.44	81	5.6	0.0006	0.212404
	USGS-NWIS	458.7	77.7	4.4	1.34	81	5.6	0.0006	0.204064
	USGS-NWIS	447.3	77.7	4.36	1.32	81	5.6	0.0006	0.201938
	USGS-NWIS	407.7	77.1	4.19	1.26	81	5.6	0.0006	0.19663
	USGS-NWIS	351.1	76.2	4	1.15	81	5.6	0.0006	0.183677
	USGS-NWIS	314.3	74.7	3.83	1.1	81	5.6	0.0006	0.179548
	USGS-NWIS	308.6	63.1	3.14	1.56	81	5.6	0.0006	0.28122
	USGS-NWIS	266.4	62.5	2.99	1.43	81	5.6	0.0006	0.264172
	USGS-NWIS	250.8	76.5	3.5	0.94	81	5.6	0.0006	0.160502
	USGS-NWIS	217.4	77.1	3.42	0.82	81	5.6	0.0006	0.141641
	USGS-NWIS	176.7	75.9	3.15	0.74	81	5.6	0.0006	0.133187
	USGS-NWIS	163.6	76.2	3.07	0.7	81	5.6	0.0006	0.127619
	USGS-NWIS	135.6	74.7	2.95	0.62	81	5.6	0.0006	0.11531
	USGS-NWIS	103.3	74.7	2.7	0.82	81	5.6	0.0006	0.159411
	USGS-NWIS	77.3	76.2	2.6	0.39	81	5.6	0.0006	0.077262
	USGS-NWIS	49.3	81.7	1.36	0.44	81	5.6	0.0006	0.120523
	USGS-NWIS	42.5	74.1	2.28	0.25	81	5.6	0.0006	0.052888
	USGS-NWIS	36	82.3	1.03	0.42	81	5.6	0.0006	0.132196
Sacramento near Red Bluff	USGS-NWIS	3708.9	377.9	5.24	1.87	378	5.2	0.000575	0.260953
	USGS-NWIS	3397.5	367.3	4.58	2.02	378	5.2	0.000575	0.301513
	USGS-NWIS	3001.1	352	4.35	1.96	378	5.2	0.000575	0.300192
	USGS-NWIS	2757.6	213.3	5.83	2.22	378	5.2	0.000575	0.293701
	USGS-NWIS	2406.6	210.3	5.48	2.09	378	5.2	0.000575	0.285196
	USGS-NWIS	2253.7	229.5	4.82	2.04	378	5.2	0.000575	0.29682
	USGS-NWIS	1970.6	204.2	4.98	1.94	378	5.2	0.000575	0.277699
	USGS-NWIS	1653.5	189	4.56	1.92	378	5.2	0.000575	0.287214
	USGS-NWIS	1376	166.1	4.42	1.87	378	5.2	0.000575	0.28413
	USGS-NWIS	1090	155.4	3.93	1.79	378	5.2	0.000575	0.288432
	USGS-NWIS	787.1	118.9	3.94	1.68	378	5.2	0.000575	0.270364
	USGS-NWIS	504	117	2.9	1.48	378	5.2	0.000575	0.277619
	USGS-NWIS	450.2	115.8	2.58	1.51	378	5.2	0.000575	0.300299
	USGS-NWIS	376.6	115.8	2.39	1.36	378	5.2	0.000575	0.281013
	USGS-NWIS	331.3	114.3	2.07	1.4	378	5.2	0.000575	0.310835
	USGS-NWIS	267.6	112.5	1.56	1.52	378	5.2	0.000575	0.388748
	USGS-NWIS	225.4	111.2	1.41	1.44	378	5.2	0.000575	0.387382
	USGS-NWIS	165.9	109.7	1.13	1.34	378	5.2	0.000575	0.402673
	USGS-NWIS	138.2	106.4	0.94	1.38	378	5.2	0.000575	0.454676
	USGS-NWIS	107	105.2	0.83	1.22	378	5.2	0.000575	0.427767
Susquehanna at Waverley	USGS-NWIS	2514.2	301.1	4.6	1.89	301	4.6	0.00048	0.281494
	USGS-NWIS	2301.8	260	3.97	2.23	301	4.6	0.00048	0.357517
	USGS-NWIS	2027.2	301.1	4.01	1.68	301	4.6	0.00048	0.267993
	USGS-NWIS	1860.1	301.1	3.52	1.76	301	4.6	0.00048	0.29966

River Name	Source	Discharge (m^3/s) Q	Width (m) W	Mean Depth (m) Y	Mean Velocity (m) V	Maximum Width (m) Wm	Maximum Depth (m) Ym	Slope (m/m) Sa	Froude Number F
	USGS-NWIS	1053.2	162.1	4.04	1.61	301	4.6	0.00048	0.255872
	USGS-NWIS	789.9	203.6	2.64	1.47	301	4.6	0.00048	0.289003
	USGS-NWIS	719.1	198.7	2.41	1.5	301	4.6	0.00048	0.308652
	USGS-NWIS	656.9	195.1	2.26	1.49	301	4.6	0.00048	0.316606
	USGS-NWIS	583.2	163.1	2.92	1.23	301	4.6	0.00048	0.229933
	USGS-NWIS	532.3	159.7	2.95	1.13	301	4.6	0.00048	0.210162
	USGS-NWIS	396.4	161.5	2.76	0.89	301	4.6	0.00048	0.171129
	USGS-NWIS	356.7	181.3	1.63	1.23	301	4.6	0.00048	0.30775
	USGS-NWIS	242.4	173.7	1.36	1.04	301	4.6	0.00048	0.284873
	USGS-NWIS	194.2	172.2	1.2	0.95	301	4.6	0.00048	0.277026
	USGS-NWIS	140.1	172.2	0.98	0.84	301	4.6	0.00048	0.271052
	USGS-NWIS	77.3	167.6	0.73	0.64	301	4.6	0.00048	0.23928
	USGS-NWIS	25.4	88.4	0.56	0.52	301	4.6	0.00048	0.221971
Tanana near Fairbanks	USGS-NWIS	2420.7	409.6	3.38	1.75	410	7.7	0.00043	0.304065
	USGS-NWIS	1922.4	156.7	7.71	1.59	410	7.7	0.00043	0.182918
	USGS-NWIS	1639.3	408.4	2.32	1.73	410	7.7	0.00043	0.362818
	USGS-NWIS	1305.2	423.7	2.12	1.46	410	7.7	0.00043	0.320311
	USGS-NWIS	1039.1	277	2.45	1.53	410	7.7	0.00043	0.312245
	USGS-NWIS	755.9	254.8	2.32	1.28	410	7.7	0.00043	0.268444
	USGS-NWIS	535.1	195.4	1.7	1.61	410	7.7	0.00043	0.394447
	USGS-NWIS	450.2	192.9	2.3	1.01	410	7.7	0.00043	0.212738
	USGS-NWIS	390.7	146.3	1.71	1.56	410	7.7	0.00043	0.381078
	USGS-NWIS	278.9	152.4	2.41	0.76	410	7.7	0.00043	0.156384
	USGS-NWIS	271.2	103	2.68	0.98	410	7.7	0.00043	0.191225
	USGS-NWIS	222.5	125	2.4	0.74	410	7.7	0.00043	0.152585
	USGS-NWIS	167.9	128.9	1.87	0.69	410	7.7	0.00043	0.161182
	USGS-NWIS	158.8	149.3	1.26	0.84	410	7.7	0.00043	0.239046
	USGS-NWIS	152.9	125	1.86	0.66	410	7.7	0.00043	0.154588
	USGS-NWIS	147.5	137.2	1.64	0.66	410	7.7	0.00043	0.16463
	USGS-NWIS	141	103.6	1.8	0.76	410	7.7	0.00043	0.180952
	USGS-NWIS	139.9	122.2	1.35	0.85	410	7.7	0.00043	0.233689
	USGS-NWIS	137	118.9	1.2	0.96	410	7.7	0.00043	0.279942
Yukon at Eagle	USGS-NWIS	15062.3	487.7	10.42	2.97	488	10.4	0.00036	0.293907
	USGS-NWIS	10957	481.6	9.14	2.49	488	10.4	0.00036	0.263095
	USGS-NWIS	6483.6	472.4	6.65	2.07	488	10.4	0.00036	0.256417
	USGS-NWIS	5294.5	470	5.79	1.94	488	10.4	0.00036	0.257543
	USGS-NWIS	4756.5	448	5.7	1.86	488	10.4	0.00036	0.248864
	USGS-NWIS	4331.8	460.2	5.13	1.83	488	10.4	0.00036	0.258095
	USGS-NWIS	3963.8	441.9	5.19	1.73	488	10.4	0.00036	0.242577
	USGS-NWIS	3510.8	417.6	5.09	1.65	488	10.4	0.00036	0.233621
	USGS-NWIS	3227.6	396.2	5.23	1.56	488	10.4	0.00036	0.217902
	USGS-NWIS	2732.2	381	4.8	1.49	488	10.4	0.00036	0.217246
	USGS-NWIS	2531.1	414.5	3.72	1.64	488	10.4	0.00036	0.271618
	USGS-NWIS	1896.9	368.8	4.31	1.19	488	10.4	0.00036	0.183103
	USGS-NWIS	787.1	438.9	1.71	1.05	488	10.4	0.00036	0.256495
	USGS-NWIS	705	449.6	2.21	0.71	488	10.4	0.00036	0.152563
	USGS-NWIS	622.9	359.6	2.3	0.75	488	10.4	0.00036	0.157974
	USGS-NWIS	506.8	344.4	2.19	0.67	488	10.4	0.00036	0.144624
	USGS-NWIS	489.8	313.9	2.94	0.53	488	10.4	0.00036	0.098739
	USGS-NWIS	475.7	214.9	3.99	0.55	488	10.4	0.00036	0.087956
	USGS-NWIS	470	320	2.66	0.55	488	10.4	0.00036	0.107723
	USGS-NWIS	407.7	297.2	2.5	0.55	488	10.4	0.00036	0.111117
Tremper	Coon, 1998	2.4	11.3	0.29	0.73	16	0.9	0.0104	0.433023
Kill	Coon, 1998	6.8	12.6	0.48	1.11	16	0.9	0.0104	0.511787
	Coon, 1998	7	12.8	0.52	1.06	16	0.9	0.0104	0.46956
	Coon, 1998	7.7	12.8	0.52	1.17	16	0.9	0.0104	0.518288
	Coon, 1998	8.9	13.1	0.56	1.2	16	0.9	0.0104	0.512241
	Coon, 1998	10.1	13.3	0.61	1.25	16	0.9	0.0104	0.511249
	Coon, 1998	16.9	14.5	0.77	1.52	16	0.9	0.0104	0.553331
	Coon, 1998	29.4	16.2	0.94	1.93	16	0.9	0.0104	0.635888
	Coon, 1998	5	12.5	0.46	0.88	16	0.9	0.0104	0.414468
	Coon, 1998	11.7	13.9	0.71	1.19	16	0.9	0.0104	0.451133
	Coon, 1998	11.9	13.9	0.71	1.21	16	0.9	0.0104	0.458715
	Coon, 1998	14	14.1	0.73	1.36	16	0.9	0.0104	0.508469
	Coon, 1998	19.6	15.3	0.86	1.5	16	0.9	0.0104	0.516689
	Coon, 1998	23.6	15.9	0.91	1.63	16	0.9	0.0104	0.545826
Moordenor	Coon, 1998	2.2	11.3	0.38	0.51	14	0.8	0.0015	0.264281
Kill	Coon, 1998	3.5	11.6	0.45	0.67	14	0.8	0.0015	0.319048
	Coon, 1998	4	11.8	0.47	0.71	14	0.8	0.0015	0.330824
	Coon, 1998	7.1	12.9	0.67	0.82	14	0.8	0.0015	0.32001

River Name	Source	Discharge (m^3/s) Q	Width (m) W	Mean Depth (m) Y	Mean Velocity (m) V	Maximum Width (m) Wm	Maximum Depth (m) Ym	Slope (m/m) Sa	Froude Number F
	Coon, 1998	9.4	13.3	0.73	0.97	14	0.8	0.0015	0.362658
	Coon, 1998	10.6	14	0.81	0.93	14	0.8	0.0015	0.330086
	Coon, 1998	11.6	14.2	0.83	0.98	14	0.8	0.0015	0.343616
Canisteo	Coon, 1998	4.1	9.2	0.58	0.77	12	1	0.00274	0.322971
River	Coon, 1998	5.8	9.4	0.62	1	12	1	0.00274	0.405687
	Coon, 1998	7.4	9.7	0.68	1.12	12	1	0.00274	0.433861
	Coon, 1998	12.8	10.5	0.81	1.51	12	1	0.00274	0.535946
	Coon, 1998	13.8	10.8	0.83	1.53	12	1	0.00274	0.536462
	Coon, 1998	14.3	11.1	0.86	1.49	12	1	0.00274	0.513244
	Coon, 1998	14.5	10.7	0.83	1.63	12	1	0.00274	0.571525
	Coon, 1998	14.6	11.1	0.86	1.54	12	1	0.00274	0.530467
	Coon, 1998	14.6	11.1	0.87	1.51	12	1	0.00274	0.517135
	Coon, 1998	14.8	11.4	0.88	1.48	12	1	0.00274	0.503973
	Coon, 1998	16	11.3	0.88	1.6	12	1	0.00274	0.544836
	Coon, 1998	16.3	11.4	0.89	1.61	12	1	0.00274	0.545152
	Coon, 1998	5	9.1	0.55	1	12	1	0.00274	0.43073
	Coon, 1998	13.8	10.9	0.84	1.5	12	1	0.00274	0.522804
	Coon, 1998	16.5	11.2	0.87	1.7	12	1	0.00274	0.582205
	Coon, 1998	17	11.8	0.93	1.55	12	1	0.00274	0.513425
	Coon, 1998	17.9	11.8	0.94	1.61	12	1	0.00274	0.530455
	Coon, 1998	19	12	0.97	1.64	12	1	0.00274	0.531918
Mill	Coon, 1998	3.1	11.6	0.35	0.76	19	1.2	0.01025	0.410361
Brook	Coon, 1998	4.8	13.2	0.45	0.81	19	1.2	0.01025	0.385714
	Coon, 1998	5.7	13.1	0.44	1	19	1.2	0.01025	0.481571
	Coon, 1998	6.1	13.4	0.44	1.03	19	1.2	0.01025	0.496018
	Coon, 1998	22.9	17.1	0.72	1.86	19	1.2	0.01025	0.700219
	Coon, 1998	48.7	18.9	1.06	2.44	19	1.2	0.01025	0.757049
	Coon, 1998	70.8	19.1	1.19	3.11	19	1.2	0.01025	0.910697
E.Branch	Coon, 1998	107.3	53.9	1.16	1.72	70	1.9	0.00842	0.510137
Ausable	Coon, 1998	119.2	57.3	1.18	1.76	70	1.9	0.00842	0.517558
River	Coon, 1998	161.9	63.7	1.32	1.92	70	1.9	0.00842	0.533828
	Coon, 1998	178.1	64.9	1.4	1.96	70	1.9	0.00842	0.52915
	Coon, 1998	248.9	68.3	1.67	2.18	70	1.9	0.00842	0.538872
	Coon, 1998	305.8	70.1	1.86	2.35	70	1.9	0.00842	0.550425
Beaver	Coon, 1998	16.3	53	0.48	0.64	68	2.6	0.00451	0.295084
Kill	Coon, 1998	71.3	57.6	0.94	1.32	68	2.6	0.00451	0.434908
	Coon, 1998	140.7	60.7	1.26	1.84	68	2.6	0.00451	0.523624
	Coon, 1998	246.6	63.4	1.7	2.29	68	2.6	0.00451	0.561045
	Coon, 1998	269.5	63.7	1.75	2.42	68	2.6	0.00451	0.584364
	Coon, 1998	286	64	1.8	2.48	68	2.6	0.00451	0.590476
	Coon, 1998	297.3	64	1.79	2.6	68	2.6	0.00451	0.620774
	Coon, 1998	560.6	66.7	2.38	3.53	68	2.6	0.00451	0.730926
	Coon, 1998	676.7	67.7	2.61	3.83	68	2.6	0.00451	0.757296
Tioughnioga	Coon, 1998	14.2	64.3	0.53	0.41	88	2.1	0.00118	0.179901
River	Coon, 1998	129.1	80.8	1.29	1.24	88	2.1	0.00118	0.34875
	Coon, 1998	153.5	82	1.39	1.34	88	2.1	0.00118	0.363065
	Coon, 1998	159.7	82.3	1.44	1.34	88	2.1	0.00118	0.356706
	Coon, 1998	171.6	82.9	1.49	1.39	88	2.1	0.00118	0.363755
	Coon, 1998	182.9	83.2	1.55	1.42	88	2.1	0.00118	0.364342
	Coon, 1998	187.1	83.5	1.54	1.46	88	2.1	0.00118	0.37582
	Coon, 1998	214.3	84.4	1.67	1.52	88	2.1	0.00118	0.375727
	Coon, 1998	281.4	86.6	1.91	1.7	88	2.1	0.00118	0.392934
	Coon, 1998	286	86.9	1.93	1.7	88	2.1	0.00118	0.390892
	Coon, 1998	305.8	87.2	1.99	1.76	88	2.1	0.00118	0.398541
	Coon, 1998	308.6	87.2	2	1.77	88	2.1	0.00118	0.399802
	Coon, 1998	322.8	87.5	2.05	1.8	88	2.1	0.00118	0.40159
Kayderasasa	Coon, 1998	24.8	24	1.13	0.91	30	1.4	0.00363	0.273457
Creek	Coon, 1998	27	24.4	1.16	0.95	30	1.4	0.00363	0.281761
	Coon, 1998	28.6	24.8	1.19	0.97	30	1.4	0.00363	0.284044
	Coon, 1998	29.7	25.1	1.2	0.98	30	1.4	0.00363	0.285774
	Coon, 1998	30	26.8	1.16	0.96	30	1.4	0.00363	0.284727
	Coon, 1998	30.3	26.7	1.16	0.98	30	1.4	0.00363	0.290659
	Coon, 1998	31.4	26.8	1.17	1	30	1.4	0.00363	0.295321
	Coon, 1998	48.1	30.2	1.37	1.16	30	1.4	0.00363	0.316581
Indian	Coon, 1998	2.8	13.9	0.43	0.47	19	0.8	0.01217	0.228955
River	Coon, 1998	3.7	14	0.44	0.61	19	0.8	0.01217	0.293759
	Coon, 1998	5.5	14.5	0.49	0.77	19	0.8	0.01217	0.351382
	Coon, 1998	6	14.4	0.49	0.86	19	0.8	0.01217	0.392453
	Coon, 1998	8.4	16.5	0.52	0.98	19	0.8	0.01217	0.434122
	Coon, 1998	9.4	16.6	0.54	1.06	19	0.8	0.01217	0.460782

River Name	Source	Discharge (m^3/s) Q	Width (m) W	Mean Depth (m) Y	Mean Velocity (m) V	Maximum Width (m) Wm	Maximum Depth (m) Ym	Slope (m/m) Sa	Froude Number F
	Coon, 1998	10.2	16.8	0.55	1.1	19	0.8	0.01217	0.473804
	Coon, 1998	12.8	17.6	0.6	1.21	19	0.8	0.01217	0.498996
	Coon, 1998	18.1	18.3	0.7	1.4	19	0.8	0.01217	0.534522
	Coon, 1998	20.3	18.6	0.74	1.48	19	0.8	0.01217	0.549582
	Coon, 1998	22.5	18.8	0.78	1.54	19	0.8	0.01217	0.557007
Sacandaga	Coon, 1998	109.6	83.2	1.47	0.89	89	2.6	0.0009	0.234487
River	Coon, 1998	112.4	83.2	1.51	0.9	89	2.6	0.0009	0.23396
	Coon, 1998	116.9	83.2	1.53	0.92	89	2.6	0.0009	0.237591
	Coon, 1998	119.5	83.2	1.54	0.93	89	2.6	0.0009	0.239392
	Coon, 1998	376.6	89	2.57	1.65	89	2.6	0.0009	0.328779
Esopus	Coon, 1998	63.4	46.6	1.12	1.22	67	4.3	0.00406	0.368246
Creek	Coon, 1998	156.3	51.8	1.62	1.86	67	4.3	0.00406	0.466812
	Coon, 1998	173.8	53	1.73	1.9	67	4.3	0.00406	0.461442
	Coon, 1998	246.3	54.9	2.01	2.23	67	4.3	0.00406	0.502451
	Coon, 1998	255.7	54.6	1.97	2.37	67	4.3	0.00406	0.539389
	Coon, 1998	345.4	56.7	2.31	2.64	67	4.3	0.00406	0.554862
	Coon, 1998	1058.9	64.9	3.79	4.3	67	4.3	0.00406	0.705563
	Coon, 1998	1463.8	67.1	4.28	5.1	67	4.3	0.00406	0.787472
E.B. Delaware	Coon, 1998	40.2	32	0.96	1.31	39	2.1	0.00202	0.427093
River	Coon, 1998	52.1	32.9	1.09	1.45	39	2.1	0.00202	0.443651
	Coon, 1998	56.3	33.2	1.26	1.34	39	2.1	0.00202	0.381335
	Coon, 1998	59.5	33.5	1.16	1.54	39	2.1	0.00202	0.45675
	Coon, 1998	81	34.7	1.42	1.65	39	2.1	0.00202	0.44231
	Coon, 1998	186.9	39.3	2.14	2.22	39	2.1	0.00202	0.484767
Oueleot	Coon, 1998	27.4	23.6	0.84	1.38	28	1.1	0.00836	0.480979
River	Coon, 1998	30	24	0.86	1.45	28	1.1	0.00836	0.499466
	Coon, 1998	31.1	24	0.86	1.51	28	1.1	0.00836	0.520133
	Coon, 1998	33.7	24.8	0.91	1.5	28	1.1	0.00836	0.502293
	Coon, 1998	40.2	25.9	0.95	1.64	28	1.1	0.00836	0.537488
	Coon, 1998	41.1	26.3	0.96	1.62	28	1.1	0.00836	0.528161
	Coon, 1998	44.2	27	1.01	1.63	28	1.1	0.00836	0.5181
	Coon, 1998	47	27.3	1.03	1.67	28	1.1	0.00836	0.525636
	Coon, 1998	47.6	26.9	1.03	1.72	28	1.1	0.00836	0.541373
	Coon, 1998	50.4	28	1.05	1.71	28	1.1	0.00836	0.533075
	Coon, 1998	53.2	28.2	1.06	1.77	28	1.1	0.00836	0.549171
	Coon, 1998	24.8	23.2	0.81	1.33	28	1.1	0.00836	0.472059
	Coon, 1998	29.7	23.7	0.86	1.46	28	1.1	0.00836	0.50291
	Coon, 1998	36.5	24.9	0.94	1.56	28	1.1	0.00836	0.513982
	Coon, 1998	45.6	27.1	1.03	1.64	28	1.1	0.00836	0.516193
	Coon, 1998	45.9	27	1.02	1.67	28	1.1	0.00836	0.528206
	Coon, 1998	49.5	27.9	1.05	1.7	28	1.1	0.00836	0.529958
Susquenhanna	Coon, 1998	100.2	57.9	1.84	0.94	60	2.3	0.00081	0.221363
River	Coon, 1998	118.9	58.5	1.95	1.04	60	2.3	0.00081	0.237905
	Coon, 1998	174.4	59.7	2.29	1.28	60	2.3	0.00081	0.270196
	Coon, 1998	194.5	60	2.43	1.33	60	2.3	0.00081	0.272543
	Coon, 1998	257.6	61.6	2.67	1.57	60	2.3	0.00081	0.306924
	Coon, 1998	294.5	62.2	2.85	1.66	60	2.3	0.00081	0.314103
	Coon, 1998	404.9	64	3.22	1.96	60	2.3	0.00081	0.348911
	Coon, 1998	537.9	66.4	3.62	2.24	60	2.3	0.00081	0.37608
	Coon, 1998	105.3	57.9	1.88	0.97	60	2.3	0.00081	0.225985
	Coon, 1998	119.2	58.5	1.97	1.03	60	2.3	0.00081	0.234418
	Coon, 1998	122.3	58.5	1.97	1.06	60	2.3	0.00081	0.241246
	Coon, 1998	126	58.5	2.02	1.07	60	2.3	0.00081	0.240489
	Coon, 1998	166.5	59.7	2.29	1.22	60	2.3	0.00081	0.257531
Unadilla	Coon, 1998	40.5	45.1	1.03	0.87	49	3.2	0.00094	0.273834
River	Coon, 1998	46.7	45.1	1.09	0.95	49	3.2	0.00094	0.290668
	Coon, 1998	51	45.1	1.17	0.97	49	3.2	0.00094	0.286461
	Coon, 1998	58.9	45.4	1.24	1.05	49	3.2	0.00094	0.301207
	Coon, 1998	63.4	45.7	1.28	1.08	49	3.2	0.00094	0.304934
	Coon, 1998	68.8	45.7	1.32	1.14	49	3.2	0.00094	0.31696
	Coon, 1998	81.3	46	1.43	1.23	49	3.2	0.00094	0.328567
	Coon, 1998	114.4	46.9	1.72	1.42	49	3.2	0.00094	0.345869
	Coon, 1998	117.5	47.2	1.76	1.42	49	3.2	0.00094	0.341916
	Coon, 1998	129.7	47.5	1.85	1.48	49	3.2	0.00094	0.347586
	Coon, 1998	131.9	47.5	1.84	1.51	49	3.2	0.00094	0.355594
	Coon, 1998	174.7	47.9	2.23	1.64	49	3.2	0.00094	0.350815
	Coon, 1998	179.2	47.9	2.25	1.66	49	3.2	0.00094	0.353512
	Coon, 1998	180.4	48.2	2.31	1.62	49	3.2	0.00094	0.340483
	Coon, 1998	234.4	48.5	2.6	1.86	49	3.2	0.00094	0.368479
	Coon, 1998	368.1	49.4	3.2	2.33	49	3.2	0.00094	0.416071

River Name	Source	Discharge (m^3/s) Q	Width (m) W	Mean Depth (m) Y	Mean Velocity (m) V	Maximum Width (m) Wm	Maximum Depth (m) Ym	Slope (m/m) Sa	Froude Number F
	Coon, 1998	51.8	45.4	1.18	0.96	49	3.2	0.00094	0.282304
	Coon, 1998	73.6	45.7	1.37	1.17	49	3.2	0.00094	0.31931
	Coon, 1998	88.9	46	1.54	1.26	49	3.2	0.00094	0.324337
	Coon, 1998	94.3	46.3	1.57	1.3	49	3.2	0.00094	0.331421
	Coon, 1998	213.5	48.5	2.47	1.78	49	3.2	0.00094	0.361792
Tiouhgnioga	Coon, 1998	39.4	56.4	0.96	0.73	66	2.5	0.00051	0.237998
River	Coon, 1998	45	56.7	1.03	0.77	66	2.5	0.00051	0.242359
	Coon, 1998	47.6	57	1.06	0.79	66	2.5	0.00051	0.24511
	Coon, 1998	54.4	57.3	1.14	0.83	66	2.5	0.00051	0.248321
	Coon, 1998	56.3	57.6	1.18	0.83	66	2.5	0.00051	0.244075
	Coon, 1998	64.8	57.9	1.27	0.88	66	2.5	0.00051	0.249441
	Coon, 1998	66	57.9	1.28	0.89	66	2.5	0.00051	0.251288
	Coon, 1998	77.9	58.8	1.41	0.94	66	2.5	0.00051	0.252875
	Coon, 1998	77.9	58.5	1.38	0.97	66	2.5	0.00051	0.263766
	Coon, 1998	79.6	58.8	1.43	0.95	66	2.5	0.00051	0.253771
	Coon, 1998	79.8	59.1	1.43	0.95	66	2.5	0.00051	0.253771
	Coon, 1998	101.6	60.3	1.63	1.03	66	2.5	0.00051	0.257709
	Coon, 1998	118.1	61.3	1.76	1.1	66	2.5	0.00051	0.264864
	Coon, 1998	122.3	61.3	1.79	1.12	66	2.5	0.00051	0.267411
	Coon, 1998	159.7	65.5	1.96	1.25	66	2.5	0.00051	0.285213
	Coon, 1998	252	66.1	2.49	1.53	66	2.5	0.00051	0.309727
Chenango	Coon, 1998	149.5	117.3	1.3	0.98	131	2.8	0.00088	0.274563
River	Coon, 1998	182.1	118.3	1.42	1.08	131	2.8	0.00088	0.289512
	Coon, 1998	187.4	118.6	1.43	1.1	131	2.8	0.00088	0.29384
	Coon, 1998	209.8	119.2	1.52	1.16	131	2.8	0.00088	0.300554
	Coon, 1998	234.1	119.8	1.57	1.25	131	2.8	0.00088	0.318674
	Coon, 1998	239.2	120.1	1.62	1.23	131	2.8	0.00088	0.308699
	Coon, 1998	253.7	120.7	1.65	1.27	131	2.8	0.00088	0.315827
	Coon, 1998	302.9	121.9	1.82	1.36	131	2.8	0.00088	0.322025
	Coon, 1998	317.1	121.9	1.84	1.42	131	2.8	0.00088	0.3344
	Coon, 1998	325.6	122.5	1.87	1.42	131	2.8	0.00088	0.331707
	Coon, 1998	385.1	124.4	2.02	1.54	131	2.8	0.00088	0.346124
	Coon, 1998	399.2	124.7	2.03	1.58	131	2.8	0.00088	0.354239
	Coon, 1998	416.2	125	2.1	1.59	131	2.8	0.00088	0.350489
	Coon, 1998	419	125	2.1	1.6	131	2.8	0.00088	0.352693
	Coon, 1998	424.7	125.3	2.11	1.6	131	2.8	0.00088	0.351857
	Coon, 1998	447.3	125.6	2.16	1.65	131	2.8	0.00088	0.358628
	Coon, 1998	569.1	127.7	2.44	1.82	131	2.8	0.00088	0.372189
	Coon, 1998	750.3	130.8	2.78	2.07	131	2.8	0.00088	0.396584
	Coon, 1998	164.2	117.6	1.37	1.02	131	2.8	0.00088	0.278373
	Coon, 1998	212.9	119.2	1.53	1.17	131	2.8	0.00088	0.302153
	Coon, 1998	231.6	120.1	1.59	1.22	131	2.8	0.00088	0.309064
	Coon, 1998	235	120.1	1.6	1.22	131	2.8	0.00088	0.308097
	Coon, 1998	270.1	121.3	1.72	1.3	131	2.8	0.00088	0.31664
Genesee	Coon, 1998	94	41.5	1.95	1.16	48	3.2	0.00038	0.265355
River	Coon, 1998	111	42.1	2.09	1.26	48	3.2	0.00038	0.27841
	Coon, 1998	151.8	44.2	2.59	1.33	48	3.2	0.00038	0.263991
	Coon, 1998	152.9	44.5	2.59	1.33	48	3.2	0.00038	0.263991
	Coon, 1998	158.6	44.5	2.59	1.38	48	3.2	0.00038	0.273915
	Coon, 1998	190.3	46	2.93	1.41	48	3.2	0.00038	0.263131
	Coon, 1998	196.2	46.3	3.01	1.41	48	3.2	0.00038	0.259611
	Coon, 1998	219.1	47.9	3.18	1.44	48	3.2	0.00038	0.25795
Trout	Coon, 1998	5.8	27.6	0.48	0.44	32	1.6	0.00269	0.202871
River	Coon, 1998	17.2	29.2	0.72	0.82	32	1.6	0.00269	0.308699
	Coon, 1998	23.5	29.5	0.81	0.98	32	1.6	0.00269	0.347833
	Coon, 1998	93.4	31.7	1.53	1.92	32	1.6	0.00269	0.495841
	Coon, 1998	107.9	31.7	1.62	2.1	32	1.6	0.00269	0.527046
Waiau at Sunnyside	Hicks and Mason 1991	21.5	64.8	1.03	0.32	83	3.1	0.00011	0.100721
	Hicks and Mason 1991	21.6	64.7	1.04	0.32	83	3.1	0.00011	0.100235
	Hicks and Mason 1991	64.3	70.7	1.47	0.62	83	3.1	0.00011	0.16335
	Hicks and Mason 1991	103	74.3	1.87	0.74	83	3.1	0.00011	0.172861
	Hicks and Mason 1991	109	73.7	1.79	0.83	83	3.1	0.00011	0.19817
	Hicks and Mason 1991	188	75.7	2.14	1.16	83	3.1	0.00011	0.253302
	Hicks and Mason 1991	210	76.8	2.33	1.17	83	3.1	0.00011	0.244847
	Hicks and Mason 1991	405	80.4	2.8	1.8	83	3.1	0.00011	0.343622
	Hicks and Mason 1991	527	83.1	3.08	2.06	83	3.1	0.00011	0.374955
Grey at Dobson	Hicks and Mason 1991	73	150.7	0.67	0.72	242	4	0.00094	0.280984
	Hicks and Mason 1991	116	158.4	0.77	0.95	242	4	0.00094	0.345832
	Hicks and Mason 1991	217	185.1	1.01	1.16	242	4	0.00094	0.368709
	Hicks and Mason 1991	334	191.2	1.25	1.4	242	4	0.00094	0.4

River Name	Source	Discharge (m^3/s) Q	Width (m) W	Mean Depth (m) Y	Mean Velocity (m) V	Maximum Width (m) Wm	Maximum Depth (m) Ym	Slope (m/m) Sa	Froude Number F
	Hicks and Mason 1991	358	193.2	1.32	1.4	242	4	0.00094	0.389249
	Hicks and Mason 1991	917	214.5	2.27	1.88	242	4	0.00094	0.398595
	Hicks and Mason 1991	1110	215	2.33	2.22	242	4	0.00094	0.464582
	Hicks and Mason 1991	3220	242.2	3.96	3.36	242	4	0.00094	0.53936
Ongarue at Taringamotu	Hicks and Mason 1991	10.5	29.7	0.87	0.41	48	3	0.00067	0.140414
	Hicks and Mason 1991	14.8	30.3	1.01	0.48	48	3	0.00067	0.152569
	Hicks and Mason 1991	18.7	30.7	1.08	0.56	48	3	0.00067	0.172133
	Hicks and Mason 1991	19.2	30.8	1.06	0.59	48	3	0.00067	0.183057
	Hicks and Mason 1991	35.1	31.8	1.31	0.84	48	3	0.00067	0.234439
	Hicks and Mason 1991	35.8	32	1.32	0.85	48	3	0.00067	0.23633
	Hicks and Mason 1991	41.7	32.2	1.38	0.94	48	3	0.00067	0.255608
	Hicks and Mason 1991	241	47.5	3.03	1.67	48	3	0.00067	0.306466
Hutt at Kaitoke	Hicks and Mason 1991	3.53	27	0.26	0.5	35	1.5	0.00473	0.313235
	Hicks and Mason 1991	8.38	28.1	0.42	0.71	35	1.5	0.00473	0.349962
	Hicks and Mason 1991	8.69	28.8	0.48	0.63	35	1.5	0.00473	0.290474
	Hicks and Mason 1991	17.2	30.3	0.67	0.85	35	1.5	0.00473	0.331718
	Hicks and Mason 1991	77.2	33.5	1.32	1.75	35	1.5	0.00473	0.486562
	Hicks and Mason 1991	104	34.8	1.45	2.06	35	1.5	0.00473	0.546475
Clarence at Jollies	Hicks and Mason 1991	7.62	31.1	0.38	0.65	37	1.4	0.00321	0.336828
	Hicks and Mason 1991	12.4	32	0.46	0.84	37	1.4	0.00321	0.395628
	Hicks and Mason 1991	17.5	32.8	0.53	1.01	37	1.4	0.00321	0.44317
	Hicks and Mason 1991	18.1	32.8	0.58	0.95	37	1.4	0.00321	0.398471
	Hicks and Mason 1991	24	33.4	0.62	1.16	37	1.4	0.00321	0.470597
	Hicks and Mason 1991	39.7	34.5	0.77	1.49	37	1.4	0.00321	0.54241
	Hicks and Mason 1991	64.8	35.4	0.99	1.85	37	1.4	0.00321	0.593938
	Hicks and Mason 1991	106	36.3	1.23	2.38	37	1.4	0.00321	0.685506
	Hicks and Mason 1991	120	36.8	1.38	2.36	37	1.4	0.00321	0.64174
Arnold at Lake Brunner	Hicks and Mason 1991	24.3	40.7	0.84	0.71	51	1.9	0.00106	0.24746
	Hicks and Mason 1991	36.8	42.6	0.98	0.88	51	1.9	0.00106	0.28396
	Hicks and Mason 1991	44.4	43.5	1.1	0.93	51	1.9	0.00106	0.283252
	Hicks and Mason 1991	72.2	40.8	1.55	1.14	51	1.9	0.00106	0.2925
	Hicks and Mason 1991	84.4	46.2	1.44	1.27	51	1.9	0.00106	0.338072
	Hicks and Mason 1991	125	50.5	1.89	1.31	51	1.9	0.00106	0.304388
Rangitikei at Mangaweka	Hicks and Mason 1991	15.3	35.3	0.57	0.76	94	2.3	0.00362	0.321561
	Hicks and Mason 1991	21.9	38.4	0.62	0.92	94	2.3	0.00362	0.373232
	Hicks and Mason 1991	42.5	45.6	0.72	1.3	94	2.3	0.00362	0.4894
	Hicks and Mason 1991	144	71.5	1.12	1.8	94	2.3	0.00362	0.543313
	Hicks and Mason 1991	173	79.7	1.28	1.7	94	2.3	0.00362	0.479989
	Hicks and Mason 1991	342	86.3	1.83	2.16	94	2.3	0.00362	0.510053
	Hicks and Mason 1991	413	89.2	2.04	2.27	94	2.3	0.00362	0.507689
	Hicks and Mason 1991	542	94	2.34	2.46	94	2.3	0.00362	0.513705
Buller at Woolfs	Hicks and Mason 1991	92.1	120.6	1.6	0.48	160	5.6	0.00076	0.121218
	Hicks and Mason 1991	124	129.5	1.46	0.66	160	5.6	0.00076	0.174484
	Hicks and Mason 1991	149	124.1	1.74	0.69	160	5.6	0.00076	0.167094
	Hicks and Mason 1991	285	127.3	2.16	1.04	160	5.6	0.00076	0.226044
	Hicks and Mason 1991	573	133.7	2.85	1.5	160	5.6	0.00076	0.283828
	Hicks and Mason 1991	1079	140.5	3.75	2.05	160	5.6	0.00076	0.338162
	Hicks and Mason 1991	2810	159.8	5.64	3.12	160	5.6	0.00076	0.419664
Ngongotaha at SH5 Bridge	Hicks and Mason 1991	1.89	6.9	0.64	0.43	22	2	0.00101	0.171698
	Hicks and Mason 1991	2.07	7	0.67	0.44	22	2	0.00101	0.171713
	Hicks and Mason 1991	4.05	8	0.92	0.55	22	2	0.00101	0.183171
	Hicks and Mason 1991	5.5	9.2	1.06	0.56	22	2	0.00101	0.173749
	Hicks and Mason 1991	5.95	9.5	1.08	0.58	22	2	0.00101	0.17828
	Hicks and Mason 1991	7.19	10.5	1.15	0.59	22	2	0.00101	0.175748
	Hicks and Mason 1991	7.79	11.3	1.17	0.59	22	2	0.00101	0.174239
	Hicks and Mason 1991	8.98	12.8	1.24	0.56	22	2	0.00101	0.160644
	Hicks and Mason 1991	12	14.5	1.42	0.58	22	2	0.00101	0.155479
	Hicks and Mason 1991	27.7	22.1	2.02	0.62	22	2	0.00101	0.139349
Wanganui at Paetawa	Hicks and Mason 1991	32.6	83.1	1.54	0.25	155	9.2	0.00026	0.064353
	Hicks and Mason 1991	45.9	84.7	1.76	0.31	155	9.2	0.00026	0.074644
	Hicks and Mason 1991	130	87.5	2.32	0.64	155	9.2	0.00026	0.134222
	Hicks and Mason 1991	381	89.6	3.57	1.19	155	9.2	0.00026	0.201187
	Hicks and Mason 1991	962	102.4	5.52	1.7	155	9.2	0.00026	0.231135
	Hicks and Mason 1991	1190	107.2	6.14	1.81	155	9.2	0.00026	0.233336
	Hicks and Mason 1991	1810	124	7.38	1.98	155	9.2	0.00026	0.232822
	Hicks and Mason 1991	2130	131.7	7.97	2.03	155	9.2	0.00026	0.229696
	Hicks and Mason 1991	2960	154.9	9.17	2.08	155	9.2	0.00026	0.219415
Hutt at Taita Gorge	Hicks and Mason 1991	23.8	52.4	0.63	0.72	60	2.1	0.00187	0.289767
	Hicks and Mason 1991	59.4	53.9	0.97	1.14	60	2.1	0.00187	0.369748
	Hicks and Mason 1991	79	55	1.12	1.28	60	2.1	0.00187	0.386356

River Name	Source	Discharge (m^3/s) Q	Width (m) W	Mean Depth (m) Y	Mean Velocity (m) V	Maximum Width (m) Wm	Maximum Depth (m) Ym	Slope (m/m) Sa	Froude Number F
	Hicks and Mason 1991	93	55.8	1.24	1.34	60	2.1	0.00187	0.384398
	Hicks and Mason 1991	137	58.1	1.65	1.43	60	2.1	0.00187	0.355616
	Hicks and Mason 1991	298	60.2	2.06	2.4	60	2.1	0.00187	0.534152
Hoteo at Gubbs	Hicks and Mason 1991	24.1	16.6	1.82	0.8	43	3	0.00078	0.189427
	Hicks and Mason 1991	27.9	17.6	1.88	0.84	43	3	0.00078	0.195698
	Hicks and Mason 1991	39.4	20.1	2.01	0.97	43	3	0.00078	0.218555
	Hicks and Mason 1991	39.8	20.5	2.03	0.96	43	3	0.00078	0.215234
	Hicks and Mason 1991	52.3	22.4	2.16	1.08	43	3	0.00078	0.234738
	Hicks and Mason 1991	54.3	23	2.21	1.07	43	3	0.00078	0.229919
	Hicks and Mason 1991	72.1	24.9	2.43	1.19	43	3	0.00078	0.243855
	Hicks and Mason 1991	99.2	30.6	2.62	1.24	43	3	0.00078	0.244714
	Hicks and Mason 1991	149	41.1	2.92	1.24	43	3	0.00078	0.231802
	Hicks and Mason 1991	156	42.6	3.03	1.21	43	3	0.00078	0.22205
Mokau at Totoro Bridge	Hicks and Mason 1991	8.86	27	1.12	0.29	52	4.2	0.00137	0.087534
	Hicks and Mason 1991	98.2	31.9	2.15	1.43	52	4.2	0.00137	0.311533
	Hicks and Mason 1991	195	40.5	3.11	1.55	52	4.2	0.00137	0.280762
	Hicks and Mason 1991	240	46.6	3.52	1.46	52	4.2	0.00137	0.248581
	Hicks and Mason 1991	255	45.3	3.44	1.63	52	4.2	0.00137	0.280734
	Hicks and Mason 1991	271	49.1	3.77	1.46	52	4.2	0.00137	0.240198
	Hicks and Mason 1991	327	53.7	4.28	1.42	52	4.2	0.00137	0.219257
	Hicks and Mason 1991	349	51.8	4.21	1.6	52	4.2	0.00137	0.249096
Waipapa at Ngaroma Rd.	Hicks and Mason 1991	3.5	19.1	0.33	0.55	25	1	0.00748	0.305839
	Hicks and Mason 1991	12.5	22	0.55	1.03	25	1	0.00748	0.443652
	Hicks and Mason 1991	22.9	22.8	0.67	1.5	25	1	0.00748	0.585384
	Hicks and Mason 1991	31.4	23.6	0.74	1.79	25	1	0.00748	0.664698
	Hicks and Mason 1991	38.5	23.9	0.79	2.04	25	1	0.00748	0.733168
	Hicks and Mason 1991	57.4	24.9	0.96	2.4	25	1	0.00748	0.782461
Whareama at Waiteko	Hicks and Mason 1991	23.1	17.9	2.01	0.64	43	4	0.00075	0.144201
	Hicks and Mason 1991	26.6	18.4	2.04	0.71	43	4	0.00075	0.158793
	Hicks and Mason 1991	30	19.5	2.14	0.72	43	4	0.00075	0.157222
	Hicks and Mason 1991	36	21	2.29	0.75	43	4	0.00075	0.158318
	Hicks and Mason 1991	200	37.9	3.67	1.44	43	4	0.00075	0.240113
	Hicks and Mason 1991	220	41	3.88	1.38	43	4	0.00075	0.223795
	Hicks and Mason 1991	289	42.9	3.96	1.7	43	4	0.00075	0.27289
Awanui at School Cut	Hicks and Mason 1991	8.8	12.3	1.08	0.66	37	3.7	0.00134	0.202871
	Hicks and Mason 1991	10.8	13.3	1.15	0.71	37	3.7	0.00134	0.211493
	Hicks and Mason 1991	13.6	14.5	1.33	0.7	37	3.7	0.00134	0.193892
	Hicks and Mason 1991	22.7	18	1.69	0.74	37	3.7	0.00134	0.181834
	Hicks and Mason 1991	25.3	19.7	1.81	0.71	37	3.7	0.00134	0.16858
	Hicks and Mason 1991	47.5	25.8	2.47	0.74	37	3.7	0.00134	0.150408
	Hicks and Mason 1991	49.5	26.1	2.51	0.76	37	3.7	0.00134	0.153237
	Hicks and Mason 1991	56	27	2.62	0.79	37	3.7	0.00134	0.155906
	Hicks and Mason 1991	115	32.2	3.29	1.08	37	3.7	0.00134	0.190201
	Hicks and Mason 1991	143	34.5	3.54	1.17	37	3.7	0.00134	0.198642
	Hicks and Mason 1991	172	37.2	3.74	1.24	37	3.7	0.00134	0.20482
Kaipara at Waimauku	Hicks and Mason 1991	13.6	16.8	1.57	0.52	35	2.4	0.0005	0.132569
	Hicks and Mason 1991	26.4	25.6	1.77	0.58	35	2.4	0.0005	0.139261
	Hicks and Mason 1991	34.8	28.8	2.04	0.59	35	2.4	0.0005	0.131954
	Hicks and Mason 1991	35.4	28.8	2.05	0.6	35	2.4	0.0005	0.133863
	Hicks and Mason 1991	36.2	29	2.07	0.6	35	2.4	0.0005	0.133215
	Hicks and Mason 1991	72	34.5	2.43	0.86	35	2.4	0.0005	0.176231
Ruakokapatuna at Iraia	Hicks and Mason 1991	0.08	4.8	0.13	0.13	12	0.8	0.00601	0.115175
	Hicks and Mason 1991	0.2	5.8	0.17	0.2	12	0.8	0.00601	0.15495
	Hicks and Mason 1991	0.22	6	0.14	0.26	12	0.8	0.00601	0.221971
	Hicks and Mason 1991	0.29	7.1	0.16	0.25	12	0.8	0.00601	0.199649
	Hicks and Mason 1991	0.41	7.1	0.19	0.3	12	0.8	0.00601	0.219853
	Hicks and Mason 1991	0.89	7.8	0.24	0.48	12	0.8	0.00601	0.312984
	Hicks and Mason 1991	3.89	9.5	0.42	0.98	12	0.8	0.00601	0.483046
	Hicks and Mason 1991	6.63	10.3	0.53	1.22	12	0.8	0.00601	0.535314
	Hicks and Mason 1991	10	11	0.63	1.45	12	0.8	0.00601	0.583559
	Hicks and Mason 1991	10.9	11.1	0.64	1.53	12	0.8	0.00601	0.610926
	Hicks and Mason 1991	15.2	12.3	0.78	1.59	12	0.8	0.00601	0.575091
Patea at McColls Bridge	Hicks and Mason 1991	2.8	21	1.3	0.1	38	3.5	0.00113	0.028017
	Hicks and Mason 1991	46	27.1	2.1	0.81	38	3.5	0.00113	0.178551
	Hicks and Mason 1991	61	28.3	2.32	0.93	38	3.5	0.00113	0.195041
	Hicks and Mason 1991	62	28.5	2.32	0.94	38	3.5	0.00113	0.197138
	Hicks and Mason 1991	130	32.7	2.97	1.34	38	3.5	0.00113	0.248378
	Hicks and Mason 1991	218	37.6	3.51	1.65	38	3.5	0.00113	0.281331
Pelorus at Bryants	Hicks and Mason 1991	6.13	35.4	0.76	0.23	55	2.3	0.00359	0.084277
	Hicks and Mason 1991	11.8	38.2	0.83	0.37	55	2.3	0.00359	0.129733

River Name	Source	Discharge (m^3/s) Q	Width (m) W	Mean Depth (m) Y	Mean Velocity (m) V	Maximum Width (m) Wm	Maximum Depth (m) Ym	Slope (m/m) Sa	Froude Number F
	Hicks and Mason 1991	13.1	40.5	0.82	0.39	55	2.3	0.00359	0.137577
	Hicks and Mason 1991	27.3	44	0.97	0.64	55	2.3	0.00359	0.207576
	Hicks and Mason 1991	79.7	58.2	1.14	1.2	55	2.3	0.00359	0.359018
	Hicks and Mason 1991	164	50.2	1.84	1.78	55	2.3	0.00359	0.419178
	Hicks and Mason 1991	290	55.1	2.25	2.34	55	2.3	0.00359	0.498324
Collins at Drop Structure	Hicks and Mason 1991	0.07	5.6	0.12	0.1	15	1	0.00858	0.092214
	Hicks and Mason 1991	0.16	6.6	0.18	0.13	15	1	0.00858	0.09788
	Hicks and Mason 1991	0.23	6.8	0.2	0.17	15	1	0.00858	0.121429
	Hicks and Mason 1991	0.55	7.2	0.25	0.31	15	1	0.00858	0.198052
	Hicks and Mason 1991	2.35	8	0.41	0.71	15	1	0.00858	0.354204
	Hicks and Mason 1991	5.31	8.7	0.51	1.2	15	1	0.00858	0.536764
	Hicks and Mason 1991	13	11.2	0.69	1.68	15	1	0.00858	0.646058
	Hicks and Mason 1991	30.9	15.4	0.98	2.05	15	1	0.00858	0.661497
Mangere at Kara Weir	Hicks and Mason 1991	0.65	8.2	0.43	0.18	25	1.9	0.00293	0.087685
	Hicks and Mason 1991	0.86	8.4	0.45	0.23	25	1.9	0.00293	0.109524
	Hicks and Mason 1991	1.34	8.7	0.52	0.3	25	1.9	0.00293	0.132894
	Hicks and Mason 1991	6.95	11.5	0.87	0.7	25	1.9	0.00293	0.239732
	Hicks and Mason 1991	7.67	11.8	0.9	0.72	25	1.9	0.00293	0.242437
	Hicks and Mason 1991	7.69	11.7	0.9	0.73	25	1.9	0.00293	0.245804
	Hicks and Mason 1991	9.24	12.8	1.09	0.66	25	1.9	0.00293	0.201938
	Hicks and Mason 1991	12.5	13.6	1.29	0.71	25	1.9	0.00293	0.199687
	Hicks and Mason 1991	20.4	14.8	1.45	0.95	25	1.9	0.00293	0.252015
	Hicks and Mason 1991	29.5	16.1	1.58	1.16	25	1.9	0.00293	0.294792
	Hicks and Mason 1991	46.6	19.8	1.68	1.4	25	1.9	0.00293	0.345033
	Hicks and Mason 1991	87	25.4	1.9	1.8	25	1.9	0.00293	0.417141
Waiwakaiho at SH3	Hicks and Mason 1991	2.44	19	0.45	0.29	35	1.7	0.01077	0.138095
	Hicks and Mason 1991	2.8	19.5	0.46	0.31	35	1.7	0.01077	0.146006
	Hicks and Mason 1991	3.43	20.3	0.49	0.35	35	1.7	0.01077	0.159719
	Hicks and Mason 1991	9.12	24.6	0.7	0.53	35	1.7	0.01077	0.202355
	Hicks and Mason 1991	21.8	26.3	0.92	0.9	35	1.7	0.01077	0.299734
	Hicks and Mason 1991	26.4	26.8	0.96	1.03	35	1.7	0.01077	0.335806
	Hicks and Mason 1991	31.2	27.2	1.01	1.13	35	1.7	0.01077	0.359174
	Hicks and Mason 1991	77.4	31.5	1.3	1.89	35	1.7	0.01077	0.529514
	Hicks and Mason 1991	216	35	1.71	3.61	35	1.7	0.01077	0.881853
Orere at Bridge	Hicks and Mason 1991	9.41	12.7	0.64	1.16	17	1.1	0.003	0.463186
	Hicks and Mason 1991	11.6	13.2	0.7	1.25	17	1.1	0.003	0.477252
	Hicks and Mason 1991	23.1	13.7	0.84	2.01	17	1.1	0.003	0.700557
	Hicks and Mason 1991	25.1	14	0.89	2.01	17	1.1	0.003	0.680594
	Hicks and Mason 1991	26.5	14.4	0.93	1.98	17	1.1	0.003	0.655859
	Hicks and Mason 1991	28.5	14.7	0.96	2.02	17	1.1	0.003	0.658571
	Hicks and Mason 1991	35.5	16.6	1.08	1.98	17	1.1	0.003	0.608612
	Hicks and Mason 1991	50.6	17.4	1.12	2.59	17	1.1	0.003	0.781768
Avon at Gloucester Street Brid	Hicks and Mason 1991	1.83	11	0.4	0.42	15	1	0.00105	0.212132
	Hicks and Mason 1991	2.32	11	0.42	0.5	15	1	0.00105	0.246452
	Hicks and Mason 1991	3.74	11.3	0.54	0.61	15	1	0.00105	0.265167
	Hicks and Mason 1991	4.48	11.6	0.59	0.65	15	1	0.00105	0.270318
	Hicks and Mason 1991	4.87	11.5	0.62	0.68	15	1	0.00105	0.275867
	Hicks and Mason 1991	6	11.7	0.69	0.74	15	1	0.00105	0.284573
	Hicks and Mason 1991	8.91	12	0.83	0.89	15	1	0.00105	0.31206
	Hicks and Mason 1991	12.2	13.3	0.92	1	15	1	0.00105	0.333037
	Hicks and Mason 1991	15.6	14.9	1	1.05	15	1	0.00105	0.33541
	Hicks and Mason 1991	17.3	15.4	1.01	1.11	15	1	0.00105	0.352817
Monowai below Control Gates	Hicks and Mason 1991	5.64	22.6	0.47	0.53	28	0.9	0.00078	0.246953
	Hicks and Mason 1991	11.5	25	0.6	0.77	28	0.9	0.00078	0.317543
	Hicks and Mason 1991	14.1	25.5	0.67	0.82	28	0.9	0.00078	0.32001
	Hicks and Mason 1991	19.2	26.9	0.8	0.89	28	0.9	0.00078	0.317857
	Hicks and Mason 1991	20.3	27.2	0.81	0.92	28	0.9	0.00078	0.326537
	Hicks and Mason 1991	20.3	27	0.81	0.93	28	0.9	0.00078	0.330086
	Hicks and Mason 1991	21.5	27	0.83	0.96	28	0.9	0.00078	0.336604
	Hicks and Mason 1991	21.7	27.8	0.85	0.92	28	0.9	0.00078	0.318761
	Hicks and Mason 1991	23	28.3	0.87	0.93	28	0.9	0.00078	0.318501
	Hicks and Mason 1991	23.1	28	0.86	0.96	28	0.9	0.00078	0.330681
	Hicks and Mason 1991	24.1	28.1	0.88	0.98	28	0.9	0.00078	0.333712
Waikato at Ngaruawahia Cable	Hicks and Mason 1991	237	157.6	2.24	0.67	198	4.3	0.00016	0.143001
	Hicks and Mason 1991	290	164	2.5	0.71	198	4.3	0.00016	0.143442
	Hicks and Mason 1991	448	183.9	2.98	0.82	198	4.3	0.00016	0.151737
	Hicks and Mason 1991	641	194.1	3.74	0.88	198	4.3	0.00016	0.145356
	Hicks and Mason 1991	738	196.8	4.03	0.93	198	4.3	0.00016	0.147985
	Hicks and Mason 1991	874	197.9	4.32	1.02	198	4.3	0.00016	0.156764

River Name	Source	Discharge (m^3/s) Q	Width (m) W	Mean Depth (m) Y	Mean Velocity (m) V	Maximum Width (m) Wm	Maximum Depth (m) Ym	Slope (m/m) Sa	Froude Number F
Heathcote at Sloan Terrace	Hicks and Mason 1991	1.22	7.5	0.37	0.44	9	1.3	0.0005	0.231067
	Hicks and Mason 1991	1.74	7.6	0.45	0.51	9	1.3	0.0005	0.242857
	Hicks and Mason 1991	1.96	7.8	0.48	0.53	9	1.3	0.0005	0.244367
	Hicks and Mason 1991	2.12	7.9	0.5	0.54	9	1.3	0.0005	0.243947
	Hicks and Mason 1991	2.94	7.9	0.63	0.59	9	1.3	0.0005	0.237448
	Hicks and Mason 1991	4.22	8.7	0.76	0.64	9	1.3	0.0005	0.234509
	Hicks and Mason 1991	4.83	8.9	0.83	0.66	9	1.3	0.0005	0.231415
	Hicks and Mason 1991	5.74	9.7	0.99	0.6	9	1.3	0.0005	0.192629
	Hicks and Mason 1991	6.27	10.1	1.08	0.58	9	1.3	0.0005	0.17828
	Hicks and Mason 1991	7.92	10.4	1.11	0.69	9	1.3	0.0005	0.209206
	Hicks and Mason 1991	8.01	10.4	1.12	0.68	9	1.3	0.0005	0.205252
	Hicks and Mason 1991	8.21	9.4	1.27	0.69	9	1.3	0.0005	0.195584
Taieri below Patearoa Power St	Hicks and Mason 1991	0.78	19.1	0.3	0.14	23	1	0.0009	0.08165
	Hicks and Mason 1991	1.24	19.5	0.34	0.19	23	1	0.0009	0.104088
	Hicks and Mason 1991	6.13	20.2	0.54	0.56	23	1	0.0009	0.243432
	Hicks and Mason 1991	6.66	20	0.57	0.58	23	1	0.0009	0.245402
	Hicks and Mason 1991	9.1	20.3	0.65	0.69	23	1	0.0009	0.273388
	Hicks and Mason 1991	11.3	20.7	0.71	0.77	23	1	0.0009	0.29191
	Hicks and Mason 1991	11.8	20.1	0.72	0.81	23	1	0.0009	0.304934
	Hicks and Mason 1991	12	20.8	0.74	0.78	23	1	0.0009	0.289645
	Hicks and Mason 1991	12.3	20	0.74	0.83	23	1	0.0009	0.308212
	Hicks and Mason 1991	18.7	21.7	0.84	1.03	23	1	0.0009	0.358992
	Hicks and Mason 1991	20.4	21.6	0.88	1.07	23	1	0.0009	0.364359
	Hicks and Mason 1991	21.2	22.1	0.87	1.1	23	1	0.0009	0.376721
	Hicks and Mason 1991	27.1	23	0.96	1.23	23	1	0.0009	0.401011
Tahunatara at Ohakuri Road	Hicks and Mason 1991	2.93	13.4	0.88	0.25	20	1.6	0.00039	0.085131
	Hicks and Mason 1991	7.45	14.4	1.06	0.49	20	1.6	0.00039	0.15203
	Hicks and Mason 1991	9.97	15	1.14	0.58	20	1.6	0.00039	0.173525
	Hicks and Mason 1991	15.6	15.8	1.3	0.76	20	1.6	0.00039	0.212926
	Hicks and Mason 1991	18.1	16.4	1.36	0.81	20	1.6	0.00039	0.221872
	Hicks and Mason 1991	21.8	16.4	1.36	0.98	20	1.6	0.00039	0.268438
	Hicks and Mason 1991	36	20.2	1.58	1.13	20	1.6	0.00039	0.287169
Rangitaiki at Te Teko	Hicks and Mason 1991	47.5	40.1	1.71	0.69	55	2.7	0.00052	0.168554
	Hicks and Mason 1991	53	40.6	1.78	0.73	55	2.7	0.00052	0.174783
	Hicks and Mason 1991	74	42.9	2.07	0.83	55	2.7	0.00052	0.184281
	Hicks and Mason 1991	98	46.8	2.35	0.89	55	2.7	0.00052	0.185457
	Hicks and Mason 1991	107	48	2.46	0.91	55	2.7	0.00052	0.185336
	Hicks and Mason 1991	120	49.4	2.61	0.93	55	2.7	0.00052	0.183886
	Hicks and Mason 1991	144	54.9	2.73	0.96	55	2.7	0.00052	0.1856
Mill Creek at Papanui	Hicks and Mason 1991	0.01	2.9	0.18	0.02	10	0.8	0.0029	0.015058
	Hicks and Mason 1991	0.02	4.4	0.19	0.02	10	0.8	0.0029	0.014657
	Hicks and Mason 1991	0.05	3.1	0.2	0.08	10	0.8	0.0029	0.057143
	Hicks and Mason 1991	0.26	3.8	0.36	0.19	10	0.8	0.0029	0.101155
	Hicks and Mason 1991	0.29	4	0.39	0.19	10	0.8	0.0029	0.097187
	Hicks and Mason 1991	0.47	4	0.4	0.29	10	0.8	0.0029	0.146472
	Hicks and Mason 1991	0.69	4.3	0.46	0.35	10	0.8	0.0029	0.164845
	Hicks and Mason 1991	1.08	4.7	0.49	0.47	10	0.8	0.0029	0.21448
	Hicks and Mason 1991	2.06	5.8	0.56	0.64	10	0.8	0.0029	0.273195
	Hicks and Mason 1991	2.14	5.9	0.56	0.64	10	0.8	0.0029	0.273195
	Hicks and Mason 1991	2.34	6.1	0.58	0.66	10	0.8	0.0029	0.276832
	Hicks and Mason 1991	8.52	10.1	0.8	1.05	10	0.8	0.0029	0.375
Ngunguru at Dugmores Rock	Hicks and Mason 1991	0.38	7.3	0.42	0.12	16	1.2	0.00611	0.059148
	Hicks and Mason 1991	0.61	7.5	0.43	0.19	16	1.2	0.00611	0.092556
	Hicks and Mason 1991	2.19	8.1	0.58	0.46	16	1.2	0.00611	0.192944
	Hicks and Mason 1991	5.03	8.2	0.77	0.8	16	1.2	0.00611	0.291227
	Hicks and Mason 1991	7.72	10.1	0.81	0.94	16	1.2	0.00611	0.333636
	Hicks and Mason 1991	12.2	12.3	0.92	1.08	16	1.2	0.00611	0.35968
	Hicks and Mason 1991	12.3	12.3	0.91	1.1	16	1.2	0.00611	0.368349
	Hicks and Mason 1991	17.9	13.7	1	1.31	16	1.2	0.00611	0.418464
	Hicks and Mason 1991	20.2	14.2	1.06	1.34	16	1.2	0.00611	0.415756
	Hicks and Mason 1991	25.1	15.7	1.17	1.36	16	1.2	0.00611	0.401636
	Hicks and Mason 1991	29.3	16.3	1.23	1.47	16	1.2	0.00611	0.423401
Butchers Creek at Lake Kaniere	Hicks and Mason 1991	0.02	4.1	0.1	0.05	9	0.7	0.01517	0.050508
	Hicks and Mason 1991	0.05	5.4	0.14	0.07	9	0.7	0.01517	0.059761
	Hicks and Mason 1991	0.29	5.3	0.16	0.34	9	0.7	0.01517	0.271523
	Hicks and Mason 1991	1.75	6.6	0.31	0.85	9	0.7	0.01517	0.487669
	Hicks and Mason 1991	1.95	6.8	0.34	0.84	9	0.7	0.01517	0.460179
	Hicks and Mason 1991	1.99	6.7	0.33	0.9	9	0.7	0.01517	0.500464
	Hicks and Mason 1991	4.31	7.4	0.44	1.33	9	0.7	0.01517	0.64049
	Hicks and Mason 1991	4.8	7.4	0.45	1.44	9	0.7	0.01517	0.685714

River Name	Source	Discharge (m^3/s) Q	Width (m) W	Mean Depth (m) Y	Mean Velocity (m) V	Maximum Width (m) Wm	Maximum Depth (m) Ym	Slope (m/m) Sa	Froude Number F
	Hicks and Mason 1991	12.6	9	0.67	2.1	9	0.7	0.01517	0.819538
	Hicks and Mason 1991	14.5	9.3	0.68	2.31	9	0.7	0.01517	0.894838
	Hicks and Mason 1991	16.7	9.4	0.72	2.48	9	0.7	0.01517	0.933625
	Hicks and Mason 1991	18.9	9.3	0.72	2.81	9	0.7	0.01517	1.057857
Waihua at Gorge	Hicks and Mason 1991	0.42	9.2	0.21	0.22	18	0.9	0.01668	0.153356
	Hicks and Mason 1991	1.1	10.9	0.27	0.38	18	0.9	0.01668	0.233609
	Hicks and Mason 1991	6.55	14.5	0.51	0.88	18	0.9	0.01668	0.393627
	Hicks and Mason 1991	19.2	16.7	0.76	1.51	18	0.9	0.01668	0.553295
	Hicks and Mason 1991	19.8	16.6	0.77	1.55	18	0.9	0.01668	0.564252
	Hicks and Mason 1991	20.3	16.9	0.78	1.54	18	0.9	0.01668	0.557007
	Hicks and Mason 1991	30.2	17.8	0.86	1.97	18	0.9	0.01668	0.678585
	Hicks and Mason 1991	32.1	18.2	0.89	1.98	18	0.9	0.01668	0.670436
Wanganui at TePorere	Hicks and Mason 1991	0.93	7.8	0.4	0.3	12	1.1	0.01907	0.151523
	Hicks and Mason 1991	0.96	7.9	0.41	0.3	12	1.1	0.01907	0.149664
	Hicks and Mason 1991	1.17	8.1	0.42	0.34	12	1.1	0.01907	0.167587
	Hicks and Mason 1991	1.17	8	0.43	0.34	12	1.1	0.01907	0.165627
	Hicks and Mason 1991	2.66	8.5	0.53	0.59	12	1.1	0.01907	0.258882
	Hicks and Mason 1991	13.1	10.5	0.87	1.44	12	1.1	0.01907	0.493162
	Hicks and Mason 1991	15.8	10.6	0.89	1.67	12	1.1	0.01907	0.565469
	Hicks and Mason 1991	16.2	10.6	0.88	1.73	12	1.1	0.01907	0.589104
	Hicks and Mason 1991	29.3	12	1.07	2.29	12	1.1	0.01907	0.707181
Opahi at Pond	Hicks and Mason 1991	0.25	6.1	0.57	0.07	11	1.1	0.00113	0.029617
	Hicks and Mason 1991	0.31	6.3	0.6	0.08	11	1.1	0.00113	0.032991
	Hicks and Mason 1991	0.38	6.4	0.62	0.1	11	1.1	0.00113	0.040569
	Hicks and Mason 1991	1.03	7.6	0.71	0.19	11	1.1	0.00113	0.07203
	Hicks and Mason 1991	5.8	9.8	1.02	0.58	11	1.1	0.00113	0.183449
	Hicks and Mason 1991	5.88	9.7	1.01	0.6	11	1.1	0.00113	0.190712
	Hicks and Mason 1991	7.46	10.5	1.09	0.65	11	1.1	0.00113	0.198878
Huka Huka at Lathams Bridge	Hicks and Mason 1991	0.09	5.5	0.11	0.15	9	0.5	0.04042	0.144471
	Hicks and Mason 1991	0.48	6.8	0.24	0.3	9	0.5	0.04042	0.195615
	Hicks and Mason 1991	0.63	7	0.25	0.36	9	0.5	0.04042	0.229996
	Hicks and Mason 1991	1.08	7.4	0.29	0.5	9	0.5	0.04042	0.296591
	Hicks and Mason 1991	1.63	7.5	0.33	0.66	9	0.5	0.04042	0.367007
	Hicks and Mason 1991	1.93	7.7	0.34	0.74	9	0.5	0.04042	0.405396
	Hicks and Mason 1991	3.55	8.3	0.42	1.02	9	0.5	0.04042	0.502762
	Hicks and Mason 1991	4.17	8.3	0.44	1.14	9	0.5	0.04042	0.548991
	Hicks and Mason 1991	5.09	8.5	0.46	1.3	9	0.5	0.04042	0.612282
	Hicks and Mason 1991	8.17	9.4	0.51	1.71	9	0.5	0.04042	0.764888
Clark Fork	Barnes 1967	1950.75	130.8	5	2.98	131	5	0.00019	0.425714
Clark Fork	Barnes 1967	891.85	88.4	3.9	2.59	88	3.9	0.00073	0.418943
Blackfoot	Barnes 1967	232.16	59.1	1.86	2.11	59	1.9	0.00027	0.494212
Coer d'Alene	Barnes 1967	319.93	49.4	2.41	2.69	49	2.4	0.00233	0.553517
Salt	Barnes 1967	36.24	57.9	0.67	0.93	58	0.7	0.00247	0.362938
Clearwater	Barnes 1967	2802.96	171.9	6	2.72	172	6	0.00188	0.354716
Etowah	Barnes 1967	63.99	19.5	2.96	1.11	20	3	0.00084	0.206093
WF Bitterroot	Barnes 1967	109.85	32	1.46	2.35	32	1.5	0.00066	0.621267
Yakima	Barnes 1967	784.26	67.4	3.57	3.26	67	3.6	0.00462	0.551151
MF Vermillion	Barnes 1967	45.87	35.7	1.01	1.27	36	1	0.00295	0.403673
Wenatchee	Barnes 1967	642.7	70.1	3.26	2.81	70	3.3	0.00311	0.497147
Moyie	Barnes 1967	227.35	44.8	2.16	2.35	45	2.2	0.00236	0.510773
Spokane	Barnes 1967	1121.18	89.9	4.45	2.8	90	4.5	0.00177	0.423999
Bull	Barnes 1967	91.17	32.9	2.19	1.27	33	2.2	0.00121	0.274138
MF Flathead	Barnes 1967	410.53	55.5	2.68	2.76	56	2.7	0.00401	0.538553
M Oconee	Barnes 1967	172.99	43	3.32	1.21	43	3.3	0.00043	0.212131
Chiwawa	Barnes 1967	166.48	41.8	1.71	2.33	42	1.7	0.00502	0.569174
Grande Ronde	Barnes 1967	130.8	34.7	1.65	2.28	35	1.7	0.00525	0.566996
Deep	Barnes 1967	235	66.7	3.17	1.11	67	3.2	0.00076	0.19915
Chattahoochee	Barnes 1967	144.39	44.8	2.35	1.37	45	2.4	0.00243	0.285479
sf Clearwater	Barnes 1967	356.74	46.3	2.71	2.84	46	2.7	0.00628	0.551088
MB Westfield	Barnes 1967	96.26	36.3	1.34	1.98	36	1.3	0.00868	0.546386

Appendix 2 - Slope Control Flow Measurement Data

Table A2 - Slope Control Flow Measurement Data

River Name	Source	Discharge (m^3/s)	Width (m)	Mean Depth (m)	Mean Velocity (m/s)	Maximum Width (m)	Maximum Depth (m)	Slope (m/m)	Froude number
Connecticut at Thompsonville	USGS-NWIS	2712.3	303.3	4.14	2.16	310	4.1	0.00042	0.34
	USGS-NWIS	2273.5	303.3	3.83	1.96	310	4.1	0.00042	0.32
	USGS-NWIS	1976.2	310.9	3.71	1.72	310	4.1	0.00042	0.29
	USGS-NWIS	1387.3	310.9	3.11	1.43	310	4.1	0.00042	0.26
	USGS-NWIS	1177.8	310.9	3.11	1.22	310	4.1	0.00042	0.22
	USGS-NWIS	1010.2	310.9	2.92	1.11	310	4.1	0.00042	0.21
	USGS-NWIS	925.8	310.9	2.87	1.04	310	4.1	0.00042	0.20
	USGS-NWIS	792.8	310.9	2.78	0.95	310	4.1	0.00042	0.18
	USGS-NWIS	628.5	307.8	2.58	0.79	310	4.1	0.00042	0.16
	USGS-NWIS	535.1	306.3	2.56	0.68	310	4.1	0.00042	0.14
	USGS-NWIS	407.7	301.7	2.43	0.56	310	4.1	0.00042	0.11
	USGS-NWIS	351.1	297.2	2.16	0.54	310	4.1	0.00042	0.12
	USGS-NWIS	257.1	303.3	2.22	0.37	310	4.1	0.00042	0.08
	USGS-NWIS	241.5	301.7	2.18	0.37	310	4.1	0.00042	0.08
	USGS-NWIS	209.5	298.7	2.04	0.34	310	4.1	0.00042	0.08
	USGS-NWIS	195.4	298.7	2.09	0.31	310	4.1	0.00042	0.07
	USGS-NWIS	165.1	282.8	1.93	0.3	310	4.1	0.00042	0.07
	USGS-NWIS	129.7	296.6	1.8	0.24	310	4.1	0.00042	0.06
	USGS-NWIS	94.6	297.5	1.8	0.18	310	4.1	0.00042	0.04
	USGS-NWIS	66.3	214.9	1.93	0.16	310	4.1	0.00042	0.04
Androscoggin at Auburn	USGS-NWIS	1874.3	125	6.94	2.16	126	6.9	0.00051	0.26
	USGS-NWIS	1466.6	124	6.19	1.91	126	6.9	0.00051	0.25
	USGS-NWIS	1313.7	126.5	5.91	1.76	126	6.9	0.00051	0.23
	USGS-NWIS	1073	124.4	5.3	1.63	126	6.9	0.00051	0.23
	USGS-NWIS	823.9	123.4	4.92	1.33	126	6.9	0.00051	0.19
	USGS-NWIS	526.6	120.4	4.26	1.03	126	6.9	0.00051	0.16
	USGS-NWIS	489.8	118.9	4.23	0.98	126	6.9	0.00051	0.15
	USGS-NWIS	359.6	121.9	3.83	0.77	126	6.9	0.00051	0.13
	USGS-NWIS	336.9	118.9	3.8	0.75	126	6.9	0.00051	0.12
	USGS-NWIS	245.2	121.9	3.46	0.58	126	6.9	0.00051	0.10
	USGS-NWIS	204.1	119.5	3.37	0.51	126	6.9	0.00051	0.09
	USGS-NWIS	188.8	118.9	3.36	0.47	126	6.9	0.00051	0.08
	USGS-NWIS	158.3	118.9	3.22	0.41	126	6.9	0.00051	0.07
	USGS-NWIS	131.1	114.3	3.15	0.37	126	6.9	0.00051	0.07
	USGS-NWIS	101.4	115.8	3.02	0.29	126	6.9	0.00051	0.05
	USGS-NWIS	80.1	115.8	2.9	0.24	126	6.9	0.00051	0.05
	USGS-NWIS	48.7	111.2	2.73	0.16	126	6.9	0.00051	0.03
	USGS-NWIS	40.5	112.8	2.65	0.13	126	6.9	0.00051	0.03
	USGS-NWIS	27.5	106.7	2.71	0.09	126	6.9	0.00051	0.02
Delaware at Port Jervis	USGS-NWIS	1959.2	195.4	4.09	2.45	196	4.1	0.00098	0.39
	USGS-NWIS	1758.2	196	4.1	2.19	196	4.1	0.00098	0.35
	USGS-NWIS	1220.3	193.8	3.22	1.96	196	4.1	0.00098	0.35
	USGS-NWIS	1030.6	193.2	3.04	1.76	196	4.1	0.00098	0.32
	USGS-NWIS	775.8	192	2.62	1.54	196	4.1	0.00098	0.30
	USGS-NWIS	577.6	190.8	2.26	1.34	196	4.1	0.00098	0.28
	USGS-NWIS	474.5	190.2	2.04	1.23	196	4.1	0.00098	0.28
	USGS-NWIS	438.8	191.7	1.97	1.16	196	4.1	0.00098	0.26
	USGS-NWIS	419	191.1	1.92	1.14	196	4.1	0.00098	0.26
	USGS-NWIS	365.2	191.7	1.77	1.07	196	4.1	0.00098	0.26
	USGS-NWIS	334.1	189	1.75	1.01	196	4.1	0.00098	0.24
	USGS-NWIS	308.6	189.6	1.72	0.94	196	4.1	0.00098	0.23
	USGS-NWIS	281.7	190.5	1.6	0.92	196	4.1	0.00098	0.23
	USGS-NWIS	241.2	189	1.5	0.85	196	4.1	0.00098	0.22
	USGS-NWIS	186.6	186.2	1.38	0.73	196	4.1	0.00098	0.20
	USGS-NWIS	163.6	186.2	1.3	0.68	196	4.1	0.00098	0.19
	USGS-NWIS	131.7	190.8	1.14	0.6	196	4.1	0.00098	0.18
	USGS-NWIS	103.6	185.3	1.1	0.51	196	4.1	0.00098	0.16
	USGS-NWIS	75	182.3	0.97	0.42	196	4.1	0.00098	0.14
	USGS-NWIS	47.8	179.2	0.79	0.34	196	4.1	0.00098	0.12
Pee Dee at Rockingham	USGS-NWIS	2686.9	324.6	3.95	2.1	325	4	0.00068	0.34
	USGS-NWIS	863.5	193.5	3.71	1.2	325	4	0.00068	0.20
	USGS-NWIS	7.3	193.8	0.19	0.2	325	4	0.00068	0.15
	USGS-NWIS	7	186.8	0.18	0.21	325	4	0.00068	0.16
	USGS-NWIS	8.1	192	0.23	0.18	325	4	0.00068	0.12
	USGS-NWIS	10.4	203.6	0.21	0.24	325	4	0.00068	0.17
	USGS-NWIS	2194.2	262.1	4.32	1.94	325	4	0.00068	0.30
	USGS-NWIS	8.4	195.7	0.15	0.29	325	4	0.00068	0.24
	USGS-NWIS	10.3	203	0.19	0.27	325	4	0.00068	0.20

River Name	Source	Discharge (m^3/s)	Width (m)	Mean Depth (m)	Mean Velocity (m/s)	Maximum Width (m)	Maximum Depth (m)	Slope (m/m)	Froude number
	USGS-NWIS	145	184.4	2.36	0.33	325	4	0.00068	0.07
	USGS-NWIS	222.5	184.4	2.65	0.46	325	4	0.00068	0.09
	USGS-NWIS	175.8	185.6	2.39	0.4	325	4	0.00068	0.08
	USGS-NWIS	564.8	189	3.26	0.91	325	4	0.00068	0.16
	USGS-NWIS	509.6	192	3.09	0.86	325	4	0.00068	0.16
	USGS-NWIS	223.4	189	2.56	0.46	325	4	0.00068	0.09
	USGS-NWIS	897.5	202.4	4.02	1.1	325	4	0.00068	0.18
Penobscot at W. Enfield	USGS-NWIS	3086.1	270	6.04	1.89	272	6	0.00021	0.25
	USGS-NWIS	2534	271.6	5.54	1.68	272	6	0.00021	0.23
	USGS-NWIS	1922.4	271.6	4.55	1.55	272	6	0.00021	0.23
	USGS-NWIS	1480.7	270.3	3.88	1.41	272	6	0.00021	0.23
	USGS-NWIS	959.8	270	3.03	1.2	272	6	0.00021	0.22
	USGS-NWIS	639.9	264.6	2.4	1.01	272	6	0.00021	0.21
	USGS-NWIS	475.7	257.2	1.97	0.94	272	6	0.00021	0.21
	USGS-NWIS	444.5	258.5	1.9	0.9	272	6	0.00021	0.21
	USGS-NWIS	402	260.9	1.87	0.82	272	6	0.00021	0.19
	USGS-NWIS	342.6	258.5	1.66	0.8	272	6	0.00021	0.20
	USGS-NWIS	334.1	179.8	4.42	0.42	272	6	0.00021	0.06
	USGS-NWIS	302.9	256.3	1.54	0.76	272	6	0.00021	0.20
	USGS-NWIS	276.9	252.4	1.46	0.75	272	6	0.00021	0.20
	USGS-NWIS	245.2	189	2.76	0.47	272	6	0.00021	0.09
	USGS-NWIS	235.8	253	2.01	0.46	272	6	0.00021	0.10
	USGS-NWIS	223.7	252.4	1.31	0.68	272	6	0.00021	0.19
	USGS-NWIS	196.8	182.9	2.39	0.45	272	6	0.00021	0.09
	USGS-NWIS	167	239.3	1.12	0.62	272	6	0.00021	0.19
	USGS-NWIS	137.3	227.7	1.06	0.57	272	6	0.00021	0.18
	USGS-NWIS	112.1	182.9	3.85	0.16	272	6	0.00021	0.03
Taku near Juneau	USGS-NWIS	2992.6	240.2	5.23	2.38	240	5.2	0.0006	0.33
	USGS-NWIS	2304.6	231	5.05	1.98	240	5.2	0.0006	0.28
	USGS-NWIS	2024.3	238.6	4.21	2.01	240	5.2	0.0006	0.31
	USGS-NWIS	1809.2	207.3	4.44	1.97	240	5.2	0.0006	0.30
	USGS-NWIS	1492.1	213.3	3.88	1.8	240	5.2	0.0006	0.29
	USGS-NWIS	1183.5	219.1	3.56	1.51	240	5.2	0.0006	0.26
	USGS-NWIS	917.3	207.3	3.14	1.41	240	5.2	0.0006	0.25
	USGS-NWIS	461.5	205.7	2.28	0.98	240	5.2	0.0006	0.21
	USGS-NWIS	393.5	50.6	7.36	1.06	240	5.2	0.0006	0.12
	USGS-NWIS	334.1	196.6	1.98	0.86	240	5.2	0.0006	0.20
	USGS-NWIS	278.9	196.9	1.77	0.8	240	5.2	0.0006	0.19
	USGS-NWIS	204.4	198.1	1.5	0.69	240	5.2	0.0006	0.18
	USGS-NWIS	156	195.1	1.24	0.64	240	5.2	0.0006	0.18
	USGS-NWIS	95.7	112.8	1.91	0.44	240	5.2	0.0006	0.10
	USGS-NWIS	66.8	158.5	1.41	0.3	240	5.2	0.0006	0.08
	USGS-NWIS	40.9	190.5	0.82	0.26	240	5.2	0.0006	0.09
	USGS-NWIS	37.7	181.3	0.66	0.31	240	5.2	0.0006	0.12
	USGS-NWIS	35.1	144.8	1.17	0.21	240	5.2	0.0006	0.06
	USGS-NWIS	27.1	79.9	0.93	0.37	240	5.2	0.0006	0.12
Tanana near Nenana	USGS-NWIS	2273.5	263	4.49	1.93	314	4.5	0.000203	0.29
	USGS-NWIS	2015.9	263.9	4.26	1.79	314	4.5	0.000203	0.28
	USGS-NWIS	1823.3	251.1	4.29	1.69	314	4.5	0.000203	0.26
	USGS-NWIS	1585.5	313.9	2.83	1.79	314	4.5	0.000203	0.34
	USGS-NWIS	1299.5	265.8	3.6	1.36	314	4.5	0.000203	0.23
	USGS-NWIS	1101.4	271	3.01	1.35	314	4.5	0.000203	0.25
	USGS-NWIS	724.8	209.1	3.11	1.12	314	4.5	0.000203	0.20
	USGS-NWIS	546.4	227.1	2.33	1.03	314	4.5	0.000203	0.22
	USGS-NWIS	461.5	208.8	2.69	0.82	314	4.5	0.000203	0.16
	USGS-NWIS	242.9	228.6	2.4	0.44	314	4.5	0.000203	0.09
	USGS-NWIS	222.3	248.4	3.48	0.26	314	4.5	0.000203	0.04
	USGS-NWIS	195.1	201.2	2.22	0.44	314	4.5	0.000203	0.09
	USGS-NWIS	193.1	196.6	2.24	0.44	314	4.5	0.000203	0.09
	USGS-NWIS	192.2	214.9	2.19	0.41	314	4.5	0.000203	0.09
	USGS-NWIS	186	213.3	2.88	0.3	314	4.5	0.000203	0.06
	USGS-NWIS	180.1	225.5	1.92	0.41	314	4.5	0.000203	0.09
	USGS-NWIS	175	202.7	2.42	0.36	314	4.5	0.000203	0.07
	USGS-NWIS	169.3	228.6	2.01	0.37	314	4.5	0.000203	0.08
	USGS-NWIS	165.9	210.3	2.04	0.39	314	4.5	0.000203	0.09
	USGS-NWIS	156.9	214.9	1.79	0.41	314	4.5	0.000203	0.10
Susquehanna at Marietta	USGS-NWIS	6427	298.7	9.27	2.32	299	9.3	0.00044	0.24
	USGS-NWIS	5124.6	323.1	7.53	2.11	299	9.3	0.00044	0.25
	USGS-NWIS	3708.9	270	7.5	1.83	299	9.3	0.00044	0.21
	USGS-NWIS	2658.6	264.9	5.47	1.82	299	9.3	0.00044	0.25

River Name	Source	Discharge (m^3/s)	Width (m)	Mean Depth (m)	Mean Velocity (m/s)	Maximum Width (m)	Maximum Depth (m)	Slope (m/m)	Froude number
	USGS-NWIS	2064	243.8	6.06	1.42	299	9.3	0.00044	0.18
	USGS-NWIS	1891.3	243.8	5.94	1.31	299	9.3	0.00044	0.17
	USGS-NWIS	1449.6	271.3	3.85	1.39	299	9.3	0.00044	0.23
	USGS-NWIS	1160.8	240.8	4.48	1.08	299	9.3	0.00044	0.16
	USGS-NWIS	897.5	237.7	4.1	0.92	299	9.3	0.00044	0.15
	USGS-NWIS	620	226.8	3.12	0.88	299	9.3	0.00044	0.16
	USGS-NWIS	506.8	230.1	2.7	0.81	299	9.3	0.00044	0.16
	USGS-NWIS	413.4	225.5	2.7	0.68	299	9.3	0.00044	0.13
	USGS-NWIS	345.4	228.3	1.42	1.06	299	9.3	0.00044	0.28
	USGS-NWIS	261.3	203	1.29	1	299	9.3	0.00044	0.28
	USGS-NWIS	206.1	228.6	1.87	0.48	299	9.3	0.00044	0.11
	USGS-NWIS	153.2	224	1.68	0.36	299	9.3	0.00044	0.08
	USGS-NWIS	87.8	222.5	1.59	0.25	299	9.3	0.00044	0.06
	USGS-NWIS	30.9	102.1	0.45	0.66	299	9.3	0.00044	0.31
Mississippi at St. Cloud	USGS-NWIS	1282.6	195.1	5.24	1.26	195	5.2	0.00053	0.18
	USGS-NWIS	891.8	190.5	4.97	0.94	195	5.2	0.00053	0.13
	USGS-NWIS	651.2	185.9	4.52	0.77	195	5.2	0.00053	0.12
	USGS-NWIS	535.1	185.9	4.57	0.63	195	5.2	0.00053	0.09
	USGS-NWIS	501.1	190.5	4.41	0.6	195	5.2	0.00053	0.09
	USGS-NWIS	433.2	190.2	3.96	0.58	195	5.2	0.00053	0.09
	USGS-NWIS	393.5	186.8	4.06	0.52	195	5.2	0.00053	0.08
	USGS-NWIS	346	192	4.31	0.42	195	5.2	0.00053	0.06
	USGS-NWIS	317.1	187.4	4.32	0.39	195	5.2	0.00053	0.06
	USGS-NWIS	302.9	190.5	4.27	0.37	195	5.2	0.00053	0.06
	USGS-NWIS	273.8	189.9	4.11	0.35	195	5.2	0.00053	0.06
	USGS-NWIS	221.1	184.7	3.97	0.3	195	5.2	0.00053	0.05
	USGS-NWIS	188.8	170.7	3.97	0.28	195	5.2	0.00053	0.04
	USGS-NWIS	132.2	169.2	1.36	0.57	195	5.2	0.00053	0.16
	USGS-NWIS	73.9	152.4	0.92	0.53	195	5.2	0.00053	0.18
	USGS-NWIS	55.8	149	0.79	0.47	195	5.2	0.00053	0.17
	USGS-NWIS	52.7	147.8	1.09	0.33	195	5.2	0.00053	0.10
	USGS-NWIS	35.4	120.4	0.6	0.49	195	5.2	0.00053	0.20
	USGS-NWIS	25.7	90.2	0.62	0.46	195	5.2	0.00053	0.19
Kennebec at Sydney	USGS-NWIS	5549.3	207.3	10.4	2.58	207	10.4	0.000061	0.26
	USGS-NWIS	2944.5	196.6	7.04	2.13	207	10.4	0.000061	0.26
	USGS-NWIS	2491.5	195.1	6.33	2.02	207	10.4	0.000061	0.26
	USGS-NWIS	2154.6	190.8	5.06	2.23	207	10.4	0.000061	0.32
	USGS-NWIS	1837.5	190.5	5.32	1.81	207	10.4	0.000061	0.25
	USGS-NWIS	1511.9	189	4.81	1.66	207	10.4	0.000061	0.24
	USGS-NWIS	1169.3	182.9	5.44	1.18	207	10.4	0.000061	0.16
	USGS-NWIS	872	178.3	5.15	0.95	207	10.4	0.000061	0.13
	USGS-NWIS	586.1	176.8	4.35	0.76	207	10.4	0.000061	0.12
	USGS-NWIS	526.6	182.9	3.03	0.95	207	10.4	0.000061	0.17
	USGS-NWIS	396.4	182.9	2.39	0.91	207	10.4	0.000061	0.19
	USGS-NWIS	351.1	179.8	2.32	0.84	207	10.4	0.000061	0.18
	USGS-NWIS	268.1	182.6	2.8	0.52	207	10.4	0.000061	0.10
	USGS-NWIS	219.7	169.2	3.25	0.4	207	10.4	0.000061	0.07
	USGS-NWIS	164.5	175.3	2.26	0.41	207	10.4	0.000061	0.09
	USGS-NWIS	105	173.7	2.1	0.29	207	10.4	0.000061	0.06
	USGS-NWIS	75.9	179.8	1.96	0.22	207	10.4	0.000061	0.05
	USGS-NWIS	62.9	173.7	1.38	0.26	207	10.4	0.000061	0.07
	USGS-NWIS	26.8	158.5	1.08	0.16	207	10.4	0.000061	0.05
Allegheny at Salamanca	USGS-NWIS	852.2	114.9	4.07	1.82	115	4.1	0.00056	0.29
	USGS-NWIS	637	111.6	3.41	1.68	115	4.1	0.00056	0.29
	USGS-NWIS	472.8	114.3	2.75	1.51	115	4.1	0.00056	0.29
	USGS-NWIS	342.6	114.9	2.24	1.33	115	4.1	0.00056	0.28
	USGS-NWIS	317.1	114	2.18	1.28	115	4.1	0.00056	0.28
	USGS-NWIS	302.9	108.8	2.07	1.34	115	4.1	0.00056	0.30
	USGS-NWIS	276.9	114.6	1.93	1.26	115	4.1	0.00056	0.29
	USGS-NWIS	251.1	114.3	2.07	1.06	115	4.1	0.00056	0.24
	USGS-NWIS	203	105.8	1.77	1.09	115	4.1	0.00056	0.26
	USGS-NWIS	194.2	106.1	1.7	1.08	115	4.1	0.00056	0.26
	USGS-NWIS	166.5	107.6	1.58	0.98	115	4.1	0.00056	0.25
	USGS-NWIS	142.7	106.7	1.52	0.88	115	4.1	0.00056	0.23
	USGS-NWIS	137.9	108.2	1.43	0.89	115	4.1	0.00056	0.24
	USGS-NWIS	115.2	108.2	1.54	0.69	115	4.1	0.00056	0.18
	USGS-NWIS	110.1	106.7	1.57	0.66	115	4.1	0.00056	0.17
	USGS-NWIS	89.2	107.6	1.44	0.58	115	4.1	0.00056	0.15
	USGS-NWIS	81.3	109.7	1.2	0.62	115	4.1	0.00056	0.18
	USGS-NWIS	64.6	106.7	1.11	0.54	115	4.1	0.00056	0.16

River Name	Source	Discharge (m^3/s)	Width (m)	Mean Depth (m)	Mean Velocity (m/s)	Maximum Width (m)	Maximum Depth (m)	Slope (m/m)	Froude number
	USGS-NWIS	49	99.7	0.69	0.71	115	4.1	0.00056	0.27
	USGS-NWIS	32.6	95.7	0.51	0.67	115	4.1	0.00056	0.30
Hudson at Hadley	USGS-NWIS	487	118.3	3.49	1.18	118	3.5	0.00052	0.20
	USGS-NWIS	314.3	114.6	2.75	1	118	3.5	0.00052	0.19
	USGS-NWIS	240.7	112.8	2.44	0.87	118	3.5	0.00052	0.18
	USGS-NWIS	214.3	114.3	2.32	0.81	118	3.5	0.00052	0.17
	USGS-NWIS	184	114.3	2.08	0.77	118	3.5	0.00052	0.17
	USGS-NWIS	161.4	112.8	2.01	0.71	118	3.5	0.00052	0.16
	USGS-NWIS	141	112.8	1.95	0.64	118	3.5	0.00052	0.15
	USGS-NWIS	101.6	109.7	1.79	0.52	118	3.5	0.00052	0.12
	USGS-NWIS	90	107.9	1.72	0.48	118	3.5	0.00052	0.12
	USGS-NWIS	87.2	106.4	1.76	0.47	118	3.5	0.00052	0.11
	USGS-NWIS	73.6	106.7	1.67	0.41	118	3.5	0.00052	0.10
	USGS-NWIS	59.5	98.1	1.59	0.38	118	3.5	0.00052	0.10
	USGS-NWIS	54.4	91.4	1.65	0.36	118	3.5	0.00052	0.09
	USGS-NWIS	43.3	88.4	1.3	0.38	118	3.5	0.00052	0.11
	USGS-NWIS	39.6	85.9	1.63	0.28	118	3.5	0.00052	0.07
	USGS-NWIS	38.5	85.9	1.65	0.27	118	3.5	0.00052	0.07
	USGS-NWIS	35.1	83.8	1.66	0.25	118	3.5	0.00052	0.06
	USGS-NWIS	33.1	85.3	1.57	0.25	118	3.5	0.00052	0.06
	USGS-NWIS	29.7	76.5	1.68	0.23	118	3.5	0.00052	0.06
	USGS-NWIS	18.8	76.2	1.54	0.16	118	3.5	0.00052	0.04
Matanuska at Palmer	USGS-NWIS	878.8	93.9	3.34	2.8	94	3.3	0.0043	0.49
	USGS-NWIS	693.7	84.7	2.92	2.81	94	3.3	0.0043	0.53
	USGS-NWIS	651.2	93.3	2.41	2.9	94	3.3	0.0043	0.60
	USGS-NWIS	617.2	93.6	2.59	2.54	94	3.3	0.0043	0.50
	USGS-NWIS	506.8	85.3	2.34	2.54	94	3.3	0.0043	0.53
	USGS-NWIS	450.2	68.6	2.52	2.61	94	3.3	0.0043	0.53
	USGS-NWIS	419	85.3	2.26	2.16	94	3.3	0.0043	0.46
	USGS-NWIS	390.7	90.5	1.86	2.32	94	3.3	0.0043	0.54
	USGS-NWIS	356.7	70.7	2.4	2.1	94	3.3	0.0043	0.43
	USGS-NWIS	331.3	68.6	2.14	2.25	94	3.3	0.0043	0.49
	USGS-NWIS	297.3	80.2	1.67	2.21	94	3.3	0.0043	0.55
	USGS-NWIS	272.4	87.8	1.72	1.8	94	3.3	0.0043	0.44
	USGS-NWIS	235.8	83.2	1.63	1.74	94	3.3	0.0043	0.44
	USGS-NWIS	212.6	84.7	1.32	1.91	94	3.3	0.0043	0.53
	USGS-NWIS	188.6	74.1	1.73	1.47	94	3.3	0.0043	0.36
	USGS-NWIS	132.5	67.1	1.43	1.38	94	3.3	0.0043	0.37
	USGS-NWIS	101.9	92	0.82	1.34	94	3.3	0.0043	0.47
	USGS-NWIS	47.3	83.5	0.59	0.96	94	3.3	0.0043	0.40
	USGS-NWIS	24.3	38.1	0.7	0.91	94	3.3	0.0043	0.35
Merrimack at Franklin	USGS-NWIS	458.7	83.8	4.72	1.17	84	4.7	0.0002	0.17
	USGS-NWIS	421.9	80.8	4.69	1.11	84	4.7	0.0002	0.16
	USGS-NWIS	295	79.2	4.09	0.91	84	4.7	0.0002	0.14
	USGS-NWIS	185.4	77.1	3.54	0.68	84	4.7	0.0002	0.12
	USGS-NWIS	163.1	78	3.36	0.62	84	4.7	0.0002	0.11
	USGS-NWIS	145	77.7	3.27	0.58	84	4.7	0.0002	0.10
	USGS-NWIS	113.8	74.7	3.11	0.49	84	4.7	0.0002	0.09
	USGS-NWIS	95.7	77.7	2.98	0.41	84	4.7	0.0002	0.08
	USGS-NWIS	90.3	77.4	2.94	0.4	84	4.7	0.0002	0.07
	USGS-NWIS	84.4	76.8	2.85	0.39	84	4.7	0.0002	0.07
	USGS-NWIS	74.2	76.2	2.84	0.34	84	4.7	0.0002	0.06
	USGS-NWIS	51	75.3	2.67	0.25	84	4.7	0.0002	0.05
	USGS-NWIS	32.8	75.6	2.43	0.18	84	4.7	0.0002	0.04
	USGS-NWIS	27.4	73.1	2.45	0.15	84	4.7	0.0002	0.03
	USGS-NWIS	25.9	74.7	2.44	0.14	84	4.7	0.0002	0.03
	USGS-NWIS	24	85.3	0.87	0.33	84	4.7	0.0002	0.11
	USGS-NWIS	20.8	73.1	2.39	0.12	84	4.7	0.0002	0.02
	USGS-NWIS	20.2	84.7	0.76	0.31	84	4.7	0.0002	0.11
White at W. Hartford	USGS-NWIS	308.6	47.9	3.24	1.98	48	3.2	0.0012	0.35
	USGS-NWIS	233	42.7	3.12	1.75	48	3.2	0.0012	0.32
	USGS-NWIS	145.2	38.7	3.12	1.2	48	3.2	0.0012	0.22
	USGS-NWIS	109.6	38.1	2.97	0.97	48	3.2	0.0012	0.18
	USGS-NWIS	89.5	37.8	2.8	0.84	48	3.2	0.0012	0.16
	USGS-NWIS	82.4	36.9	2.85	0.79	48	3.2	0.0012	0.15
	USGS-NWIS	62.3	72.2	1.58	0.55	48	3.2	0.0012	0.14
	USGS-NWIS	47.3	35.4	2.61	0.51	48	3.2	0.0012	0.10
	USGS-NWIS	32.6	84.4	0.81	0.48	48	3.2	0.0012	0.17
	USGS-NWIS	30.9	95.4	0.44	0.73	48	3.2	0.0012	0.35
	USGS-NWIS	28.9	83.2	0.72	0.48	48	3.2	0.0012	0.18

River Name	Source	Discharge (m³/s)	Width (m)	Mean Depth (m)	Mean Velocity (m/s)	Maximum Width (m)	Maximum Depth (m)	Slope (m/m)	Froude number
	USGS-NWIS	28	93.9	0.38	0.79	48	3.2	0.0012	0.41
	USGS-NWIS	24.7	75.3	0.71	0.46	48	3.2	0.0012	0.17
	USGS-NWIS	22.3	76.8	0.74	0.39	48	3.2	0.0012	0.14
	USGS-NWIS	19.6	57.6	0.52	0.65	48	3.2	0.0012	0.29
	USGS-NWIS	16.7	80.5	0.6	0.34	48	3.2	0.0012	0.14
	USGS-NWIS	13.5	74.4	0.65	0.28	48	3.2	0.0012	0.11
	USGS-NWIS	10.4	79.9	0.49	0.27	48	3.2	0.0012	0.12
	USGS-NWIS	8.1	81.1	0.49	0.2	48	3.2	0.0012	0.09
	USGS-NWIS	5.3	82	0.43	0.15	48	3.2	0.0012	0.07
Columbia	Barnes 1967	11494.96	529.4	8.53	2.55	529	8.5	0.00019	0.28
Columbia	Barnes 1967	28312.7	510.8	16.79	3.3	511	16.8	0.000266	0.26
Amazon at Obidos	Oltman 1968	216000	2290	48.03	1.96	2300	50	7.3E-06	0.09
	Oltman 1968	72500	2260	40.88	0.78	2300	50	7.3E-06	0.04
	Dury 1976	283170	2300	50.33	2.45	2300	50	7.3E-06	0.11
	Oltman 1968	165000	2280	46.49	1.56	2300	50	7.3E-06	0.07

Appendix 3 - Bankfull River Discharge and Channel Geometry Data

Table A3 - Bankfull River Discharge and Channel Geometry Data Base

River Name	Discharge (m^3/s)	Water surface slope (m/m)	Channel width (m)	Average Channel Depth (m)	Average Channel Velocity (m/s)	Froude Number	Source
NA	368	0.0042	47	2.41	3.25	0.67	**Church and Rood**
NA	116	0.001	32	1.73	2.10	0.51	1983
NA	91.8	0.0007	42	2.58	0.85	0.17	(includes data from
NA	581	0.00085	99	7.01	0.84	0.10	Bray, 1979; and
NA	668	0.0008	69	5.95	1.63	0.21	Williams, 1978).
NA	69.4	0.0025	33	3.08	0.68	0.12	
NA	17.6	0.0048	13	0.65	2.08	0.83	
NA	23.8	0.0073	31	1.03	0.75	0.23	
NA	5.7	0.0037	10	0.58	0.98	0.41	
NA	3	0.0412	3	0.33	3.03	1.69	
NA	7.5	0.0146	7	0.44	2.44	1.17	
NA	89.2	0.0063	26	1.58	2.17	0.55	
NA	60.9	0.0061	34	0.76	2.36	0.86	
NA	27.5	0.0036	24	0.7	1.64	0.62	
NA	8.2	0.003	25	0.71	0.46	0.18	
NA	365	0.003	37	3.38	2.92	0.51	
NA	1.7	0.0184	4	0.59	0.72	0.30	
NA	10.5	0.0026	27	0.81	0.48	0.17	
NA	10.9	0.0042	13	0.66	1.27	0.50	
NA	275	0.0042	29	2.49	3.81	0.77	
NA	10.5	0.001	20	0.88	0.60	0.20	
NA	187	0.001	32	2.51	2.33	0.47	
NA	226	0.0008	58	1.78	2.19	0.52	
NA	73.6	0.0135	16	1.07	4.30	1.33	
NA	13.2	0.0039	8	0.81	2.04	0.72	
NA	12.2	0.0025	14	0.7	1.24	0.48	
NA	79.3	0.0008	29	1.43	1.91	0.51	
NA	22.2	0.004	17	0.55	2.37	1.02	
NA	12	0.0064	17	0.93	0.76	0.25	
NA	12.6	0.0074	15	0.9	0.93	0.31	
NA	24.5	0.0092	13	0.83	2.27	0.80	
NA	6.2	0.0237	4	0.41	3.78	1.89	
NA	5	0.0066	7	0.39	1.83	0.94	
NA	4.5	0.0154	3	0.5	3.00	1.36	
NA	5.5	0.0013	17	0.65	0.50	0.20	
NA	45.3	0.0029	29	1.71	0.91	0.22	
NA	850	0.0012	141	2.76	2.18	0.42	
NA	229	0.00127	90	1.25	2.04	0.58	
NA	354	0.00019	149	2.36	1.01	0.21	
NA	10.2	0.0118	12	0.55	1.55	0.67	
NA	5.5	0.0152	10	0.37	1.49	0.78	
NA	5.5	0.0162	8	0.37	1.86	0.98	
NA	4.9	0.0263	8	0.46	1.33	0.63	
NA	28.3	0.004	24	0.76	1.55	0.57	
NA	13.5	0.0099	10	0.82	1.65	0.58	
NA	20.2	0.0036	16	0.98	1.29	0.42	
NA	106	0.0041	35	1.9	1.59	0.37	
NA	6.29	0.051	9	0.37	1.89	0.99	
NA	2.75	0.052	3	0.46	1.99	0.94	
NA	5.83	0.0128	10	0.37	1.58	0.83	
NA	1.52	0.081	5	0.24	1.27	0.83	
NA	7.73	0.0148	12	0.34	1.89	1.04	
NA	9.29	0.0107	9	0.64	1.61	0.64	
NA	1.51	0.0369	2	0.27	2.80	1.72	
NA	12.9	0.0124	9	0.73	1.96	0.73	
NA	145	0.0046	50	1.3	2.23	0.62	
NA	8.86	0.0157	9	0.55	1.79	0.77	
NA	3.51	0.0307	4	0.52	1.69	0.75	
NA	6.2	0.0208	7	0.52	1.70	0.75	
NA	25.3	0.0106	15	0.73	2.31	0.86	
NA	11.6	0.013	10	0.61	1.90	0.78	
NA	1.9	0.0755	2	0.37	2.57	1.35	
NA	7.62	0.0025	10	0.73	1.04	0.39	
NA	8.92	0.046	13	0.4	1.72	0.87	
NA	5.24	0.0495	13	0.3	1.34	0.78	
NA	2.25	0.0625	3	0.4	1.88	0.95	
NA	6.85	0.0604	7	0.46	2.13	1.00	
NA	1.06	0.0165	3	0.4	0.88	0.45	

River Name	Discharge (m^3/s)	Water surface slope (m/m)	Channel width (m)	Average Channel Depth (m)	Average Channel Velocity (m/s)	Froude Number	Source
NA	0.535	0.013	3	0.3	0.59	0.35	
NA	2.42	0.0356	7	0.37	0.93	0.49	
NA	156	0.0018	50	1.5	2.08	0.54	
NA	17	0.0089	14	0.52	2.34	1.03	
NA	3.4	0.026	6	0.3	1.89	1.10	
NA	31	0.0143	13	0.76	3.14	1.15	
NA	1.7	0.0009	5	0.27	1.26	0.77	
NA	6.3	0.035	6	0.49	2.14	0.98	
NA	16.7	0.0169	9	0.76	2.44	0.89	
NA	510	0.0022	104	1.87	2.62	0.61	
NA	666	0.0022	106	2.03	3.10	0.69	
NA	9621	0.00004	832	7.92	1.46	0.17	
NA	10895	0.00004	881	8.1	1.53	0.17	
NA	16696	0.00007	738	11.18	2.02	0.19	
NA	9055	0.00007	725	8.22	1.52	0.17	
NA	10753	0.0007	728	8.86	1.67	0.18	
NA	107	0.0011	59	2.62	0.69	0.14	
NA	68	0.00011	51	2.16	0.62	0.13	
NA	101	0.00011	58	2.52	0.69	0.14	
NA	141	0.00021	54	2.92	0.89	0.17	
NA	127	0.00021	54	2.74	0.86	0.17	
NA	848	0.0003	225	2.74	1.38	0.27	
NA	396	0.0003	203	2.07	0.94	0.21	
NA	679	0.0003	219	2.52	1.23	0.25	
NA	1058	0.00036	235	3.53	1.28	0.22	
NA	2263	0.00036	253	4.78	1.87	0.27	
NA	565	0.00033	79	4.14	1.73	0.27	
NA	96	0.00033	51	2.01	0.94	0.21	
NA	152	0.00033	55	2.46	1.12	0.23	
NA	396	0.0005	39	7.19	1.41	0.17	
NA	79	0.0005	30	1.79	1.47	0.35	
NA	141	0.0005	33	2.92	1.46	0.27	
NA	148	0.0002	42	3.77	0.93	0.15	
NA	148	0.0002	42	3.77	0.93	0.15	
NA	130	0.00051	46	3.2	0.88	0.16	
NA	48	0.00051	33	1.73	0.84	0.20	
NA	121	0.00051	46	3.04	0.87	0.16	
NA	2605	0.00009	442	5.33	1.11	0.15	
NA	7782	0.00074	479	5.82	2.79	0.37	
NA	6084	0.00074	475	4.99	2.57	0.37	
NA	6933	0.00074	475	5.36	2.72	0.38	
NA	121	0.0054	51	1.15	2.06	0.61	
NA	48	0.0054	40	0.85	1.41	0.49	
NA	84	0.0054	47	1.03	1.74	0.55	
NA	52	0.016	35	0.76	1.95	0.72	
NA	40	0.016	28	0.73	1.96	0.73	
NA	20	0.019	24	0.58	1.44	0.60	
NA	13	0.019	23	0.55	1.03	0.44	
NA	2829	0.0025	201	3.47	4.06	0.70	
NA	690	0.0025	151	1.79	2.55	0.61	
NA	933	0.0025	162	2.01	2.87	0.65	
NA	165	0.0057	49	1.09	3.09	0.95	
NA	84	0.0057	40	0.97	2.16	0.70	
NA	155	0.0057	48	1.09	2.96	0.91	
NA	18	0.001	21	0.97	0.88	0.29	
NA	37	0.001	25	1.09	1.36	0.42	
NA	169	0.0049	72	1.21	1.94	0.56	
NA	311	0.0049	73	1.64	2.60	0.65	
NA	152	0.0025	95	1.24	1.29	0.37	
NA	52	0.0077	35	0.73	2.04	0.76	
NA	101	0.0077	41	0.82	3.00	1.06	
NA	65	0.0038	45	0.76	1.90	0.70	
NA	181	0.0038	62	1.03	2.83	0.89	
NA	486	0.0017	121	1.98	2.03	0.46	
NA	299	0.0017	110	1.58	1.72	0.44	
NA	9004	0.00069	549	7.6	2.16	0.25	
NA	7220	0.00069	546	6.8	1.94	0.24	
NA	8212	0.00069	548	7.22	2.08	0.25	
NA	1416	0.0012	82	5	3.45	0.49	
NA	159	0.0012	67	2.1	1.13	0.25	

River Name	Discharge (m³/s)	Water surface slope (m/m)	Channel width (m)	Average Channel Depth (m)	Average Channel Velocity (m/s)	Froude Number	Source
NA	278	0.0012	71	2.5	1.57	0.32	
NA	55	0.0014	29	1.5	1.26	0.33	
NA	18	0.0014	22	1	0.82	0.26	
NA	39	0.0014	27	1.3	1.11	0.31	
NA	2378	0.0018	149	3.4	4.69	0.81	
NA	439	0.0018	126	1.7	2.05	0.50	
NA	595	0.0018	130	1.9	2.41	0.56	
NA	178	0.0019	76	1.7	1.38	0.34	
NA	68	0.0019	55	0.94	1.32	0.43	
NA	101	0.0019	62	1.2	1.36	0.40	
NA	749	0.00081	166	2.4	1.86	0.39	
NA	1358	0.00081	174	3.23	2.42	0.43	
NA	14998	0.00022	475	11.15	2.83	0.27	
NA	8206	0.00022	469	6.91	2.53	0.31	
NA	9763	0.00022	472	7.89	2.62	0.30	
NA	2405	0.00052	271	4.2	2.11	0.33	
NA	3395	0.00052	274	5.18	2.39	0.34	
NA	5433	0.00052	280	6.94	2.80	0.34	
NA	834	0.00051	168	2.65	1.87	0.37	
NA	1584	0.00051	182	3.53	2.47	0.42	
NA	1839	0.00094	111	3.84	4.31	0.70	
NA	679	0.00094	99	2.8	2.45	0.47	
NA	919	0.00094	103	3.07	2.91	0.53	
NA	905	0.00092	191	2.59	1.83	0.36	
NA	1075	0.00092	194	2.83	1.96	0.37	
NA	1075	0.0012	168	2.46	2.60	0.53	
NA	481	0.0012	160	1.58	1.90	0.48	
NA	792	0.0012	165	2.07	2.32	0.51	
NA	1811	0.00084	134	4.57	2.96	0.44	
NA	305	0.00084	111	1.67	1.65	0.41	
NA	543	0.00084	117	2.19	2.12	0.46	
NA	113	0.00055	38	2.04	1.46	0.33	
NA	28	0.00055	29	1.34	0.72	0.20	
NA	56	0.00055	32	1.67	1.05	0.26	
NA	203	0.0033	80	1.37	1.85	0.51	
NA	79	0.0033	61	1	1.30	0.41	
NA	166	0.0033	78	1.24	1.72	0.49	
NA	155	0.0018	69	1.7	1.32	0.32	
NA	288	0.0018	75	2.31	1.66	0.35	
NA	481	0.0026	95	2.37	2.14	0.44	
NA	594	0.0026	98	2.56	2.37	0.47	
NA	367	0.004	94	1.58	2.47	0.63	
NA	509	0.004	97	1.7	3.09	0.76	
NA	314	0.002	104	1.43	2.11	0.56	
NA	404	0.002	107	1.61	2.35	0.59	
NA	933	0.0012	85	3.29	3.34	0.59	
NA	124	0.0012	63	1.4	1.41	0.38	
NA	234	0.0012	69	1.79	1.89	0.45	
NA	62	0.0036	31	1.21	1.65	0.48	
NA	28	0.0036	26	0.88	1.22	0.42	
NA	59	0.0036	31	1.18	1.61	0.47	
NA	53	0.0035	44	0.79	1.52	0.55	
NA	53	0.0035	44	0.79	1.52	0.55	
NA	130	0.0012	28	3.41	1.36	0.24	
NA	10	0.0012	16	1.12	0.56	0.17	
NA	18	0.0012	19	1.4	0.68	0.18	
NA	339	0.0012	112	1.82	1.66	0.39	
NA	650	0.0012	130	2.46	2.03	0.41	
NA	1018	0.00035	123	3.84	2.16	0.35	
NA	350	0.00035	111	2.28	1.38	0.29	
NA	693	0.00035	119	3.2	1.82	0.32	
NA	141	0.0036	41	1.67	2.06	0.51	
NA	28	0.0036	27	0.88	1.18	0.40	
NA	59	0.0036	30	1.31	1.50	0.42	
NA	891	0.00044	180	2.62	1.89	0.37	
NA	1584	0.00044	192	3.56	2.32	0.39	
NA	42	0.0024	30	0.94	1.49	0.49	
NA	32	0.0024	28	0.91	1.26	0.42	
NA	65	0.0032	31	1.24	1.69	0.49	
NA	33	0.0032	27	0.88	1.39	0.47	

River Name	Discharge (m^3/s)	Water surface slope (m/m)	Channel width (m)	Average Channel Depth (m)	Average Channel Velocity (m/s)	Froude Number	Source
NA	57	0.0032	30	1.15	1.65	0.49	
NA	277	0.0037	77	1.49	2.41	0.63	
NA	127	0.0037	57	1.12	1.99	0.60	
NA	203	0.0037	69	1.34	2.20	0.61	
NA	12	0.0067	19	0.73	0.87	0.32	
NA	27	0.0067	22	0.91	1.35	0.45	
NA	100	0.0008	35	2.04	1.40	0.31	
NA	29	0.0008	27	0.94	1.14	0.38	
NA	65	0.0008	36	1.37	1.32	0.36	
NA	203	0.00079	50	2.16	1.88	0.41	
NA	42	0.00079	34	1.21	1.02	0.30	
NA	96	0.00079	42	1.58	1.45	0.37	
NA	46	0.0085	29	1	1.59	0.51	
NA	67	0.0085	30	1.24	1.80	0.52	
NA	118	0.0019	75	0.97	1.62	0.53	
NA	161	0.0019	76	1.12	1.89	0.57	
NA	42	0.00051	27	1.58	0.98	0.25	
NA	3	0.00051	12	0.85	0.29	0.10	
NA	16	0.00051	20	1.37	0.58	0.16	
NA	11	0.011	18	0.57	1.07	0.45	
NA	5	0.011	14	0.42	0.85	0.42	
NA	8	0.011	17	0.48	0.98	0.45	
NA	110	0.0041	46	1.06	2.26	0.70	
NA	161	0.0041	50	1.18	2.73	0.80	
NA	489	0.002	119	2.31	1.78	0.37	
NA	99	0.002	91	1.03	1.06	0.33	
NA	175	0.002	101	1.37	1.26	0.35	
NA	10	0.0051	16	0.51	1.23	0.55	
NA	39	0.0051	22	0.76	2.33	0.85	
NA	268	0.00059	53	2.22	2.28	0.49	
NA	46	0.00059	37	1.12	1.11	0.34	
NA	77	0.00059	41	1.43	1.31	0.35	
NA	23	0.0025	26	0.7	1.26	0.48	
NA	79	0.0025	31	0.85	3.00	1.04	
NA	13	0.0018	14	0.76	1.22	0.45	
NA	29	0.0018	16	0.97	1.87	0.61	
NA	73	0.0059	37	0.94	2.10	0.69	
NA	124	0.0059	43	1.06	2.72	0.84	
NA	93	0.0042	52	0.85	2.10	0.73	
NA	164	0.0042	57	0.88	3.27	1.11	
NA	110	0.0016	64	1.24	1.39	0.40	
NA	220	0.0016	70	1.64	1.92	0.48	
NA	186	0.0021	59	1.28	2.46	0.70	
NA	45	0.0021	43	0.82	1.28	0.45	
NA	142	0.0021	56	1.18	2.15	0.63	
NA	104	0.0038	45	1.09	2.12	0.65	
NA	169	0.0038	49	1.4	2.46	0.67	
NA	101	0.0046	45	1	2.24	0.72	
NA	174	0.0046	57	1.18	2.59	0.76	
NA	509	0.0016	126	2.37	1.70	0.35	
NA	226	0.0016	116	1.79	1.09	0.26	
NA	382	0.0016	122	2.16	1.45	0.32	
NA	413	0.0012	109	1.92	1.97	0.45	
NA	549	0.0012	111	2.22	2.23	0.48	
NA	127	0.0041	61	1.17	1.78	0.53	
NA	510	0.0042	152	1.01	3.32	1.06	
NA	630	0.0031	108	2.3	2.54	0.53	
NA	199	0.004	46	1.5	2.88	0.75	
NA	153	0.0044	55	1.25	2.23	0.64	
NA	8.5	0.0156	12	0.49	1.45	0.66	
NA	161	0.0007	90	1.19	1.50	0.44	
NA	141	0.002	27	3.51	1.49	0.25	
NA	11553	0.0004	594	8.84	2.20	0.24	
NA	368	0.0008	99	2.79	1.33	0.25	
NA	163	0.0017	68	1.23	1.95	0.56	
NA	73	0.002	37	3.51	0.56	0.10	
NA	2265	0.0001	197	5.15	2.23	0.31	
NA	4474	0.0015	229	7.01	2.79	0.34	
NA	258	0.0007	85	2.45	1.24	0.25	
NA	1954	0.0015	161	4.57	2.66	0.40	

River Name	Discharge (m^3/s)	Water surface slope (m/m)	Channel width (m)	Average Channel Depth (m)	Average Channel Velocity (m/s)	Froude Number	Source
NA	40	0.0015	48	0.98	0.85	0.27	
NA	733	0.0005	111	3.86	1.71	0.28	
NA	255	0.0014	104	1.36	1.80	0.49	
NA	354	0.00159	87	1.98	2.06	0.47	
NA	9628	0.00056	493	6.77	2.88	0.35	
NA	6478	0.0004	582	4.55	2.45	0.37	
NA	2890	0.00047	311	4.63	2.01	0.30	
NA	2661	0.00056	242	4.6	2.39	0.36	
NA	2280	0.00026	333	4.64	1.48	0.22	
NA	1402	0.0004	289	3.16	1.54	0.28	
NA	2718	0.00032	356	4.24	1.80	0.28	
NA	55	0.00053	31	2.53	0.70	0.14	
NA	425	0.0042	61	2.3	3.03	0.64	
NA	481	0.0019	79	3.29	1.85	0.33	
NA	198	0.00092	82	1.98	1.22	0.28	
NA	23	0.0007	18	1.2	1.06	0.31	
NA	64	0.0044	17	1.78	2.12	0.51	
NA	10	0.0064	14	0.73	0.98	0.37	
NA	10.7	0.013	10	0.73	1.47	0.55	
NA	29.5	0.0045	14	1.34	1.57	0.43	
NA	66	0.0048	18	1.79	2.05	0.49	
NA	66	0.0105	19	1.36	2.55	0.70	
NA	140	0.0017	34	3.06	1.35	0.25	
NA	58	0.0057	18	1.36	2.37	0.65	
NA	67	0.0018	31	1.77	1.22	0.29	
NA	25	0.0052	25	0.78	1.28	0.46	
NA	66	0.0024	26	1.16	2.19	0.65	
NA	81	0.0014	29	1.63	1.71	0.43	
NA	170	0.0074	40	1.89	2.25	0.52	
NA	260	0.0007	56	2.77	1.68	0.32	
NA	14.2	0.0032	17	0.69	1.21	0.47	
NA	36.5	0.0137	14	1.06	2.46	0.76	
NA	370	0.0015	58	3.6	1.77	0.30	
NA	66	0.0014	19	2.47	1.41	0.29	
NA	2.7	0.0023	5	0.65	0.83	0.33	
NA	212	0.0036	43	2.09	2.36	0.52	
NA	157	0.0009	39	2.64	1.52	0.30	
NA	550	0.0007	59	4.19	2.22	0.35	
NA	38	0.002	19	1.67	1.20	0.30	
NA	24	0.0037	17	0.74	1.91	0.71	
NA	40	0.0028	20	1.29	1.55	0.44	
NA	45	0.00066	18	1.27	1.97	0.56	
NA	66	0.00069	27	1.6	1.53	0.39	
NA	68	0.00062	23	1.5	1.97	0.51	
NA	13	0.003	12	1.17	0.93	0.27	
NA	4.8	0.0094	10	0.53	0.91	0.40	
NA	1.1	0.0193	3	0.4	0.92	0.46	
NA	3.8	0.0115	10	0.42	0.90	0.45	
NA	3.5	0.0125	5	0.56	1.25	0.53	
NA	2270	0.0015	244	4.36	2.13	0.33	
NA	0.61	0.0286	4	0.1	1.53	1.54	
NA	4.9	0.0175	31	0.11	1.44	1.38	
NA	3.6	0.0151	24	0.13	1.15	1.02	
NA	0.06	0.032	2	0.04	0.75	1.20	
NA	2096	0.00121	121	4.87	3.56	0.51	
NA	1042	0.00189	170	2.25	2.72	0.58	
NA	1700	0.00221	178	3.33	2.87	0.50	
NA	3820	0.01003	212	4.77	3.78	0.55	
NA	16300	0.00007	776	11.34	1.85	0.18	
NA	16950	0.00009	625	13.92	1.95	0.17	
NA	1500	0.00013	515	3	0.97	0.18	
NA	4000	0.00013	525	6	1.27	0.17	
NA	3426	0.0011	195	5.67	3.10	0.42	
NA	5154	0.0013	206	7.01	3.57	0.43	
NA	2662	0.00055	146	5.94	3.07	0.40	
NA	3341	0.00065	148	6.55	3.45	0.43	
NA	1133	0.00027	226	3.76	1.33	0.22	
NA	850	0.0003	186	2.97	1.54	0.29	
NA	850	0.00031	187	2.2	2.07	0.44	
NA	133	0.015	22	2.59	2.33	0.46	

River Name	Discharge (m^3/s)	Water surface slope (m/m)	Channel width (m)	Average Channel Depth (m)	Average Channel Velocity (m/s)	Froude Number	Source
NA	159	0.015	23	2.74	2.52	0.49	
NA	184	0.011	35	2.01	2.62	0.59	
NA	221	0.011	35	2.16	2.92	0.64	
NA	317	0.0063	109	1.19	2.44	0.72	
NA	428	0.0063	113	1.37	2.76	0.75	
NA	3.4	0.0108	6	0.45	1.26	0.60	
NA	2832	0.00091	900	2.14	1.47	0.32	
NA	6.7	0.0023	10	0.48	1.40	0.64	
NA	0.7	0.026	2	0.2	1.75	1.25	
NA	85.2	0.0014	47	0.97	1.87	0.61	
NA	7.1	0.017	9	0.52	1.52	0.67	
NA	9.8	0.019	12	0.46	1.78	0.84	
NA	12.2	0.0046	12	0.73	1.39	0.52	
NA	2.2	0.011	7	0.34	0.92	0.51	
NA	2.7	0.014	7	0.29	1.33	0.79	
NA	1.9	0.0061	5	0.31	1.23	0.70	
NA	8.4	0.015	9	0.43	2.17	1.06	
NA	22.6	0.0044	18	0.73	1.72	0.64	
NA	4.5	0.0206	8	0.49	1.15	0.52	
NA	3.2	0.01	6	0.39	1.37	0.70	
NA	2.5	0.0092	6	0.41	1.02	0.51	
NA	49	0.0058	34	0.84	1.72	0.60	
NA	37.5	0.0067	26	0.91	1.58	0.53	
NA	7.1	0.0046	12	0.52	1.14	0.50	
NA	42	0.0058	25	0.88	1.91	0.65	
NA	101	0.0037	37	1.45	1.88	0.50	
NA	167	0.0018	53	1.63	1.93	0.48	
NA	46.7	0.002	24	1.62	1.20	0.30	
NA	255	0.00088	84	1.85	1.64	0.39	
NA	72.2	0.0071	31	1.13	2.06	0.62	
NA	114	0.0024	37	1.65	1.87	0.46	
Diamond	132.9	0.0196	33.2	1	4.00	1.28	**Dingman and**
Wild	205	0.0198	43.5	0.8	5.89	2.10	**and Palaia, 1999**
Ellis	33.7	0.049	20.2	1.3	1.28	0.36	
Lucy	16.1	0.039	14.4	1	1.12	0.36	
Saco	462.6	0.0018	69.8	2.2	3.01	0.65	
Oyster	8.5	0.0022	12.1	0.7	1.00	0.38	
Dudley	4.6	0.0015	8	0.6	0.96	0.40	
Pemii W	302.9	0.0026	61.4	1.6	3.08	0.78	
Stevens	5.8	0.022	8.4	0.3	2.30	1.34	
Baker	144.8	0.0007	34.4	1.8	2.34	0.56	
Pemi P	588.3	0.0017	81.8	4.3	1.67	0.26	
Smith	49.1	0.0037	19.1	1.3	1.98	0.55	
Beards	33.9	0.0125	17.2	0.6	3.28	1.35	
W Br War	8.9	0.0085	8.1	0.8	1.37	0.49	
Warner	60.3	0.001	27.6	1.2	1.82	0.53	
Soucock	32.2	0.0011	14.6	1.4	1.58	0.43	
S Br Pisc	57.6	0.0018	26.7	0.8	2.70	0.96	
Stony	5.2	0.0126	6	0.5	1.73	0.78	
Halls	89.4	0.0045	19.9	1.6	2.81	0.71	
E Br Pass	35.7	0.004	17.3	1.2	1.72	0.50	
Moose	58.6	0.01	19.3	1	3.04	0.97	
Moose St	75.2	0.008	32.8	0.9	2.55	0.86	
Ammon	119	0.0075	25.7	1	4.63	1.48	
E Orange	6.9	0.011	8.4	0.6	1.37	0.56	
Mink	6.1	0.016	7.7	0.6	1.32	0.54	
Ayers	20.1	0.0021	17.1	2	0.59	0.13	
White	487.8	0.0012	86.8	4.1	1.37	0.22	
Williams	113.8	0.003	37	1.2	2.56	0.75	
Saxtons	73.3	0.004	19.1	0.7	5.48	2.09	
Cold	55.5	0.011	21.2	1	2.62	0.84	
S Br Ashu	26.6	0.0154	9.6	0.5	5.54	2.50	
Batten	90.5	0.0024	32.8	1.4	1.97	0.53	
Dog	88.7	0.0036	24.8	2.3	1.56	0.33	
Mad	161.7	0.0013	40	1.8	2.25	0.53	
Missisq	267.9	0.001	56	2.8	1.84	0.35	
Black	58.2	0.0024	18.4	1.7	1.86	0.46	
Paradise Creek near Paradise KS	36.81	0.001	9.75	2.38	1.59	0.33	**Schumm, 1960**
North Fork Solomon River near Downs, KS	226.5	0.0006	24.99	2.62	3.46	0.68	
Prairie Dog Creek at Norton KS	73.61	0.0005	13.72	1.89	2.84	0.66	

River Name	Discharge (m^3/s)	Water surface slope (m/m)	Channel width (m)	Average Channel Depth (m)	Average Channel Velocity (m/s)	Froude Number	Source
Sappa Creek at Stamford NE	50.96	0.0013	13.11	1.83	2.12	0.50	
Sappa Creek at Beaver city NE	38.22	0.003	7.92	1.92	2.51	0.58	
Beaver Creek at Beaver City NE	28.31	0.001	12.19	1.37	1.70	0.46	
Beaver Creek at Ludell KS	12.74	0.001	8.53	2.44	0.61	0.13	
Frenchman Creek at Hamlet, NE	24.07	0.0013	10.97	1.98	1.11	0.25	
Blackwood Creek at Culbertson, NE	19.54	0.0021	8.23	2.56	0.93	0.19	
Red Willow Creek near Red Willow, NE	62.85	0.001	13.72	2.16	2.12	0.46	
South Loup River near Cumro, NE	58.89	0.003	43.58	2.22	0.61	0.13	
White River at Interior, SD	308.61	0.002	89.3	1.77	1.95	0.47	
Cheyenne River at Edgemont, SD	103.62	0.0025	67.36	1.52	1.01	0.26	
Smoky Hill River near Russel, KS	226.5	0.00066	35.05	1.07	6.04	1.87	
Smoky Hill River near Danopolis, KS	260.48	0.0005	28.04	1.68	5.53	1.36	
Smoky Hill River near Junction city , KS	368.06	0.0004	46.63	1.52	5.19	1.35	
Kansas River at Wamego, KS	1104.19	0.0008	193.84	3.05	1.87	0.34	
Kansas River near topeka, KS	1359	0.0005	243.83	5.49	1.02	0.14	
Arikaree River at Haigler, NE	99.09	0.002	20.73	0.91	5.25	1.76	
S. F. Republican River near Benkleman, NE	127.41	0.002	30.48	0.7	5.97	2.28	
Republican river near Benkleman, NE	61.58	0.003	37.49	0.76	2.16	0.79	
Republican River near Bostwick, NE	339.75	0.0008	46.94	1.52	4.76	1.23	
Republican River at Concordia, KS	368.06	0.0007	76.2	1.52	3.18	0.82	
Republican River at Junction City , KS	424.69	0.0007	91.44	1.98	2.35	0.53	
South Fork powder River near Kaycee, WY	110.42	0.004	36.27	0.7	4.35	1.66	
Middle Fork Powder River above Kaycee WY	16.25	0.005	10.67	0.76	2.00	0.73	
Middle Fork Powder River near Kaycee, WY	46.15	0.0015	14.32	1.34	2.41	0.66	
Owl Creek near Thermopolis , WY	16.56	0.0015	10.67	1.19	1.30	0.38	
Gooseberry Creek at Pulliam, WY	8.81	0.006	17.98	0.73	0.67	0.25	
Greybull River near Basin,WY	88.9	0.0015	40.84	0.94	2.32	0.76	
Bates Creek near Alcova, WY	14.16	0.0035	21.03	0.85	0.79	0.27	
Powder River at Moorhead, MT	210.93	0.0016	64.61	1.22	2.68	0.77	
Red Fork at Barnum WY	18.12	0.005	10.67	0.76	2.23	0.82	
Tongue River near Acme, WY	97.68	0.002	30.48	1.31	2.45	0.68	
Horseshoe Creek near Glendo, WY	14.86	0.0025	19.51	0.82	0.93	0.33	
Smoky Hill River near Elkader, KS	84.94	0.006	152.39	1.22	0.46	0.13	
Republican River near Naponee, KS	321.35	0.0007	38.71	1.37	6.06	1.65	
Powder River near Sussex, WY	165.63	0.0008	53.95	1.13	2.72	0.82	
Powder River near Arvada WY	243.49	0.0007	51.81	1.37	3.43	0.94	
Missouri Landusky	850	0.00049	190	6.33	0.71	0.09	**Osterkamp and**
Missouri Culbertson	683	0.00016	320	10.7	0.20	0.02	**Hedman, 1982.**
Yellowstone Corwin	487	0.0023	82.3	3.05	1.94	0.35	
Yellowstone Livngston	584	0.0027	88.4	3.66	1.81	0.30	
Bighorn Bighorn	407	0.00045	82.3	3.2	1.55	0.28	
Yellowstone Miles City	1544	0.00068	219	7.3	0.97	0.11	
Missouri at Sioux City	963	0.00021	350	17	0.16	0.01	
Missouri Omaha	1811	0.00016	290	11.6	0.54	0.05	
Middle Loup St. Paul	235	0.001	134	1.07	1.64	0.51	
North Loup Ord	75.1	0.0013	75.6	0.98	1.01	0.33	
North Loup St. Paul	181	0.0011	85.3	1.52	1.40	0.36	
Elkhorn Norfolk	108	0.00069	80.8	1.01	1.32	0.42	
Missouri Nebraska City	2554	0.00024	270	10	0.95	0.10	
Missouri St. Joseph	2790	0.00021	270	10	1.03	0.10	
Kansas Wamego	1080	0.00025	223	11	0.44	0.04	
Kansas Topeka	1312	0.00027	159	8	1.03	0.12	
Kansas Lecompton	1561	0.00027	171	8.5	1.07	0.12	
Kansas DeSoto	1420	0.00034	165	8.5	1.01	0.11	
Missouri Waverly	3200	0.00015	320	13	0.77	0.07	
Thompson Trenton	640	0.00076	82.3	2.13	3.65	0.80	
Missouri Booneville	2148	0.00016	430	17.2	0.29	0.02	
Missouri Herman	4941	0.00013	424	17	0.69	0.05	
ColumbiaVenita	11494.9	0.00019	529.4	8.53	2.55	0.28	**Barnes, 1967**
Indian fork	21.7	0.00028	15.8	1.65	0.83	0.21	
Champlin	67.7	0.0035	23.8	1.37	2.08	0.57	
Clark Fork	1950.7	0.00073	130.8	5	2.98	0.43	
Clark Fork	891.8	0.00125	88.4	3.9	2.59	0.42	
Columbia	28312.6	0.00026	510.8	16.79	3.30	0.26	
Esopus	393.5	0.0034	89.3	1.68	2.62	0.65	
Salt Cr.	52.7	0.00056	22.9	2.07	1.11	0.25	
Blackfoot	232.2	0.0023	59.1	1.86	2.11	0.49	
Coer d'Alene	319.9	0.0025	49.4	2.41	2.69	0.55	
Rio Chama	30	0.0012	27.4	1.04	1.05	0.33	
Salt	36.2	0.0019	57.9	0.67	0.93	0.36	

River Name	Discharge (m³/s)	Water surface slope (m/m)	Channel width (m)	Average Channel Depth (m)	Average Channel Velocity (m/s)	Froude Number	Source
Beaver Kill	438.8	0.0034	68.3	2.26	2.84	0.60	
Clearwater	2802.9	0.00079	171.9	6	2.72	0.35	
Etowah	64	0.00066	19.5	2.96	1.11	0.21	
WF Bitteroot	109.9	0.0046	32	1.46	2.35	0.62	
Yakima	784.3	0.003	67.4	3.57	3.26	0.55	
MF Vermilion	45.9	0.0031	35.7	1.01	1.27	0.40	
Weneatchee	642.7	0.0024	70.1	3.26	2.81	0.50	
Moyie	227.3	0.0036	44.8	2.16	2.35	0.51	
Spokane	1121.2	0.0018	89.9	4.45	2.80	0.42	
Tobesfokee	71.9	0.00077	25	2.74	1.05	0.20	
Bull Cr	91.2	0.0012	32.9	2.19	1.27	0.27	
NF Flathead	410.5	0.0036	55.5	2.68	2.76	0.54	
Middle Oconee	173	0.00047	43	3.32	1.21	0.21	
Beaver Cr	45.3	0.0012	14.9	2.65	1.15	0.23	
Catherine Cr	49.3	0.0067	17.4	1.28	2.21	0.62	
Chiwawa	166.5	0.0052	41.8	1.71	2.33	0.57	
Esopus	393.5	0.0045	54.3	2.53	2.86	0.58	
Grande Ronde	130.8	0.0053	34.7	1.62	2.33	0.58	
Murder Cr	23.8	0.0027	13.7	1.4	1.24	0.34	
Provo	34	0.0089	15.5	1.07	2.05	0.63	
S Beaverdam	23.2	0.0016	18.6	1.4	0.89	0.24	
Deep	235	0.00077	66.7	3.17	1.11	0.20	
Clear Cr	39.1	0.0168	15.2	1.16	2.22	0.66	
Chattahoochee	144.4	0.0024	44.8	2.35	1.37	0.29	
SF Clearwater	356.7	0.0063	46.3	2.71	2.84	0.55	
EB Ausable	220.6	0.0056	46.6	2.16	2.19	0.48	
MB Westfield	96.3	0.0087	36.3	1.34	1.98	0.55	
Mission Cr	3.5	0.0169	6.4	0.43	1.27	0.62	
NF Cedar	28.2	0.0237	18.6	0.79	1.92	0.69	
Merced	55.2	0.013	21.6	1.31	1.95	0.54	
Pond Cr	41.9	0.00064	31.4	2.47	0.54	0.11	
Boundary	71.6	0.0187	25.6	1.34	2.09	0.58	
Amazon	283170	0.000013	3870	33	2.22	0.12	**Dury, 1976***
Reference							

*Discharge Prediction, Present and Future from Channel Dimensions, Journal of Hydrology vol. 30 pg. 219-245.

Appendix 4 - Prandtl-von Karmen Synthetic River Channel Data Base

Table A4 - Prandtl von-Karmen Synthetic River Channel Data Base

Channel Data				Scalars			Estimated Data				
Channel Width W_m (m)	Channel Slope S (m/m)	Channel Max Depth Y_m (m)	Roughness Height k_s (m)	Max Y[1] Y (m)	Distance[2] x (m)	Integral[3] Q' (m^2)	Discharge Q (m^3/s)	Top Width W (m)	Mean Depth Y (m)	Mean Velocity V (m/s)	Froude Number F
30	0.008	1.47	0.0210	0.15	4.7	0.31	0.14	9.5	0.10	0.15	0.15
30	0.008	1.47	0.0210	0.29	6.7	1.79	1.11	13.4	0.20	0.42	0.30
30	0.008	1.47	0.0210	0.44	8.2	4.27	3.24	16.4	0.29	0.67	0.39
30	0.008	1.47	0.0210	0.59	9.5	7.64	6.70	19.0	0.39	0.90	0.46
30	0.008	1.47	0.0210	0.74	10.6	11.84	11.60	21.2	0.49	1.12	0.51
30	0.008	1.47	0.0210	0.88	11.6	16.81	18.04	23.2	0.59	1.32	0.55
30	0.008	1.47	0.0210	1.03	12.5	22.51	26.10	25.1	0.69	1.52	0.58
30	0.008	1.47	0.0210	1.18	13.4	28.90	35.83	26.8	0.78	1.70	0.61
30	0.008	1.47	0.0210	1.32	14.2	35.97	47.29	28.5	0.88	1.88	0.64
30	0.008	1.47	0.0210	1.47	15.0	43.67	60.53	30.0	0.98	2.06	0.66
30	0.004	1.74	0.0156	0.17	4.7	0.62	0.21	9.5	0.12	0.19	0.18
30	0.004	1.74	0.0156	0.35	6.7	2.83	1.35	13.4	0.23	0.43	0.29
30	0.004	1.74	0.0156	0.52	8.2	6.36	3.71	16.4	0.35	0.65	0.35
30	0.004	1.74	0.0156	0.69	9.5	11.05	7.44	19.0	0.46	0.85	0.40
30	0.004	1.74	0.0156	0.87	10.6	16.82	12.66	21.2	0.58	1.03	0.43
30	0.004	1.74	0.0156	1.04	11.6	23.58	19.45	23.2	0.69	1.21	0.46
30	0.004	1.74	0.0156	1.22	12.5	31.28	27.87	25.1	0.81	1.37	0.49
30	0.004	1.74	0.0156	1.39	13.4	39.87	37.98	26.8	0.93	1.53	0.51
30	0.004	1.74	0.0156	1.56	14.2	49.32	49.84	28.5	1.04	1.68	0.53
30	0.004	1.74	0.0156	1.74	15.0	59.60	63.47	30.0	1.16	1.83	0.54
30	0.002	2.05	0.0108	0.21	4.7	1.08	0.28	9.5	0.14	0.22	0.19
30	0.002	2.05	0.0108	0.41	6.7	4.32	1.58	13.4	0.27	0.43	0.26
30	0.002	2.05	0.0108	0.62	8.2	9.31	4.17	16.4	0.41	0.62	0.31
30	0.002	2.05	0.0108	0.82	9.5	15.82	8.19	19.0	0.55	0.79	0.34
30	0.002	2.05	0.0108	1.03	10.6	23.73	13.74	21.2	0.68	0.95	0.37
30	0.002	2.05	0.0108	1.23	11.6	32.94	20.88	23.2	0.82	1.10	0.39
30	0.002	2.05	0.0108	1.44	12.5	43.36	29.69	25.1	0.96	1.24	0.40
30	0.002	2.05	0.0108	1.64	13.4	54.93	40.21	26.8	1.09	1.37	0.42
30	0.002	2.05	0.0108	1.85	14.2	67.61	52.49	28.5	1.23	1.50	0.43
30	0.002	2.05	0.0108	2.05	15.0	81.34	66.57	30.0	1.37	1.62	0.44
50	0.005	2.01	0.0189	0.20	7.9	1.15	0.47	15.8	0.13	0.22	0.19
50	0.005	2.01	0.0189	0.40	11.2	5.35	3.07	22.4	0.27	0.51	0.31
50	0.005	2.01	0.0189	0.60	13.7	12.06	8.47	27.4	0.40	0.77	0.39
50	0.005	2.01	0.0189	0.81	15.8	21.01	17.05	31.6	0.54	1.00	0.44
50	0.005	2.01	0.0189	1.01	17.7	32.01	29.04	35.4	0.67	1.22	0.48
50	0.005	2.01	0.0189	1.21	19.4	44.93	44.64	38.7	0.81	1.43	0.51
50	0.005	2.01	0.0189	1.41	20.9	59.65	64.01	41.8	0.94	1.63	0.54
50	0.005	2.01	0.0189	1.61	22.4	76.08	87.29	44.7	1.07	1.82	0.56
50	0.005	2.01	0.0189	1.81	23.7	94.16	114.58	47.4	1.21	2.00	0.58
50	0.005	2.01	0.0189	2.01	25.0	113.82	146.00	50.0	1.34	2.17	0.60
50	0.002	2.51	0.0115	0.25	7.9	2.38	0.68	15.8	0.17	0.26	0.20
50	0.002	2.51	0.0115	0.50	11.2	9.34	3.78	22.4	0.33	0.51	0.28
50	0.002	2.51	0.0115	0.75	13.7	19.94	9.89	27.4	0.50	0.72	0.32
50	0.002	2.51	0.0115	1.00	15.8	33.74	19.33	31.6	0.67	0.91	0.36
50	0.002	2.51	0.0115	1.26	17.7	50.46	32.31	35.4	0.84	1.09	0.38
50	0.002	2.51	0.0115	1.51	19.4	69.88	49.01	38.7	1.00	1.26	0.40
50	0.002	2.51	0.0115	1.76	20.9	91.83	69.57	41.8	1.17	1.42	0.42
50	0.002	2.51	0.0115	2.01	22.4	116.19	94.11	44.7	1.34	1.57	0.43
50	0.002	2.51	0.0115	2.26	23.7	142.85	122.72	47.4	1.51	1.72	0.45
50	0.002	2.51	0.0115	2.51	25.0	171.72	155.50	50.0	1.67	1.86	0.46
50	0.001	2.96	0.0072	0.30	7.9	3.82	0.84	15.8	0.20	0.27	0.19
50	0.001	2.96	0.0072	0.59	11.2	13.86	4.31	22.4	0.40	0.49	0.25
50	0.001	2.96	0.0072	0.89	13.7	28.75	10.96	27.4	0.59	0.67	0.28
50	0.001	2.96	0.0072	1.19	15.8	47.85	21.06	31.6	0.79	0.84	0.30
50	0.001	2.96	0.0072	1.48	17.7	70.78	34.83	35.4	0.99	1.00	0.32
50	0.001	2.96	0.0072	1.78	19.4	97.23	52.41	38.7	1.19	1.14	0.33
50	0.001	2.96	0.0072	2.08	20.9	126.98	73.93	41.8	1.38	1.28	0.35
50	0.001	2.96	0.0072	2.37	22.4	159.86	99.50	44.7	1.58	1.41	0.36
50	0.001	2.96	0.0072	2.67	23.7	195.72	129.21	47.4	1.78	1.53	0.37
50	0.001	2.96	0.0072	2.96	25.0	234.44	163.14	50.0	1.98	1.65	0.38
100	0.002	3.30	0.0125	0.33	15.8	6.95	2.28	31.6	0.22	0.33	0.22
100	0.002	3.30	0.0125	0.66	22.4	26.49	12.30	44.7	0.44	0.62	0.30
100	0.002	3.30	0.0125	0.99	27.4	55.99	31.86	54.8	0.66	0.88	0.35

Channel Data				Scalars			Estimated Data				
Channel Width W_m (m)	Channel Slope S (m/m)	Channel Max Depth Y_m (m)	Roughness Height k_s (m)	Max Y[1] Y (m)	Distance[2] x (m)	Integral[3] Q' (m^2)	Discharge Q (m^3/s)	Top Width W (m)	Mean Depth Y (m)	Mean Velocity V (m/s)	Froude Number F
100	0.002	3.30	0.0125	1.32	31.6	94.22	61.90	63.2	0.88	1.11	0.38
100	0.002	3.30	0.0125	1.65	35.4	140.36	103.10	70.7	1.10	1.32	0.40
100	0.002	3.30	0.0125	1.98	38.7	193.84	155.97	77.5	1.32	1.52	0.42
100	0.002	3.30	0.0125	2.31	41.8	254.21	220.93	83.7	1.54	1.71	0.44
100	0.002	3.30	0.0125	2.64	44.7	321.10	298.34	89.4	1.76	1.89	0.46
100	0.002	3.30	0.0125	2.97	47.4	394.22	388.49	94.9	1.98	2.07	0.47
100	0.002	3.30	0.0125	3.30	50.0	473.32	491.67	100.0	2.20	2.23	0.48
100	0.001	3.90	0.0075	0.39	15.8	10.97	2.77	31.6	0.26	0.34	0.21
100	0.001	3.90	0.0075	0.78	22.4	39.08	13.95	44.7	0.52	0.60	0.27
100	0.001	3.90	0.0075	1.17	27.4	80.46	35.18	54.8	0.78	0.82	0.30
100	0.001	3.90	0.0075	1.56	31.6	133.34	67.32	63.2	1.04	1.02	0.32
100	0.001	3.90	0.0075	1.95	35.4	196.61	110.97	70.7	1.30	1.21	0.34
100	0.001	3.90	0.0075	2.34	38.7	269.46	166.61	77.5	1.56	1.38	0.35
100	0.001	3.90	0.0075	2.73	41.8	351.30	234.62	83.7	1.82	1.54	0.36
100	0.001	3.90	0.0075	3.12	44.7	441.64	315.31	89.4	2.08	1.69	0.38
100	0.001	3.90	0.0075	3.51	47.4	540.06	408.97	94.9	2.34	1.84	0.38
100	0.001	3.90	0.0075	3.90	50.0	646.22	515.83	100.0	2.60	1.98	0.39
100	0.0005	4.61	0.0041	0.46	15.8	16.72	3.24	31.6	0.31	0.33	0.19
100	0.0005	4.61	0.0041	0.92	22.4	56.82	15.59	44.7	0.61	0.57	0.23
100	0.0005	4.61	0.0041	1.38	27.4	114.61	38.51	54.8	0.92	0.76	0.25
100	0.0005	4.61	0.0041	1.84	31.6	187.64	72.79	63.2	1.23	0.94	0.27
100	0.0005	4.61	0.0041	2.30	35.4	274.34	118.99	70.7	1.54	1.10	0.28
100	0.0005	4.61	0.0041	2.76	38.7	373.65	177.53	77.5	1.84	1.24	0.29
100	0.0005	4.61	0.0041	3.22	41.8	484.71	248.75	83.7	2.15	1.38	0.30
100	0.0005	4.61	0.0041	3.69	44.7	606.88	332.95	89.4	2.46	1.52	0.31
100	0.0005	4.61	0.0041	4.15	47.4	739.60	430.38	94.9	2.76	1.64	0.32
100	0.0005	4.61	0.0041	4.61	50.0	882.41	541.26	100.0	3.07	1.76	0.32
200	0.0012	4.91	0.0091	0.49	31.6	28.05	8.70	63.2	0.33	0.42	0.23
200	0.0012	4.91	0.0091	0.98	44.7	99.64	43.73	89.4	0.66	0.75	0.29
200	0.0012	4.91	0.0091	1.47	54.8	204.88	110.12	109.5	0.98	1.02	0.33
200	0.0012	4.91	0.0091	1.97	63.2	339.27	210.57	126.5	1.31	1.27	0.35
200	0.0012	4.91	0.0091	2.46	70.7	499.98	346.94	141.4	1.64	1.50	0.37
200	0.0012	4.91	0.0091	2.95	77.5	685.00	520.70	154.9	1.97	1.71	0.39
200	0.0012	4.91	0.0091	3.44	83.7	892.77	733.01	167.3	2.29	1.91	0.40
200	0.0012	4.91	0.0091	3.93	89.4	1122.05	984.87	178.9	2.62	2.10	0.41
200	0.0012	4.91	0.0091	4.42	94.9	1371.82	1277.14	189.7	2.95	2.28	0.42
200	0.0012	4.91	0.0091	4.91	100.0	1641.21	1610.59	200.0	3.28	2.46	0.43
200	0.0006	5.80	0.0049	0.58	31.6	42.70	10.18	63.2	0.39	0.42	0.21
200	0.0006	5.80	0.0049	1.16	44.7	144.76	48.82	89.4	0.77	0.71	0.26
200	0.0006	5.80	0.0049	1.74	54.8	291.72	120.49	109.5	1.16	0.95	0.28
200	0.0006	5.80	0.0049	2.32	63.2	477.28	227.63	126.5	1.55	1.16	0.30
200	0.0006	5.80	0.0049	2.90	70.7	697.54	371.95	141.4	1.93	1.36	0.31
200	0.0006	5.80	0.0049	3.48	77.5	949.72	554.75	154.9	2.32	1.54	0.32
200	0.0006	5.80	0.0049	4.06	83.7	1231.71	777.12	167.3	2.71	1.72	0.33
200	0.0006	5.80	0.0049	4.64	89.4	1541.82	1039.94	178.9	3.09	1.88	0.34
200	0.0006	5.80	0.0049	5.22	94.9	1878.67	1344.00	189.7	3.48	2.03	0.35
200	0.0006	5.80	0.0049	5.80	100.0	2241.08	1690.00	200.0	3.87	2.18	0.35
200	0.0003	6.85	0.0023	0.69	31.6	63.52	11.64	63.2	0.46	0.40	0.19
200	0.0003	6.85	0.0023	1.37	44.7	207.98	53.90	89.4	0.91	0.66	0.22
200	0.0003	6.85	0.0023	2.06	54.8	412.52	130.93	109.5	1.37	0.87	0.24
200	0.0003	6.85	0.0023	2.74	63.2	668.37	244.95	126.5	1.83	1.06	0.25
200	0.0003	6.85	0.0023	3.43	70.7	970.12	397.51	141.4	2.28	1.23	0.26
200	0.0003	6.85	0.0023	4.11	77.5	1313.97	589.79	154.9	2.74	1.39	0.27
200	0.0003	6.85	0.0023	4.80	83.7	1697.04	822.77	167.3	3.20	1.54	0.27
200	0.0003	6.85	0.0023	5.48	89.4	2117.03	1097.26	178.9	3.65	1.68	0.28
200	0.0003	6.85	0.0023	6.17	94.9	2572.08	1413.98	189.7	4.11	1.81	0.29
200	0.0003	6.85	0.0023	6.85	100.0	3060.59	1773.55	200.0	4.57	1.94	0.29
300	0.0008	6.36	0.0065	0.64	47.4	66.39	19.14	94.9	0.42	0.48	0.23
300	0.0008	6.36	0.0065	1.27	67.1	227.21	92.62	134.2	0.85	0.81	0.28
300	0.0008	6.36	0.0065	1.91	82.2	459.78	229.55	164.3	1.27	1.10	0.31
300	0.0008	6.36	0.0065	2.54	94.9	754.15	434.77	189.7	1.70	1.35	0.33
300	0.0008	6.36	0.0065	3.18	106.1	1104.13	711.67	212.1	2.12	1.58	0.35
300	0.0008	6.36	0.0065	3.82	116.2	1505.29	1062.84	232.4	2.54	1.80	0.36
300	0.0008	6.36	0.0065	4.45	125.5	1954.29	1490.43	251.0	2.97	2.00	0.37
300	0.0008	6.36	0.0065	5.09	134.2	2448.45	1996.22	268.3	3.39	2.19	0.38

Channel Data				Scalars			Estimated Data				
Channel Width W_m (m)	Channel Slope S (m/m)	Channel Max Depth Y_m (m)	Roughness Height k_s (m)	Max Y[1] Y (m)	Distance[2] x (m)	Integral[3] Q' (m^2)	Discharge Q (m^3/s)	Top Width W (m)	Mean Depth Y (m)	Mean Velocity V (m/s)	Froude Number F
300	0.0008	6.36	0.0065	5.72	142.3	2985.54	2581.76	284.6	3.82	2.38	0.39
300	0.0008	6.36	0.0065	6.36	150.0	3563.70	3248.43	300.0	4.24	2.55	0.40
300	0.0004	7.51	0.0032	0.75	47.4	99.22	21.98	94.9	0.50	0.46	0.21
300	0.0004	7.51	0.0032	1.50	67.1	327.19	102.49	134.2	1.00	0.76	0.24
300	0.0004	7.51	0.0032	2.25	82.2	651.12	249.81	164.3	1.50	1.01	0.26
300	0.0004	7.51	0.0032	3.00	94.9	1057.12	468.31	189.7	2.00	1.23	0.28
300	0.0004	7.51	0.0032	3.75	106.1	1536.61	761.08	212.1	2.50	1.43	0.29
300	0.0004	7.51	0.0032	4.51	116.2	2083.56	1130.48	232.4	3.00	1.62	0.30
300	0.0004	7.51	0.0032	5.26	125.5	2693.39	1578.44	251.0	3.50	1.79	0.31
300	0.0004	7.51	0.0032	6.01	134.2	3362.45	2106.59	268.3	4.01	1.96	0.31
300	0.0004	7.51	0.0032	6.76	142.3	4087.74	2716.34	284.6	4.51	2.12	0.32
300	0.0004	7.51	0.0032	7.51	150.0	4866.74	3408.93	300.0	5.01	2.27	0.32
300	0.0001	10.47	0.0005	1.05	47.4	210.85	27.58	94.9	0.70	0.42	0.16
300	0.0001	10.47	0.0005	2.09	67.1	661.30	122.32	134.2	1.40	0.65	0.18
300	0.0001	10.47	0.0005	3.14	82.2	1284.67	291.04	164.3	2.09	0.85	0.19
300	0.0001	10.47	0.0005	4.19	94.9	2054.11	537.34	189.7	2.79	1.01	0.19
300	0.0001	10.47	0.0005	5.24	106.1	2953.34	863.77	212.1	3.49	1.17	0.20
300	0.0001	10.47	0.0005	6.28	116.2	3971.02	1272.26	232.4	4.19	1.31	0.20
300	0.0001	10.47	0.0005	7.33	125.5	5098.62	1764.41	251.0	4.89	1.44	0.21
300	0.0001	10.47	0.0005	8.38	134.2	6329.39	2341.56	268.3	5.59	1.56	0.21
300	0.0001	10.47	0.0005	9.43	142.3	7657.83	3004.87	284.6	6.28	1.68	0.21
300	0.0001	10.47	0.0005	10.47	150.0	9079.32	3755.36	300.0	6.98	1.79	0.22
400	0.0007	7.36	0.0057	0.74	63.2	110.84	32.15	126.5	0.49	0.52	0.24
400	0.0007	7.36	0.0057	1.47	89.4	374.34	153.55	178.9	0.98	0.87	0.28
400	0.0007	7.36	0.0057	2.21	109.5	753.07	378.33	219.1	1.47	1.17	0.31
400	0.0007	7.36	0.0057	2.94	126.5	1230.83	714.01	253.0	1.96	1.44	0.33
400	0.0007	7.36	0.0057	3.68	141.4	1797.54	1165.84	282.8	2.45	1.68	0.34
400	0.0007	7.36	0.0057	4.41	154.9	2446.07	1737.87	309.8	2.94	1.91	0.35
400	0.0007	7.36	0.0057	5.15	167.3	3170.97	2433.40	334.7	3.43	2.12	0.37
400	0.0007	7.36	0.0057	5.89	178.9	3967.92	3255.23	357.8	3.92	2.32	0.37
400	0.0007	7.36	0.0057	6.62	189.7	4833.36	4205.75	379.5	4.41	2.51	0.38
400	0.0007	7.36	0.0057	7.36	200.0	5764.26	5287.09	400.0	4.91	2.69	0.39
400	0.0003	9.02	0.0022	0.90	63.2	179.26	37.68	126.5	0.60	0.50	0.20
400	0.0003	9.02	0.0022	1.80	89.4	581.58	172.89	178.9	1.20	0.80	0.23
400	0.0003	9.02	0.0022	2.71	109.5	1148.53	418.16	219.1	1.80	1.06	0.25
400	0.0003	9.02	0.0022	3.61	126.5	1855.79	780.19	253.0	2.40	1.28	0.26
400	0.0003	9.02	0.0022	4.51	141.4	2688.40	1263.63	282.8	3.01	1.49	0.27
400	0.0003	9.02	0.0022	5.41	154.9	3635.87	1872.09	309.8	3.61	1.68	0.28
400	0.0003	9.02	0.0022	6.31	167.3	4690.27	2608.49	334.7	4.21	1.85	0.29
400	0.0003	9.02	0.0022	7.21	178.9	5845.29	3475.31	357.8	4.81	2.02	0.29
400	0.0003	9.02	0.0022	8.12	189.7	7095.77	4474.69	379.5	5.41	2.18	0.30
400	0.0003	9.02	0.0022	9.02	200.0	8437.34	5608.51	400.0	6.01	2.33	0.30
400	0.0001	11.74	0.0005	1.17	63.2	323.41	44.78	126.5	0.78	0.45	0.16
400	0.0001	11.74	0.0005	2.35	89.4	1011.76	198.12	178.9	1.57	0.71	0.18
400	0.0001	11.74	0.0005	3.52	109.5	1963.00	470.78	219.1	2.35	0.92	0.19
400	0.0001	11.74	0.0005	4.70	126.5	3136.14	868.48	253.0	3.13	1.10	0.20
400	0.0001	11.74	0.0005	5.87	141.4	4506.36	1395.23	282.8	3.91	1.26	0.20
400	0.0001	11.74	0.0005	7.04	154.9	6056.38	2054.11	309.8	4.70	1.41	0.21
400	0.0001	11.74	0.0005	8.22	167.3	7773.20	2847.64	334.7	5.48	1.55	0.21
400	0.0001	11.74	0.0005	9.39	178.9	9646.57	3777.93	357.8	6.26	1.69	0.22
400	0.0001	11.74	0.0005	10.56	189.7	11668.09	4846.82	379.5	7.04	1.81	0.22
400	0.0001	11.74	0.0005	11.74	200.0	13830.73	6055.93	400.0	7.83	1.93	0.22
500	0.0006	8.34	0.0049	0.83	79.1	169.55	48.48	158.1	0.56	0.55	0.24
500	0.0006	8.34	0.0049	1.67	111.8	565.76	228.75	223.6	1.11	0.92	0.28
500	0.0006	8.34	0.0049	2.50	136.9	1131.99	560.56	273.9	1.67	1.23	0.30
500	0.0006	8.34	0.0049	3.34	158.1	1843.98	1054.41	316.2	2.22	1.50	0.32
500	0.0006	8.34	0.0049	4.17	176.8	2686.72	1717.62	353.6	2.78	1.75	0.33
500	0.0006	8.34	0.0049	5.00	193.6	3649.58	2555.87	387.3	3.34	1.98	0.35
500	0.0006	8.34	0.0049	5.84	209.2	4724.49	3573.76	418.3	3.89	2.19	0.36
500	0.0006	8.34	0.0049	6.67	223.6	5905.05	4775.19	447.2	4.45	2.40	0.36
500	0.0006	8.34	0.0049	7.51	237.2	7185.96	6163.50	474.3	5.00	2.60	0.37
500	0.0006	8.34	0.0049	8.34	250.0	8562.77	7741.69	500.0	5.56	2.78	0.38
500	0.0003	9.85	0.0022	0.99	79.1	250.27	54.98	158.1	0.66	0.53	0.21
500	0.0003	9.85	0.0022	1.97	111.8	809.66	251.56	223.6	1.31	0.86	0.24
500	0.0003	9.85	0.0022	2.96	136.9	1596.81	607.64	273.9	1.97	1.13	0.26

Channel Data				Scalars			Estimated Data				
Channel Width W_m (m)	Channel Slope S (m/m)	Channel Max Depth Y_m (m)	Roughness Height k_s (m)	Max Y[1] Y (m)	Distance[2] x (m)	Integral[3] Q' (m^2)	Discharge Q (m^3/s)	Top Width W (m)	Mean Depth Y (m)	Mean Velocity V (m/s)	Froude Number F
500	0.0003	9.85	0.0022	3.94	158.1	2577.94	1132.75	316.2	2.63	1.36	0.27
500	0.0003	9.85	0.0022	4.93	176.8	3732.31	1833.55	353.6	3.28	1.58	0.28
500	0.0003	9.85	0.0022	5.91	193.6	5045.36	2715.18	387.3	3.94	1.78	0.29
500	0.0003	9.85	0.0022	6.90	209.2	6506.11	3781.82	418.3	4.60	1.97	0.29
500	0.0003	9.85	0.0022	7.88	223.6	8105.80	5036.99	447.2	5.25	2.14	0.30
500	0.0003	9.85	0.0022	8.87	237.2	9837.30	6483.76	474.3	5.91	2.31	0.30
500	0.0003	9.85	0.0022	9.85	250.0	11694.56	8124.82	500.0	6.57	2.47	0.31
500	0.0001	12.82	0.0005	1.28	79.1	450.61	65.21	158.1	0.85	0.48	0.17
500	0.0001	12.82	0.0005	2.56	111.8	1407.01	287.96	223.6	1.71	0.75	0.18
500	0.0001	12.82	0.0005	3.85	136.9	2727.22	683.61	273.9	2.56	0.97	0.19
500	0.0001	12.82	0.0005	5.13	158.1	4354.37	1260.32	316.2	3.42	1.17	0.20
500	0.0001	12.82	0.0005	6.41	176.8	6254.02	2023.80	353.6	4.27	1.34	0.21
500	0.0001	12.82	0.0005	7.69	193.6	8402.20	2978.47	387.3	5.13	1.50	0.21
500	0.0001	12.82	0.0005	8.98	209.2	10780.92	4127.90	418.3	5.98	1.65	0.22
500	0.0001	12.82	0.0005	10.26	223.6	13375.95	5475.12	447.2	6.84	1.79	0.22
500	0.0001	12.82	0.0005	11.54	237.2	16175.68	7022.76	474.3	7.69	1.92	0.22
500	0.0001	12.82	0.0005	12.82	250.0	19170.34	8773.12	500.0	8.55	2.05	0.22
750	0.0005	10.23	0.0040	1.02	118.6	345.65	99.91	237.2	0.68	0.62	0.24
750	0.0005	10.23	0.0040	2.05	167.7	1136.22	464.49	335.4	1.36	1.02	0.28
750	0.0005	10.23	0.0040	3.07	205.4	2257.79	1130.43	410.8	2.05	1.34	0.30
750	0.0005	10.23	0.0040	4.09	237.2	3662.26	2117.28	474.3	2.73	1.64	0.32
750	0.0005	10.23	0.0040	5.12	265.2	5319.96	3438.68	530.3	3.41	1.90	0.33
750	0.0005	10.23	0.0040	6.14	290.5	7210.02	5105.18	580.9	4.09	2.15	0.34
750	0.0005	10.23	0.0040	7.16	313.7	9316.60	7125.33	627.5	4.77	2.38	0.35
750	0.0005	10.23	0.0040	8.19	335.4	11627.11	9506.39	670.8	5.46	2.60	0.36
750	0.0005	10.23	0.0040	9.21	355.8	14131.20	12254.60	711.5	6.14	2.81	0.36
750	0.0005	10.23	0.0040	10.23	375.0	16820.17	15375.49	750.0	6.82	3.01	0.37
750	0.0002	12.75	0.0012	1.27	118.6	571.12	116.55	237.2	0.85	0.58	0.20
750	0.0002	12.75	0.0012	2.55	167.7	1812.96	523.22	335.4	1.70	0.92	0.22
750	0.0002	12.75	0.0012	3.82	205.4	3542.96	1252.30	410.8	2.55	1.20	0.24
750	0.0002	12.75	0.0012	5.10	237.2	5686.70	2320.98	474.3	3.40	1.44	0.25
750	0.0002	12.75	0.0012	6.37	265.2	8198.85	3741.27	530.3	4.25	1.66	0.26
750	0.0002	12.75	0.0012	7.65	290.5	11047.73	5522.43	580.9	5.10	1.86	0.26
750	0.0002	12.75	0.0012	8.92	313.7	14209.47	7672.00	627.5	5.95	2.06	0.27
750	0.0002	12.75	0.0012	10.20	335.4	17665.16	10196.34	670.8	6.80	2.24	0.27
750	0.0002	12.75	0.0012	11.47	355.8	21399.33	13100.96	711.5	7.65	2.41	0.28
750	0.0002	12.75	0.0012	12.75	375.0	25399.00	16390.72	750.0	8.50	2.57	0.28
750	0.0001	15.06	0.0004	1.51	118.6	823.07	129.07	237.2	1.00	0.54	0.17
750	0.0001	15.06	0.0004	3.01	167.7	2561.35	568.03	335.4	2.01	0.84	0.19
750	0.0001	15.06	0.0004	4.52	205.4	4956.27	1346.19	410.8	3.01	1.09	0.20
750	0.0001	15.06	0.0004	6.02	237.2	7904.62	2479.14	474.3	4.01	1.30	0.21
750	0.0001	15.06	0.0004	7.53	265.2	11343.99	3977.78	530.3	5.02	1.49	0.21
750	0.0001	15.06	0.0004	9.03	290.5	15231.00	5850.52	580.9	6.02	1.67	0.22
750	0.0001	15.06	0.0004	10.54	313.7	19533.07	8104.19	627.5	7.03	1.84	0.22
750	0.0001	15.06	0.0004	12.04	335.4	24224.47	10744.58	670.8	8.03	1.99	0.22
750	0.0001	15.06	0.0004	13.55	355.8	29284.19	13776.68	711.5	9.03	2.14	0.23
750	0.0001	15.06	0.0004	15.06	375.0	34694.63	17204.91	750.0	10.04	2.29	0.23
1000	0.0003	12.96	0.0021	1.30	158.1	704.90	177.65	316.2	0.86	0.65	0.22
1000	0.0003	12.96	0.0021	2.59	223.6	2261.63	806.07	447.2	1.73	1.04	0.25
1000	0.0003	12.96	0.0021	3.89	273.9	4442.74	1939.30	547.7	2.59	1.37	0.27
1000	0.0003	12.96	0.0021	5.18	316.2	7154.50	3606.15	632.5	3.46	1.65	0.28
1000	0.0003	12.96	0.0021	6.48	353.6	10339.58	5826.69	707.1	4.32	1.91	0.29
1000	0.0003	12.96	0.0021	7.78	387.3	13957.85	8616.45	774.6	5.18	2.15	0.30
1000	0.0003	12.96	0.0021	9.07	418.3	17978.97	11988.04	836.7	6.05	2.37	0.31
1000	0.0003	12.96	0.0021	10.37	447.2	22378.92	15952.11	894.4	6.91	2.58	0.31
1000	0.0003	12.96	0.0021	11.67	474.3	27137.99	20517.91	948.7	7.78	2.78	0.32
1000	0.0003	12.96	0.0021	12.96	500.0	32239.62	25693.55	1000.0	8.64	2.97	0.32
1000	0.0001	16.87	0.0004	1.69	158.1	1261.79	209.47	316.2	1.12	0.59	0.18
1000	0.0001	16.87	0.0004	3.37	223.6	3917.55	919.72	447.2	2.25	0.91	0.19
1000	0.0001	16.87	0.0004	5.06	273.9	7571.71	2177.12	547.7	3.37	1.18	0.20
1000	0.0001	16.87	0.0004	6.75	316.2	12066.73	4006.34	632.5	4.50	1.41	0.21
1000	0.0001	16.87	0.0004	8.44	353.6	17307.48	6424.61	707.1	5.62	1.62	0.22
1000	0.0001	16.87	0.0004	10.12	387.3	23227.84	9445.23	774.6	6.75	1.81	0.22
1000	0.0001	16.87	0.0004	11.81	418.3	29778.18	13079.02	836.7	7.87	1.99	0.23
1000	0.0001	16.87	0.0004	13.50	447.2	36919.33	17335.12	894.4	9.00	2.15	0.23

Channel Data				Scalars			Estimated Data					
Channel Width	Channel Slope	Channel Max Depth	Roughness Height	Max Y[1]	Distance[2]	Integral[3]	Discharge	Top Width	Mean Depth	Mean Velocity	Froude Number
W_m	S	Y_m	k_s	Y	x	Q'	Q	W	Y	V	F
(m)	(m/m)	(m)	(m)	(m)	(m)	(m^2)	(m^3/s)	(m)	(m)	(m/s)	
1000	0.0001	16.87	0.0004	15.19	474.3	44619.32	22221.44	948.7	10.12	2.31	0.23
1000	0.0001	16.87	0.0004	16.87	500.0	52851.34	27744.96	1000.0	11.25	2.47	0.23
1000	0.00005	19.93	0.0001	1.99	158.1	1799.54	229.56	316.2	1.33	0.55	0.15
1000	0.00005	19.93	0.0001	3.99	223.6	5501.67	992.54	447.2	2.66	0.84	0.16
1000	0.00005	19.93	0.0001	5.98	273.9	10549.74	2330.98	547.7	3.99	1.07	0.17
1000	0.00005	19.93	0.0001	7.97	316.2	16725.79	4267.30	632.5	5.31	1.27	0.18
1000	0.00005	19.93	0.0001	9.96	353.6	23899.03	6817.13	707.1	6.64	1.45	0.18
1000	0.00005	19.93	0.0001	11.96	387.3	31978.91	9992.54	774.6	7.97	1.62	0.18
1000	0.00005	19.93	0.0001	13.95	418.3	40897.69	13803.35	836.7	9.30	1.77	0.19
1000	0.00005	19.93	0.0001	15.94	447.2	50602.03	18257.85	894.4	10.63	1.92	0.19
1000	0.00005	19.93	0.0001	17.93	474.3	61048.46	23363.22	948.7	11.96	2.06	0.19
1000	0.00005	19.93	0.0001	19.93	500.0	72200.63	29125.78	1000.0	13.28	2.19	0.19
1500	0.00008	20.90	0.0002	2.09	237.2	2583.35	426.92	474.3	1.39	0.65	0.17
1500	0.00008	20.90	0.0002	4.18	335.4	7954.72	1859.12	670.8	2.79	0.99	0.19
1500	0.00008	20.90	0.0002	6.27	410.8	15310.02	4382.33	821.6	4.18	1.28	0.20
1500	0.00008	20.90	0.0002	8.36	474.3	24331.90	8042.19	948.7	5.57	1.52	0.21
1500	0.00008	20.90	0.0002	10.45	530.3	34829.34	12870.59	1060.7	6.97	1.74	0.21
1500	0.00008	20.90	0.0002	12.54	580.9	46669.90	18892.12	1161.9	8.36	1.94	0.21
1500	0.00008	20.90	0.0002	14.63	627.5	59754.28	26126.81	1255.0	9.75	2.13	0.22
1500	0.00008	20.90	0.0002	16.72	670.8	74004.25	34591.55	1341.6	11.15	2.31	0.22
1500	0.00008	20.90	0.0002	18.81	711.5	89356.00	44300.97	1423.0	12.54	2.48	0.22
1500	0.00008	20.90	0.0002	20.90	750.0	105756.07	55267.98	1500.0	13.93	2.64	0.23
1500	0.00004	24.68	0.0001	2.47	237.2	3670.16	466.08	474.3	1.65	0.60	0.15
1500	0.00004	24.68	0.0001	4.94	335.4	11145.96	2001.75	670.8	3.29	0.91	0.16
1500	0.00004	24.68	0.0001	7.41	410.8	21298.72	4684.80	821.6	4.94	1.16	0.17
1500	0.00004	24.68	0.0001	9.87	474.3	33689.76	8556.67	948.7	6.58	1.37	0.17
1500	0.00004	24.68	0.0001	12.34	530.3	48056.57	13646.29	1060.7	8.23	1.56	0.17
1500	0.00004	24.68	0.0001	14.81	580.9	64217.82	19975.98	1161.9	9.87	1.74	0.18
1500	0.00004	24.68	0.0001	17.28	627.5	82037.95	27563.90	1255.0	11.52	1.91	0.18
1500	0.00004	24.68	0.0001	19.75	670.8	101410.41	36425.41	1341.6	13.16	2.06	0.18
1500	0.00004	24.68	0.0001	22.22	711.5	122248.41	46573.77	1423.0	14.81	2.21	0.18
1500	0.00004	24.68	0.0001	24.68	750.0	144479.41	58020.69	1500.0	16.46	2.35	0.19
2000	0.00005	26.22	0.0001	2.62	316.2	5021.98	734.88	632.5	1.75	0.66	0.16
2000	0.00005	26.22	0.0001	5.24	447.2	15288.02	3163.78	894.4	3.50	1.01	0.17
2000	0.00005	26.22	0.0001	7.87	547.7	29250.49	7413.69	1095.4	5.24	1.29	0.18
2000	0.00005	26.22	0.0001	10.49	632.5	46306.26	13552.21	1264.9	6.99	1.53	0.19
2000	0.00005	26.22	0.0001	13.11	707.1	66094.02	21626.58	1414.2	8.74	1.75	0.19
2000	0.00005	26.22	0.0001	15.73	774.6	88364.04	31673.19	1549.2	10.49	1.95	0.19
2000	0.00005	26.22	0.0001	18.35	836.7	112929.53	43721.71	1673.3	12.24	2.14	0.20
2000	0.00005	26.22	0.0001	20.98	894.4	139643.60	57797.17	1788.9	13.98	2.31	0.20
2000	0.00005	26.22	0.0001	23.60	948.7	168386.60	73921.26	1897.4	15.73	2.48	0.20
2000	0.00005	26.22	0.0001	26.22	1000.0	199058.45	92113.06	2000.0	17.48	2.63	0.20
2000	0.00002	32.67	0.0000	3.27	316.2	7923.21	818.51	632.5	2.18	0.59	0.13
2000	0.00002	32.67	0.0000	6.53	447.2	23760.48	3471.31	894.4	4.36	0.89	0.14
2000	0.00002	32.67	0.0000	9.80	547.7	45101.85	8070.09	1095.4	6.53	1.13	0.14
2000	0.00002	32.67	0.0000	13.07	632.5	71023.93	14674.32	1264.9	8.71	1.33	0.14
2000	0.00002	32.67	0.0000	16.33	707.1	100977.23	23325.55	1414.2	10.89	1.51	0.15
2000	0.00002	32.67	0.0000	19.60	774.6	134583.52	34055.78	1549.2	13.07	1.68	0.15
2000	0.00002	32.67	0.0000	22.87	836.7	171560.89	46891.13	1673.3	15.25	1.84	0.15
2000	0.00002	32.67	0.0000	26.14	894.4	211688.19	61853.60	1788.9	17.42	1.98	0.15
2000	0.00002	32.67	0.0000	29.40	948.7	254785.66	78962.27	1897.4	19.60	2.12	0.15
2000	0.00002	32.67	0.0000	32.67	1000.0	300703.23	98233.92	2000.0	21.78	2.26	0.15
30	0.01	1.39	0.0227	0.14	4.7	0.23	0.11	9.5	0.09	0.13	0.13
30	0.01	1.39	0.0227	0.28	6.7	1.53	1.03	13.4	0.19	0.41	0.31
30	0.01	1.39	0.0227	0.42	8.2	3.74	3.09	16.4	0.28	0.67	0.41
30	0.01	1.39	0.0227	0.56	9.5	6.77	6.46	19.0	0.37	0.92	0.48
30	0.01	1.39	0.0227	0.70	10.6	10.56	11.26	21.2	0.46	1.14	0.54
30	0.01	1.39	0.0227	0.84	11.6	15.06	17.60	23.2	0.56	1.36	0.58
30	0.01	1.39	0.0227	0.98	12.5	20.23	25.54	25.1	0.65	1.56	0.62
30	0.01	1.39	0.0227	1.11	13.4	26.05	35.15	26.8	0.74	1.76	0.65
30	0.01	1.39	0.0227	1.25	14.2	32.48	46.49	28.5	0.84	1.95	0.68
30	0.01	1.39	0.0227	1.39	15.0	39.51	59.62	30.0	0.93	2.14	0.71
500	0.00005	15.14	0.0001	1.51	79.1	644.37	71.66	158.1	1.01	0.45	0.14
500	0.00005	15.14	0.0001	3.03	111.8	1979.02	311.24	223.6	2.02	0.69	0.15
500	0.00005	15.14	0.0001	4.54	136.9	3803.84	732.68	273.9	3.03	0.88	0.16

Channel Data				Scalars			Estimated Data				
Channel Width W_m (m)	Channel Slope S (m/m)	Channel Max Depth Y_m (m)	Roughness Height k_s (m)	Max Y[1] Y (m)	Distance[2] x (m)	Integral[3] Q' (m^2)	Discharge Q (m^3/s)	Top Width W (m)	Mean Depth Y (m)	Mean Velocity V (m/s)	Froude Number F
500	0.00005	15.14	0.0001	6.06	158.1	6040.08	1343.40	316.2	4.04	1.05	0.17
500	0.00005	15.14	0.0001	7.57	176.8	8640.39	2148.58	353.6	5.05	1.20	0.17
500	0.00005	15.14	0.0001	9.09	193.6	11571.94	3152.21	387.3	6.06	1.34	0.17
500	0.00005	15.14	0.0001	10.60	209.2	14810.17	4357.54	418.3	7.07	1.47	0.18
500	0.00005	15.14	0.0001	12.11	223.6	18335.71	5767.34	447.2	8.08	1.60	0.18
500	0.00005	15.14	0.0001	13.63	237.2	22132.77	7383.97	474.3	9.09	1.71	0.18
500	0.00005	15.14	0.0001	15.14	250.0	26188.12	9209.52	500.0	10.10	1.82	0.18
100	0.0003	5.21	0.0024	0.52	15.8	22.47	3.59	31.6	0.35	0.33	0.18
100	0.0003	5.21	0.0024	1.04	22.4	74.31	16.79	44.7	0.69	0.54	0.21
100	0.0003	5.21	0.0024	1.56	27.4	148.08	40.97	54.8	1.04	0.72	0.22
100	0.0003	5.21	0.0024	2.08	31.6	240.63	76.88	63.2	1.39	0.88	0.24
100	0.0003	5.21	0.0024	2.60	35.4	349.98	125.02	70.7	1.74	1.02	0.25
100	0.0003	5.21	0.0024	3.12	38.7	474.77	185.78	77.5	2.08	1.15	0.25
100	0.0003	5.21	0.0024	3.65	41.8	613.95	259.49	83.7	2.43	1.28	0.26
100	0.0003	5.21	0.0024	4.17	44.7	766.69	346.42	89.4	2.78	1.39	0.27
100	0.0003	5.21	0.0024	4.69	47.4	932.31	446.80	94.9	3.12	1.51	0.27
100	0.0003	5.21	0.0024	5.21	50.0	1110.22	560.85	100.0	3.47	1.62	0.28
50	0.002	2.51	0.0115	0.25	7.9	2.38	0.68	15.8	0.17	0.26	0.20
50	0.002	2.51	0.0115	0.50	11.2	9.34	3.78	22.4	0.33	0.51	0.28
50	0.002	2.51	0.0115	0.75	13.7	19.94	9.89	27.4	0.50	0.72	0.32
50	0.002	2.51	0.0115	1.00	15.8	33.74	19.33	31.6	0.67	0.91	0.36
50	0.002	2.51	0.0115	1.26	17.7	50.46	32.31	35.4	0.84	1.09	0.38
50	0.002	2.51	0.0115	1.51	19.4	69.88	49.01	38.7	1.00	1.26	0.40
50	0.002	2.51	0.0115	1.76	20.9	91.83	69.57	41.8	1.17	1.42	0.42
50	0.002	2.51	0.0115	2.01	22.4	116.19	94.11	44.7	1.34	1.57	0.43
50	0.002	2.51	0.0115	2.26	23.7	142.85	122.72	47.4	1.51	1.72	0.45
50	0.002	2.51	0.0115	2.51	25.0	171.72	155.50	50.0	1.67	1.86	0.46
50	0.0005	3.50	0.0040	0.35	7.9	5.87	0.99	15.8	0.23	0.27	0.18
50	0.0005	3.50	0.0040	0.70	11.2	20.23	4.84	22.4	0.47	0.46	0.22
50	0.0005	3.50	0.0040	1.05	13.7	41.05	12.02	27.4	0.70	0.63	0.24
50	0.0005	3.50	0.0040	1.40	15.8	67.45	22.81	31.6	0.93	0.77	0.26
50	0.0005	3.50	0.0040	1.75	17.7	98.87	37.39	35.4	1.17	0.91	0.27
50	0.0005	3.50	0.0040	2.10	19.4	134.92	55.88	38.7	1.40	1.03	0.28
50	0.0005	3.50	0.0040	2.45	20.9	175.28	78.42	41.8	1.63	1.15	0.29
50	0.0005	3.50	0.0040	2.80	22.4	219.73	105.09	44.7	1.87	1.26	0.29
50	0.0005	3.50	0.0040	3.15	23.7	268.06	135.98	47.4	2.10	1.36	0.30
50	0.0005	3.50	0.0040	3.50	25.0	320.11	171.17	50.0	2.33	1.47	0.31
100	0.0004	4.86	0.0033	0.49	15.8	19.05	3.39	31.6	0.32	0.33	0.19
100	0.0004	4.86	0.0033	0.97	22.4	63.93	16.11	44.7	0.65	0.56	0.22
100	0.0004	4.86	0.0033	1.46	27.4	128.24	39.58	54.8	0.97	0.74	0.24
100	0.0004	4.86	0.0033	1.94	31.6	209.23	74.57	63.2	1.30	0.91	0.26
100	0.0004	4.86	0.0033	2.43	35.4	305.19	121.61	70.7	1.62	1.06	0.27
100	0.0004	4.86	0.0033	2.92	38.7	414.92	181.11	77.5	1.94	1.20	0.28
100	0.0004	4.86	0.0033	3.40	41.8	537.48	253.41	83.7	2.27	1.34	0.28
100	0.0004	4.86	0.0033	3.89	44.7	672.16	338.79	89.4	2.59	1.46	0.29
100	0.0004	4.86	0.0033	4.37	47.4	818.34	437.49	94.9	2.92	1.58	0.30
100	0.0004	4.86	0.0033	4.86	50.0	975.52	549.73	100.0	3.24	1.70	0.30
200	0.0015	4.66	0.0108	0.47	31.6	24.34	8.22	63.2	0.31	0.42	0.24
200	0.0015	4.66	0.0108	0.93	44.7	88.10	42.08	89.4	0.62	0.76	0.31
200	0.0015	4.66	0.0108	1.40	54.8	182.53	106.79	109.5	0.93	1.05	0.35
200	0.0015	4.66	0.0108	1.86	63.2	303.62	205.12	126.5	1.24	1.31	0.37
200	0.0015	4.66	0.0108	2.33	70.7	448.81	339.00	141.4	1.55	1.54	0.40
200	0.0015	4.66	0.0108	2.79	77.5	616.29	509.93	154.9	1.86	1.77	0.41
200	0.0015	4.66	0.0108	3.26	83.7	804.64	719.12	167.3	2.17	1.98	0.43
200	0.0015	4.66	0.0108	3.73	89.4	1012.75	967.60	178.9	2.48	2.18	0.44
200	0.0015	4.66	0.0108	4.19	94.9	1239.68	1256.26	189.7	2.79	2.37	0.45
200	0.0015	4.66	0.0108	4.66	100.0	1484.65	1585.88	200.0	3.10	2.55	0.46

notes:
[1] maximum depth of flow (prescribed)
[2] distance from center of channel to bank
[3] value of equation (6) divided by 2.5V*